



PB94-146768

UILU-ENG-94-2005

CIVIL ENGINEERING STUDIES

STRUCTURAL RESEARCH SERIES NO. 589



ISSN: 0069-4274

BEHAVIOR OF REINFORCED CONCRETE FRAMES WITH MASONRY INFILLS

by

RICHARD ANGEL

DANIEL ABRAMS

University of Illinois at Urbana-Champaign

and

DANIEL SHAPIRO

JOE UZARSKI


MARK WEBSTER

SOH and Associates, Structural Engineers
San Francisco, California

A Report on Research Sponsored by the
NATIONAL SCIENCE FOUNDATION

Grants: BCS-90-16509 (UIUC) and
BCS-90-16875 (SOHA)

DEPARTMENT OF CIVIL ENGINEERING
UNIVERSITY OF ILLINOIS AT
URBANA-CHAMPAIGN
March 1994

REPORT DOCUMENTATION PAGE	1. REPORT NO. UILU-ENG-94-2005	2.	3. Ri  PB94-146768
4. Title and Subtitle BEHAVIOR OF REINFORCED CONCRETE FRAMES WITH MASONRY INFILLS			5. Report Date March 1994
7. Author(s) R. Angel, D. Abrams, D. Shapiro, J. Uzarski, and M. Webster			8. Performing Organization Report No. SRS 589
9. Performing Organization Name and Address University of Illinois at Urbana-Champaign Department of Civil Engineering 205 N. Mathews Avenue Urbana, Illinois 61801			10. Project/Task/Work Unit No. 11. Contract(C) or Grant(G) No. BCS-90-16509
12. Sponsoring Organization Name and Address National Science Foundation 4201 Wilson Boulevard, Rm 545 Arlington, VA 22230			13. Type of Report & Period Covered Sept. 90 to Feb. 94 14.
15. Supplementary Notes			
16. Abstract (Limit: 200 words) The primary objective of the research project was to determine the transverse (out-of-plane) seismic strength of unreinforced masonry infill panels that have been cracked with in-plane lateral forces. The goal of the research was to develop a simple method that practicing engineers could use for evaluating strength of infill panels that have been damaged in earthquakes. In addition, the feasibility of using a low-cost repair or rehabilitation technique for improving transverse strength was examined. A total of 22 tests were run on eight large-scale masonry infill panels that were constructed in a single bay, single story reinforced concrete frame. Test panels were first subjected to in-plane load reversals to create a pre-existing cracked, damaged state for the subsequent out-of-plane tests which were done with an air bag. Following this test sequence, selected damaged panels were repaired and retested. Previous in-plane cracking was found to reduce out-of-plane strength by as much as a factor of two. However, transverse strength of a cracked masonry infill was found to be appreciable because of arching action. A simple equation was developed for out-of-plane strength based on the masonry compressive strength, the h/t ratio, the amount of in-plane damage and the stiffness of the bounding frame. An evaluation procedure was developed based on this procedure.			
17. Document Analysis a. Descriptors arching action, cracking, earthquakes, infills, frames, seismic evaluation, rehabilitation, reinforced concrete, retrofit, unreinforced masonry b. Identifiers/Open-Ended Terms c. COSATI Field/Group			
18. Availability Statement Release Unlimited	19. Security Class (This Report) UNCLASSIFIED 20. Security Class (This Page) UNCLASSIFIED	21. No. of Pages 183 22. Price	



ABSTRACT

This report provides a summary of a combined experimental and analytical research project that investigated the loss of transverse (out-of-plane) strength for unreinforced masonry infill panels as a result of in-plane cracking.

Large-scale test panels were constructed and subjected to repeated and reversed horizontal forces applied parallel with their plane to a lateral drift equal to twice that at initial cracking. Then, they were subjected to monotonically increasing transverse pressures with an air bag until their ultimate strengths were developed. Selected test panels were then repaired and retested.

Test specimens consisted of either clay-unit or concrete masonry infills placed in a single-bay, single-story reinforced concrete frame. Parameters of the experimental sequence were the masonry-unit type, the mortar type, and the height-to-thickness ratio of the infill panel.

An analytical model was developed to predict the out-of-plane behavior and strength of masonry panels with and without previous in-plane damage. The analytical model was based on an arching action theory. Analytical model parameters included the masonry compressive strength, the infill slenderness ratio, and the extent of in-plane damage.

Based on the analytical model and on the supporting experimental results, recommendations were developed for practical seismic evaluation and rehabilitation of cracked unreinforced masonry infill panels loaded normal to their plane.

ACKNOWLEDGEMENTS

The research project was one part of the national coordinated program on Repair and Rehabilitation Research for Seismic Resistance of Structures that was funded by the National Science Foundation (Grant #BCS 90-165509). The project was also one component of an ongoing research program at the University of Illinois on seismic evaluation and rehabilitation of unreinforced masonry buildings.

This report was written as a doctoral dissertation of the first author under the direction of the second author. Professors G. R. Gurfinkel, W. L. Gamble and J. P. Murtha are thanked for serving on the faculty review committee. Their critical and constructive suggestions were found to be of great value for the development of the report.

The authors thank support staff of the Civil Engineering department including H. Dalrymple, D. C. Hines, and M. J. Lawson from the electronic shop, and C. E. Swan and his associates from the machine shop. Civil Engineering graduate students Mauricio Angulo, Mario Salazar, Kyle Koppenhoefer, Pedro Vargas, Nirav Shah, Arturo Tena-Colunga, Weijia Xu, Paul Blaszczyk, Ming Tang, and Andrew Costley are thanked for their assistance and consultation with technical research problems.

The authors express great gratitude to Mr. Benli Gao of the Nanjing Technical Institute for his assistance in the analytical phase of the program while in residence as a visiting scholar at the University of Illinois.

TABLE OF CONTENTS

	PAGE
LIST OF TABLES	XII
LIST OF FIGURES	XIII
CHAPTER 1	
INTRODUCTION	1
1.1 Objective and Scope	2
1.2 Relevant Present Research	4
1.3 Uniqueness of Study	4
1.4 Outline	6
CHAPTER 2	
LITERATURE REVIEW	7
2.1 Previous Experimental Research	7
2.1.1 Specimens Subjected to In–Plane Forces	7
2.1.2 Specimens Subjected to Out–of–Plane Forces	9
2.1.3 Out–of–Plane Behavior of Repaired Infills	12
2.1.4 Summary	12
2.2 Existing Analytical Models	13
2.2.1 In–Plane Direction	13
2.2.2 Out–of–Plane Direction	16
2.2.3 Conclusions	20
CHAPTER 3	
DESCRIPTION OF EXPERIMENTAL PROGRAM	21
3.1 Specimen Description	21
3.1.1 Reinforced Concrete Frame	21
3.1.2 Masonry Infills	22
3.2 Considerations for Specimen Design	24

3.3	Specimen Construction	27
3.4	Description of Infill Repairing Method	28
3.5	General Testing Procedure	29
3.6	Description of Nondestructive Evaluation Methods	31

CHAPTER 4

RESPONSE RESULTING FROM IN-PLANE FORCES	32
4.1 Cracking and Damage of Test Specimens	32
4.2 Conventions	34
4.3 Measured Behavior of Reinforced Concrete Frame	34
4.4 Measured Cracking Strength and Behavior of Masonry Infill	35
4.5 Specimen Lateral Stiffness	38
4.6 Cracking Strength and Shear Strain Distribution	39
4.7 Correlation between Measured Experimental Results and NDE Estimates .	40
4.7.1 Flat-Jack Test	40
4.7.2 In-Place Shear Test (Shove Test)	41
4.8 Summary and Conclusions	43

CHAPTER 5

MEASURED RESPONSE RESULTING FROM OUT-OF-PLANE FORCES .	44
5.1 Cracking and Damage of Test Specimens	44
5.1.1 Virgin Specimen (Test #1)	44
5.1.2 In-Plane Cracked Specimens (Tests # 2b, 3b, 4b, 5b, 6b, 7b and 8b)	46
5.1.3 Repaired Specimens (Tests # 2c, 3c, 6c)	46
5.1.4 In-Plane Cracked Specimen with In-Plane Shear (Tests #5d and 6d)	47
5.2 Measured Experimental Test Results	47
5.2.1 Virgin Specimen (Test# 1)	47
5.2.2 In-Plane Cracked Specimens Loaded to Ultimate Out-of-Plane Strengths (Tests# 2b, 3b and 6b)	48
5.2.3 In-Plane Cracked Specimen Not Loaded to Ultimate Out-of-Plane Strength (Tests# 4b, 5b, 7b and 8b)	50
5.2.4 Repaired Specimen (Tests# 2c, 3c and 6c)	50

5.2.5	In–Plane Cracked Specimen with In–Plane Shear	50
5.3	Out–of–Plane Tests – Discussion of Observed Response	51
5.3.1	Effects of In–Plane Cracking	51
5.3.2	Effects of Deterioration in the Frame–Infill Boundary	51
5.3.3	Effects of Gravity Loads	52
5.3.4	Effects of Tensile Bond	52
5.3.5	Effects of Repair Method	52
5.4	Existing Analytical Model Predictions	53
5.5	Correlation with Dynamic Test of Half–Scale Model	55
5.6	Correlation with Existing Structures	57
5.7	Conclusions	59

CHAPTER 6

DESCRIPTION OF ANALYTICAL MODEL	61
6.1 Analytical Derivation	61
6.1.1 Parameters	62
6.1.2 Lateral Force Capacity	62
6.1.3 Axial Shortening of Extreme Fiber	63
6.1.4 Location of Thrust Centroid	64
6.1.5 Bearing Width at Support	64
6.1.6 Derivation of Angles	66
6.1.7 Lateral Deflection	66
6.2 Critical Slenderness Ratio (h/t)	66
6.3 Failure Modes	68
6.4 In–Plane Cracking Effects	70
6.5 Slenderness Ratio and Crushing Strain Effects	71
6.6 Correlation Between Analytical and Experimental Data	72
6.6.1 Correlation Between Experimental Data and Developed Arching Action Theory	73
6.6.2 Correlation of Arching Theory and McDowell Theory	74
6.7 Concluding Remarks	76

CHAPTER 7

SUGGESTED EVALUATION PROCEDURE	77
---	-----------

7.1	Effects of Masonry Strain and Stress	77
7.2	Effects of In–Plane Damage	78
7.3	Effects of Confining Frame Stiffness	80
7.4	Out–of–Plane Strength	81
7.5	Correlation With Experimental Results	82
7.6	Suggested Evaluation Procedure	83
7.7	Example	87
7.8	Summary and Conclusions	90

CHAPTER 8

SUMMARY AND CONCLUSIONS	91
8.1 Experimental Program Overview	91
8.2 In–Plane Tests	92
8.3 Out–of–Plane Tests	92
8.4 Development of a New Analytical Model and a Suggested Evaluation Procedure	93
8.5 Further Studies	93
8.6 Summary	94

APPENDIX A

DESCRIPTION OF TESTING EQUIPMENT	95
A.1 Loading Apparatus	95
A.1.1 In–Plane Test Set–Up	95
A.1.2 Out–of–Plane Test Set–Up	96
A.1.3 Gravity Loading	98
A.1.4 Base–Beam	99
A.2 Instrumentation and Data Acquisition	99
A.2.1 In–Plane Test	100
A.2.2 Out–of–Plane Test	102
A.2.3 Masonry Strain Distribution	103

APPENDIX B

CONSTRUCTION MATERIALS	105
-------------------------------------	------------

B.1	Frame Properties	105
B.1.1	Base Beam	105
B.1.2	Concrete	105
B.1.3	Steel	106
B.2	Masonry Unit	106
B.2.1	Brick Type (ASTM C-62, ASTM C-67)	106
B.2.2	Block Type (ASTM C-90)	107
B.3	Mortar (ASTM C-109)	107
B.4	Prism Test (ASTM E447-84)	107
B.5	Diagonal Tension Test (ASTM E519-81)	107
B.6	Quadlet Test	109
B.7	Test for Flexural Tensile Strength	109
B.7.1	Perpendicular to bed joint (ASTM E518-80)	109
B.7.2	Parallel to bed joint	110

APPENDIX C

NDE TESTING	113
C.1	Effect of Column Axial Compression and Infill Compression Stress . 113
C.2	Masonry Shear Strength

APPENDIX D

CRACK PATTERNS	118
-----------------------------	------------

APPENDIX E

IN-PLANE TEST RESULTS	124
E.1	Lateral Force vs. Shear Strain Relations
E.2	Frame Monitoring Instrumentation
E.3	Derivation of Frame Axial Loads and Resisting Moments
E.4	Test Results

APPENDIX F

OUT-OF-PLANE TEST RESULTS	164
--	------------

APPENDIX G

SENSITIVITY ANALYSIS FOR K1 AND K2	169
---	------------

APPENDIX H

THE MAXIMUM COMPRESSIVE STRESS FB AT THE SUPPORT	172
---	------------

APPENDIX I

NOTATION	174
-----------------------	------------

REFERENCES	177
-------------------------	------------

VITA	184
-------------------	------------

LIST OF TABLES

Table #		Page #
Table 1	Experimental Testing Sequence	3
Table 2	Research Projects on Infills in Progress in the United States	5
Table 3	Frame Properties	24
Table 4	Specimen Properties	32
Table 5	Specimen In-Plane Test Results	35
Table 6	Specimen In-Plane Stiffness	38
Table 7	Relative Predicted/Measured Specimen Stiffness	39
Table 8	Shear Modulus	41
Table 9	Specimen In-Plane Test Results	42
Table 10	Specimen Out-of-Plane Test Results	48
Table 11	Critical Slenderness Ratios	70
Table 12	Parameter Approximation	83
Table 13	Frame-Infill Specimen Properties	85
Table 14	Frame-Infill Properties	89
Table 15	Example-Parameter Approximation	89
Table 16	In-Plane Test Instrumentation	103
Table 17	Out-of-Plane Test Instrumentation	104
Table 18	Concrete Mix for Concrete Frame	111
Table 19	Concrete Properties for Frame	111
Table 20	Steel Properties for Frame	111
Table 21	Results for Prism Tests in Concrete Frame	112
Table 22	Shear Test Results	117
Table 23	Summary of In-Plane Data	124
Table 24	Summary of In-Plane Data	128
Table 25	Specimen Chronological Information	164

LIST OF FIGURES

Figure #	Page #
Fig. 1 General Overview of Data	7
Fig. 2 Range of Literature Survey for Specimens Loaded in the In–Plane Direction	8
Fig. 3 Relative Frame/Infill Shear Strength vs. Infill Shear Stress	9
Fig. 4 Drift at First Cracking vs. Infill Shear Stress	10
Fig. 5 Drift at Ultimate Load vs. Infill Shear Stress	10
Fig. 6 Range of Literature Survey for Specimens Loaded in the Out–of–Plane Direction	11
Fig. 7 Equivalent Strut Method	14
Fig. 8 Existing Analytical Model Predictions	16
Fig. 9 Effect of h/t on Lateral Strength	19
Fig. 10 Description of Clay Brick Specimen	21
Fig. 11 Description of Concrete Block Specimen	22
Fig. 12 Reinforcing Design for Reinforced Concrete Frame	23
Fig. 13 Relative Frame–Infill Strength for Brick and Block Infills	25
Fig. 14 P–M Interaction Diagram	26
Fig. 15 Collapse Mechanism for R/C Frames	27
Fig. 16 Repairing Method	28
Fig. 17 Elevation of Overall In–Plane Test Setup	29
Fig. 18 Displacement Histogram	30
Fig. 19 Elevation of Overall Out–of–Plane Test Setup	30
Fig. 20 Frame/Infill Crack Development	33
Fig. 21 Cracking of Reinforced Concrete Frame	34
Fig. 22 Load–Displacement Hysteresis	36

Fig. 23 Shear Stress vs. Lateral Drift	36
Fig. 24 Shear Stress vs. Lateral Drift	37
Fig. 25 Masonry Stiffness vs. Masonry Compressive Strength	37
Fig. 26 Measured/Predicted Specimen Stiffness	38
Fig. 27 Shear Strain Monitoring System	40
Fig. 28 Shear Stress— Shear Strain	41
Fig. 29 Shear Stress at Cracking vs. In—Place Shear Test Results	42
Fig. 30 Infill Crack Development	45
Fig. 31 Infill Stress Distribution (psi)	45
Fig. 32 Deflection Shape of Typical Infill During Out—of—Plane Test	46
Fig. 33 Specimen Test Results	49
Fig. 34 Equivalent Lateral Load	49
Fig. 35 Comparison of Various Theories with Experimental Results	53
Fig. 36 Effect of h/t on Lateral Strength	54
Fig. 37 Directions of Applied Motions	55
Fig. 38 Dynamic Out—of—Plane Test Results	56
Fig. 39 Static—Dynamic Out—of—Plane Test Results Comparison	57
Fig. 40 Testing Rig For Testing of Existing Structure	58
Fig. 41 Results for Full Scale Testing	58
Fig. 42 Idealized Loading and Behavior of Unit Strip of Infill Panel	61
Fig. 43 Masonry Deformed Shape	62
Fig. 44 Equilibrium of Strip Segment	63
Fig. 45 Deflected Shape of Half—Strip Segment	65
Fig. 46 Arching Action Vanishing	67
Fig. 47 Lateral Strength vs. Masonry Strain For Snap—Through	69

Fig. 48 Lateral Strength vs. Masonry Strain For Arching Mechanism	70
Fig. 49 In-Plane Damage Reduction Factor of the Panel vs. Slenderness Ratio	71
Fig. 50 Lateral Strength of Walls vs. Slenderness Ratio	71
Fig. 51 Lateral Strength of Walls vs. Slenderness Ratio	72
Fig. 52 Predicted Behavior	75
Fig. 53 Masonry Strain vs. Slenderness Ratio of the Panel	77
Fig. 54 Predicted Masonry Strain vs. Slenderness Ratio of the Panel	78
Fig. 55 In-Plane Damage Reduction Factor vs. the Slenderness Ratio of the panel	79
Fig. 56 Approximate In-Plane Damage Reduction Factor vs. the Slenderness Ratio of the panel	80
Fig. 57 Lateral Strength of Panels vs. Slenderness Ratio	82
Fig. 58 Physical Infill Cracking Damage	86
Fig. 59 Example Problem	88
Fig. 60 Elevation of Overall In-Plane Test Setup	95
Fig. 61 Air Bag Location	96
Fig. 62 Airbag Reaction Wall	97
Fig. 63 Air Bag Reaction System	97
Fig. 64 Elevation of Vertical Loading System (Top-Beam Column Joint) ..	98
Fig. 65 Elevation of Vertical Loading System (Column-Base Beam Joint)	99
Fig. 66 Detail For Base Beam	100
Fig. 67 Reinforcing Strain Gage Locations For Concrete Frame	101
Fig. 68 Location for LVDT's and Load Cells	102
Fig. 69 Out-of-Plane LVDT'S Location	103
Fig. 70 Masonry Strain Monitoring Setup	104
Fig. 71 Cylinder Test (ASTM C-39)	105

Fig. 122 Test 2A – West End Top LVDT Strain vs. Reinf Strain	132
Fig. 123 Test 2A – Lateral Force vs. East Column Axial Force	133
Fig. 124 Test 2A – Lateral Force vs. East Column Moment	133
Fig. 125 Test 2A – Lateral Force vs. West Column Axial Force	133
Fig. 126 Test 2A – Lateral Force vs. West Column Moment	133
Fig. 127 Test 3A – Lateral Force vs. Deflection	134
Fig. 128 Test 3A – Lateral Force vs. Drift	134
Fig. 129 Test 3A – Lateral Force vs. Shear Distortion	134
Fig. 130 Test 3A – Infill Shear Stress vs. Shear Distortion	134
Fig. 131 Test 3A – Lateral Force vs. East Column Base Rotation	135
Fig. 132 Test 3A – Lateral Force vs. West Column Base Rotation	135
Fig. 133 Test 3A – Lateral Force vs. Beam East End Rotation	135
Fig. 134 Test 3A – Lateral Force vs. Beam West End Rotation	135
Fig. 135 Test 3A – East Column East Base LVDT Strain vs. Reinf Strain ...	136
Fig. 136 Test 3A – East Column West Base LVDT Strain vs. Reinf Strain ...	136
Fig. 137 Test 3A – West Column East Base LVDT Strain vs. Reinf Strain ...	136
Fig. 138 Test 3A – West Column West Base LVDT Strain vs. Reinf Strain ..	136
Fig. 139 Test 3A – East End Beam Bottom LVDT Strain vs. Reinf Strain ...	137
Fig. 140 Test 3A – East End Beam Top LVDT Strain vs. Reinf Strain	137
Fig. 141 Test 3A – West End Beam Bottom LVDT Strain vs. Reinf Strain ..	137
Fig. 142 Test 3A – West End Top LVDT Strain vs. Reinf Strain	137
Fig. 143 Test 3A – Lateral Force vs. East Column Axial Force	138
Fig. 144 Test 3A – Lateral Force vs. East Column Moment	138
Fig. 145 Test 3A – Lateral Force vs. West Column Axial Force	138
Fig. 146 Test 3A – Lateral Force vs. West Column Moment	138

Fig. 147 Test 4A–Lateral Force vs. Deflection	139
Fig. 148 Test 4A–Lateral Force vs. Drift	139
Fig. 149 Test 4A– Lateral Force vs. Shear Distortion	139
Fig. 150 Test 4A–Infill Shear Stress vs. Shear Distortion	139
Fig. 151 Test 4A– Lateral Force vs. East Column Base Rotation	140
Fig. 152 Test 4A–Lateral Force vs. West Column Base Rotation	140
Fig. 153 Test 4A– Lateral Force vs. Beam East End Rotation	140
Fig. 154 Test 4A– Lateral Force vs. Beam West End Rotation	140
Fig. 155 Test 4A– East Column East Base LVDT Strain vs. Reinf Strain ...	141
Fig. 156 Test 4A– East Column West Base LVDT Strain vs. Reinf Strain ...	141
Fig. 157 Test 4A– West Column East Base LVDT Strain vs. Reinf Strain ...	141
Fig. 158 Test 4A– West Column West Base LVDT Strain vs. Reinf Strain ..	141
Fig. 159 Test 4A– East End Beam Bottom LVDT Strain vs. Reinf Strain ...	142
Fig. 160 Test 4A– East End Beam Top LVDT Strain vs. Reinf Strain	142
Fig. 161 Test 4A– West End Beam Bottom LVDT Strain vs. Reinf Strain ..	142
Fig. 162 Test 4A– West End Top LVDT Strain vs. Reinf Strain	142
Fig. 163 Test 4A– Lateral Force vs. East Column Axial Force	143
Fig. 164 Test 4A– Lateral Force vs. East Column Moment	143
Fig. 165 Test 4A– Lateral Force vs. West Column Axial Force	143
Fig. 166 Test 4A– Lateral Force vs. West Column Moment	143
Fig. 167 Test 5A–Lateral Force vs. Deflection	144
Fig. 168 Test 5A–Lateral Force vs. Drift	144
Fig. 169 Test 5A– Lateral Force vs. Shear Distortion	144
Fig. 170 Test 5A–Infill Shear Stress vs. Shear Distortion	144
Fig. 171 Test 5A– Lateral Force vs. East Column Base Rotation	145

Fig. 172 Test 5A—Lateral Force vs. West Column Base Rotation	145
Fig. 173 Test 5A— Lateral Force vs. Beam East End Rotation	145
Fig. 174 Test 5A— Lateral Force vs. Beam West End Rotation	145
Fig. 175 Test 5A— East Column East Base LVDT Strain vs. Reinf Strain ...	146
Fig. 176 Test 5A— East Column West Base LVDT Strain vs. Reinf Strain ...	146
Fig. 177 Test 5A— West Column East Base LVDT Strain vs. Reinf Strain ...	146
Fig. 178 Test 5A— West Column West Base LVDT Strain vs. Reinf Strain ..	146
Fig. 179 Test 5A— East End Beam Bottom LVDT Strain vs. Reinf Strain ...	147
Fig. 180 Test 5A— East End Beam Top LVDT Strain vs. Reinf Strain	147
Fig. 181 Test 5A— West End Beam Bottom LVDT Strain vs. Reinf Strain ..	147
Fig. 182 Test 5A— West End Top LVDT Strain vs. Reinf Strain	147
Fig. 183 Test 5A— Lateral Force vs. East Column Axial Force	148
Fig. 184 Test 5A— Lateral Force vs. East Column Moment	148
Fig. 185 Test 5A— Lateral Force vs. West Column Axial Force	148
Fig. 186 Test 5A— Lateral Force vs. West Column Moment	148
Fig. 187 Test 6A—Lateral Force vs. Deflection	149
Fig. 188 Test 6A—Lateral Force vs. Drift	149
Fig. 189 Test 6A— Lateral Force vs. Shear Distortion	149
Fig. 190 Test 6A—Infill Shear Stress vs. Shear Distortion	149
Fig. 191 Test 6A— Lateral Force vs. East Column Base Rotation	150
Fig. 192 Test 6A—Lateral Force vs. West Column Base Rotation	150
Fig. 193 Test 6A— Lateral Force vs. Beam East End Rotation	150
Fig. 194 Test 6A— Lateral Force vs. Beam West End Rotation	150
Fig. 195 Test 6A— East Column East Base LVDT Strain vs. Reinf Strain ...	151
Fig. 196 Test 6A— East Column West Base LVDT Strain vs. Reinf Strain ...	151

Fig. 197 Test 6A– West Column East Base LVDT Strain vs. Reinf Strain . . .	151
Fig. 198 Test 6A– West Column West Base LVDT Strain vs. Reinf Strain ..	151
Fig. 199 Test 6A– East End Beam Bottom LVDT Strain vs. Reinf Strain ...	152
Fig. 200 Test 6A– East End Beam Top LVDT Strain vs. Reinf Strain	152
Fig. 201 Test 6A– West End Beam Bottom LVDT Strain vs. Reinf Strain ..	152
Fig. 202 Test 6A– West End Top LVDT Strain vs. Reinf Strain	152
Fig. 203 Test 6A– Lateral Force vs. East Column Axial Force	153
Fig. 204 Test 6A– Lateral Force vs. East Column Moment	153
Fig. 205 Test 6A– Lateral Force vs. West Column Axial Force	153
Fig. 206 Test 6A– Lateral Force vs. West Column Moment	153
Fig. 207 Test 7A–Lateral Force vs. Deflection	154
Fig. 208 Test 7A–Lateral Force vs. Drift	154
Fig. 209 Test 7A– Lateral Force vs. Shear Distortion	154
Fig. 210 Test 7A–Infill Shear Stress vs. Shear Distortion	154
Fig. 211 Test 7A– Lateral Force vs. East Column Base Rotation	155
Fig. 212 Test 7A–Lateral Force vs. West Column Base Rotation	155
Fig. 213 Test 7A– Lateral Force vs. Beam East End Rotation	155
Fig. 214 Test 7A– Lateral Force vs. Beam West End Rotation	155
Fig. 215 Test 7A– East Column East Base LVDT Strain vs. Reinf Strain ...	156
Fig. 216 Test 7A– East Column West Base LVDT Strain vs. Reinf Strain ...	156
Fig. 217 Test 7A– West Column East Base LVDT Strain vs. Reinf Strain ...	156
Fig. 218 Test 7A– West Column West Base LVDT Strain vs. Reinf Strain ..	156
Fig. 219 Test 7A– East End Beam Bottom LVDT Strain vs. Reinf Strain ...	157
Fig. 220 Test 7A– East End Beam Top LVDT Strain vs. Reinf Strain	157
Fig. 221 Test 7A– West End Beam Bottom LVDT Strain vs. Reinf Strain ..	157

Fig. 222 Test 7A– West End Top LVDT Strain vs. Reinf Strain	157
Fig. 223 Test 7A– Lateral Force vs. East Column Axial Force	158
Fig. 224 Test 7A– Lateral Force vs. East Column Moment	158
Fig. 225 Test 7A– Lateral Force vs. West Column Axial Force	158
Fig. 226 Test 7A– Lateral Force vs. West Column Moment	158
Fig. 227 Test 8A–Lateral Force vs. Deflection	159
Fig. 228 Test 8A–Lateral Force vs. Drift	159
Fig. 229 Test 8A– Lateral Force vs. Shear Distortion	159
Fig. 230 Test 8A–Infill Shear Stress vs. Shear Distortion	159
Fig. 231 Test 8A– Lateral Force vs. East Column Base Rotation	160
Fig. 232 Test 8A–Lateral Force vs. West Column Base Rotation	160
Fig. 233 Test 8A– Lateral Force vs. Beam East End Rotation	160
Fig. 234 Test 8A– Lateral Force vs. Beam West End Rotation	160
Fig. 235 Test 8A– East Column East Base LVDT Strain vs. Reinf Strain ...	161
Fig. 236 Test 8A– East Column West Base LVDT Strain vs. Reinf Strain ...	161
Fig. 237 Test 8A– West Column East Base LVDT Strain vs. Reinf Strain ...	161
Fig. 238 Test 8A– West Column West Base LVDT Strain vs. Reinf Strain ..	161
Fig. 239 Test 8A– East End Beam Bottom LVDT Strain vs. Reinf Strain ...	162
Fig. 240 Test 8A– East End Beam Top LVDT Strain vs. Reinf Strain	162
Fig. 241 Test 8A– West End Beam Bottom LVDT Strain vs. Reinf Strain ..	162
Fig. 242 Test 8A– West End Top LVDT Strain vs. Reinf Strain	162
Fig. 243 Test 8A– Lateral Force vs. East Column Axial Force	163
Fig. 244 Test 8A– Lateral Force vs. East Column Moment	163
Fig. 245 Test 8A– Lateral Force vs. West Column Axial Force	163
Fig. 246 Test 8A– Lateral Force vs. West Column Moment	163

Fig. 247 Results for Test #1	165
Fig. 248 Results for Test #2b	165
Fig. 249 Results for Test #2c	165
Fig. 250 Results for Test #3b	165
Fig. 251 Results for Test #3c	166
Fig. 252 Results for Test #4b	166
Fig. 253 Results for Test #5b	166
Fig. 254 Results for Test #5d	166
Fig. 255 Results for Test #6b	167
Fig. 256 Results for Test #6b2	167
Fig. 257 Results for Test #6c	167
Fig. 258 Results for Test #6d	167
Fig. 259 Results for Test #7b	168
Fig. 260 Results for Test #8b	168
Fig. 261 Idealized Stress–Strain Relation in Compression	169
Fig. 262 Panel Strength Reduction vs. k_1	170
Fig. 263 Panel Strength Reduction vs. k_2	171
Fig. 264 Panel Strength Reduction vs. k_2	171
Fig. 265 Idealized Stress–Strain Relation in Compression Zone for Flexural Compressive Masonry Member	172
Fig. 266 Parameters for The Idealized Stress–Strain Relation	173

CHAPTER 1

INTRODUCTION

Masonry is one of the oldest types of construction materials currently in use around the globe. This material has been used for centuries, by various cultures, in typical constructions to satisfy the demands of economics, accessibility, aesthetics and functionality.

Masonry has many uses in the construction industry. Often it is used for infill walls in frame structures. In such cases, the masonry is not considered as a part of the lateral force resisting system. For this reason masonry infill panels are considered as simply an environmental divider that forms the envelope of a building.

Contrary to popular assumptions made in the design and analysis of frame structures, the presence of infills influences the behavior of structures during large ground motions. Structural interaction of the frame and the masonry infill walls cannot be predicted by simple means. If it is considered that the infill and the frame act as a whole, the lateral stiffness and the lateral load capacity largely increases. This being the case, the building may not have to be rehabilitated as would have to be done if the elements were to act separately. On the other hand, because of element interaction, and shifting of critical sections in the frame to weaker sections, the frame–infill system might become brittle and behave in an undesirable manner; therefore, it might be required to rehabilitate the system to make it behave in a ductile manner as assumed in design. In either case, the abundance of this type of structure in earthquake prone zones, makes it important to increase the knowledge on how masonry infills behave under repeated in–plane cyclic loadings. This enhances present earthquake hazard mitigation practice by improving existing techniques and creating new methods for the evaluation of existing buildings.

Masonry infills are stiff but brittle elements that often attract large lateral story shears when loaded parallel to their plane. Following moderate or strong earthquakes, it is common to observe an x pattern of cracks from each corner of an infill panel which is a result of large in–plane stiffness, but small in–plane diagonal tensile strength. The probability of occurrence for a second earthquake with equal intensity is small. However, it is probable that a lighter earthquake may occur and shake a cracked infill panel loose from its surrounding frame with inertial forces applied normal to its plane. The x pattern of cracks resulting from in–plane forces is similar to the crack pattern for a square panel subjected to out–of–plane forces. This implies that the out–of–plane strength may be related to the in–plane damage. The out–of–plane strength may be substantially weakened by in–plane cracking of the panels. Because of this, evaluation of out–of–plane strength for a cracked infill is often surmised to be quite small, and repair measures may be prescribed unnecessarily.

Past research on out–of–plane strength of unreinforced masonry infills has shown that arching effects may be dominant for panels that are restrained at their edges by relatively stiff frames, or for panels that have continuity with an adjacent infill. The ultimate limit state of an infill panel has

been found to be precipitated by the formation of fracture lines that form along the edges of four or more segments. As the segments rotate about their boundaries, arching action develops until crushing of the masonry along the segment edges occurs. This suggests that a yield-line analysis might be applicable even for a brittle material such as unreinforced masonry. Both of these previous findings suggest that an infill panel may possess significant transverse strength even though it is cracked. If an evaluation procedure can be developed based on arching action, then the conservatism associated with future strength assessments can be diminished.

This research examines losses in out-of-plane strength resulting from in-plane shear cracking for unreinforced masonry infills. A full-scale, single-story, single-bay reinforced concrete frame was constructed, and filled with clay brick or concrete block masonry. Test specimens were first subjected to in-plane lateral forces until the masonry infills cracked in shear. Then, the same panels were subjected to normal pressures using an air bag. Finally, repair techniques to enhance the out-of-plane performance of various cracked infills were developed and tested. Estimates of transverse strength and behavior were determined using a variety of analytical models in an effort to propose a suitable formulation for cracked infills. This report summarizes the experimental research done, and presents correlations between measured and calculated behavior. In addition, an analytical model based on arching action was developed to estimate the out-of-plane strength of uncracked, cracked and repaired infill panels. Finally, an evaluation method to predict the out-of-plane strength of the panels based on the analytical model was developed.

1.1 Objective and Scope

The overall goal of this research was to increase the knowledge and the understanding of how masonry infills behave under strong seismic motions, and how the infill-frame system interacts during an earthquake. The most important objective was to assess the out-of-plane capacity of infill panels previously cracked with in-plane loads, and to postulate a repair technique to increase the corresponding strength.

The scope of the research entailed: 1) design and construction of testing specimens, 2) experimental testing of specimens in the in-plane and out-of-plane directions, 3) analysis of in-plane and out-of-plane results, 4) development of an analytical model to predict the out-of-plane strength of panels, and 5) development of a suggested evaluation procedure for masonry infill panels.

The experimental program consisted of several full-scale tests. Specimens consisted of a one-story, single-bay reinforced concrete frame with different brick and concrete block masonry infills. A reinforced concrete frame was built and tested with different widths of brick and concrete block infills to consider different relative frame/infill strengths and different h/t ratios for infills. The sequence followed for testing is as shown in Table 1.

The specimens were loaded in-plane, up to twice the cracking drift. The loading levels required became apparent as the results of the experiment were available. This was done with the

Table 1 Experimental Testing Sequence

Test Number	Infill Type	Infill h/t	Mortar Type	In-Plane Test	Out-of-Plane Test		
					Unrepaired	Repaired	Combined*
1	brick	34	S		○		
2a	brick	34	N	○			
2b					○		
2c						○	
3a	brick	34	lime	○			
3b					○		
3c						○	
4a	block	18	N	○			
4b					○		
5a	block	11	N	○			
5b					○		
5d							○
6a	brick	17	lime	○			
6b					○		
6c						○	
6d							○
7a	brick	17	N	○			
7b					○		
8a	brick	9	lime	○			
8b					○		

* Out-of-plane test done with in-plane forces

purpose of keeping a constant relative value of how much in-plane damage was “severe”. The specimens were then tested out-of-plane by applying a monotonically increasing uniform load across the surface of the infill with an airbag. Some of these specimens were then repaired in order to increase the infill resistance to out-of-plane failure.

Results from the in-plane and out-of-plane tests are presented. Experimental information is given on panel damage and corresponding crack patterns, and their relation to the in-plane lateral behavior and the out-of-plane strength of the panels. In addition, measurements were analyzed to show tendencies between each of the specimens. Experimental static results were compared to predictions calculated from existing analytical models, and to dynamic results obtained from similar specimens tested on a Biaxial Shock Testing Machine (BSTM).

An analytical model is presented for determining the transverse uniform pressure that cracked, uncracked, or repaired masonry infill panels can resist. The model was based on arching action for a strip of infill that spans between two fully restrained supports. Expressions evaluating the out-of-plane strength of panels were developed. The analytical model was modified to account for existing in-plane damage and the corresponding effects on the out-of-plane strength of the panel.

Based on the developed analytical model, and on the experimental results, a suggested evaluation procedure is proposed. The suggested evaluation procedure is a way to determine the out-of-plane strength of panels based on geometrical and mechanical properties. In addition, the evaluation procedure considers the extent of existing damage in the panel, and the effects of the flexibility of the confining frame. A series of tables and figures are presented to aid in the evaluation process.

1.2 Relevant Present Research

The National Science Foundation (NSF) presently sponsors a coordinated program entitled "Repair and Rehabilitation Research for Seismic Resistance of Structures". The research done at the University of Illinois is part of this coordinated program. In addition to this coordinated program, NSF, NCEER, U.S. Department of Defense and the U.S. Department of Energy are currently sponsoring a number of parallel research projects on infill behavior. The name and the corresponding research areas of the institutions where the infill behavior research projects are underway are presented in Table 2. Parameters of interest in these studies include: type of frames, type of infills, scale factors, and testing mode. Research done at some of the institutions listed in Table 2 include the development of repair methods.

Specimen configuration and testing methods used in the research projects varied to cover a wide range of parameters. Specimens tested at the University of Illinois consisted of a reinforced concrete frame with both clay brick and concrete block infills. Similar but half-scale specimens were tested at USACERL (United States Army Civil Engineering Research Laboratories) dynamically using a shaking table. Correlation between results obtained from the University of Illinois and USACERL showed effects relating static and dynamic testing. Testing laboratory specimens were also compared to results obtained by James A. Hill & Associates from panels in buildings scheduled to be demolished. Martin-Marietta Corporation focused on the testing of hollow clay tile infills encased within a steel frame and the interaction between out-of-plane cracking and effects on in-plane strength reduction. Cornell University in conjunction with the State University of New York (SUNY) undertook the analytical modeling of infills as the main objective for research to predict their corresponding experimental results.

1.3 Uniqueness of Study

This research was unique in that full scale tests were done on the interaction of in-plane and out-of-plane loading. Development of analytical models for out-of-plane strength of panels damaged with in-plane forces had not been addressed in previous research. After reviewing previous

Table 2 Research Projects on Infills in Progress in the United

Name of institution	States	Frame Type	Infill Type	In-Plane Test		Out-of-Plane Test	
				Static	Dynamic	Static	Dynamic
University of Illinois Urbana, IL	Concrete	Brick		○		○	
		Block		○		○	
University of Arizona Tucson, AZ	Steel	Brick		○		○	
ANA & University of Colorado Boulder, CO	Concrete 1/2 scale	Block		○		○	
James A. Hill & Assoc. Long Beach, CA	Concrete	Brick	Out-of-Plane Test Of Actual Buildings			○	
SUNY Buffalo, NY	Steel	Brick		○			○
Cornell University Ithaca, NY	Steel 1/4 scale	Block		○			
Martin-Marietta Corp. Oak Ridge, TN	Steel	**HCT		○		○	
Martin-Marietta Corp. Oak Ridge, TN	Steel	**HCT			○		○
USACERL Champaign, IL	Concrete 1/2 scale	Brick			○		○
Rice University Houston, TX	Concrete	Brick		○			
Nabih Yousseff & Ass. Los Angeles, CA	Concrete Steel	Brick		○	In-Plane Evaluation Of Actual Buildings		

** Hollow Clay Tile

analytical models, a more accurate method of determining the strength of both undamaged and damaged infill-frame structural systems resulted. Results from this study allowed better evaluation of the structural behavior of existing masonry infill-frame structures under earthquake loadings, and also aided in the determination of repair techniques for these types of structures when damaged by earthquakes.

1.4 Outline

The layout of this report has been arranged to include the most important information in the first part of the text followed by all the supporting information and test results presented in the appendices. A literature review has been performed on the experimental work previously done on masonry infill panels and results are presented in Chapter 2, along with a description of the existing analytical models used to analyze the out-of-plane behavior and strength of masonry infill panels. A detailed description of features of the experimental program are presented in Chapter 3. Experimental results and discussion of the observed response for the in-plane tests are presented in Chapter 4 and for the out-of-plane tests in Chapter 5. Development of an analytical model to predict the out-of-plane strength of the panel is presented in Chapter 6. Chapter 7 describes a suggested evaluation procedure for the out-of-plane strength of the panels, and Chapter 8 provides a summary of the experimental program, principal conclusions, and a selection of further studies to be made.

CHAPTER 2

LITERATURE REVIEW

The chapter is divided into two parts: previous experimental research, and existing analytical models.

2.1 Previous Experimental Research

Studies on the behavior and strength of masonry infills, for both in-plane and out-of-plane forces have been of interest to researchers and engineers for over four decades. This section summarizes previous experimental research on masonry infills in order to understand the type of work that has already been completed, and to visualize the gaps or locations where more experimental data is required. The section is separated into two sections according to loading direction: in-plane and out-of-plane.

2.1.1 Specimens Subjected to In-Plane Forces

Experimental evaluation of the behavior of masonry infills loaded within their plane is extensive. Several parameters, including the number of bays and the number of stories in the test specimen, are addressed in previous programs. A summary of test specimens found in the literature is presented in Fig. 1 with respect to the number of bays and stories. Test specimens represent various

		Number of Bays		
		1	2	3
Number of Stories	1	72	0	0
	2	1	0	4
	3	9	0	1
	4	0	0	0
	5	10	0	0
	6	0	0	0
	7	1	0	0

Fig. 1 General Overview of Data

construction configurations from low and wide systems to tall and slender multi-story specimens. The most commonly used specimen consisted of a single-bay, single-story specimen. These studies provided evaluations of the importance of infill confinement from adjacent infills, the types of failure that can be observed in an inner or outer frame or infill, the effects of the system rigidity on strength,

and failure mechanisms for the specimen. Basic limitations of these studies consisted in the scale of the specimens (smaller than full scale) and the capacities of the testing equipment.

Important parameters studied for the evaluation of masonry infills included the type of confining frame, the type of masonry unit used for the infill, and the relative frame/infill strength. A summary of the parameters studied is presented in Fig. 2. Two frequent types of confinement frames

		Number of Specimens
Frame type	Steel	22
	Concrete	76
Infill type	Clay Brick	23
	Concrete Block	75
Failure type	Diagonal Cracking of Infill	50
	Crushing of Masonry along Diagonal	6
	Column Shear	25
	Column Hinging	17
Scale	1/8 to Full	

Fig. 2 Range of Literature Survey for Specimens Loaded in the In-Plane Direction

used for masonry infill testing are structural steel or reinforced concrete. The two common types of masonry infills are clay brick or concrete block, with a few others using hollow clay tile (HCT). Infill behavior and mode of failure are largely controlled by the strength and flexibility of the confining frame and the interaction with the masonry infill. For strong and stiff frames coupled with weak infills, the behavior of the system is controlled by the frame. For this case the infill deforms and cracks as it adapts to the deformed shape of the frame. For weak and brittle frames coupled with strong infills, the behavior of the system is controlled by the infill and the type of failure may be brittle. As the infill tries to deform, it typically cracks in an X-type crack pattern under the applied cyclic lateral loading. Once cracking occurs, the columns may fail in a brittle fashion from the continuing propagation of the infill cracks through the columns critical sections. Possible types of failure encountered for these types of specimens are summarized in Fig. 2.

The type of behavior that is observed in frame–infill specimens varies according to the interaction of the frame and the infill as previously mentioned. The relative frame/infill shear strength

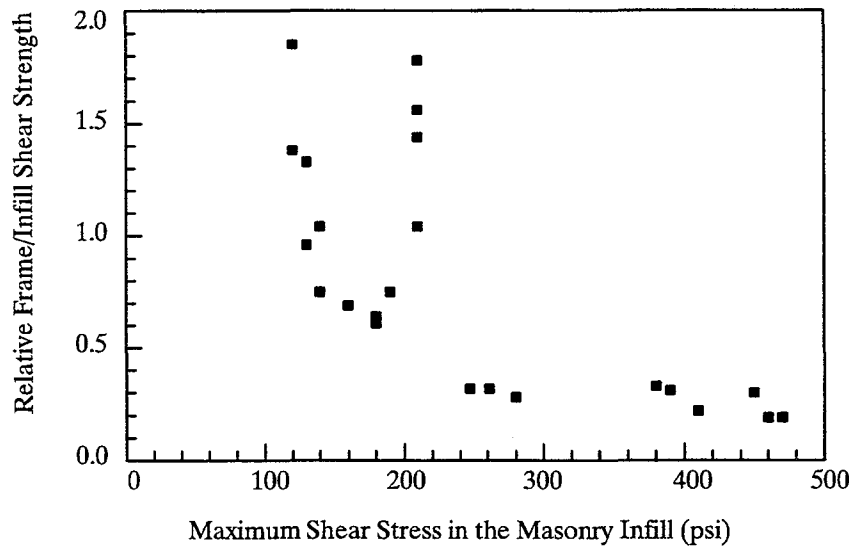


Fig. 3 Relative Frame/Infill Shear Strength vs. Infill Shear Stress

vs. the observed maximum shear stress in the masonry infill is shown in Fig. 3. The frame strength was calculated based on the steel and concrete components resisting shear forces. The infill shear strength was estimated as the masonry shear strength multiplied by the shear area of the panel that resists shear. The maximum shear stress in the masonry was estimated from test results and from mechanical and physical properties of the specimens. For a typical infill size with masonry shear strength values ranging from 100psi to 200psi, the relative frame/infill shear strength reached values as high as 2.0. For the same type of infills with moderate to high shear strength values, the infill strength becomes relatively large with the relative frame/infill shear strength ratio near 0.25.

The lateral drift observed at first cracking of the infill versus the shear stress in the masonry is illustrated in Fig. 4. The lateral drift observed at ultimate load of the frame–infill specimen versus the shear stress in the masonry is illustrated in Fig. 5. Lateral drifts at initial cracking for infills with moderate shear stresses (100 to 200 psi) were as large as 1.5%. Drifts at peak load were as large as 3%. These large lateral drifts were obtained for specimens where the frame–infill relative strength ranged from 0.5 to 2.0. The ductile behavior of these specimens under the applied lateral loads was due to the strong ductile frame that was used. Frame/infill specimens with relative strengths up to 0.5 reached lateral drifts of 0.5% at first cracking of the infill, and up to 1.0% at ultimate. The behavior of these specimens was primarily controlled by the infill strength.

2.1.2 Specimens Subjected to Out–of–Plane Forces

Previous research done on the out–of–plane behavior of masonry infills is not as extensive as the amount of research done for the in–plane direction. A summary of the most important parameters studied is presented in Fig. 6.

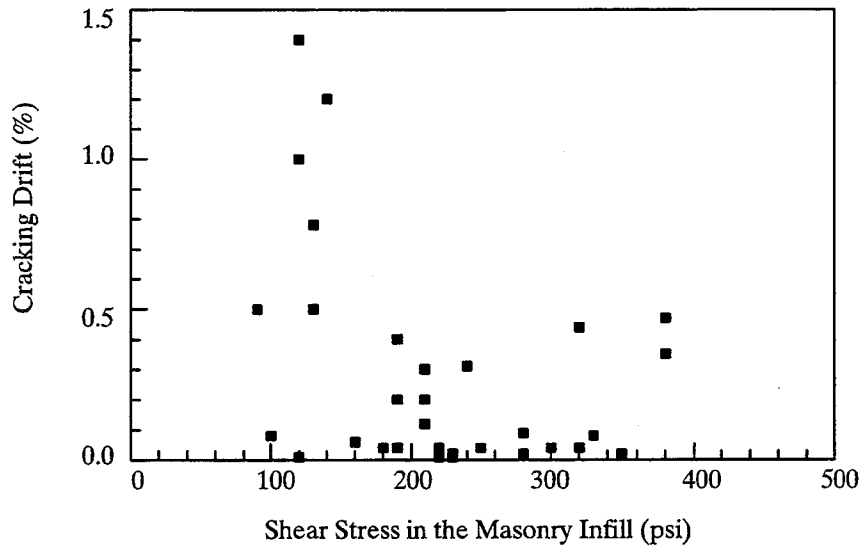


Fig. 4 Drift at First Cracking vs. Infill Shear Stress

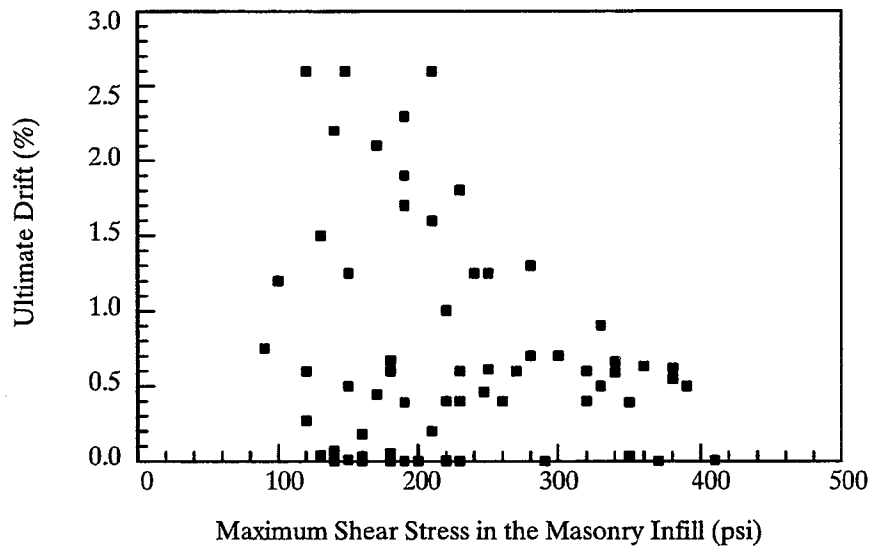


Fig. 5 Drift at Ultimate Load vs. Infill Shear Stress

The most common specimen layout for evaluation of the behavioral response of infills when loaded by uniform loads in the out-of-plane direction consists of a single-bay, single-story frame, with a single-wythe masonry infill.

Out-of-plane testing of masonry infills has been performed in a series of different ways. In 1958, Monk [55] tested a series of infills by building them in an octagon shaped test fixture and detonating a high explosive at the center. The magnitude of the blast was adjusted to reproduce approximately the effects of the atomic blast experienced in Operation "Cue" at the 5 psi overpressure level. This type of testing was done for the assessment of damage expected in an atomic blast. For this

Frame type	<div> <div></div> <div>Steel</div> <div>Concrete</div> </div>
Frame Stiffness	<div> <div></div> <div>Flexible</div> <div>Rigid</div> </div>
Infill type	<div> <div></div> <div>Clay Brick</div> <div>Concrete Block</div> <div>Hollow Clay Tile</div> </div>
Boundary Condition	<div> <div></div> <div>Free</div> <div>Simply Support</div> <div>Fixed Support</div> </div>
Scale	1/2 to Full

Fig. 6 Range of Literature Survey for Specimens Loaded in the Out-of-Plane Direction

test, it was determined that the time–pressure effects of the high explosive could be approximately equated to the impulse resulting from an atomic explosion. Following this, Gabrielsen [33] then tested several full–scale masonry walls statically and dynamically. In addition, an extensive dynamic testing program involving full–scale walls was done for the Defense Civil Preparedness Agency and the Veterans Administration. For these tests, a shock tunnel was used which enabled full–scale walls to be subjected to air blast loadings over one entire face. These types of testing methods are not as commonly used when compared to the following types of testing methods.

A new method for dynamic testing of infill specimens is done using shake tables. Shake tables are able to represent and simulate the behavior of a structure when subjected to a specified recorded earthquake. Currently, research using half scale infill specimens is being done at the United States Army Civil Engineering Research Laboratories (USACERL). These specimens consist of a set of reinforced concrete frames with a series of clay masonry infills that are subjected to the 1940 El Centro earthquake, NS Component.

Static testing simulating dynamic inertial loads on structures has also been done. Panels have been loaded with concentrated loads. Presently, a research project headed by James A. Hill [42] is under way for testing of several infill specimens on actual buildings. These test specimens are loaded by a pair of hydraulic actuators that apply concentrated loads to the central part of the infill following a specified load or displacement sequence.

One other method consists of applying a uniform lateral load to the specimens with an air bag that covers the entire specimen surface area. This system has been used by many researchers including Drysdale [24] for his tests on full-scaled concrete block walls, and Dawe [22] for his tests on full-scaled concrete masonry infills.

Masonry infills are confined within frames that are an integral part of large steel or reinforced concrete structures. Researchers have used the frame strengths, frame sizes and materials used to build the test frames, as variables to understand their effect on the behavior of the infills. Monk [55] used large reinforced concrete frames to represent rigid supports for the infill, as was also done by Gabrielsen [33]. Those studies evaluated the behavior of the infill with no concern for the frame. Others, including Drysdale [24] and Dawe [22] used steel frames to observe the effect of the frame flexibility on the infill. The flexibility of these frames complicates the understanding of the observed behavior of the infill, and the development of a realistic and accurate analytical model to predict its behavior. A detailed description of the procedure used to account for the frame flexibility is presented by Dawe [22].

For former out-of-plane tests, masonry infills were built with different types of masonry units as illustrated in Fig. 6. The masonry units varied in physical properties (unit size, size and number of openings), as well as in mechanical properties (initial rate of absorption, compressive strength, modulus of elasticity). Different frame dimensions and different infill thicknesses were used for these specimens. Two non-dimensional parameters were used to illustrate the range of main physical properties of the tested infills: the aspect ratio of the frame (l/h), and the slenderness ratio of the infill (h/t). The aspect ratio of the frames ranged from 1 to 3, while the slenderness ratio ranged from 8 to 31 for concrete masonry units and 8 to 24 for clay brick units.

2.1.3 Out-of-Plane Behavior of Repaired Infills

Structures damaged by earthquakes are not always safe and often require extensive repairs. Existing structures may require rehabilitation in order to meet earthquake standards that are periodically upgraded. Research on rehabilitation and repair methods for masonry infills is a topic of interest in many countries; therefore, investigations are being made in several parts of the world. Zarnic [88, 89, 90] and a number of Slovenian investigators [17, 63, 69, 91] have researched different methods and have invested great effort into the pressure injection of cement grout to walls and infills as well as attaching steel tie-bars in the diagonal direction. An alternative method tried in Slovenia is a reinforced light-weight foam-concrete topping, connected to the surrounding wall by steel anchors.

2.1.4 Summary

In-plane and out-of-plane behavior of test specimens has been studied within the realm of uni-directional loading with no concern for the interaction between the two loading directions. Biaxial testing is an area of research that has not been addressed and should be extended to cover: reduction of out-of-plane strength for a certain in-plane damage, reduction in the in-plane

stiffness after cracking in the out-of-plane direction, and the effect of openings with both in-plane and out-of-plane loading combinations. Based on these effects, effective rehabilitation and repairing techniques must be developed.

Henderson [39] is presently examining the deterioration in in-plane strength due to pre-existing out-of-plane damage for hollow clay tile infills. Although this is a new problem that has not been extensively addressed, the in-plane strength of infills does not deteriorate greatly even after cracking in the masonry. However, the amount of deterioration in the out-of-plane strength given a known amount of in-plane damage may become significant. Also, research on the effect of deterioration along the frame/infill boundaries due to in-plane cyclic motion of the specimen and the reduction in the mechanical properties of cracked masonry on the out-of-plane strength of infills has never been evaluated. Therefore, the present research on the out-of-plane behavior of infills as affected by their in-plane damage is a unique extension of current work that should allow better prediction of masonry behavior for combined loading directions.

2.2 Existing Analytical Models

2.2.1 In-Plane Direction

In-plane stiffness and strength predictions of masonry infill panels can be evaluated using a number of different analytical procedures: shear beam method, finite element models and the most commonly used equivalent strut methods.

Whitney, Anderson and Cohen [84] proposed a simple, approximate method for calculation of stiffness and strength of infilled frames, using results from investigations done at MIT. This proposed method was later modified by Benjamin and Williams [16] after completing a series of tests of different sizes and types of frames with infills.

Modelling the frame-infill specimen as a shear beam is one simple approach to estimate the lateral stiffness. Lateral load causes lateral deflection due to shear and flexural deformations.

$$\delta_{total} = \delta_{shear} + \delta_{flexure} \quad \text{Eq. [1]}$$

$$\delta_{total} = \left(\frac{PL}{A'G} \right) + \left(\frac{PL^3}{12EI} \right) \quad \text{Eq. [2]}$$

Although this method is simple, the estimated predictions largely over estimate the stiffness of the specimen at cracking of the panel (Eq. [3]).

$$K = \frac{1}{\left(\frac{L}{A'G} + \frac{L^3}{12EI} \right)} \quad \text{Eq. [3]}$$

where:

L = height of the specimen

A' = shear area of the specimen

I = moment of inertia of the specimen

E = modulus of elasticity.

Storm [76] used finite elements to represent bricks in the panel, but did not represent the mortar joints or the boundary between frame and infill. Finite elements were also used by Franklin

[32] who modeled masonry with brittle type material elements larger in dimension than bricks. Page [58] focused on modeling each brick with an element, and the mortar with joint elements. Linear analysis can only be used to analyze infill panels prior to initial major cracking. The effectiveness of linear analysis is limited since the infilled frame still provides stiffness after cracking in the panel occurs. Considering material non-linearity and the whole range of behavior of infill frames, requires nonlinear finite element analysis as proposed by Mehrabi [54].

Replacing the infill panel with an equivalent strut permits a simplified static analysis of an equivalent frame. The equivalent strut concept, the first practical attempt to predict infilled frame behavior by theory, was proposed by Polyakov in 1960 and then by Holmes [44, 45] and Stafford Smith [74, 75] later in the sixties. Since then, others have published methods for determining the equivalent infill panel strut width, and consequently its lateral stiffness.

Holmes [44, 45] considered steel frames with non-structural concrete or clay brick infill panels. The first model considered a single frame-infill specimen subjected to a horizontal force P . Force P produces a compressive resultant and a vertical force in the infill as illustrated in Fig. 7. By

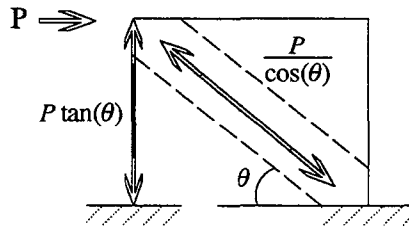


Fig. 7 Equivalent Strut Method

considering the forces in the frame and infill panel separately, the horizontal force causing failure may be determined by evaluating the shortening on the equivalent strut. An expression proposed to evaluate the horizontal stiffness of the specimen is presented in Eq. [4].

$$K = \left[\frac{24E_c I_c}{h'^3 \left[1 + \frac{I_c}{I_b} \cot \theta \right]} + \frac{t f_m}{3 \epsilon_{cr}} \right] \quad \text{Eq. [4]}$$

where:

- E_c = elastic modulus of frame
- I_c = moment of inertia of the columns
- I_b = moment of inertia of the beam
- h' = height of frame
- θ = angle between diagonal and horizontal
- t = thickness of the panel
- f_m = masonry compressive strength
- ϵ_{cr} = masonry crushing strain.

This method could be applied to both concrete block and clay brick masonry infill panels. This

expression in its original form was to be used for single-bay, single story frames, but it may be modified to account for additional stories or bays. Eq. [4] suggests that the in-plane stiffness depends primarily on the relative geometry of the frame and the infill along with the mechanical properties of both the masonry panel and of the frame. The compressive area of the equivalent strut was determined to be dependent primarily on the thickness and the aspect ratio of the panel. The specimen behavior prediction assumes an idealized linear relationship for the force-deflection up to crushing of the masonry at which point failure of the system occurs.

Stiffness predicted by the Stafford Smith method [74, 75] is affected not only by the size, thickness, proportions, and material properties, but also by the length and distribution of the applied load on the corner. The equivalent strut method developed by Stafford Smith combined the effects of the strain energies of the tension in the windward column, A , the compression in the equivalent strut, B , and the bending of the frame, C . The expression proposed to evaluate the in-plane stiffness is presented in Eq. [5], with expressions for the corresponding terms presented in Eq. [6] to Eq. [8]:

$$K = \frac{A + B + C}{C(A + B)} \quad \text{Eq. [5]}$$

$$A = \frac{h' \tan 2\theta}{A_c E_c} \quad \text{Eq. [6]}$$

$$B = \frac{d}{wt E_m (\cos 2\theta)} \quad \text{Eq. [7]}$$

$$C = \frac{h_3(3I_b h' + I_c L')}{12E_c I_c (6I_b h' + I_c L')} \quad \text{Eq. [8]}$$

where:

- E_c = elastic modulus of frame
- E_m = elastic modulus of masonry
- I_c = moment of inertia of the columns
- I_b = moment of inertia of the beam
- A_c = area of the columns
- L' = length of beam
- h' = height of frame
- d = diagonal length of infill panel
- w = width of equivalent strut ($0.2 d$ for $L/h = 1.5$)
- θ = angle between diagonal and horizontal
- t = thickness of the panel.

The effect of the stiffnesses of the frame members in flexure compared to that of the infill panel in compression was considered in later studies by Stafford Smith. Results from these studies concluded that the stiffer the frame compared to the infill panel, the greater the contact length, and consequently the stiffer the infilled frame.

2.2.2 Out-of-Plane Direction

In this section, a summary and discussion of analytical models developed by others to predict the out-of-plane behavior and strength of infill panels is presented. A number of different methods are used to estimate the out-of-plane forces and deflections of the test panels of this study for comparison. Predictions by existing analytical models and experimental results are presented and discussed in detail in Chapter 5. Numerical models vary from simple elastic plate analyses to more refined models based on arching action and inelastic behavior. For each model, an expression for the transverse load capacity is computed as a function of the h/t ratio of an infill panel.

2.2.2.1 Elastic and Inelastic Plate Theories

The simplest model to represent two-way bending of an infill is an elastic plate. Classical solutions derived by Timoshenko [79] are available for determining deflections of rectangular plates subjected to uniform pressures. Linearly elastic, isotropic, homogeneous material behavior is assumed in this theory. An expression for the pressure, q_a , for a given tensile stress, f_t , is given in Eq. [9]. The term β_1 represents the aspect ratio of a panel, and is equal to 0.498 for the test panel

$$q_a = \frac{f_t}{6\beta_1\left(\frac{h}{t}\right)^2} \quad \text{Eq. [9]}$$

$$q_a = 0.335 \frac{f_t}{\left(\frac{h}{t}\right)^2} \quad \text{Eq. [10]}$$

(assuming pinned edges). Eq. [10] is based on this coefficient. Since the analysis is elastic, no post-cracking behavior is considered. The solution does not model the flexibility of a cracked infill, and is overly stiff when compared with other models as illustrated in Fig. 8. Failure is assumed to occur

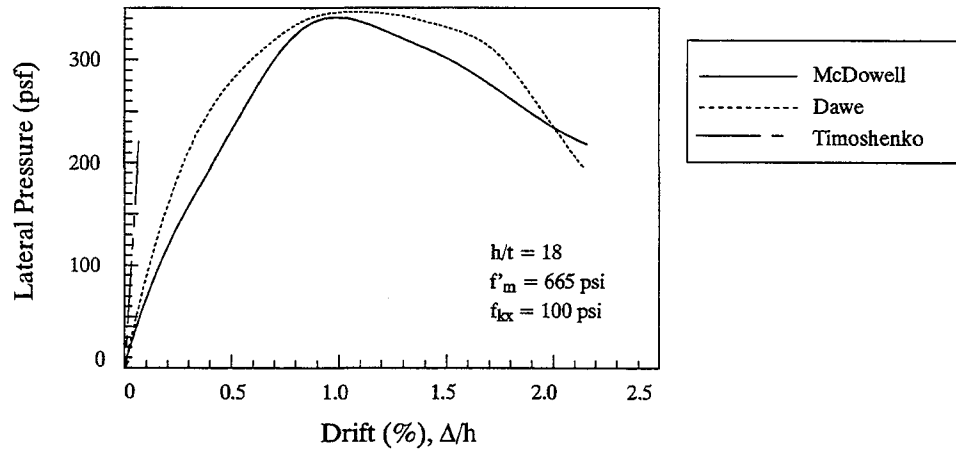


Fig. 8 Existing Analytical Model Predictions

once the maximum tensile stress reaches the tensile strength of the masonry.

Inelastic two-way action has been modeled through the use of modified yield-line analyses by Drysdale [24], Haseltine [36, 37], and Hendry [40, 41]. Strength and behavior of unrestrained, rectangular unreinforced masonry wall panels can be calculated with this type of model. Haseltine

[36, 37] developed a design methodology and formulated the following equation for the out-of-plane bending strength, q_a , of a rectangular panel.

$$q_a = \frac{f_{kx}}{6\alpha\left(\frac{h}{t}\right)^2 \gamma_m \gamma_f} \quad \text{Eq. [11]}$$

$$q_a = 0.420 \frac{f_{kx}}{\left(\frac{h}{t}\right)^2} \quad \text{Eq. [12]}$$

The term, f_{kx} is the flexural tensile strength normal to the bed joints; α is a bending moment coefficient based on the panel aspect ratio and the edge boundary condition (0.081 for test panels with pinned edges); γ_m and γ_f are factors of safety included in the expression to obtain a conservative expression for the allowable strength of the panel. γ_m is a factor ranging from 2.5 to 3.5 based on quality control of materials; and γ_f is a panel importance factor ranging from 1.1 to 1.4. As with the Timoshenko approach, Eq. [11] limits strength to a critical flexural tension stress, and is thus conservative for panels whose strength may be appreciable in the post-cracking range. If the largest values for γ_m and γ_f are considered, the coefficient term becomes 0.420 as noted in Eq. [12]. This is close to the strength given by Eq. [10] and is therefore not represented on Fig. 8. The difference in the coefficient term is attributed to the consideration of a different flexural tensile strength of the masonry vertical to the joint (f_{kx}), and parallel to the joint (f_{ky}). The ratio f_{kx}/f_{ky} is approximately 3 according to experimental data. If the γ_m and γ_f factors are taken to be 1.0 to exclude the factors of safety, Eq. [11] reduces to Eq. [13].

$$q_u = \frac{2 f_{kx}}{\left(\frac{h}{t}\right)^2} \quad \text{Eq. [13]}$$

Hendry [40, 41] considered that the most useful and informative approach would be to calculate coefficients which give the effective bending moment on a strip of panel of unit width. Following this criteria, expressions for simply supported panels with and without precompression, Eq. [14] and Eq. [15] respectively, were developed in a similar format.

$$q_u = 8 \frac{\sigma_c}{\left(\frac{h}{t}\right)^2} \quad \text{Eq. [14]}$$

$$q_u = \frac{f_{kx}}{6\alpha\left(\frac{h}{t}\right)^2} \quad \text{Eq. [15]}$$

The term, σ_c is the precompression stress applied to the panel; f_{kx} is the flexural tensile strength normal to the bed joints; a ratio f_{kx}/f_{ky} of 5; α is a bending moment coefficient based on the panel aspect ratio and the edge boundary condition designed to fit the experimental data (0.025 for test panels with pinned edges). If the corresponding value for α is considered for the expression evaluating panels with no precompression, the new expression becomes Eq. [16].

The out-of-plane strength of a masonry panel can be evaluated based on Eq. [13] and Eq. [16], and limited by f_{kx} . The difference between the coefficient terms in these two mentioned

$$q_u = 6.67 \frac{f_{kx}}{\left(\frac{h}{t}\right)^2} \quad \text{Eq. [16]}$$

equations is attributed to the use of a different bending moment coefficient which in turn depends on the corresponding estimated f_{kx}/f_{ky} ratio. This type of analysis produces out-of-plane strength results an order of magnitude larger than results obtained using Timoshenko elastic plate theory.

2.2.2.2 Arching Action

McDowell, McKee and Sevin [50, 51] at the Armour Research Foundation (ARF) developed a theory based on arching action for a one-way strip of unreinforced masonry confined by rigid boundaries. Their theory showed that masonry walls with full end restraint could withstand much larger lateral loads than predicted by means of conventional elastic or elasto-plastic bending analyses. A paper published in 1959 by the second two authors [52] applied the ARF theory to a design method for blast. Unlike the previous formulations which are limited by flexural tension, panel strength per McDowell is limited by compressive stress. A strip is comprised of two equal segments that rotate about their ends until masonry crushes, or the two segments snap through. Ultimate capacity can be deduced from McDowell's formulation to be equal to that given in Eq. [17],

$$q_u = \frac{\gamma f'_m}{2\left(\frac{h}{t}\right)^2} \quad \text{Eq. [17]} \quad q_u = 0.504 \frac{f'_m}{\left(\frac{h}{t}\right)^2} \quad \text{Eq. [18]}$$

where γ is a variable that depends on the lateral deflection, thickness of element, and h/t ratio; and f'_m is the prism compressive strength. If an h/t ratio of 10 is assumed, the coefficient term becomes 0.504 as given in Eq. [18] which is in the range of that for Eq. [10] and Eq. [12]. However, lateral strength is a function of compressive strength, f'_m , rather than tensile strength, f_t or f_{kx} which is an order of magnitude larger.

Based on the ARF theory, Monk [55] developed procedures for blast design as part of a study of blast resistance by the Structural Clay Products Research Foundation. The theory was used with data from dynamic tests done at Coal City, Illinois. The tests revealed that effective designs in unreinforced clay masonry infills could be achieved if arching effects were considered. Thomas [78] demonstrated that arching could result in a considerable strength increase after initial cracking for clay brick infills. West et. al. [82] stated that the interface conditions between an infill and a frame are significant to transverse strength. Anderson [12, 13] proposed a more involved theory for one-way wall panels subjected to transverse loads that included the effects of boundary stiffness, initial gaps and infill shrinkage on the out-of-plane strength calculations.

Apart from arching action, one other perplexing concern when estimating transverse strength of unreinforced infills is how to model two-way action. Lefter [49] and Dawe [22] developed strength theories based on virtual work concepts and include both arching and two-way action. Both theories

consider a thrust force acting through segments bounded by yield lines. The resisting moment along a yield line is the product of the thrust force times its eccentricity about the centroid of the panel thickness. Like McDowell [50, 51], transverse strength is limited by compressive stress along the edges of a segment rather than a tensile stress as proposed by Haseltine [36, 37]. With Dawe's method, computer-aided techniques are used to predict the first crack and ultimate infill capacity. A conventional yield-line method is modified to combine arching action within flexible frame boundaries.

Lefter's theory is based on a fixed eccentricity of the thrust force (1 inch from edge), and is thus not sufficiently general to be used with the thin brick infill specimens. As shown in Fig. 8, Dawe's theory produces a stiffer and stronger response than McDowell's theory because two-way action is considered rather than one-way action. However, since edge flexibility is introduced with Dawe's theory, the differences between the two curves are minimized.

Though each of the theories described have formulated lateral strength in terms of different coefficients, each has suggested that strength is proportional to the inverse of the square of the h/t ratio. The influence of the h/t ratio on strength is shown in Fig. 9 where theoretical curves are plotted based on the Timoshenko formulation as well as the two arching action models. Again, the Haseltine theory is not plotted because it nearly duplicates the Timoshenko solution. A nominal masonry compressive strength equal to 1000 psi has been used to plot curves based on the McDowell and Dawe theories.

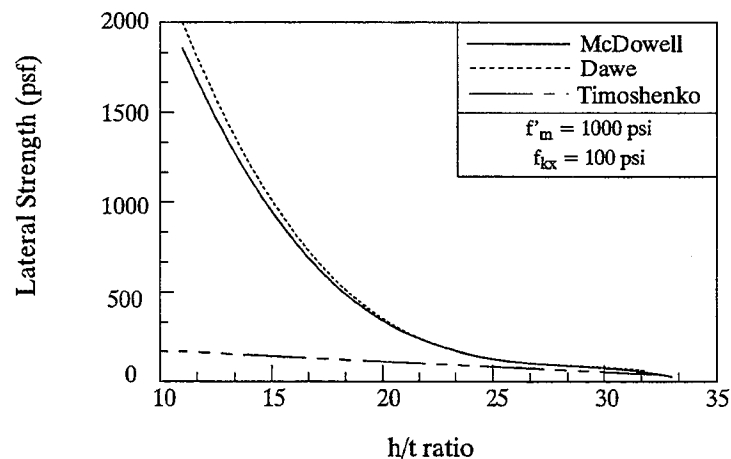


Fig. 9 Effect of h/t on Lateral Strength

Lateral strength is proportional to masonry compressive strength rather than tensile strength. According to the two arching theories, the test panels would have resisted pressures as high as 2000 psf which are two orders of magnitude larger than what would be expected during a seismic event.

One aspect of the out-of-plane infill problem that has not been studied to date is how to estimate the transverse strength of infills that have been previously cracked when subjected to

in-plane loads. If arching action is significant, then the transverse strength of a confined infill panel may be appreciable even though it is cracked. The purpose of the study described herein is to validate this concept through experimental and numerical analysis.

2.2.3 Conclusions

Analytical procedures were studied to predict the in-plane stiffness of the frame-infill specimens. Analytical procedures vary from simple shear beam analysis, to finite element models and equivalent strut methods.

Conclusions made based on the in-plane analysis were:

- The compressive area of the equivalent strut depends primarily on the thickness and the aspect ratio of the panel.
- The in-plane capacity of the specimen reaches its limit when the compression of the developed masonry strut is exceeded.
- Specimen stiffness depends on the length and distribution of the applied load on the corner of the frame.

A number of theories and analytical models have been studied to predict the out-of-plane behavior of masonry infills. Theories studied included elastic and inelastic plate theory as well as one and two way arching action. Analytical models varied from simple expressions and coefficients, to elaborate computer programs.

Conclusions made based on the out-of-plane analysis were:

- For slenderness ratios larger than 30, the arching action is small.
- Out-of-plane strength depends on compressive strength of the masonry and not on the tensile strength.
- Out-of-plane strength decreases with the square of the slenderness ratio of the panel.
- The effects of in-plane damage on the out-of-plane strength of the panels are not represented with any existing model.

CHAPTER 3

DESCRIPTION OF EXPERIMENTAL PROGRAM

Description of the experimental phase of the program is presented in this chapter. This chapter covers the overall design, construction, repairing and testing of several unreinforced masonry infills within a reinforced concrete frame. Information on material properties, test setup and instrumentation is provided in Appendices A and B.

3.1 Specimen Description

The experimental program consisted of testing eight full-scale specimens. The specimens were unreinforced clay or concrete masonry infills placed within a single-story, single-bay reinforced concrete frame as shown in Fig. 10 and Fig. 11.

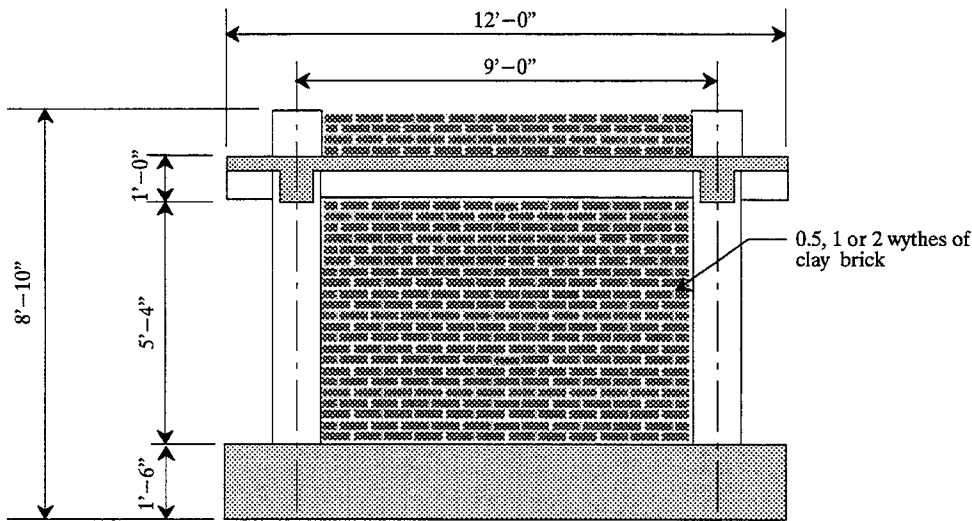


Fig. 10 Description of Clay Brick Specimen

3.1.1 Reinforced Concrete Frame

The confining reinforced concrete frame was built strong, ductile, and heavily reinforced for both flexure and shear. The elevation of the frame and corresponding cross-sections of the members are presented in Fig. 12. The frame was tested with a number of clay brick and concrete block infills, providing data for a parametric evaluation of different relative frame/infill strengths, different infill h/t ratios, and different mortar types.

The reinforced concrete frame represented typical concrete construction, particularly structures built in accordance to currently used codes and standards (1989 or newer). These codes include guidelines that require the placement of steel reinforcement within joints, continuous longitudinal steel reinforcement, and a small spacing for shear reinforcement throughout the members. Material and geometrical properties of the frame are summarized in Table 3.

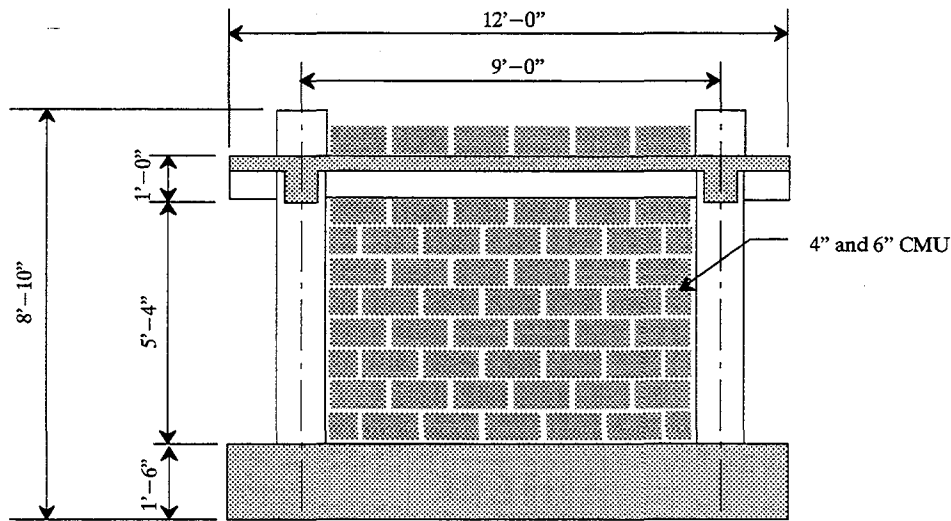


Fig. 11 Description of Concrete Block Specimen

3.1.2 Masonry Infills

Masonry infills were constructed with reclaimed Chicago common clay bricks or concrete masonry units. Brick masonry units were tested according to several ASTM standards including the initial rate of absorption test, the modulus of rupture test and the flat-wise compressive strength test. Infill thickness was varied to examine a wide range of slenderness ratios. This was felt to be important for both in-plane and out-of-plane behavior. The slenderness ratios ranged from 9 to 34. Brick infill thickness ranged from double-wythe ($7\frac{3}{8}$ inches) for smaller slenderness ratios, to half-wythe ($1\frac{5}{8}$ inches) for larger ratios. The half-wythe infill was built using bricks cut into two halves. Dimensions and shapes of the bricks were even and constant. For the double-wythe infill, a header course was included at every sixth course as is done in common U.S. practice.

Concrete blocks were also used for construction of two infills. Concrete masonry units were obtained from a local supplier. This was done to obtain a representative sample of masonry units with mechanical properties typical of newer construction. Material properties of the concrete blocks were measured based on standard ASTM tests. The slenderness ratios for concrete block infills ranged from 11 to 18 using standard 4 and 6 inch wide blocks. Mortar was placed on face shells only.

Block and brick courses were placed above the concrete slab to emulate stiffening of upper story infills.

A representative mortar mix was used for the two types of infills. The type of mortar was based on the evaluation of properties of masonry prisms and quadlets constructed with various mortars. Results of these tests are summarized in Appendix B. The two selected mortar types were: Type N and a lime mortar. The former stronger mortar contained the proportions 1:1:6 (cement:lime:sand); while the latter contained proportions of 1:3 (lime:sand), resulting in a mixture with low strength. A slight

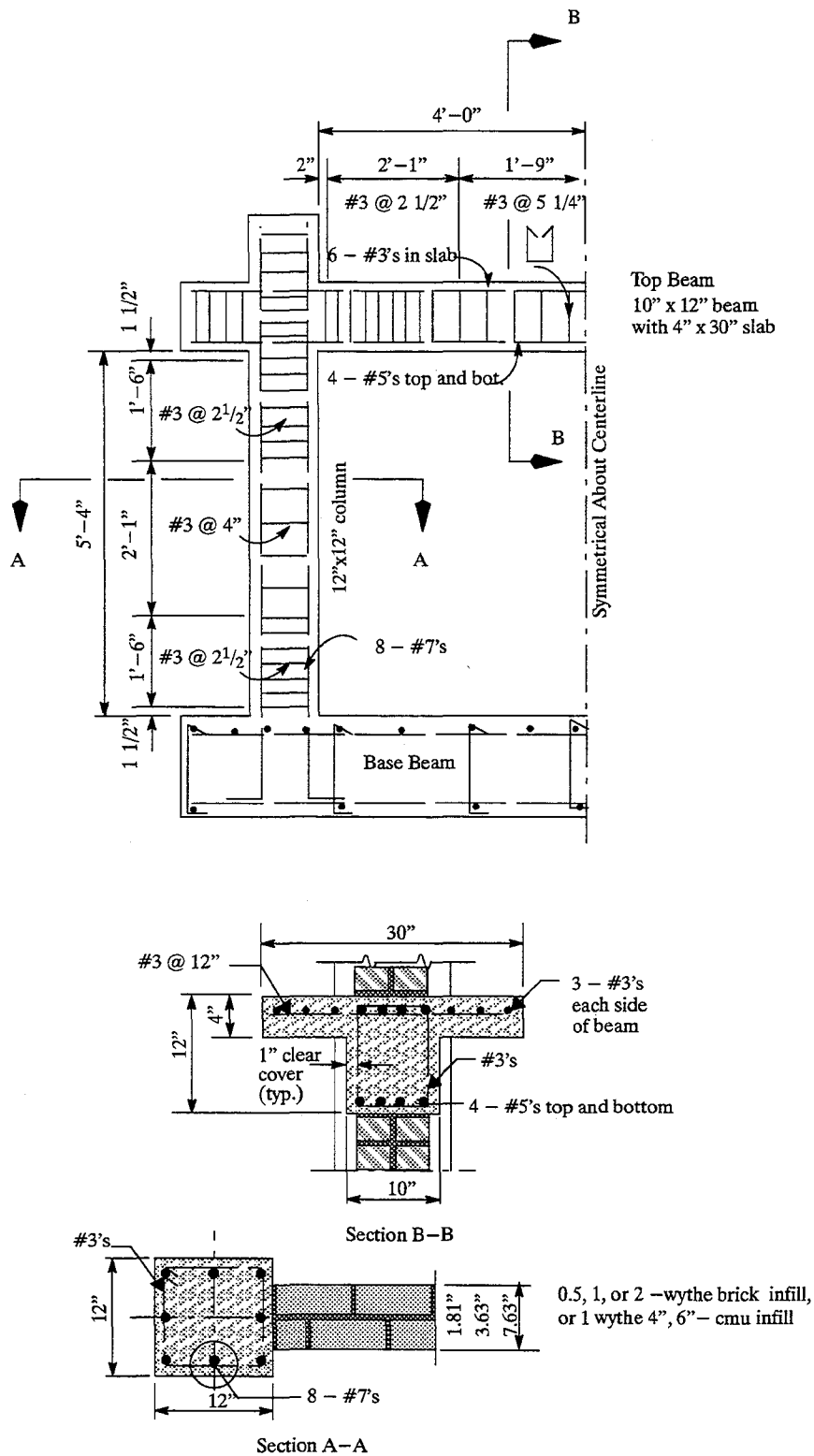


Fig. 12 Reinforcing Design for Reinforced Concrete Frame

Table 3 Frame Properties

Relative Properties	Frame
Lateral Strength	68 kips
Concrete Compressive Strength	8000 psi
Vertical Stress on Columns	350 psi
Column Area	144 in ²
Column Moment of Inertia (gross)	1728 in ⁴
M _u (k-in)	1407k-in
V _u (k)	87.5 k
Column Ratio (%) $\rho_s = \frac{A_s}{A_g}$	3.33%
Beam Area	200 in ²
Beam Moment of Inertia (gross)	2314 in ⁴
M _u top/bott.(k-in)	1230/864 k-in
V _u (k)	83.5 k
Beam Reinforcement Anchorage	Sufficient
Beam Top/Bottom Steel Ratio (%) $\rho = \frac{A_s}{bd}$	1.45/0.38
Ties	#3 @2.5"

modification of Type N mortar, namely Type S mortar, was also used. Type S mortar contained proportions 1:1/2:4 1/2 (cement:lime:sand) and produced mechanical properties similarly to Type N mortar.

3.2 Considerations for Specimen Design

Criteria used for the design of the frame/infill test specimens was based on construction currently found throughout the United States.

For in-plane lateral loadings the frame/infill test specimen represented the bottom story of a multi-story building. When actual buildings are subjected to earthquakes, lateral story shears are largest at the base level. These shears vary according to the story mass and to the local accelerations. Bottom stories carry the largest sum of lateral forces, and also the largest sum of gravity loads. These gravity loads apply a pre-compression on the affected stories. The magnitude of this pre-compression is important when determining the lateral capacity of the building. To better represent an actual building, a vertical compressive axial force was concentrically applied to both columns. This vertical load was applied to the specimen for the purpose of simulating gravity loads from upper levels. The axial compression force increased the cracking moment and the moment

capacity of the columns. The column axial force also resulted in some compressive stresses applied to the infill.

For out-of-plane loads, the frame/infill test specimen represented the upper-story of a multi-story building. When ground motions are applied to a structure, the maximum accelerations are located at the upper stories of a building. The acceleration and mass of the masonry dictates the amount of lateral inertial force that is applied to the infill. Gravity loads on an upper story from roof loads, or other sources, were also accounted for during testing of the specimens in the out-of-plane direction.

Consideration was given to the frame/infill relative lateral strength of the specimens. The specimen behavior changes depending on the frame/infill relative lateral strength. For strong and stiff frames with weak and brittle infills, the behavior of the specimen is governed by the frame. For a weak and brittle frame with a strong infill, the behavior of the specimen is governed by the infill. Thus, the study of a wide range of relative frame/infill lateral strengths would demonstrate the corresponding effects on the in-plane behavior of the specimens.

The estimated behavior of various clay brick and CMU infills encased within the frame is illustrated in Fig. 13. The depicted behavior is based on results obtained from elastic finite element

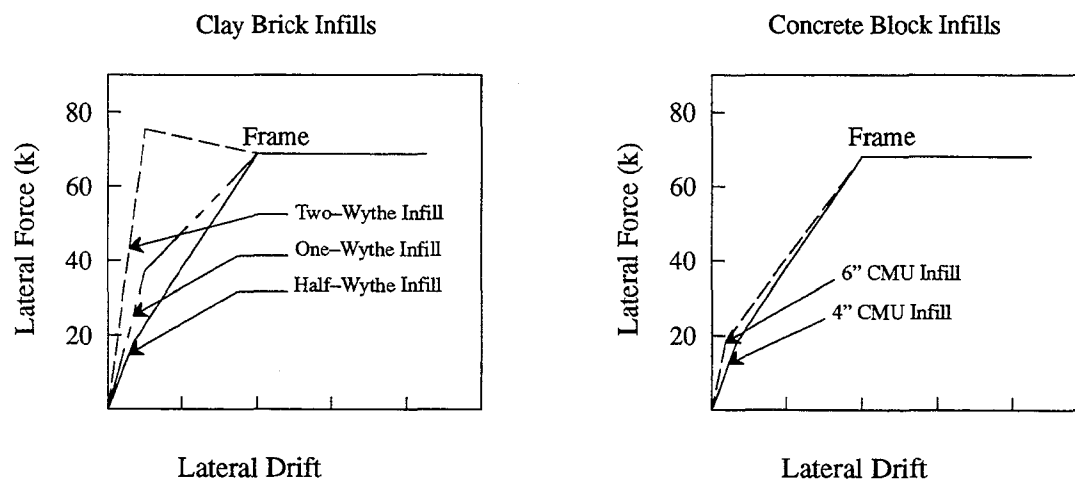


Fig. 13 Relative Frame-Infill Strength for Brick and Block Infills

analyses done for the frame in combination with different infills. The behavior of the infills is assumed to be linearly elastic up to cracking of the masonry at a shear strength of 100 psi. Once the infill cracks, the load is redistributed until the frame is the only acting structural element in the specimen. This analysis is highly qualitative and idealized. The capacity of the frame is the maximum lateral load that the specimen is able to resist once the masonry deteriorates.

The strength of the frame was required to be equal to or greater than the strength of the strongest infill. The frame was designed to be strong, and ductile. Design requirements met the special provisions for seismic design included in the 1989 ACI (American Concrete Institute) building code. All steel reinforcement in the frame was sufficiently anchored to develop the maximum flexural member capacity. Code provisions for the shear strength were met. Stirrups were placed within the joint for an overall better cyclic performance of the system to meet ACI-318. The concrete mix used, with large compressive strength and modulus of elasticity, generated the desired frame strength and rigidity in conjunction with the geometric properties of the frame. The high concrete compressive strength, as illustrated in Table 3, was reached by using a special concrete recipe mixed in-house. A detailed description of the mix is presented in Appendix B.

Flexural strength of the columns was calculated for the geometrical properties of the members including the effect of the vertical axial force applied at the top of the columns. The moment-thrust interaction diagram for the columns of the frame is shown in Fig. 14. Frame lateral strength was

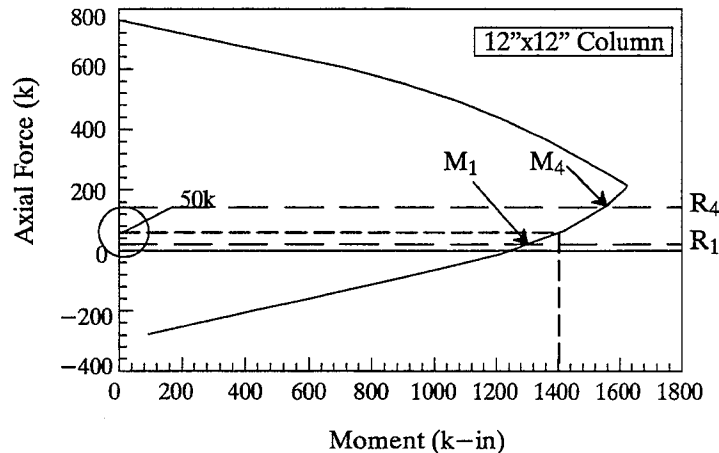
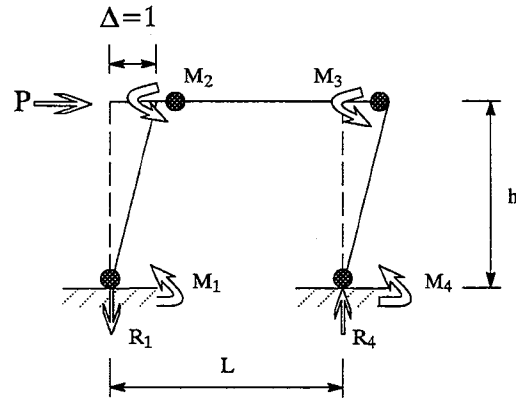


Fig. 14 P-M Interaction Diagram

calculated from the flexural strength of the members in conjunction with the virtual work method. The collapse mechanisms for the frame is presented in Fig. 15. M_1 and M_4 vary as the applied lateral force increases. The moment capacity of the column in the windward direction decreases as the applied lateral force increases. The moment capacity of the opposite column increases as the applied lateral force increases. The axial force applied to the columns of 50 kips (Fig. 14) was considered to prevent the columns from developing tension. The corresponding lateral load required to form the collapse mechanism was considered to be the lateral strength of the frame.

Masonry properties were chosen in such a way as to couple with the frame properties and closely represent actual construction. The chosen masonry units and mortar types were considered to produce the desired ranges for the frame/infill lateral strength. The half-wythe clay brick panel



$$P = (M_1 + M_2 + M_3 + M_4) \left(\frac{1}{h} \right)$$

Fig. 15 Collapse Mechanism for R/C Frames

was considered to have a low lateral strength, while the double-wythe clay brick had a high strength and stiffness in a magnitude comparable to that of the frame as illustrated in Fig. 13.

3.3 Specimen Construction

The frame included a heavily reinforced concrete base beam. Base beam geometry and reinforcement layout is presented in Fig. 66 in Appendix A. The beam was post-tensioned to the testing floor with eight 1.5 inch diameter Dywidag bars. Steel column cages were assembled. All reinforcement steel used met the A615-Grade 60 steel standards. The sizes of bars used varied from #3's to #7's as shown in Fig. 12. All bars were cut and bent in house to the exact design dimensions. The cages were built by placing the longitudinal bars on a "horse" or horizontal hanger. Longitudinal bars and stirrups were tied together by commonly used tie wire. Once the cages were assembled, they were placed in the base beam. Post-tensioning cables were introduced through the center of the column cages. The lower end of the cable was tightened and secured in place along with its corresponding anchorage connection. The remaining part of the strand was prevented from movement while the casting operation was in progress. The base beam was then cast with concrete obtained from a local distributor. At the time the base beam was curing, the top beam cage was assembled. It was built in a similar manner as the column cages. The two columns and the top beam were cast monolithically. The frame was cast with a concrete mix made in-house. Cylinders and sample beams were also cast for evaluation of material properties including the compressive strength, the modulus of elasticity and the modulus of rupture. Results of these tests are presented in Appendix B.

Masonry construction was done by professional masons. The same crew of two craftsmen was used to build all specimens. Mortar was retempered for a maximum period of 2 hours. All masonry units were pre-wetted for a period of five minutes to decrease the rate of water absorption from the

mortar joint. This resulted in better bond strength in the masonry unit/mortar interface. Masonry infills consisting of either clay brick or concrete block masonry units were laid in running bond.

Vertical forces applied to the columns during the testing of the specimen were not present during the construction of the masonry infill panel. The panel was constructed once the surrounding frame had been built, and only at the time of testing of the specimen the vertical forces were applied. The same vertical forces were applied to the columns during both the in-plane and the out-of-plane tests.

3.4 Description of Infill Repairing Method

Specimens with out-of-plane strengths lower than desired were repaired and retested to observe and quantify the improvement on the out-of-plane strength.

The repair method, similar to one studied by Prawel [61], consisted of parging a half-inch thick ferrocement coating to one or both faces of the infill panel. The repairing method is illustrated in Fig. 16. A single sheet wire mesh (0.5-in. mesh with No. 19-gage wire) was placed on each face. The wire mesh was embedded in the coating. Multiple wire sheets were lapped spliced to cover the entire infill surface area. The wire mesh was anchored to a damaged infill by steel bolts. 1/4-inch diameter steel bolts spaced at 16-inch centers were used. The plaster mix consisted of a cement-sand material mix in a ratio of 1:2. This mix ratio yielded the desired plaster strength for the coating and a good workable material for easy placement. The plaster mix was troweled on to each of the infill faces to be treated, for a total coating thickness of 0.5-in. A flexible PVC sleeve was placed over the bolts to provide relaxation to the system, and prevent premature cracking of the coating. Material testing was done to determine the mechanical properties of the coating. Results for these tests are presented in Appendix B.

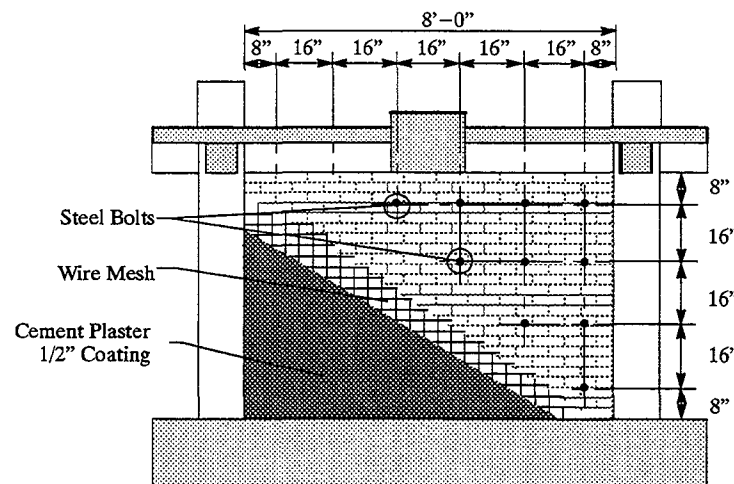


Fig. 16 Repairing Method

3.5 General Testing Procedure

The in-plane tests were run in displacement control, increasing the force until the prescribed deformation was reached. Specimens were loaded up to a defined factor in terms of Δ_{cr} (deflection at which initial cracking of the infill occurs) to assure a fully cracked condition. These forces were applied using a twin pair of 110-kip capacity servohydraulic actuators that pushed or pulled against a beam stub located at the center of the top beam (Fig. 17). One actuator was operated in displacement control, and was followed by its twin which was operated in force control. This way equal forces were applied preventing torsional moments to develop in the specimen. The test specimens were loaded parallel to their plane following the prescribed displacement histogram (adopted from Shing [71]) presented in Fig. 18. In this manner the specimen stiffness dictated the amount of force applied for a particular displacement. The general histogram shape represented a damaging earthquake. Displacements were increased slowly up to cracking to observe elastic behavior in the masonry. Once the infill cracked, two more cycles of the same magnitude were applied; the second cycle defined the behavior of an infill after cracking, and the third cycle confirmed equality with the second cycle. Decaying cycles were also included in the histogram with the purpose of illustrating the deterioration and degradation of the elastic stiffness due to cyclic loading. The displacements of the specimen were then increased until the desired maximum deformation was reached. An arbitrary value of twice the displacement required for cracking in the infill was assigned as the peak displacement.

Once an infill panel was substantially cracked with in-plane forces, it was tested in the out-of-plane direction by applying a uniform pressure with an airbag. The purpose of the

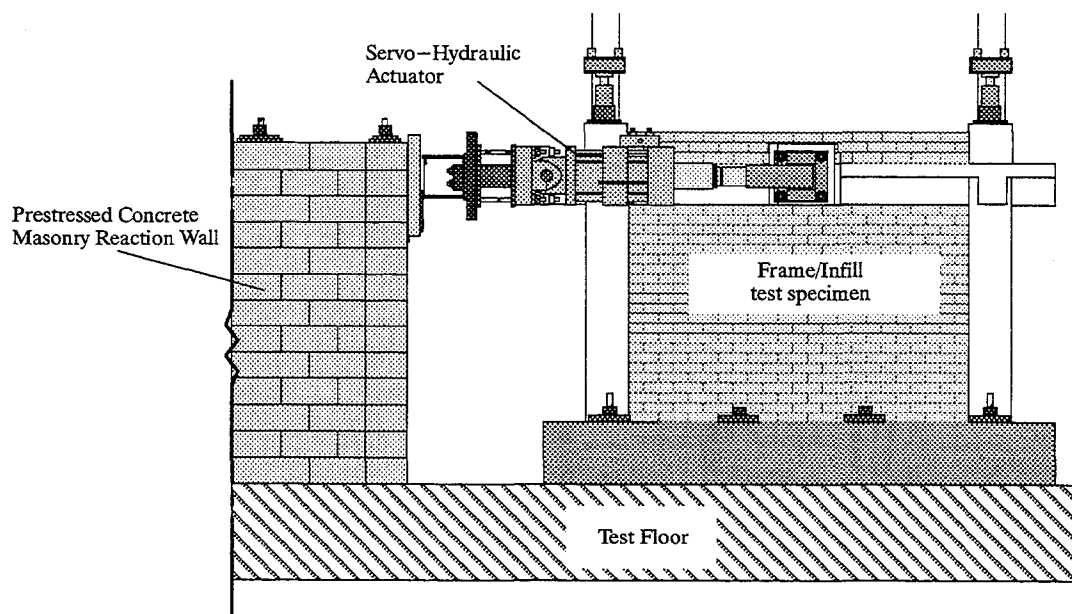


Fig. 17 Elevation of Overall In-Plane Test Setup

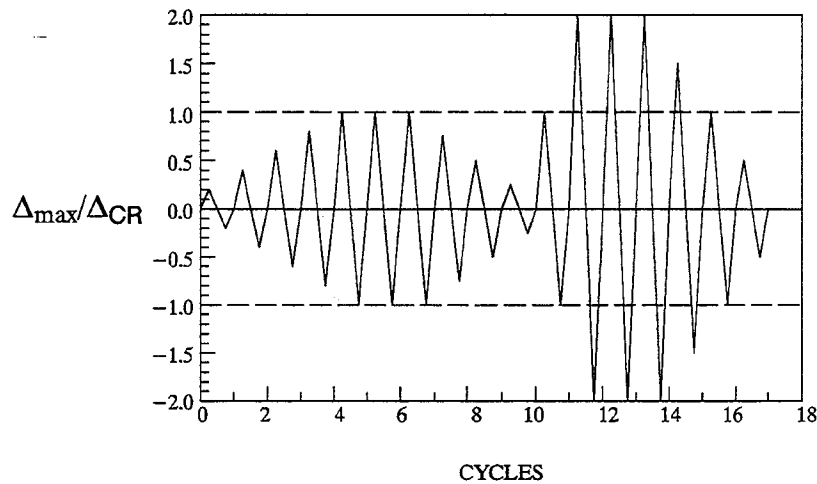


Fig. 18 Displacement Histogram

out-of-plane test was to determine the peak pressure or peak accelerations that a virgin, a damaged, or a repaired infill could resist. The pressure of the airbag was increased monotonically at a given rate until the peak pressure was reached. For some of the tested specimens, the air-bag was deflated to a zero pressure and then inflated again up to its maximum pressure. This evaluated the deterioration of the out-of-plane stiffness of the infill under repeated loading. The specimens tested for repeated loadings corresponded to those infills with capacities exceeding the capacity of the available equipment. The overall setup for the out-of-plane tests is presented in Fig. 19. The airbag applying the uniform pressure was reacted by a reinforced concrete reaction slab. Connection details between the airbag reaction frame and the frame/infill system are presented in Appendix A.

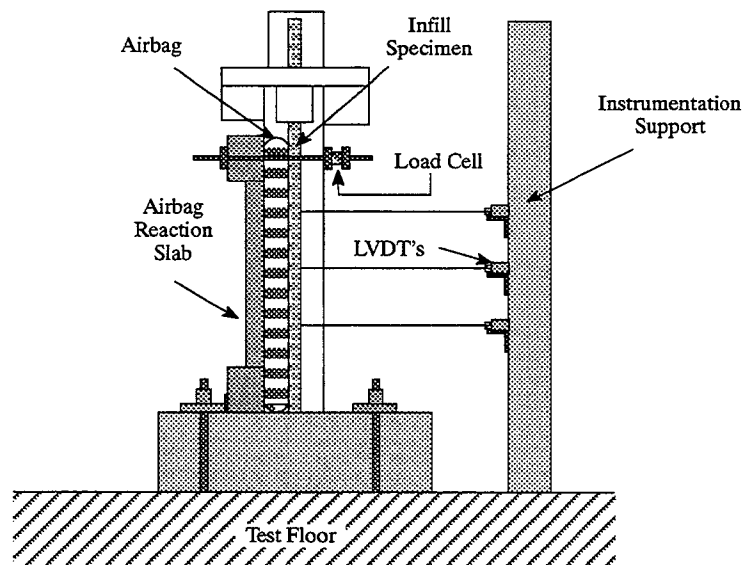


Fig. 19 Elevation of Overall Out-of-Plane Test Setup

Tests with forces applied normal and parallel to the infill plane simultaneously were also carried out for comparison. The worst possible loading case scenario that a building could ever see in any direction was chosen. This was chosen to estimate an upper bound for structural damage, and a lower bound for the expected resistance of the frame/infill system.

Although dynamic testing would have been preferred, it was not possible for the full-scale specimen because loading equipment was not available. Dynamic testing, however, was done with 1/2 scale replicas of the test infills by the Army Corps of Engineers at their Civil Engineering Research Laboratory [10] in Champaign, and the observed dynamic behavior is compared to static results in Chapter 5.

3.6 Description of Nondestructive Evaluation Methods

Non-destructive evaluation tests (NDE) were done prior to experimental testing of the specimen to determine corresponding mechanical properties. The flat-jack test and the in-place shear (shove) test were used for this purpose. The flat-jack test determines the vertical stresses present in the masonry panels. The in-place shear test (shove test) measures the shear strength along a single brick in a masonry panel. These two masonry properties are important for evaluation of the lateral strength of a structure. For this type of evaluation procedure, the combined use of both the flat-jack and the in-place shear test methods provide unique insight to accurately estimate the in-plane capacity of the structure. A detailed description of the non-destructive evaluation techniques used in this report are presented in Appendix C. Correlation of the predicted in-plane lateral capacity using the results obtained from the nondestructive tests are compared to experimental results in Chapter 4.

CHAPTER 4

RESPONSE RESULTING FROM IN-PLANE FORCES

Results from applying in-plane forces to the specimens are presented in this chapter. Experimental information is given on panel damage and corresponding crack patterns, and their relation to observed lateral behavior and stiffness characteristics. In addition, measurements are analyzed to show tendencies between each of the specimens. Topics addressed in this chapter include: (a) the relation between lateral strength and stiffness for the frame/infill specimens, (b) measured behavior of frame and infill, (c) shear stress and strain distribution, and (d) how well nondestructive estimates of masonry shear strength approach experimental results.

4.1 Cracking and Damage of Test Specimens

The crack patterns for the masonry infill specimens followed crack distributions as shown in Appendix D (the crack patterns corresponding to the in-plane loading are designated as the infill number, followed by the letter "a"). Properties of the infill test specimens are presented in Table 4. The compressive strength of the masonry (f'_m) and the measured modulus of elasticity (E_m) were measured directly from a series of prism tests carried out for the different infill panels. The estimated modulus of elasticity was obtained by multiplying 750 times the masonry compressive strength. The general behavior explained here applies to every specimen unless otherwise specified. The first occurrence of cracking was the separation of the infill from the frame. This occurred along the infill boundaries where tensile stresses between the frame and the infill developed as illustrated in Fig. 20(a). Because the specimen was symmetrical as was the loading, identical cyclic behavior was expected. The separation between the frame and infill commenced at the top and developed down. The separation at the beam-infill boundary increased with lateral drift. As the lateral load and drift increased, small diagonal cracks in the center-upper part of the infill developed. The amount of lateral drift required for the formation of these cracks is defined as the cracking drift (Δ_{cr}/h). Fig. 20(b) illustrates the typical crack pattern obtained when Δ_{cr} was reached in one direction for the

Table 4 Specimen Properties

Specimen #	Mortar Unit	Mortar	Thickness (in)	h/t	f'_m (psi)	E_m (Estimated) (ksi)	E_m (Measured) (ksi)
2a	Brick	Type N	1 ⁷ / ₈	34	1575	1181	1167
3a	Brick	Lime Mortar	1 ⁷ / ₈	34	1470	1103	756
4a	Block	Type N	3 ⁵ / ₈	18	3321	2491	1804
5a	Block	Type N	5 ⁵ / ₈	11	3113	2335	1686
6a	Brick	Lime Mortar	3 ⁷ / ₈	17	665	499	310
7a	Brick	Type N	3 ⁷ / ₈	17	1596	1197	424
8a	Brick	Lime Mortar	7 ³ / ₈	9	507	380	342

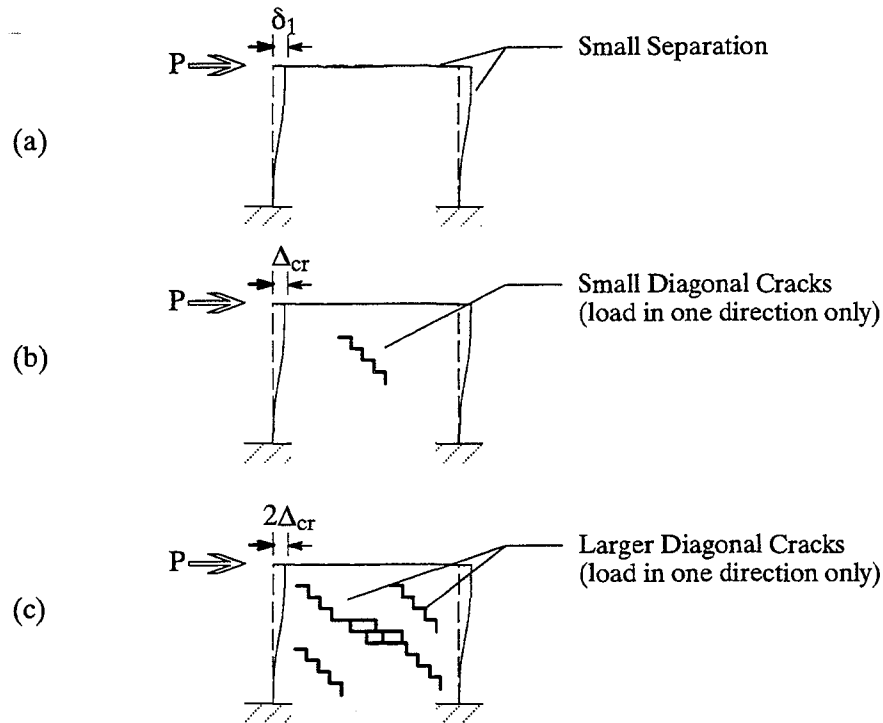


Fig. 20 Frame/Infill Crack Development

first time. A similar set of cracks developed in the opposite direction when the cycle was reversed. After cracking of the masonry, the stiffness of the infill was reduced, but the load carrying capacity of the system continued to increase. A sequence of cycles of the same amplitude, and smaller, were applied to the structure to determine the amount of strength deterioration. Following the detailed histogram (Fig. 18), the specimens were then loaded to a maximum lateral drift of $2\Delta_{cr}$. This higher load caused the masonry to develop new cracks. The final crack patterns (Fig. 20(c)) included extension of the previous cracks, and the creation of new diagonal cracks caused by the redistribution of shear stress.

Infill crack patterns depended on variables such as the shear strength of the masonry, the thickness of the infill, and the type of masonry unit. For clay brick infills, the cracks were created at locations of maximum applied stress, with no concern for the masonry unit size. Crack patterns for concrete masonry infills followed bed and head joints (Fig. 89 and Fig. 91). Even though the net bedded area was similar for some clay and concrete masonry infills, the force needed to crack a concrete masonry infill was larger because of the larger masonry unit size.

Damage was apparent at completion of the in-plane tests. Masonry panels were seen to detach from the confining frame. Mortar at the frame-infill boundary was partially dislodged. Gaps formed between the infill and the frame were large enough to see through. The in-plane lateral stiffness decreased. After cracking of the infill, the stiffness decreased with every applied loading

cycle. As the damage to the infill increased, the redistribution of in-plane forces between the frame–infill elements continued to occur.

4.2 Conventions

Electronic equipment used to monitor the in-plane behavior of the specimens is summarized in Appendix A. The sign conventions used for this equipment is explained in this section. Lateral forces were considered positive when the direction of the applied force was towards the east. Strain gages were positive for tensile movements. Displacement transducers were positive when recording extension. Sign conventions were adopted with the purpose of obtaining positive slopes for force–deflection relations.

4.3 Measured Behavior of Reinforced Concrete Frame

Behavior of reinforced concrete frames is generally well understood. Once the concrete frame is filled with a masonry infill or any other type of panel, its behavior is not as easily quantified.

Testing of the first specimen resulted in the second largest cyclic load and the second largest lateral displacement that the frame–infill system would see. These upper limits for load and drift applied to the specimens during the first test were not exceeded until the in-plane test for specimen 8a. No new damage occurred in the frame throughout the sequence of experiments.

Cracks developed in the frame after the first in-plane test are depicted in Fig. 21(a). No new

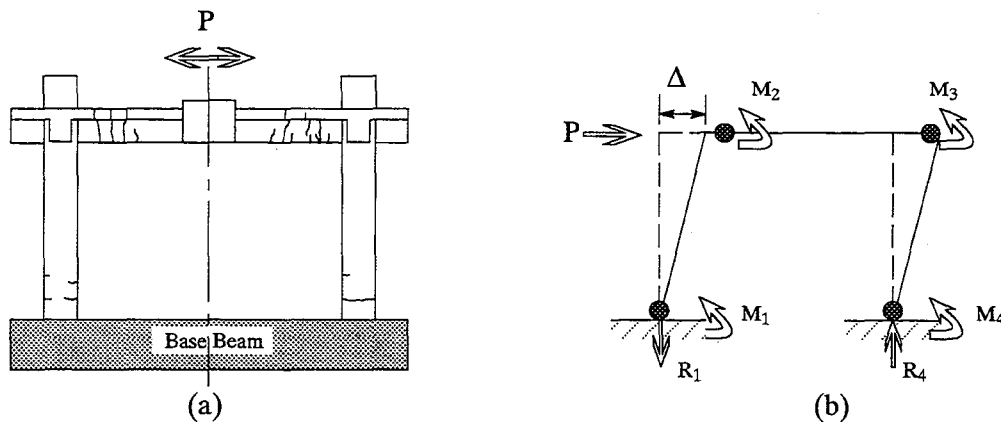


Fig. 21 Cracking of Reinforced Concrete Frame

cracks appeared after the first test. During testing of the last specimen, existing cracks propagated but no new cracks were formed. Flexural cracks in the frame occurred at predicted critical locations. The sequence for the development of these cracks followed the distribution of the applied moments to the frame (Fig. 21(b)); that is, first cracks formed in the bottom part of the windward column where moments were largest and axial compression was smallest, followed by cracking of the beam near the column face. Rotation across gage lengths at the plastic hinge regions were monitored as presented in Appendix E.

The frame cracked in flexure. Cracking of the frame was symmetrical with respect to the center line as expected from the applied cyclic loading pattern. The first bottom crack in the beam occurred before the first top crack. The crack widths were larger on the bottom face than on the top face because the neutral axis of the beam was farthest from the bottom face. Cracking in the columns occurred at the critical sections as well. The cracks that developed on the outer face of the tension column were anticipated; but the number of cracks and their size was smaller than expected from simple frame analysis (no infill).

The post-cracking behavior of the frame was of interest; whether the frame reached its capacity or not greatly influenced specimen behavior. Strain gages placed directly on the steel reinforcing bars at the critical sections of the frame as illustrated by Fig. 67 indicated reinforcement behavior. The measurements obtained from these strain gages were compared to measurements from displacement transducers placed at similar locations on the face of the beam and columns (Fig. 68). Their behavior during the course of the tests is presented by figures in Appendix E. The resisting moment and axial forces that developed in the columns were estimated based on strain and rotation measurements obtained during the tests. These quantities were evaluated following a procedure described in Appendix E.

4.4 Measured Cracking Strength and Behavior of Masonry Infill

In-plane test results for the specimens are summarized in Table 5. In-plane specimen behavior during the course of the tests was monitored and results are presented in Appendix E. A typical load displacement hysteresis loop is presented in Fig. 22 for Specimen 2a. Lateral force required to reach Δ_{cr} (lateral displacement at which initial cracking in the infill occurs) was defined as the cracking load for the masonry infill. The lateral force applied to the specimen to reach a lateral displacement of $2\Delta_{cr}$ was defined as the maximum applied load. This is not the ultimate strength, but simply the load needed to reach $2\Delta_{cr}$. These values were recorded cyclically, and the average of both positive and negative respective loads was obtained. These values were divided by the infill gross area to give a nominal shear stress for f_{v1} (at Δ_{cr}) and f_{v2} (at $2\Delta_{cr}$) respectively, which are listed in Table 5.

Table 5 Specimen In-Plane Test Results

Specimen #	Δ_{cr} (in)	Δ_{cr}/h (%)	f_{v1} at Δ_{cr} (psi)	f_{v2} at $2\Delta_{cr}$ (psi)
2a	0.11	0.172	189	271
3a	0.07	0.109	122	189
4a	0.03	0.047	75	135
5a	0.02	0.031	161	196
6a	0.08	0.125	50	95
7a	0.08	0.125	117	169
8a	0.125	0.195	47	71

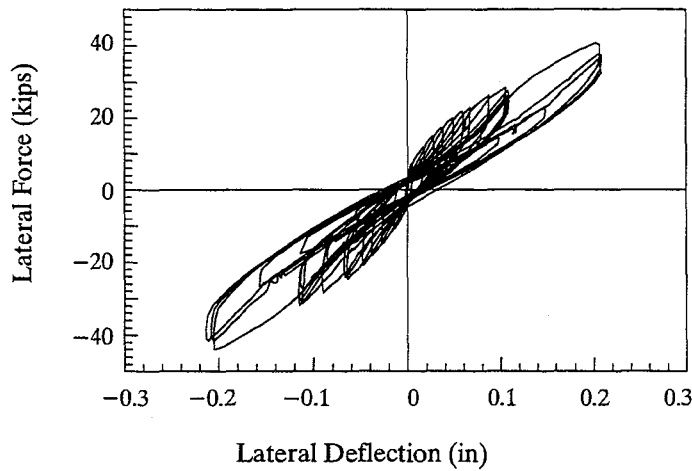


Fig. 22 Load–Displacement Hysteresis

Specimens were subjected to a sequence of cycles as described by the histogram shown in Fig. 18. The in-plane behavior of the specimens when loaded in one direction appeared not to be influenced by damage previously done to the infill in the opposite direction. The observed lateral force–displacement behavior as measured during the test was symmetrical for loading in both directions. Due to the number of repeated cycles, stiffness of the specimens gradually decreased.

Maximum infill shear stress varied with mortar type. Infills built with Type N mortar reached, on the average, 50% higher shear stress levels than infills with lime mortar. For specimens with similar stiffnesses within the linearly elastic region, Δ_{cr} was directly proportional to the maximum infill shear stress. This is shown in Fig. 23 for Specimen 2a with a maximum shear stress of 1.5 times that of Specimen 3a.

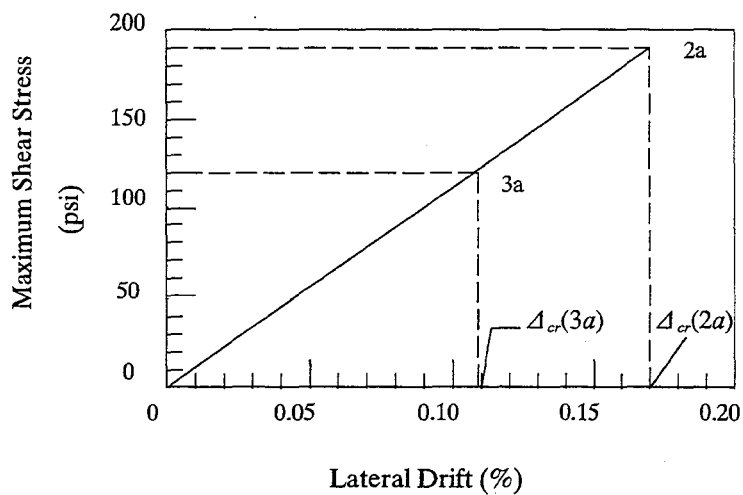


Fig. 23 Shear Stress vs. Lateral Drift

The lateral stiffness of the frame–infill system decreased gradually as the number of applied loading cycles increased. As illustrated by Fig. 22, Fig. 28 and by figures in Appendix E (Lateral Force vs. Deflection and Infill Shear Stress vs. Shear Distortion), the initial lateral stiffness was large for the first few cycles and continued to decrease until cracking of the infill occurred. The stiffness decreased at a larger rate after cracking of the specimen. Fig. 24 shows load–deflection curves for comparison of the masonry stiffness at cracking for Specimens 6a and 7a. Stiffness was directly proportional to the

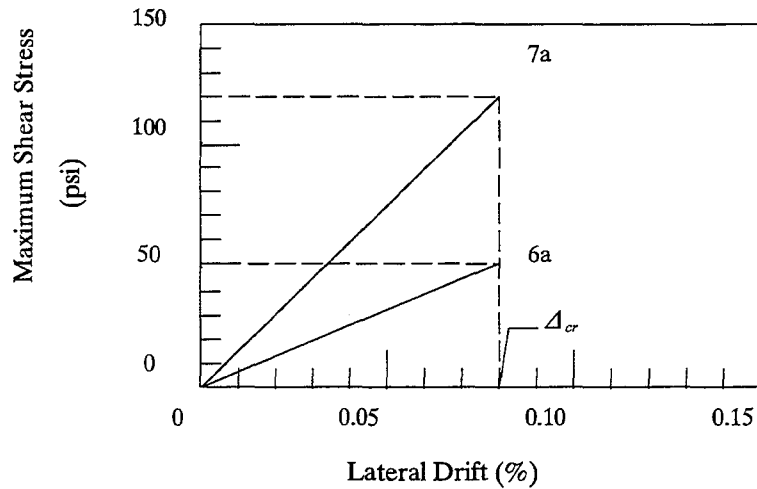


Fig. 24 Shear Stress vs. Lateral Drift

masonry compressive strength. This is shown in Fig. 25 with experimental results. The masonry stiffness was evaluated at cracking as the shear stress in the masonry (f_{vI}) over the lateral deformation (Δ_{cr}).

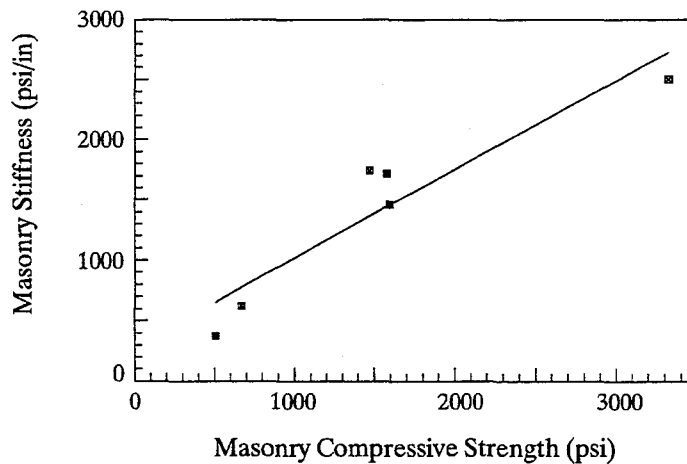


Fig. 25 Masonry Stiffness vs. Masonry Compressive Strength

The peak developed stress was on the average 1.5 times stress at initial cracking. Post–cracking strength is developed because of the confinement offered by the frame. The

confinement provided by the frame demonstrated that masonry does not behave in a brittle fashion once it cracks for these types of frame/infill arrangements, contradicting the generally accepted conception of brittle structural behavior for the masonry.

4.5 Specimen Lateral Stiffness

Specimen lateral stiffness at cracking of the panel was calculated based on the load–deflection measurements recorded during the progress of the in–plane tests. Measured specimen stiffnesses are reported in Table 6, and for Specimen 2a is also illustrated in Fig. 26. An

Table 6 Specimen In–Plane Stiffness

Specimen #	h/t	Thickness (in)	Specimen In–Plane Stiffness (k/in)			
			Measured	Holmes	S. Smith	Cracked Frame
2a	34	1 ⁷ / ₈	268	513	547	312
3a	34	1 ⁷ / ₈	272	497	491	245
4a	18	3 ⁵ / ₈	390	786	630	410
5a	11	5 ⁵ / ₈	1256	754	615	392
6a	17	3 ⁷ / ₈	218	482	475	229
7a	17	3 ⁷ / ₈	509	783	508	267
8a	9	7 ³ / ₈	257	579	570	342

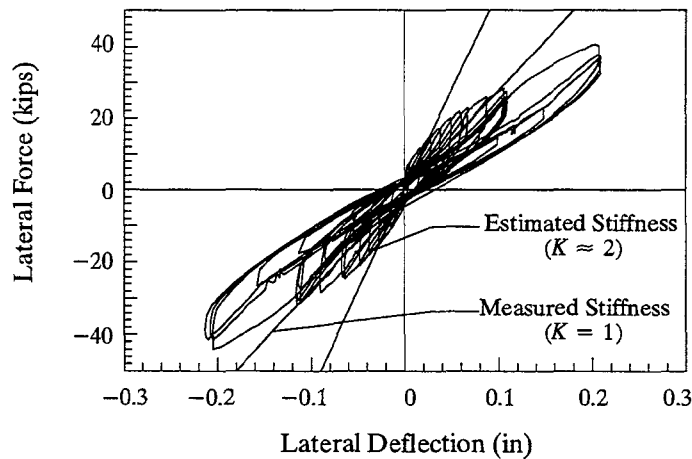


Fig. 26 Measured/Predicted Specimen Stiffness

explanation of the analytical models by Holmes and Smith included in Table 6 is presented in Section 2.2.1.

Numerical predictions for the in–plane stiffness of the specimens are presented in Table 6. The first two predictions are based on Holmes and Smith methods, and the third on results obtained from a frame analysis of the specimens with an equivalent diagonal compression strut in place of the

infill panel. Equivalent strut compressive area ranged from 0.2 (Smith) to 1/3 (Holmes) the diagonal length of the infill panel times the thickness. The third prediction is based on the cracked properties of the frame and on a strut compressive area of $t_d/8$. The factor of eight in the strut compressive area was chosen to fit the experimental data. The predicted specimen stiffnesses are normalized with the experimentally measured values, and results are presented in Table 7. Predicted and measured stiffnesses for Specimen 2a are illustrated in Fig. 26. Observations from Table 7 and Fig. 26 showed that the predicted specimen stiffness corresponded to roughly twice the values recorded during the in-plane testing; this was attributed to deterioration and degradation of the specimen that occurred during the applied cycles.

An expression based on Holmes equivalent strut method and modified to account for the degradation of the specimen under cyclic loads is presented in Eq. [19]. This expression was obtained

$$K = \left[\frac{12EJ_c}{h'^3 \left[1 + \frac{t_c}{t_b} \cot \theta \right]} + \frac{t_f^2}{6\varepsilon_{cr}} \right] \quad \text{Eq. [19]}$$

by modifying Eq. [4] by a factor of one-half. The one-half factor was obtained by comparing predicted and measured specimen response (Fig. 26) and is purely empirical based on the tested specimens. Measured specimen stiffnesses were well predicted by the modified Holmes model. Normalized prediction values and statistical information for the modified Holmes model is presented in Table 7.

4.6 Cracking Strength and Shear Strain Distribution

The nominal infill shear stress was obtained by dividing the applied lateral force by the gross area of the infill. Lateral force required to reach Δ_{cr} (lateral displacement at which initial cracking in

Table 7 Relative Predicted/Measured Specimen Stiffness

Specimen #	Predicted/Measured Stiffness			
	Holmes	S. Smith	Cracked Frame	Mod.Holmes
2a	1.91	2.04	1.16	0.96
3a	1.83	1.81	0.90	0.91
4a	2.02	1.62	1.05	1.01
5a	0.60*	0.49*	0.31*	0.30*
6a	2.22	2.19	1.04	1.11
7a	1.54	1.00	0.52	0.77
8a	2.25	2.22	1.33	1.13
Average =	1.96	1.81	1.00	0.98
Std. Deviation =	0.26	0.46	0.28	0.13

* – value not included in the statistical calculations

the infill occurs) divided by the nominal area of the corresponding specimen was defined as the cracking strength.

Infill shear deformations were monitored using displacement transducers placed diagonally across the infill surface as shown in Fig. 68. The infill shear strain was evaluated using Eq. [20]:

$$\gamma = \frac{\Delta T + \Delta C}{2h_o \cos \theta} \quad \text{Eq. [20]}$$

where:

- γ = shear strain
- ΔT = measured diagonal extension
- ΔC = measured diagonal contraction
- h_o = effective height
- θ = angle formed by diagonal and horizontal base.

The variables used in Eq. [20] are illustrated in Fig. 27. Plots of the shear stress vs. shear strain

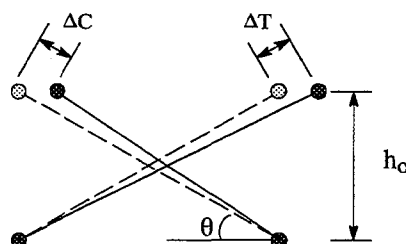


Fig. 27 Shear Strain Monitoring System

calculated from records obtained during the testing of the specimens are presented in Fig. 28 for Specimen 2a and in Appendix E for the remaining. Estimated shear modulus values ($0.4 E_m$) are compared to values obtained from measured curves in Table 8 for the test specimens. From the measured curves, the shear modulus was calculated by dividing the measured shear stress by the shear strain, and compared to the commonly estimated value of $0.4 E_m$ producing good correlation results as illustrated in Fig. 28.

4.7 Correlation between Measured Experimental Results and NDE Estimates

Nondestructive testing produced a general idea of the state of stress and the shear strength of the masonry panels. NDE testing procedures with corresponding test result values are presented in Appendix C.

4.7.1 Flat—Jack Test

It was concluded that when vertical forces were applied to the columns, the average vertical stress in the infill had an upper bound of 40psi (Specimen 2a). This conclusion was based on results from flat—jack tests. The columns carried most (over 90%) of the vertical forces applied to the specimens.

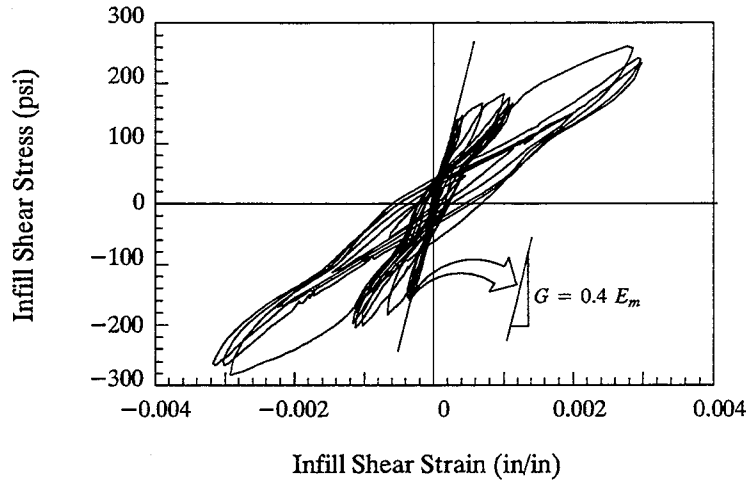


Fig. 28 Shear Stress– Shear Strain

Table 8 Shear Modulus

Specimen #	G_m (Estimate) (ksi)	G_m (Measured) (ksi)
2a	467	459
3a	302	253
4a	721	152
5a	674	625
6a	124	125
7a	170	167
8a	137	80

Values in Table 9 correspond to an average compressive stress in the infill. Average compressive stress in the infill corresponds to the mean value of results obtained from tests performed at the different infill locations. The two test locations consisted of one in the upper section of the infill, and the second in the lower part of the infill where the stresses were larger. Stresses measured in the upper section of the infill were around 15% lower than the values presented in Table 9, while stresses measured in the lower part of the infill were about 15% larger. The compressive stresses were a result of applying vertical forces at the top of the columns. Vertical compressive stresses varied according to the relative frame–infill stiffness (larger infill stiffness–larger attracted vertical load), and to the corresponding panel compressive area (larger compressive area–smaller compressive stress).

4.7.2 In–Place Shear Test (Shove Test)

The in–place shear test was done to estimate the shear strength of the masonry in situ. This is an important material property used to estimate the lateral force capacity of masonry infills. Shove test results performed on all clay brick infills ($f_{v, \text{predicted}}$) are presented in Table 9. The presented results

Table 9 Specimen In-Plane Test Results

Specimen #	Δ_{cr} (in)	Δ_{cr}/h (%)	f_a (psi)	f_{v1} at Δ_{cr} (psi)	f_v predicted (psi)	f_{v1}/f_v
2a	0.11	0.172	40	189	125	1.51
3a	0.07	0.109	35	122	87	1.40
4a	0.03	0.047	*N.T.	75	*N.T.	*N.T.
5a	0.02	0.031	*N.T.	161	*N.T.	*N.T.
6a	0.08	0.125	19	50	35	1.43
7a	0.08	0.125	28	117	70	1.67
8a	0.125	0.195	13	47	30	1.57
* Not Tested					$\bar{f}_{v1}/\bar{f}_v = 1.51$	

considered the corresponding vertical stress in the infill. These values were not modified because the in-place shear tests were performed directly in the panel that was tested; thus, any modification to the obtained test values would have produced inaccurate estimates of the masonry shear strength. Test results provided an estimate of the average expected infill shear strength. Shove tests were performed at the locations and following the procedure as described in Appendix C.

Results of shove tests are compared to measured nominal shear stresses required to reach Δ_{cr} . The shove tests produced lower, conservative values for the shear strength of the infills as measured in-situ. Measured shear stresses during the in-plane loading tests are compared with the in-place shear test results in Fig. 29 (f_a included). Underestimation of the shear strength of the masonry by the

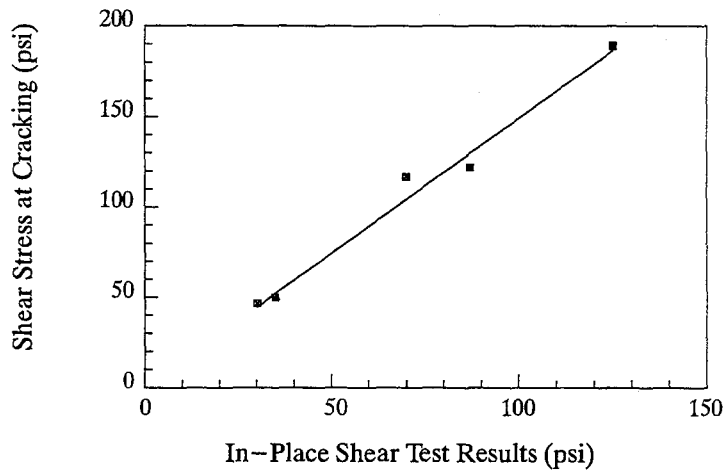


Fig. 29 Shear Stress at Cracking vs. In-Place Shear Test Results

shove tests was attributed to the added confinement by the frame during lateral loading of the specimen.

4.8 Summary and Conclusions

Results of the in-plane tests are presented in Appendix E. A discussion of the observed experimental results is presented in this chapter. Measurements are analyzed and tendencies between specimens are shown. A series of topics affecting the in-plane behavior of the frame/infill specimens are addressed; and a comparison between the tests results and results obtained from different types of nondestructive tests performed on the masonry is done.

Conclusions made based on the obtained experimental results were:

- The stiffness of the frame/infill specimen decreased greatly once cracking of the infill occurred.
- The masonry shear strength was affected by the type of mortar type used.
- Stiffness of the frame/infill specimen was directly proportional to the masonry compressive strength.
- In-plane stiffness can be approximated using an equivalent strut with a width equal to one eighth the diagonal dimension of the panel.
- The lateral force required to reach displacements of $2\Delta_{cr}$ (Δ_{cr} = the lateral displacement of the specimen to cause cracking of the panel), was approximately $1.5P_{cr}$ (P_{cr} = the lateral load applied to the specimen to cause cracking of the panel).
- The in-plane shear test estimated a lower bound for the actual lateral cracking strength of the specimens.

CHAPTER 5

MEASURED RESPONSE RESULTING FROM OUT-OF-PLANE FORCES

Results of the out-of-plane tests are presented in this chapter. Experimental information is given of panel damage and corresponding crack patterns, and their relation to the observed out-of-plane strength. In addition, measurements are analyzed to show correlation between the specimens. Topics addressed in this chapter are: (a) effect of in-plane damage on out-of-plane strength of the infill, (b) effect of panel boundary conditions on the out-of-plane strength of the infill, (c) effect of gravity loads on the out-of-plane strength of the infill, (d) effect of masonry tensile bond on the out-of-plane strength of the infill, (e) effect of the repair method on the out-of-plane strength of the infill, (f) effects of repetitive loads on the out-of-plane behavior, (g) effect of in-plane shear on out-of-plane behavior, (h) out-of-plane strength and behavior predictions by existing analytical model, (i) correlation of static results to dynamic results and (j) correlation of experimental static results to static results from testing of existing structures.

5.1 Cracking and Damage of Test Specimens

Crack patterns for the masonry infill specimens followed similar crack distributions as shown in Appendix D (crack patterns corresponding to the out-of-plane tests are designated as the infill number, followed by letters b, c, d or t). General behavior of infill panels when loaded in the out-of-plane direction is explained in this section.

5.1.1 Virgin Specimen (Test #1)

Specimen 1 was tested in the out-of-plane direction with no previous in-plane loading or damage. This specimen was tested to determine the behavior of a virgin infill specimen and to compare the experimental results with specimens that have been previously cracked with in-plane forces. The first occurrence of cracking during the out-of-plane test was the simultaneous and symmetrical development of small diagonal cracks in the upper part of the infill as illustrated in Fig. 30(a). Cracks then continued forming in the diagonal direction expanding from both ends until reaching the upper frame-infill boundaries and the mid-height of the panel. Cracking of the panel then continued by forming a series of horizontal cracks in the center part of the panel as illustrated in Fig. 30(b). A few more cracks continued forming in the horizontal direction along the mid-height of the panel up to a certain amount of lateral drift of the panel at which point diagonal cracks began developing from the mid-height of the panel, toward the bottom corners of the specimens. The cracks developed according to the amount of lateral drift that the panel experienced but not totally reaching the bottom corners as illustrated in Fig. 30(c).

The development of the upper diagonal cracks was the first indication of damage for an infill. Location of these cracks was predictable in terms of the expected distribution of vertical compressive stresses and the edge conditions. Compressive stresses within the infill resulting from compressive forces applied to the columns were deduced from the difference between measured column forces and

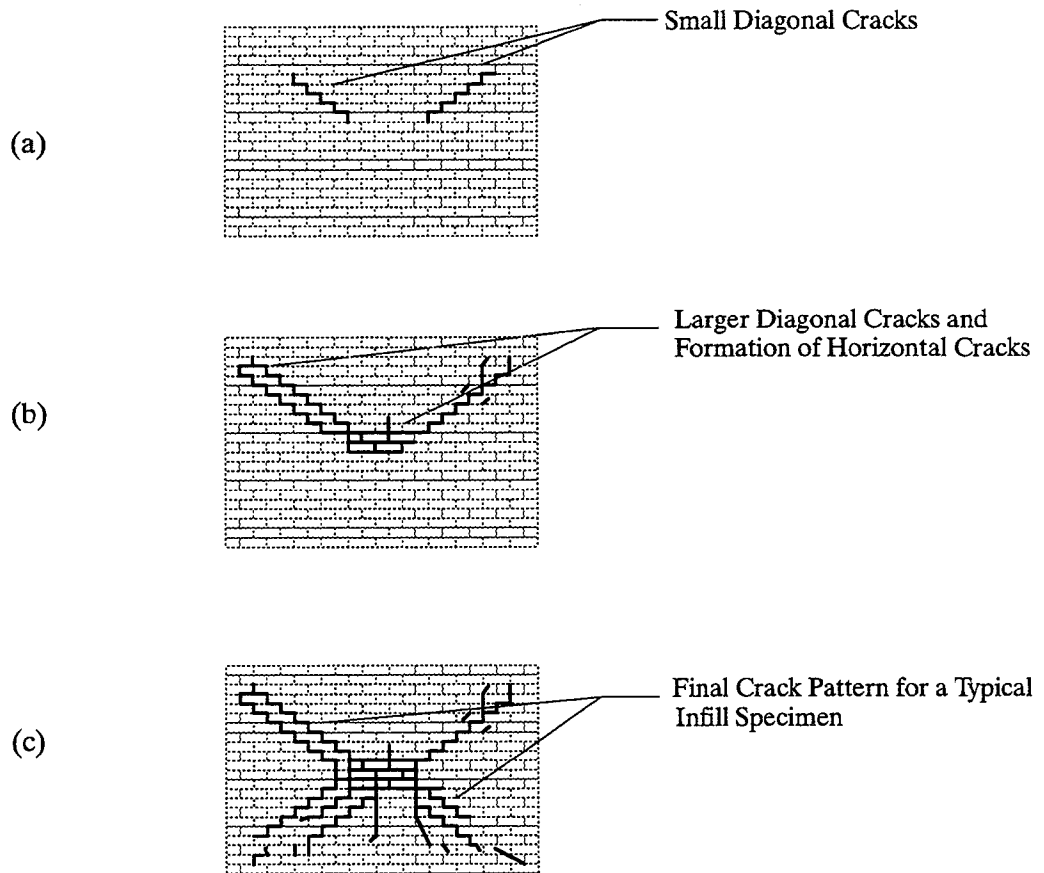


Fig. 30 Infill Crack Development

column compressive strains times the column modulus of elasticity. Instrumentation used to monitor strain distributions is presented in Appendix A.2.3. Stresses were developed primarily as a result of the force from the columns to the infill. A semi-triangular shaped stress distribution was formed (Fig. 31 for Specimen 2a). The mortar bed joint on top of the highest course was not placed as well

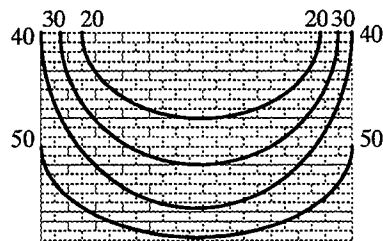


Fig. 31 Infill Stress Distribution (psi)

when compared to the bed joints along the other three infill boundaries. Therefore, the top frame-infill boundary did not provide the same amount of confinement to the infill during the

primary part of the out-of-plane testing of the specimens. Lower compressive stress applied to the upper part of the infill combined with a lower confinement by the frame on the upper portion of the panel justifies why this portion developed cracks prior to anywhere else.

The final deflected shape of a typical infill along the vertical and horizontal center line sections when loaded out-of-plane is shown in Fig. 32. This type of deformed shape is highly idealized, although similarities with a typical infill crack pattern (Fig. 30(c)) are clear.

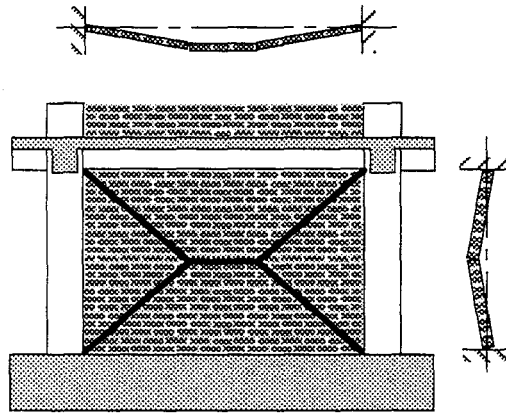


Fig. 32 Deflection Shape of Typical Infill During Out-of-Plane Test

5.1.2 In-Plane Cracked Specimens (Tests # 2b, 3b, 4b, 5b, 6b, 7b and 8b)

The cracking of previously cracked specimens was observed to follow a similar sequence as the one observed for the virgin specimen with a few distinctions. The formation of the final crack pattern observed less resistance by the previously cracked specimens. The resistance by the masonry decreased because of the presence of existing cracks that just re-open during the test; only a few new cracks were created as the out-of-plane loadings increased.

Brick masonry infills cracked in the in-plane and in the out-of-plane directions following the path of least resistance including reopening of previously formed cracks as well as forming new cracks as shown in figures in Appendix D (compare figures designated by letters “a”, and “b” for Specimens 2, 3, 6, 7 and 8). In-plane and out-of-plane cracks for each specimen compared favorably. All of the cracks for specimens built with concrete block units that formed during the in-plane test reopened during the out-of-plane test because of the low discretization in the infill. Therefore, the path of least resistance was the same for the in-plane and the out-of-plane directions. Once this path was formed and the out-of-plane test continued, these cracks extended as the deformations increased to obtain the final out-of-plane crack patterns illustrated in Fig. 90 and Fig. 92 in appendix D.

5.1.3 Repaired Specimens (Tests # 2c, 3c, 6c)

Crack patterns observed for the repaired specimens were formed in the same sequence as for the virgin specimen (Section 5.1.1). Approaching the end of test 2c, the specimen developed a large

vertical crack along the center line of the panel as illustrated in Fig. 85. This crack was a result of an insufficient lap length for the steel wire mesh. The repaired specimen behaved in a ductile fashion making it safe from brittle and unexpected failure. Specimens 3c and 6c responded similarly to Specimen 2c, however, vertical cracking did not occur because a sufficient lap length was provided for the steel mesh.

5.1.4 In-Plane Cracked Specimen with In-Plane Shear (Tests #5d and 6d)

In-plane constant lateral forces were applied to Specimens 5d (196 psi) and 6d (95 psi) during out-of-plane testing to evaluate the behavioral response of an infill when subjected to lateral forces in both parallel and perpendicular directions to their plane. Crack patterns observed for these tests were similar to the corresponding out-of-plane test with no in-plane force as observed by comparing Fig. 92 for Specimen 5b and Fig. 93 for Specimen 5d. For Specimen 6d the crack pattern was identical to the pattern obtained for Specimen 6b (Fig. 95), therefore a figure for Specimen 6d was omitted.

5.2 Measured Experimental Test Results

Physical and mechanical properties of the masonry infills are presented along with the corresponding out-of-plane test results in Table 10. Test results for five specimens are presented in Fig. 33. Results for the remaining specimens are presented in Appendix E. Values recorded for the out-of-plane tests indicate the strength of the infill panel; or the maximum measured pressure that was applied to the infill. The maximum pressure applied to the panels was recorded for cases where the capacity of the infill exceeded the capacity of the loading rig. Maximum lateral deformations in the infill were limited to 3% drift which was considered to be an upper bound for any loading condition.

Air bag contact area was smaller than the panel surface area. Conversion of the measured applied pressures to an equivalent uniform pressure consisted of equating the external virtual work required for the panel to undergo a unit displacement under both loading conditions. An illustration of the expression used in the pressure conversion is presented in Fig. 34. Because the difference between the air bag contact area with the infill and the infill panel surface area was small, the difference in the measured applied pressure and the equivalent uniform pressure was also small (5% to 10%); but with this procedure the small pressure difference was considered for better comparison of the measured experimental results.

5.2.1 Virgin Specimen (Test# 1)

The specimen was subjected to lateral pressures applied normal to the entire surface of the infill. The monotonically increasing pressures were increased gradually up to reaching the strength (171 psf) of the infill at which point the resisting capacity of the infill started to decay at a low rate. The test was continued until the limiting drift of 3% was reached. Pressure in the air bag was then released, and some elastic deformation was recovered with the larger part of the maximum deformation remaining as plastic deformation of the masonry as illustrated in Fig. 247.

Table 10 Specimen Out-of-Plane Test Results

Test Number	Infill Type	Infill h/t	Mortar Type	f_m (psi)	In-Plane Test		Out-of-Plane Test		
					Max. Values		Lateral Pressure		
					$\frac{\Delta_{max}}{h}$	Shear Stress (psi)	Unrepaired (psf)	Repaired (psf)	I.P. ** (psf)
1	brick	34	S	1670			171		
2a	brick	34	N	1575	0.344	271			
2b							84		
2c								417	
3a	brick	34	lime	1470	0.218	189			
3b							125		
3c								437	
4a	block	18	N	3321	0.094	135			
4b							622*		
5a	block	11	N	3113	0.062	196			
5b							673*		
5d									675*
6a	brick	17	lime	665	0.250	95			
6b							259		
6b2							221		
6c								644*	
6d									194
6t									637*
7a	brick	17	N	1596	0.250	169			
7b							642*		
8a	brick	9	lime	507	0.390	71			
8b							670*		

* – Maximum pressure values recorded for the infill, not the strength of the infill.

** – Maximum pressure values recorded for the infill, with in-plane forces corresponding to $2\Delta_{cr}$.

5.2.2 In-Plane Cracked Specimens Loaded to Ultimate Out-of-Plane Strengths (Tests# 2b, 3b and 6b)

A series of specimens cracked in the in-plane direction were then tested in the out-of-plane direction. Strengths, defined as the largest pressure carrying capacity, for Specimens 2b, 3b, and 6b are illustrated in Fig. 248, Fig. 250 and Fig. 255, respectively. These specimens behaved in a ductile manner by reaching their strengths at lateral drifts of approximately 1% (lateral drift was approximately half the panel thickness), and maintaining loading capacity up to the limiting

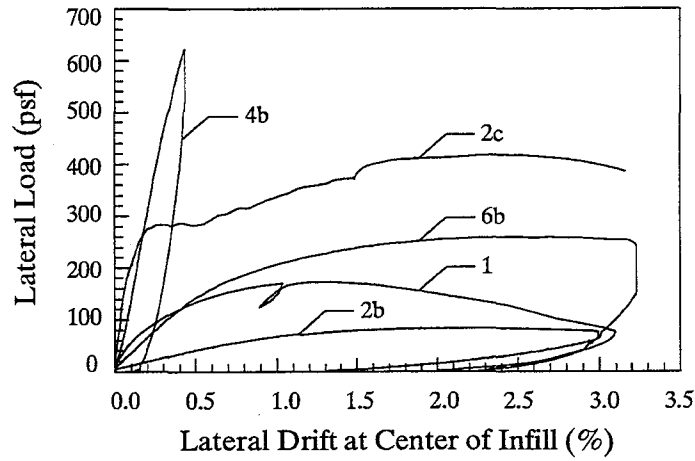


Fig. 33 Specimen Test Results

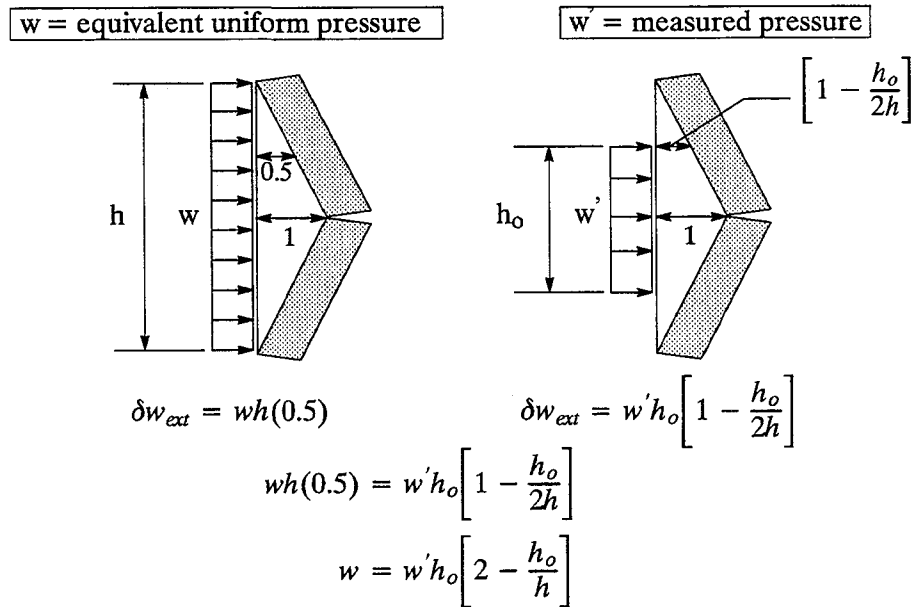


Fig. 34 Equivalent Lateral Load

deflection value of 3% drift. Removal of the applied pressure caused a recovery in the drift of the infill. A recovery of elastic deformation of over 50% of the maximum applied deformation can be obtained for these specimens as illustrated by Fig. 248.

Specimen 6b was tested for a second time in the out-of-plane direction to observe behavior under repetitive cycles. This second out-of-plane test was designated as Specimen 6b2. Its corresponding behavioral response is illustrated in Fig. 256. Comparison of results from Specimen 6b, and 6b2 indicates that even though the infill stiffness is greatly reduced, once the maximum lateral drift experienced by the infill was reached, the previously observed load capacity of the infill was again resisted as if the infill had never been unloaded.

5.2.3 In-Plane Cracked Specimen Not Loaded to Ultimate Out-of-Plane Strength (Tests# 4b, 5b, 7b and 8b)

A series of test specimens exceeded the capacity of the loading rig. For these specimens the strength of the panels was not measured; instead, the maximum applied force dictated by the capacity of the loading rig was recorded. Although it was not possible to determine the capacity of these panels, a limit for the lower bound of the load carrying capacity was defined. Maximum pressures applied to Specimens 4b, 5b, 7b and 8b, and their corresponding out-of-plane behavior is presented in Fig. 252, Fig. 253, Fig. 259, and Fig. 260 respectively. As illustrated, the stiffness of these specimens was large, and the observed behavior remained within the elastic range of the masonry. Test results for Specimens 7b, and 8b (Fig. 259 and Fig. 260) indicated that repetitive applied loadings within the elastic region did not affect the stiffness of the specimen. Small initial plastic deformations remaining in the panels was attributed to cracking of the panels, which could not be restored. Also, a slight panel rotation was needed so that the masonry could come in full contact with its surrounding frame. This rotation was small and depended mostly on the amount of damage that had been done previously during the in-plane test. Once the deformation required to close the cracks was reached, the repetitive applied loadings did not cause any additional permanent deformation of the panels.

5.2.4 Repaired Specimen (Tests# 2c, 3c and 6c)

Experimental results obtained for repaired Specimens 2c, 3c, and 6c are presented in Fig. 249, Fig. 251 and Fig. 257. Test Specimens 2c and 3c reached their corresponding strengths within the allowable capacity of the testing rig, which Specimen 6c exceeded.

The behavior of these specimens can be divided into three stages. First, the specimens were observed to possess a large stiffness up to cracking of the coating. Once the coating had cracked and the lateral deformation continued to increase, the cracks expanded and increased in size. In the third stage, the steel mesh started to debond from the repairing coating and the lateral load was resisted by arching action. The strength remained constant with no serious sign of decay at the limiting maximum lateral drift.

The large vertical crack dividing the infill into two equal halves (Specimen 2c) did not affect the lateral strength or ductility of the infill. The principal load resisting moment was developed along the short direction of the span (vertical direction).

The out-of-plane strength of Specimen 6c exceeded the capacity of the testing rig. Repetitive loadings were applied to this specimen in the same manner as was done to Specimens 7b and 8b. Out-of-plane response of Specimen 6c was similar to Specimens 7b and 8b, with a difference in having a much smaller amount of initial plastic deformation.

5.2.5 In-Plane Cracked Specimen with In-Plane Shear

Tests of Specimens 5d and 6d were done to determine the behavior of an infill panel when subjected to lateral loads in both parallel and horizontal directions. In-plane lateral forces during the out-of-plane tests were of the same magnitude as the largest forces applied during the in-plane

testing of the infills (196 psi and 95 psi respectively). On completion of the in-plane tests the infill panels were slightly “loose” from their confining frames. During tests 5d and 6d this “looseness” did not appear because the infill was confined along one diagonal of the panel while the opposite diagonal of the panel became detached from the frame as illustrated in Fig. 20(c). This confinement was an important factor when observing the out-of-plane behavior of Specimens 5d and 6d. Specimen 5d exceeded the capacity of the loading rig. When comparing results from Specimen 5d to a similar specimen with no in-plane applied forces (Specimen 5b) the measured curves indicate that the extra confinement applied by the lateral load on the infill produced a slightly stiffer response for the out-of-plane test of the same panel. Specimen 6d produced an out-of-plane strength lower than the capacity of the rig. Results for Specimen 6d can be compared to Specimen 6b2 which did not include applied lateral in-plane forces. The behavior observed for Specimen 6d was stiffer during the first part of the testing due to the development of compressive stresses in the infill resulting from the applied in-plane force. It was observed that once compressive stresses caused by the confinement provided by the in-plane lateral force were exceeded, panel stiffness reduced at a greater rate than if no in-plane load had been applied. Therefore, the stiffness for Specimen 6d reduced when compared with that of Specimen 6b2. Specimen 6d produced an out-of-plane strength close to the strength reached by Specimen 6b2 at the limiting lateral drift of 3%.

5.3 Out-of-Plane Tests – Discussion of Observed Response

In this section the effects of various parameters on out-of-plane strength of the panels are discussed.

5.3.1 Effects of In-Plane Cracking

Comparison of experimental test results for Specimens 1, 2b and 3b (Fig. 247, Fig. 248 and Fig. 250) indicates that in-plane damage decreases the out-of-plane strength. For infill panels with large slenderness ratios, the in-plane cracking reduces the out-of-plane strength by as much as a factor of 2 depending on the amount of in-plane damage. Specimen 2b resisted half the strength observed for a similar infill with no previous in-plane damage. Comparing Specimen 2b and 3b (Table 10), suggests that out-of-plane strengths of similar infills with different extents of in-plane damage are different. Strength of Specimen 3b was 50% larger than Specimen 2b. The out-of-plane strengths for panels with smaller slenderness ratios were influenced by in-plane cracking, but in a smaller magnitude.

5.3.2 Effects of Deterioration in the Frame–Infill Boundary

Frame–infill boundary conditions varied according to the amount of in-plane damage experienced by each specimen. These boundary conditions varied from almost fully restrained against translation and rotation for the virgin specimen to more flexible supports for cracked specimens. Although no specimens failed by punching out of the panel, some of the specimens were slightly loosened from the confining frame, and therefore a larger lateral deflection of the panels, and also

a larger rotation of the panel segments, was required for a panel to reach its out-of-plane strength (compare Fig. 247 and Fig. 248).

5.3.3 Effects of Gravity Loads

In order to better understand how the gravity loads affect the out-of-plane strength of infills, a set of specimen tests were carried out: one with no vertical load (Specimen 6t) while the second specimen had a vertical load producing a compressive stress of approximately 20 psi (Specimen 6c) in the infill. Load-deflection curves for out-of-plane loading were almost identical for the two specimens (figure for Specimen 6t was similar to Fig. 257 for Specimen 6c). No new cracks were created during testing of Specimen 6t. Vertical stress caused the specimen to act in a slightly stiffer manner until the vertical stress was overcome by the out-of-plane loading. Once this occurred, the behavior of the two specimens could not be distinguished from each other.

5.3.4 Effects of Tensile Bond

Effects of the masonry tensile bond strength in virgin panels was evaluated by Dawe [22]. A set of panels: one with mortar and one dry-stacked were constructed to evaluate these effects. It was concluded that although the panel acted in a more flexible manner at the start of the testing, the masonry deformed into a similar deflected dome shape. Once panels were cracked, both specimens observed a similar type of behavior for the remaining part of the testing.

Experimental results for Specimens 1, 2b and 3b confirm the notion that the tensile strength of the mortar affects the initial stiffness of the specimen. Specimen 1 (Fig. 247) tested in the virgin state acted in a stiffer manner when compared to Specimens 2b (Fig. 248) and 3b (Fig. 250). With Specimens 2b and 3b, the tensile bond strength of the panels was nonexistent since the masonry had been previously cracked with in-plane loads.

5.3.5 Effects of Repair Method

Specimens that were tested to their ultimate strength were the only ones repaired (Specimens 2b, 3b, and 6b).

Specimens 2b and 3b were repaired and retested; these specimens (once repaired became 2c and 3c) when retested produced results illustrated in Fig. 249 and Fig. 251. Observations made from these experimental results indicated that the repairing method increased the out-of-plane strength of the panels by a factor of nearly 5. Also, Specimens 2c (Fig. 249) and 3c (Fig. 251) produced comparable out-of-plane lateral strengths indicating that the strength developed by the repairing method was not affected by the amount of previous damage done to the panel.

The repairing method was also used for repairing Specimen 6b. The repaired specimen (Specimen 6c) was then retested in the out-of-plane direction as the previous specimens. This specimen resisted pressures of at least 2.5 times the original strength, and exceeded the capacity of the rig.

The repair method was effective in terms of increasing the out-of-plane strength for two different reasons: 1) repaired panels had a smaller slenderness ratio (h/t), and 2) compression

strength of the repairing materials was higher. As discussed by McDowell [50, 51], Hendry [40, 41] and other authors in Chapter 2, the lateral strength of the panel varies with the square of the slenderness ratio of the panel, and linearly with the compressive strength of the masonry.

5.4 Existing Analytical Model Predictions

In this section, a number of different analytical models used to estimate the out-of-plane strength and behavior of panels are compared to experimental results. An explanation of the existing analytical models is presented in Section 2.2.2. The comparison between the existing analytical models and the experimental results are presented to better understand model deficiencies. Presented methods do not consider effects caused by existing in-plane damage in the panel. Numerical models vary from elastic plate theory to models based on arching action and inelastic behavior. Behavior based on three such theories is contrasted with experimental results (Specimen 6b) in Fig. 35.

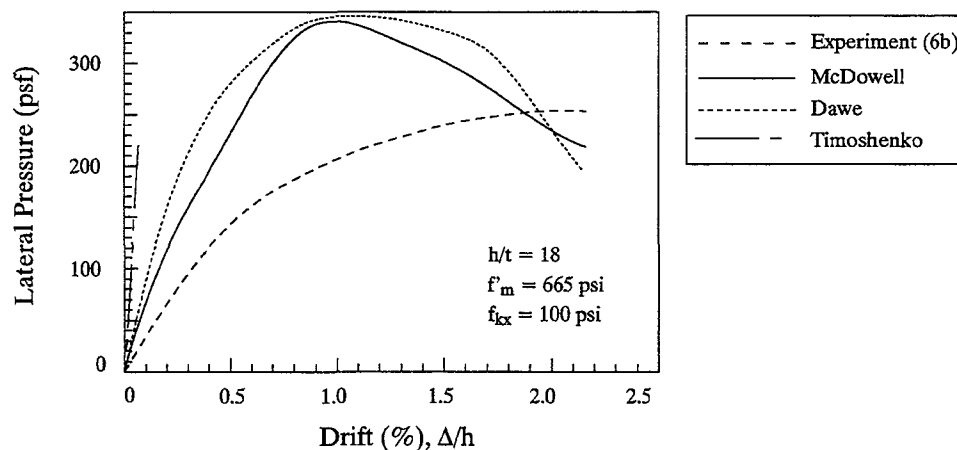


Fig. 35 Comparison of Various Theories with Experimental Results

The simplest model to represent two-way bending of an infill is an elastic plate. Classical solutions derived by Timoshenko [79] are available for determining linearly elastic, isotropic, homogeneous material behavior of rectangular plates. Since the analysis is elastic, no post-cracking behavior is considered. Failure is assumed to occur once the maximum tensile stress reaches the stress required for cracks to occur. The solution does not model the flexibility of a cracked infill; thus, predictions by the model are overly stiff when compared with the test results as illustrated in Fig. 35.

McDowell, McKee and Sevin [50, 51] at the Armour Research Foundation (ARF) developed a theory based on arching action for a one-way strip of unreinforced masonry confined by rigid boundaries. Their theory showed that masonry walls with full end restraint could withstand much larger lateral loads than predicted by means of conventional elastic or elasto-plastic bending analyses. Unlike the previous formulations which are limited by flexural tension, panel strength per McDowell is limited by compressive stress. McDowell theory results show a stiffer and stronger response than the specimen experimental results as illustrated in Fig. 35. Though the test panel spans

in two directions rather than one as assumed, measured behavior was still more flexible than that predicted by the McDowell theory. This difference is attributed to the pre-cracked condition of the infill specimen.

Dawe [22] developed a strength theory based on virtual work concepts and includes two-way arching action. Like McDowell [50, 51], transverse strength is limited by compressive stress along the edges of a segment rather than a tensile stress. With Dawe's method, computer-aided techniques were used to predict the first crack and ultimate infill capacity. The model was modified to predict behavior based on arching action of a panel confined by within a flexible frame. As shown in Fig. 35, Dawe's theory produces a stiffer and stronger response than McDowell's theory because two-way action is considered rather than one-way action. However, since edge flexibility is introduced with Dawe's theory, the differences between the two curves are minimized.

Theories by both McDowell and Dawe give peak strengths that are larger than that of the test panels. This difference is likely due to pre-existing, in-plane cracking. The test specimen required a greater deflection to reach its ultimate capacity than that predicted by the two arching action models as illustrated in Fig. 35.

Theories described suggested that strength is proportional to the inverse of the square of the h/t ratio. The influence of the h/t ratio on strength is shown in Fig. 36 where theoretical curves based

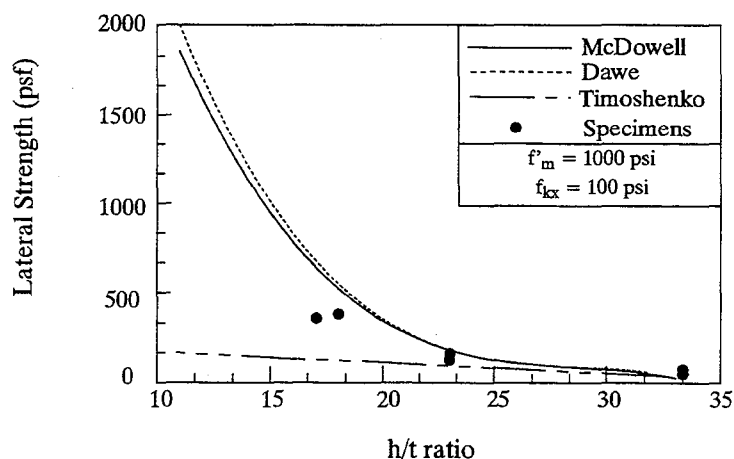


Fig. 36 Effect of h/t on Lateral Strength

on the Timoshenko formulation as well as the two arching action models are plotted along with the experimental results. A nominal masonry compressive strength equal to 1000 psi has been used to plot curves based on the McDowell and Dawe theories. Analytical model predictions based on arching action over estimates the out-of-plane strength of panels, while the elastic plate theory underestimated it. This was concluded based from comparison of experimental results to model predictions as illustrated in Fig. 36. The large overestimation by the arching action models was attributed to the lack of consideration of the existing panel damage.

5.5 Correlation with Dynamic Test of Half-Scale Model

The U.S. Army Construction Engineering Research Laboratories (USACERL) have performed a series of dynamic tests on similar but half-scaled R/C frames with masonry infills. A typical testing specimen is illustrated in Fig. 37.

The tests were performed on the Biaxial Shock Testing Machine (BSTM) at USACERL to evaluate the dynamic behavior of the masonry infill systems. Each model was constructed of two, single-bay, single-story, reinforced concrete frames with a top concrete slab spanning between them. The frames were infilled with masonry panels with a slenderness ratio (h/t) of 18. Masonry panels were constructed using half-scale bricks and a Type N mortar.

Testing of the specimens consisted of first applying dynamic accelerations to the specimen in the direction parallel to the plane of the infill. Secondly, specimens were rotated 90 degrees and accelerations were then applied normal to the infill. Dynamic testing was performed by subjecting

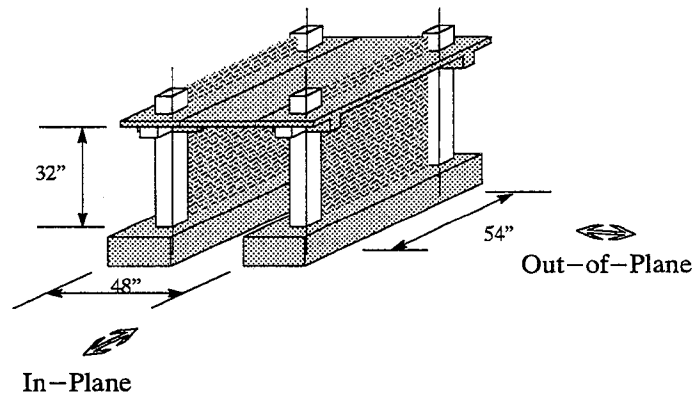


Fig. 37 Directions of Applied Motions

each test specimen to a series of scaled El Centro earthquake records. Testing of the specimens was stopped once the infill was relatively damaged. This point was arbitrarily chosen based on the mechanical properties of the masonry, on its dynamic behavior observed during the tests, and on visual inspection.

Out-of-plane dynamic results for virgin and previously cracked infills are presented in Fig. 38. Lateral deflections and lateral accelerations plotted in the figures were recorded at the center of the panel. Direct comparison of the behavioral response is reasonable for the virgin and the pre-cracked infill specimens.

The out-of-plane strength reduction resulting from in-plane cracking was obvious. Specimens were loaded up to a pressure level such that similar amounts of out-of-plane damage occurred to the panels; this relatively severe infill cracking was designated as the upper limit of loading applied to the structure. This upper limit does not refer to the strength of the panel, rather the maximum pressure applied to the specimen during the out-of-plane tests. The previously in-plane

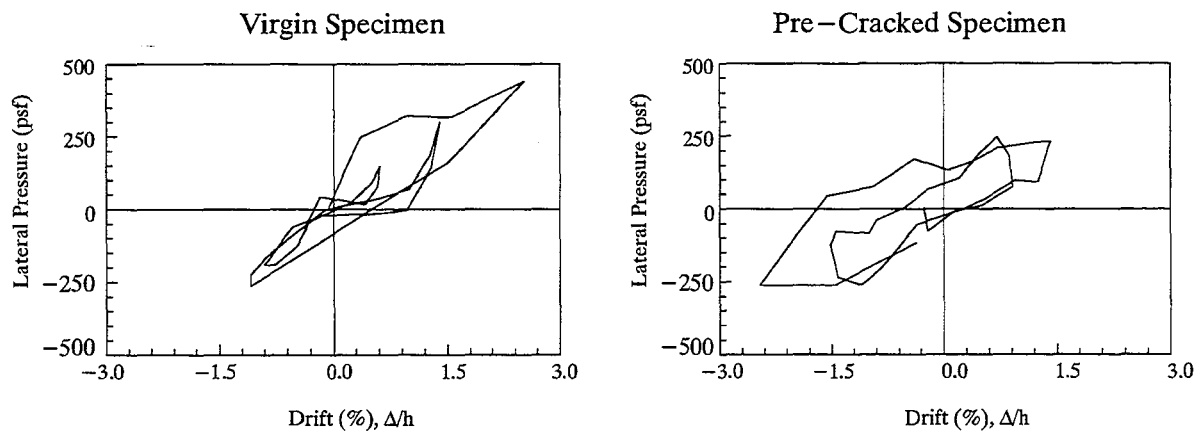


Fig. 38 Dynamic Out-of-Plane Test Results

cracked infill panel resisted smaller lateral than pressures resisted by a similar panel tested under virgin conditions. This reduction in out-of-plane capacity directly correlates with observations based on static testing as previously reported in this chapter.

Static results obtained for Specimen 6b are comparable to the specimens tested dynamically at USACERL. The masonry for Specimen 6b had a compressive strength equal to 665 psi. This corresponded to 14% the compressive strength of masonry used in the dynamic experiments. This is an important difference because the out-of-plane strength should be directly proportional to the masonry compressive strength (Section 2.2.2.2).

Static results for Specimen 6b represented the actual ultimate out-of-plane strength while the dynamic results obtained from a similar type of infill panel with a much larger compressive strength did not reach the strength of the panel. A comparison of the out-of-plane behavior observed from dynamic results with static results is presented in Fig. 39 for a normalized compressive strength of 4800 psi. In addition to being strong in the out-of-plane direction, these types of panels were observed to be ductile. For comparison of results for pre-cracked specimens shown in Fig. 39 an important factor has to be considered: dynamic tests were loaded up to cracking of the panel while static tests were tested to ultimate out-of-plane strength of the infills. Comparison of dynamic experimental results and static experimental results (Fig. 39) both agree that a considerable amount of strength and ductility remained in the panels after a severe degree of out-of-plane cracking occurred. This reserve of strength and ductility for cracked panels was attributed to arching action.

An important difference in the out-of-plane behavior was observed between the dynamic and the static tests. During dynamic out-of-plane testing displacement of the cracked panel segments relative to the frame was observed. This was not the observed during static testing. Relative displacements between each of the masonry segments caused the effective contact thickness between the segments to become smaller than the panel thickness. Because the strength and the stiffness of the panels should depend on the square of slenderness ratio (h/t), as discussed in Chapter 2, the

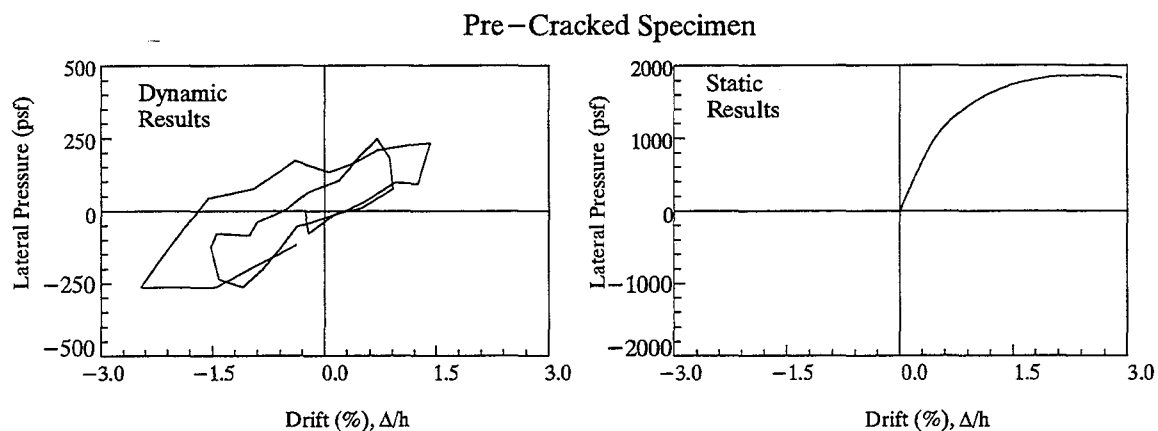


Fig. 39 Static-Dynamic Out-of-Plane Test Results Comparison

decrease in effective thickness of the panel (increase in slenderness ratio) greatly decreases panel strength and the stiffness as illustrated in Fig. 39.

Behavior observed during dynamic testing favorably compared to the behavior observed statically in several ways: 1) existing in-plane cracking affected the out-of-plane strength and stiffness of the panel, 2) the stiffness and the strength of the panels varied with the slenderness ratio of the panel, and 3) large ductility was available in the panel after cracking had occurred.

5.6 Correlation with Existing Structures

The program under the direction of James A. Hill [42] included destructive testing of three infill panels in an existing building scheduled for demolition. The program addressed the out-of-plane response of unreinforced, unanchored infill panels to lateral loading. Loads were applied by hydraulic jacks which were alternately loaded, unloaded, and reloaded in order to monitor the cyclic behavior and stiffness deterioration of the masonry under a repeated loading sequence. The test setup is illustrated in Fig. 40.

Testing was performed at the third level of a seven-story building which provided a relatively stiff confinement for the infills. Three panels were selected for testing. The selection of the panels was decided to cover a wide range of supporting conditions. The first testing panel consisted of a solid rectangular panel supported along all four edges; the second configuration represented a solid panel spanning only in the vertical direction; and the final panel was selected to represent panels with a number of openings.

Experimental results obtained at the University of Illinois are compared only to the first type of panels represented in the full scale testing program. Full scale specimens for these panels supported along the four edges consisted of a rectangular solid 13" unreinforced clay brick infill panel with a floor-to-floor height of 10'-6" and an overall length of 20 ft. The specimen was subjected to a series of loads which increased monotonically. The range of the applied loads increased as the number of

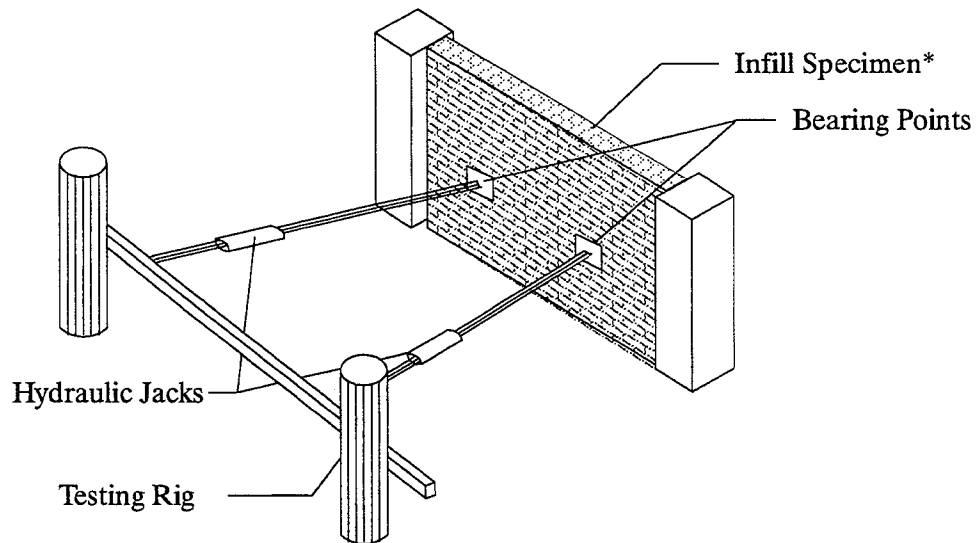


Fig. 40 Testing Rig For Testing of Existing Structure
*(not to scale)

cycles increased until reaching the limiting capacity of the loading rig. The maximum capacity of the loading rig corresponded to an equivalent lateral pressure of about 120 psf with a maximum lateral drift of about 0.6%. The behavior monitored during the testing of the specimen [42] (Fig. 41) showed that the specimen was always in the elastic region. Alike specimens tested at the University of Illinois

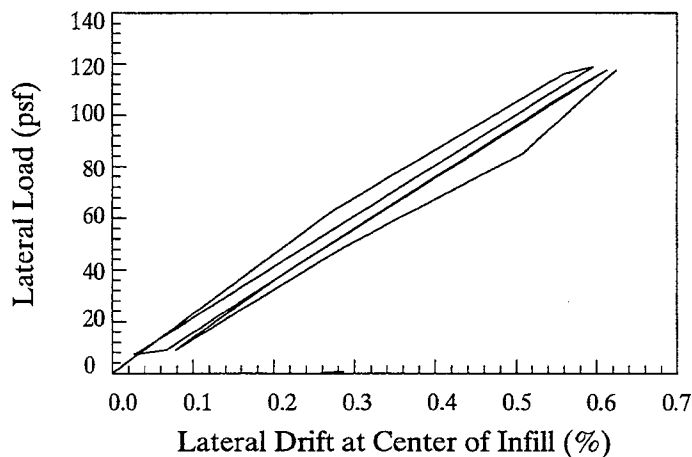


Fig. 41 Results for Full Scale Testing

with capacity exceeding the corresponding loading rig, the out-of-plane behavior of the panels was observed to be linearly elastic and only minor plastic deformations remained in the panel after removal of the lateral load. In addition, at the peak applied load there was no indication of strength decay in the infill; therefore, as for panels tested at the University of Illinois, a large reserve in out-of-plane capacity remained after cracking of the panels.

Behavior observed during testing of a panel located in a building favorably compared to the behavior observed statically in a couple of ways: 1) the stiffness of the panels remained linear within the elastic region of the masonry, and 2) a large reserve in out-of-plane capacity remained after cracking had occurred.

5.7 Conclusions

A series of experimental tests focusing on the out-of-plane strength and behavior of unreinforced masonry panels were performed. Measurements of test results were analyzed to show correlation between the specimens and to evaluate the effects of parameters on the out-of-plane strength of the panels. Finally, static test results were compared to dynamic results obtained from similar but half-scaled models, and to results from tests done on masonry panels located in an existing building.

Conclusions regarding out-of-plane behavior were:

- The final crack pattern and deformed shape of the panels were similar to yield line patterns observed in two-way slabs.
- Application of repetitive loadings within the elastic region did not affect the stiffness of the specimen.
- Application of in-plane shear stress slightly increased the initial out-of-plane stiffness.
- For infill panels with large slenderness ratios, in-plane cracking reduced the out-of-plane strength of the panels by a factor as high as two depending on the amount of in-plane damage experienced by the specimen.
- Gravity loads slightly increased the initial stiffness of the panel, but the out-of-plane strength of the panel was not affected.
- The flexural tensile bond strength of the masonry slightly increased the initial stiffness of the panel, but the out-of-plane strength of the panel was not affected.
- Repairing infill panels increased the out-of-plane strength of damaged panels by a factor as high as five.
- The out-of-plane strength of repaired infills did not depend on the amount of initial damage experienced by the panels.
- Out-of-plane strength and stiffness of the cracked test panels are overestimated by existing analytical models.
- Good comparison was found between the results obtained from the laboratory tests and the testing of existing structures.

- Comparison between dynamic and the static tests agreed in that: out-of-plane stiffness and strength depended on the compressive strength and the slenderness ratio of the panels; existing in-plane damage reduced the out-of-plane strength of the panels.

CHAPTER 6

DESCRIPTION OF ANALYTICAL MODEL

A method is presented for determining the transverse uniform pressure that cracked or uncracked masonry infill panels can resist. The method is based on arching action for a strip of infill that spans between two rigid supports. If panels are located in adjacent bays or stories, then by continuity, rotations at boundaries may be considered to be fully restrained. Two different types of failure modes are distinguished: one being crushing along the edges for panels with a low h/t ratio, and the other being snap through for panels with large h/t ratios. An expression for the critical slenderness ratio is derived to differentiate between these two failure modes.

6.1 Analytical Derivation

An infill panel is idealized as a strip of unit width that spans between two supports fully restrained against translation and rotation. A uniformly distributed lateral load is applied normal to the plane of the panel. Because of a previous in-plane loading, the panel is considered cracked in an x pattern. This is modeled with the worst case situation using a unit one-way strip that is cracked at mid-span. Cracking separates the strip into two segments that rotate as rigid bodies about their supported ends as shown in Fig. 42. Although the tensile strength of the panels is neglected and

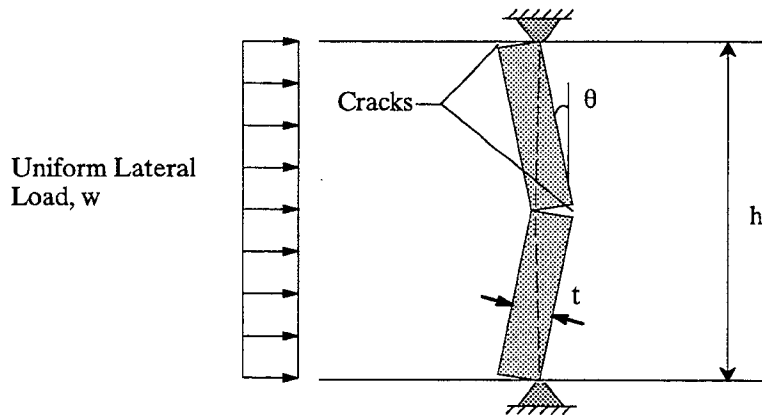


Fig. 42 Idealized Loading and Behavior of Unit Strip of Infill Panel

formation of cracks is not important for estimation of the out-of-plane strength of the panels, the deterioration in the infill caused by the repetitive in-plane cyclic loading varies the out-of-plane behavior and strength of the panels as explained in Section 5.3.1. A factor to account for this effect is developed in a later section.

For a particular lateral load, w , there is an associated rotation, θ , of the strip segments. This results in a compressive strain in the masonry which is largest at the supports and the center of the panel. Thus, the transverse strength of the strip is limited by crushing at the boundaries. Conversely, a panel may snap through the bounding frame if the length of its diagonal strut is compressed to a

length less than $h/2$. This suggests that the predominant mode of failure for panels with a low h/t ratio is the former mode while for panels with a high h/t ratio is the latter mode.

6.1.1 Parameters

The uniform lateral load, w , can be estimated based on statics. The free body diagram for the lateral load resisting mechanism is presented in Fig. 43. As shown in Fig. 43, the direction of the thrust

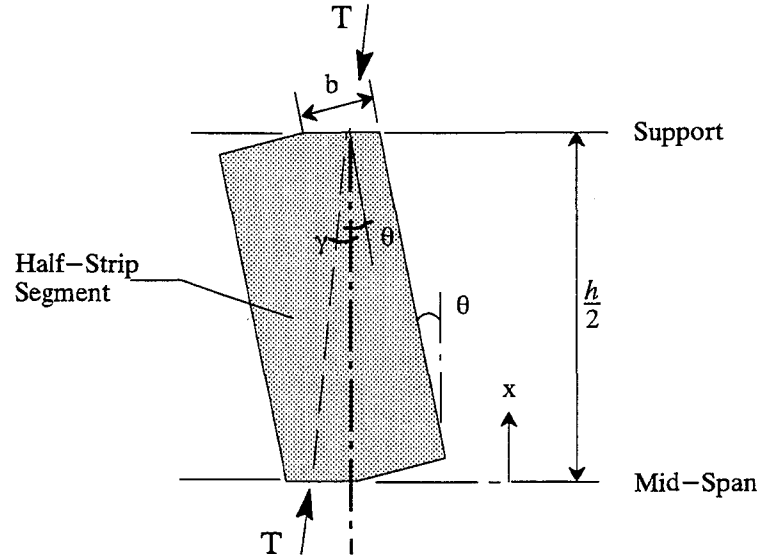


Fig. 43 Masonry Deformed Shape

force with respect to an undisturbed vertical reference line, γ , is dependent on the rotation of the half span, θ , and on the location of the thrust resultant. The centroid of the force is dependent on the bearing width, b , and on the compressive stress distribution along this width. Therefore, the primary variables for panel strength are γ , b , and θ .

These variables are functions of the compressive edge strain at the support, and the distribution of strain along the height.

6.1.2 Lateral Force Capacity

The transverse load that is applied uniformly to a strip can be related to the thrust force by summing horizontal forces that act at the mid-span hinge (Fig. 44). If the thrust force is equated to the internal compressive force, then expressions Eq. [21] through Eq. [24] can be obtained relating the load, w , to the maximum compressive stress at the support. Eq. [21] is valid only for small angles. The expressions considers only the component of the forces developed by thrust in the arch, excluding the minimal contribution by flexure as a beam. Any developed flexural stresses in the segments of the beam are at most an order of magnitude smaller than the developed axial stresses forming the thrust in the arch. The term f_b is the maximum compressive stress at the support, and may be determined from the corresponding strain if the stress-strain relation for the masonry in compression is known (k_t represents the ratio of peak stress to average stress in the masonry). The strain, ϵ_{\max} , can be

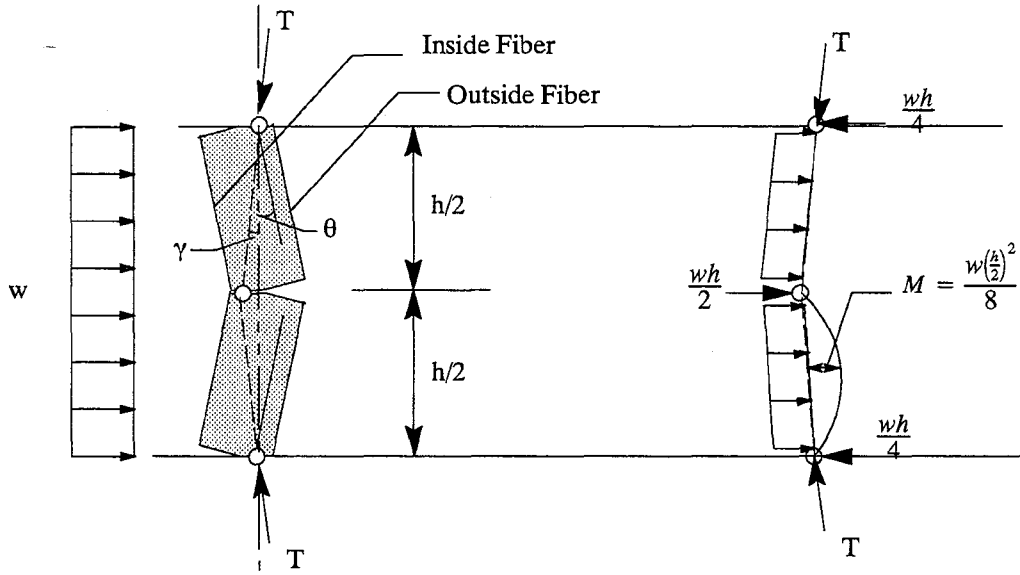


Fig. 44 Equilibrium of Strip Segment

$$\frac{wh}{2} = 2T \sin \gamma \quad \text{Eq. [21]}$$

$$T = k_1 b f_b \cos \gamma \frac{1}{\cos \theta} \quad \text{Eq. [22]}$$

$$w = \frac{4}{h} k_1 b f_b \cos \gamma \frac{1}{\cos \theta} \sin \gamma \quad \text{Eq. [23]}$$

$$w = \frac{4 k_1 \left(\frac{b}{t}\right) f_b \frac{\cos \gamma}{\cos \theta} \sin \gamma}{\left(\frac{h}{t}\right)} \quad \text{Eq. [24]}$$

expressed in terms of the total shortening along the outside face which is the variable that is used to determine the angles, γ and θ , and the compressed width, b .

6.1.3 Axial Shortening of Extreme Fiber

It is assumed that compressive strains at the outside fiber vary linearly along the length of the half-strip segment (Fig. 44). At the support, strains are maximum while at mid-span they are relieved entirely because of the open crack. The opposite strain distribution exists along the inside fiber. The total shortening of the outside fiber over the length of the half strip, Δ , is then found by integrating these strains along the half length as shown (Eq. [25]). This shortening is used as the basis for determining the rotation of the half-strip segment, and thus the angle of the thrust force. For convenience, a dimensionless parameter c is introduced in the format presented in Eq. [26].

$$\Delta = \int_0^{\frac{h}{2}} \varepsilon(x) dx = \int_0^{\frac{h}{2}} \left[\frac{\varepsilon_{\max}}{\frac{h}{2}} \right] x dx = \frac{1}{4} \varepsilon_{\max} h \quad \text{Eq. [25]}$$

$$c = \frac{\Delta_1}{h} = \frac{1}{4} \varepsilon_{\max} \quad \text{Eq. [26]}$$

6.1.4 Location of Thrust Centroid

As a secondary concern, the angle of the thrust force (T) is dependent on the location of the centroid of the compressive stress distribution at the support. This location is a function of the shape of the stress–strain curve for masonry in compression which is dependent on the strain level. It is possible to express the shape of the constitutive relation in terms of two variables: k_1 which represents the ratio of peak stress to average stress, and k_2 which represents the location of the centroid of the stress distribution. Since these values vary with the strain level, the location of the stress resultant changes with the angle of thrust. For the analytical model to be complete, it should include k_1 and k_2 factors; however, since there are no commonly accepted relations of these parameters with strain level and it would complicate the analysis unjustifiably, a simple triangular distribution of stress is assumed which remains constant for all levels of strain.

For a triangular distribution of compressive stress, the average stress across the stressed area is equal to 0.5 times the peak stress, and the centroid is located at a distance equal to 0.33 times the depth of the compressed zone from the extreme compressive fiber. Thus, k_1 and k_2 are taken to be 0.50 and 0.33 respectively. A detailed discussion of the development of k_1 and k_2 and the sensitivity analysis for the different distributions is presented in Appendix G.

6.1.5 Bearing Width at Support

The deflected shape of a half strip segment is shown in Fig. 45. From simple geometric relations, the dimensions δ and a can be derived as follows:

$$\delta = \frac{h}{4} \left(\frac{1}{\cos \theta} - 1 \right) \quad \text{Eq. [27]}$$

$$a = \frac{\delta}{\tan \theta} = \frac{h}{4} \left(\frac{1 - \cos \theta}{\cos \theta} \right) \frac{\cos \theta}{\sin \theta} \quad \text{Eq. [28]}$$

$$a = \frac{h}{4} \left(\frac{1 - \cos \theta}{\sin \theta} \right) \quad \text{Eq. [29]}$$

The compression width, b , is then determined from $t/2$ and a . A dimensionless factor representing the compression width in the panel in terms of the panel thickness is developed and presented in Eq. [31] to Eq. [34]. The derivation starts with the equation for the compression width (Eq. [30]).

Squaring both sides of the equation and substituting c for Δ/h :

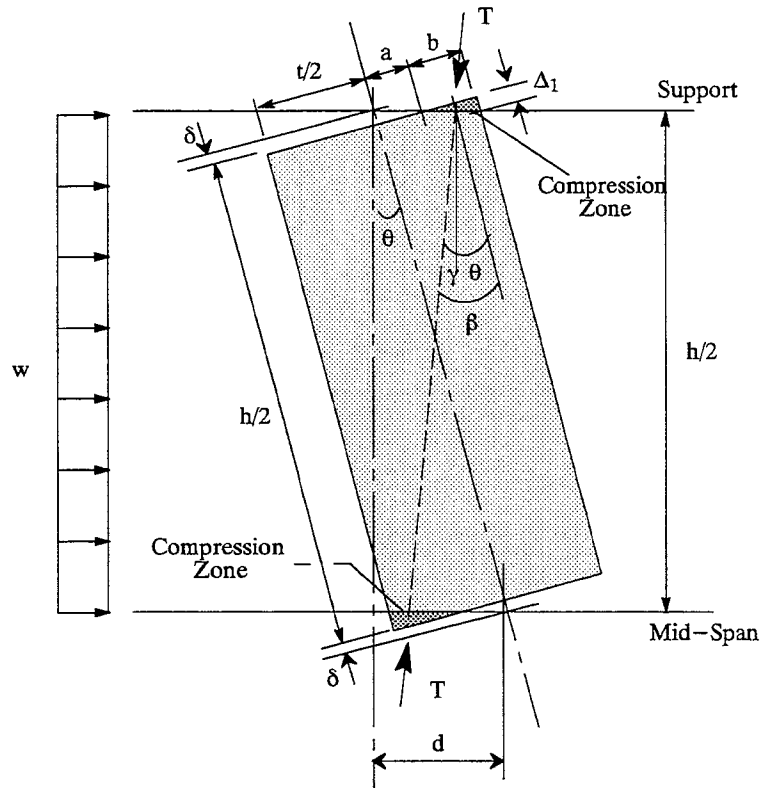


Fig. 45 Deflected Shape of Half-Strip Segment

$$b = \frac{t}{2} - a = \frac{t}{2} - \frac{h}{4} \left(\frac{1 - \cos \theta}{\sin \theta} \right) = \frac{t}{2} - \frac{h}{4} \left(\frac{\sqrt{\Delta_1^2 + b^2}}{\Delta_1} - \frac{b}{\Delta_1} \right) \quad \text{Eq. [30]}$$

$$\left(1 - \frac{h}{4\Delta_1}\right)b - \frac{t}{2} = -\frac{h}{4\Delta_1} \sqrt{\Delta_1^2 + b^2} \quad \text{Eq. [31]}$$

$$\left(1 - \frac{1}{2c}\right)b^2 - i\left(1 - \frac{1}{4c}\right)b + \left(\frac{t}{2}\right)^2 \left[1 - \frac{1}{4}\left(\frac{h}{t}\right)^2\right] = 0 \quad \text{Eq. [32]}$$

$$\frac{b}{t} = \frac{1}{2} \left[\frac{(1-4c)}{2(1-2c)} + \sqrt{\frac{1}{4(1-2c)^2} - \frac{c}{2(1-2c)} \left(\frac{h}{t}\right)^2} \right] \quad \text{Eq. [33]}$$

Since the term c is only a fraction of the strain, it is on the order of 0.001 and can be neglected when being subtracted from unity. With this simplification, Eq. [33] reduces to:

$$\frac{b}{t} \approx 0.25 \left[1 + \sqrt{1 - 2c \left(\frac{h}{t} \right)^2} \right] \quad \text{Eq. [34]}$$

6.1.6 Derivation of Angles

The angles, θ , γ and β , as illustrated in Fig. 45, can be derived based on trigonometric relations as shown below. Expressions for the tangents of these angles are given in terms of the b/t and h/t ratios.

$$\tan \theta = \frac{A_1}{b} = \frac{ch}{b} = \frac{c(\frac{h}{t})}{(\frac{b}{t})} \quad \text{Eq. [35]}$$

$$\tan \beta = \frac{t - 2k_2b}{\frac{h}{2} - \frac{2}{b}(1 - k_2)bA_1} \quad \text{Eq. [36]}$$

$$\tan \beta = \frac{2[1 - 2k_2(\frac{b}{t})]}{(\frac{h}{t})[1 - 4(1 - k_2)c]} = \frac{2[1 - 2k_2(\frac{b}{t})]}{(\frac{h}{t})} \quad \text{Eq. [37]}$$

$$\gamma = \beta - \theta \quad \text{Eq. [38]}$$

6.1.7 Lateral Deflection

In view of the rotation of the half panel, the lateral deflection at mid-span of the panel can be evaluated by Eq. [39]:

$$d = \left(\frac{h}{2} + \delta\right) \sin \theta = \frac{h}{4}(1 + \cos \theta) \tan \theta \quad \text{Eq. [39]}$$

Because the values for maximum θ are relatively small, Eq. [39] can be simplified into Eq. [40].

$$d \approx \frac{\theta h}{2} \quad \text{Eq. [40]}$$

6.2 Critical Slenderness Ratio (h/t)

The arching action theory is applicable only for a range of slenderness ratios (h/t) less than a limit at which snap-through of a panel occurs. The (h/t) ratio at which this occurs is termed the critical slenderness ratio. Based on Eq. [33], Eq. [41] and Eq. [42] are developed. The critical value for the slenderness ratio $\left(\frac{h}{t}\right)_{max1}$ of the panel is calculated using Eq. [41], and the corresponding

$\left(\frac{b}{t}\right)_{min1}$ ratio is estimated using Eq. [42].

$$\left(\frac{h}{t}\right)_{max1} = \sqrt{\frac{1}{2c(1 - 2c)}} \approx \frac{1}{\sqrt{2c}} \quad \text{Eq. [41]}$$

$$\left(\frac{b}{t}\right)_{min1} = \frac{1}{4} \left[\frac{1 - 4c}{1 - 2c} \right] \approx \frac{1}{4} \quad \text{Eq. [42]}$$

If the limiting value obtained in Eq. [41] is exceeded, Eq. [33] has no real roots. The physical interpretation of these limits occurs when the angle θ (angle of rotation of the panel) exceeds the angle

β (angle of rotation between the longitudinal fiber of the panels and the thrust force). Thus, the angle of rotation between the vertical axis and the thrust force (γ) becomes negative (refer to Fig. 45 for illustration of angles). Therefore, for values $\left(\frac{h}{t}\right) > \left(\frac{h}{t}\right)_{max1}$ the segments of the panel are then separated from each other, and the obtained results of the derived equations are not longer valid.

Further study shows that for slenderness ratio less than $\left(\frac{h}{t}\right)_{max1}$, it is still possible for the angle γ to be equal to or less than zero as illustrated in Fig. 46. Once the angle γ reaches a zero or negative

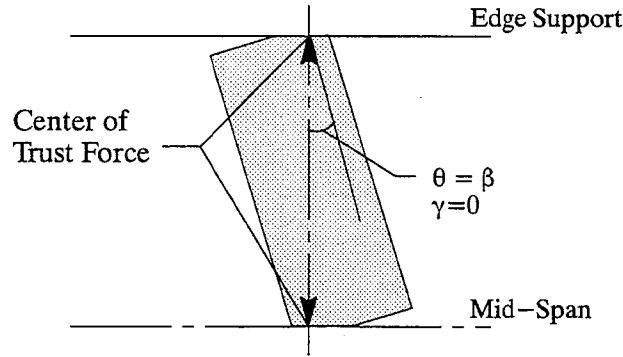


Fig. 46 Arching Action Vanishing

value, the arching action vanishes. The limiting value $\left(\frac{h}{t}\right)_{max2}$ and the corresponding $\left(\frac{b}{t}\right)_{min2}$ are estimated according to the following derivation:

$$\gamma = 0$$

$$\beta = \theta \rightarrow \tan \beta = \tan \theta \quad \text{Eq. [43]}$$

$$\frac{2[1 - 2k_2\left(\frac{b}{t}\right)_{min2}]}{\left(\frac{h}{t}\right)_{max2}[1 - 4(1 - k_2)c]} = \frac{c\left(\frac{h}{t}\right)_{max2}}{\left(\frac{b}{t}\right)_{min2}} \quad \text{Eq. [44]}$$

$$\left(\frac{h}{t}\right)_{max2} = \sqrt{\frac{2[1 - 2k_2\left(\frac{b}{t}\right)_{min2}]\left(\frac{b}{t}\right)_{min2}}{c[1 - 4(1 - k_2)c]}} \quad \text{Eq. [45]}$$

$$\left(\frac{h}{t}\right)_{max2} = \sqrt{\frac{2[1 - 2k_2\left(\frac{b}{t}\right)_{min2}]\left(\frac{b}{t}\right)_{min2}}{c}} \quad \text{Eq. [46]}$$

Similarly, from Eq. [33]:

By squaring both sides of the equation the result becomes:

$$\left(\frac{b}{t}\right)_{min2} = \frac{1}{2} \left[\frac{(1-4c)}{2(1-2c)} + \sqrt{\frac{1}{4(1-2c)^2} - \frac{c}{2(1-2c)} \left(\frac{h}{t}\right)_{max2}^2} \right] \quad \text{Eq. [47]}$$

$$\left[2\left(\frac{b}{t}\right)_{min2} - \frac{(1-4c)}{2(1-2c)} \right]^2 = \frac{1}{4(1-2c)^2} - \frac{c}{2(1-2c)} \frac{2 \left[1 - 2k_2 \left(\frac{b}{t}\right)_{min2} \right] \left(\frac{b}{t}\right)_{min2}}{c} \quad \text{Eq. [48]}$$

$$\left(\frac{b}{t}\right)_{min2}^2 - \frac{(1-8c)}{[4(1-2c) - 2k_2]} \left(\frac{b}{t}\right)_{min2} - \frac{2c}{4(1-2c) - 2k_2} = 0 \quad \text{Eq. [49]}$$

$$\left(\frac{b}{t}\right)_{min2} = \frac{1}{2} \left[\frac{\left(\frac{1}{2} - 4c\right)}{[2(1-2c) - k_2]} + \sqrt{\frac{\left(\frac{1}{2} - 4c\right)^2}{[2(1-2c) - k_2]^2} + \frac{4c}{[2(1-2c) - k_2]}} \right] \quad \text{Eq. [50]}$$

$$\left(\frac{b}{t}\right)_{min2} \approx \frac{1}{2} \left[\frac{1}{2(2-k_2)} + \sqrt{\frac{1}{4(2-k_2)^2} + \frac{4c}{(2-k_2)}} \right] \quad \text{Eq. [51]}$$

Estimation of $\left(\frac{b}{t}\right)_{min2}$ was done for a number of different values of c . The value for $\left(\frac{b}{t}\right)_{min2}$ was found to remain relatively constant at 0.30 for ϵ_{max} ranging from 0.001 to 0.004. Substituting the obtained value for $\left(\frac{b}{t}\right)_{min2}$ into Eq. [46] a simplified expression for $\left(\frac{h}{t}\right)_{max2}$ is obtained (Eq. [52]). Comparison

$$\left(\frac{h}{t}\right)_{max2} \approx \frac{0.981}{\sqrt{2c}} \quad \text{Eq. [52]}$$

of both upper limits of slenderness ratios $\left(\frac{h}{t}\right)_{max1}$ and $\left(\frac{h}{t}\right)_{max2}$ for developing arching action, evaluated by Eq. [41] and Eq. [52] respectively, shows that $\left(\frac{h}{t}\right)_{max2}$ produces a slightly smaller slenderness ratio for the limit of arching action vanishing. Therefore, it is necessary to evaluate only this second upper limit since it is the predominant for any range of c values (c is defined by Eq. [26]).

6.3 Failure Modes

The predominant failure modes for infills loaded normal to their plane vary according to a series of parameters in which the slenderness ratio (h/t) is one of the most important. The observed modes of failure of the masonry panels varied between two distinct mechanisms ranging from snap through, to crushing of the arch.

Loss of arching action occurs in slender members that form a small arch during the out-of-plane loading of the panel. The strain in the masonry needed for the strength of the panel to be reached is much smaller than the ultimate crushing strain of the masonry. Once the strength of the panel is reached, the capacity of the panel reduces rapidly until reaching zero. The lateral strength

of the panels become zero because of the excessive lateral deflection causing the arch to vanish. At this point of maximum lateral deflection, the strain observed in the edge fiber of the masonry remains less than the limit for crushing of masonry. An example of this type of behavior is shown in Fig. 47.

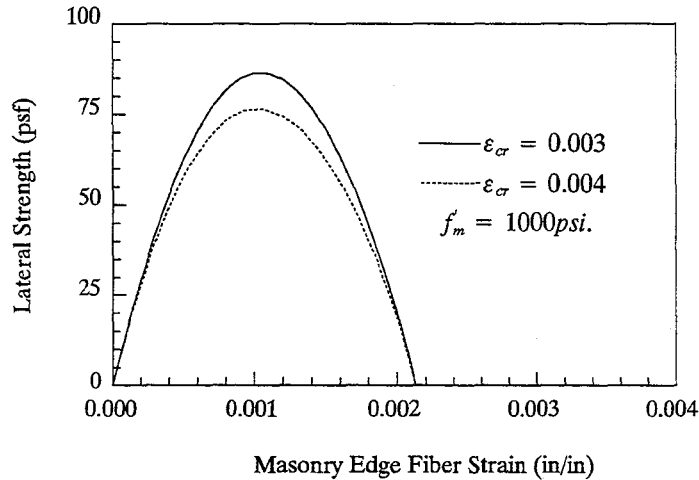


Fig. 47 Lateral Strength vs. Masonry Strain For Snap – Through

The example corresponds to an infill with a slenderness ratio (h/t) of 30. The crushing strain of the masonry (ϵ_{cr}) is varied between 0.003 and 0.004 (the effect of the crushing strain on the out-of-plane strength of the panel is explained in a later section). The strength of the panel occurs at a masonry strain (ϵ) of 0.001. Once the strength of the panel is reached, the capacity of the panel decreases with increasing lateral deformation.

The failure mode governed by excessive crushing of the masonry in the developed arch occurs in panels with low slenderness ratios. For this type of panel, the strength is developed at a masonry strain equal to the crushing strain. After the peak load is reached, the strength reduces slowly until the crushing strain is reached. An example illustrating this type of behavior is shown in Fig. 48. The example corresponds to the behavior of an infill with a slenderness ratio (h/t) of 10. The crushing strain of the masonry is varied for this example between the range of 0.003 and 0.004. As predicted, once the strength of the panel is reached, the capacity of the panel decreases with increasing lateral deformations up to the upper limit of the masonry crushing strain. At this point the strength is conservatively assumed to disappear, and the infill fails in crushing.

Critical values for slenderness ratios separating between arching and snap through mechanisms can be estimated with Eq. [52]. Critical slenderness ratios are presented in Table 11 for various crushing strains. Infills with a slenderness ratio larger than the value given in Table 11 will fail by snap through (i.e. for $\epsilon_{cr} = 0.002$, infills $h/t > 30.6$); otherwise, the failure mode will be attributable to crushing of the arch mechanism.

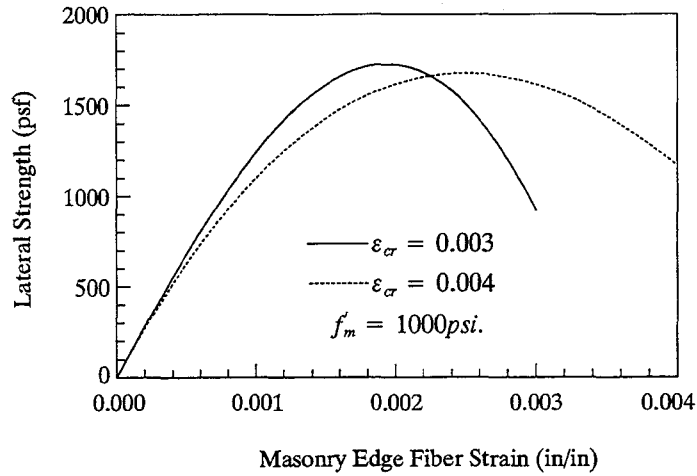


Fig. 48 Lateral Strength vs. Masonry Strain For Arching Mechanism

Table 11 Critical Slenderness Ratios

Crushing Strain (ϵ_{cr})	Slenderness Ratio
0.002	30.6
0.003	25.0
0.004	21.7
0.005	19.6

6.4 In-Plane Cracking Effects

A decreased in the out-of-plane capacity occurred in panels with existing in-plane damaged as observed from the experimental results presented in Appendix F. Based on the experimental results, the theory was modified to account for the in-plane damage done to the panels (in-plane damage effects on out-of-plane strength of panels are discussed in Chapter 5). The theory was modified to account for in-plane damage by adjusting the factor c as shown in Eq. [53].

$$c = \frac{2d}{h} = \frac{1}{2}\epsilon_{\max} \quad \text{Eq. [53]}$$

The factor of 2 in Eq. [53] was chosen to modify the theory based on the available experimental data. The adjustment made to the theory considers in-plane drifts reaching twice the drift required for cracking of the panels. For other magnitudes of in-plane damage, a different change should be applied to the constant c . The variation of the factor c corresponds physically to a larger lateral drift of the panel with a reduction in the out-of-plane stiffness and strength.

The out-of-plane strength of the panels is reduced according to the magnitude of existing in-plane damage. For the same amount of in-plane damage, the out-of-plane strength reduction

varies with the slenderness ratio of the panels. The out-of-plane strength reduction factor is illustrated in Fig. 49 for a range of slenderness ratios. The reduction factor was obtained using the

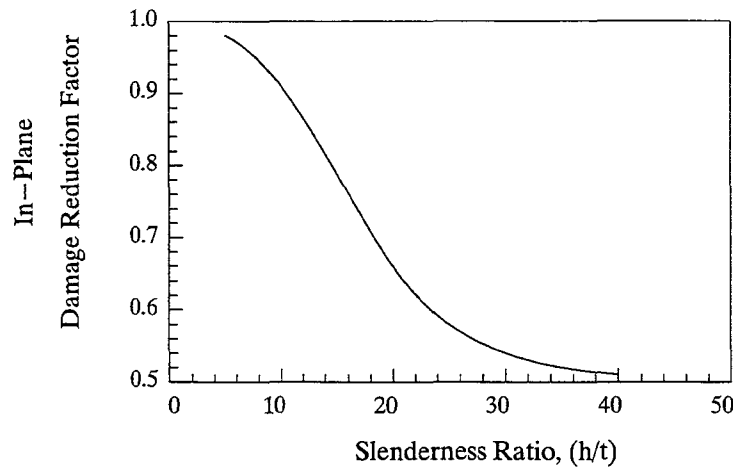


Fig. 49 In-Plane Damage Reduction Factor of the Panel vs. Slenderness Ratio ($f'_m = 1000\text{psi.}$)

analytical model modified in accordance to Eq. [53] for in-plane damaged infill panels. The reduction factor was evaluated as the panel strengths calculated based on the modified model for in-plane cracked panels normalized to the strength of the panel in a virgin state. Slender infills are greatly affected by in-plane damage. The strength for these slender panels can be reduced by a factor of two as shown in Fig. 49. Experimental results support this observation.

6.5 Slenderness Ratio and Crushing Strain Effects

As discussed in Section 2.2.2, the strength of the panels varies with the square of the slenderness ratio of the panel. This is demonstrated with Fig. 50 and Fig. 51. As the slenderness ratios

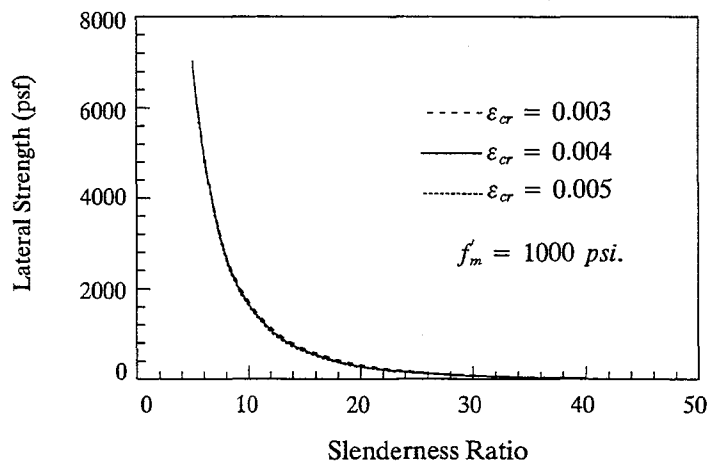


Fig. 50 Lateral Strength of Walls vs. Slenderness Ratio

of the panels decrease, the out-of-plane strength of the panels becomes very large. For a panel with a masonry compressive strength (f'_m) of 1000 psi with a slenderness ratio equal to 5, its strength reaches 7000 psf. For panels with larger slenderness ratios, the change in strength with a varying slenderness ratio becomes less accentuated, as presented in Fig. 51.

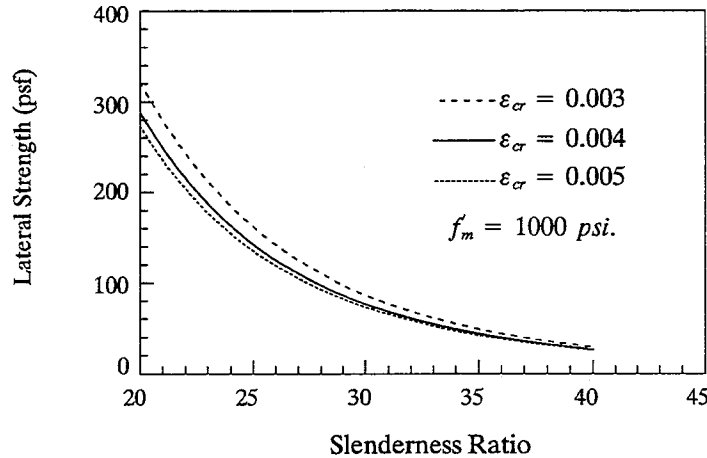


Fig. 51 Lateral Strength of Walls vs. Slenderness Ratio

The limit on masonry compressive crushing strain is another parameter in the evaluation of panel behavior. Variation in the crushing strain of the masonry affects the stiffness and the strength of the panels as illustrated by Fig. 47 and Fig. 48. The strength is slightly reduced along with the stiffness of the panels. The change in the out-of-plane strength given a change in the compressive crushing strain of the masonry for a certain range of slenderness ratios is illustrated in Fig. 50 and, Fig. 51. When the crushing strain of the masonry is varied between values of 0.003 and 0.005, the out-of-plane strength of the panels is not greatly affected. This statement is true for low values of slenderness ratios. For small values of slenderness ratios (Fig. 51) the difference in the out-of-plane strength given a change in the compressive crushing strain is more significant. Based on the illustrations presented, a maximum strength reduction of 14% was observed for slender infills by varying the crushing strain of the masonry between the range of 0.003, and 0.005. Thus, for an accurate estimation of the out-of-plane strength of the panels, an adequate value for the crushing strain of the masonry should be provided. Values used for the analytical estimation of the out-of-plane strength of the panels in this project were obtained from experiments done in this and other projects [14, 20, 35]. A nominal ultimate crushing strain value equals to 0.004 was determined for the masonry infill panels.

6.6 Correlation Between Analytical and Experimental Data

In this section experimental data is compared to results using the analytical model described in Section 6.1. In addition, the arching action model of McDowell is also contrasted with the experimental data.

compared well to the measured panel behavior. Evaluation of the panel also included the deterioration in the out-of-plane strength caused by the existing in-plane damage.

Specimen 7b (slenderness ratio of 17) was expected to follow a similar type of behavior as that observed for Specimen 6b, with a larger out-of-plane strength since its masonry compressive strength was much higher. The analytical results increased by a factor of the same magnitude as the increase in the prism compressive strength. The measured experimental data for this specimen did not agree with this relationship. The out-of-plane strength of the panel increased by such a magnitude that its capacity exceeded the capacity of the loading rig as illustrated by Fig. 259. Although the initial stiffness of the panel was relatively well predicted, the strength of the panel was not. The estimated strength of the panel under estimated the actual measured strength. This difference may be attributed to a conservative estimation of the compressive strength of the masonry from prism tests, due to variable workmanship.

6.6.1.2 Observed Behavior and Predicted Strength (Specimen 4b, 5b, 6c, 8b)

A series of panels tested out-of-plane obtained lateral strengths exceeding the capacity of the loading rig (Specimens 4b, 5b, 6c, and 8b). The behavioral response observed during the testing of the specimens is compared to their corresponding analytical predictions as evaluated from the analytical method, and results are presented in Fig. 52(a), Fig. 52(b), Fig. 52(d), and Fig. 52(e). Comparing the experimental results to the estimated analytical results shown in these figures indicates that the initial behavior and stiffness of the panels was well predicted. Based on initial panel behavior, and on the type of behavior observed throughout the loading sequence of the panel as observed for Specimen 6b (Fig. 255), it is reasonable to assume that the actual strength of the panel was well predicted by the method. Analytical evaluation of Specimens 4b, 5b, and 8b included the reduction factor for the out-of-plane strength of the panel when existing in-plane damage was present. For Specimen 6c, no in-plane damage reduction factor was considered as for Specimens 2c and 3c.

6.6.2 Correlation of Arching Theory and McDowell Theory

The arching action theory by McDowell produced larger results than predictions obtained using the developed analytical model. This difference was attributed to two different factors. First, the stress-strain relationship for the McDowell theory was different to that developed in this project. McDowell assumed a linearly elastic-plastic relationship for the stress-strain behavior of the masonry. This assumption does not represent experimental data. Secondly, and most importantly, the McDowell theory did not include a deterioration factor for existing damage. The amount of out-of-plane deterioration observed in the panels varied non-linearly with the slenderness ratio of the infill panel as explained in Section 6.4. Comparison between experimental behavior and analytical results is presented in Fig. 52(c). The expected behavior predicted by McDowell overestimated the actual strength and stiffness of the panel. This was also the case for Specimen 8b as illustrated in Fig. 52(e). The difference between the two analytical models was more pronounced

6.6.1 Correlation Between Experimental Data and Developed Arching Action Theory

A computer program evaluating the developed arching action theory was written and used to estimate analytically the predicted behavior of the experimentally tested masonry panels. The tested masonry panels were divided into two different categories: 1) those where the strength of the panel was reached, and 2) those where the strength of the panels exceeded the capacity of the loading rig and therefore the strength of the panel was not actually recorded. Because there were two different categories of experimental results, each category was discussed separately in the following sections.

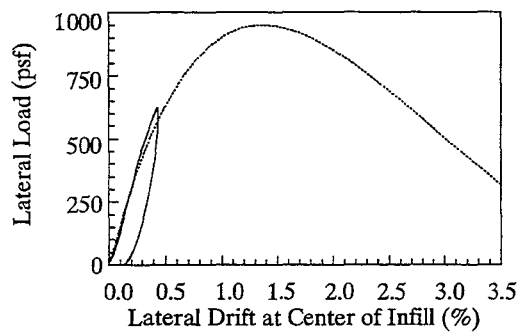
6.6.1.1 Observed Behavior and Strength (Specimen 1, 2b, 2c, 3b, 3c, 6b, 7b)

Results obtained from the analytical procedure are compared to experimental results in the figures presented in Appendix F. Figures include behavior and strength estimates for panels with capacities not exceeding the strength of the loading rig (Specimens 1, 2b, 2c, 3b, 3c, 6b, and 7b), as well as for infills with out-of-plane strengths exceeding the capacity of the loading rig, (Specimens 4b, 5b, 6c, and 8b).

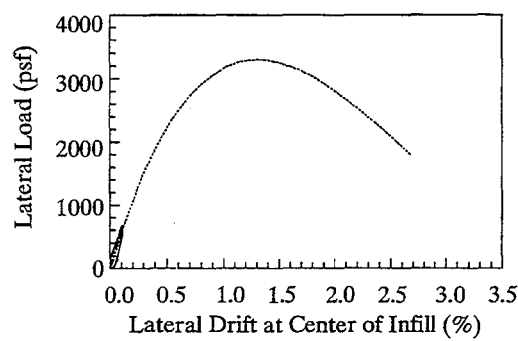
Infill panels with slenderness ratios equal to 34 (Specimens 1, 2b, and 3b) were observed to lay close to the maximum slenderness ratio limit where snap-through occurs. The analytical behavior for Specimen 1 did not include any in-plane damage done to the infill since it was tested in its virgin (uncracked) state. Behavior observed for Specimen 1 is presented in Fig. 247 along with its analytical prediction. The analytical behavioral prediction for Specimens 2b, and 3b includes a factor for reduction of strength and stiffness in the panel due to existing in-plane damage. These results are presented with the corresponding experimental data in Fig. 248 and Fig. 250. Analysis of the behavior observed for these three specimens indicate that the predicted stiffness and strength for slender panels are on the average half the actual stiffness and strength as measured experimentally. These indicate that at this range of slenderness ratios, the magnitude of out-of-plane strength resisted by arching action is measurable, but its effectiveness is decreasing.

The same analytical procedure developed for URM infill panels was used for repaired specimens (Specimens 2c, and 3c with a slenderness ratio of 22). This was done for two reasons: 1) the coating was in full contact with the infill and thus it acted as one continuous unit, and 2) steel anchors were provided for the coating to ensure that in case of bonding failure between the coating and the infill panel the stresses between both elements were fully transferable between each other allowing both elements to act as a continuous member. A compressive strength for the brick masonry-repaired coating system was used. This value was estimated based on the compressive strengths of the masonry and of the coating and calculated as a section composed of two different materials. Analytical predictions and experimental results for Specimens 2c and 3c are presented in Fig. 249, and Fig. 251 respectively. Prediction of stiffness and strength of panels are reasonable. Strength values for the panels were estimated to within 7% the measured data.

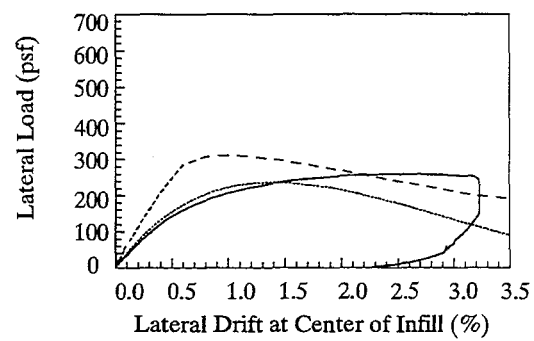
Measured data for Specimen 6b (slenderness ratio of 17) is compared to its corresponding analytical behavior in Fig. 255. As illustrated, both the predicted stiffness and strength of the panels



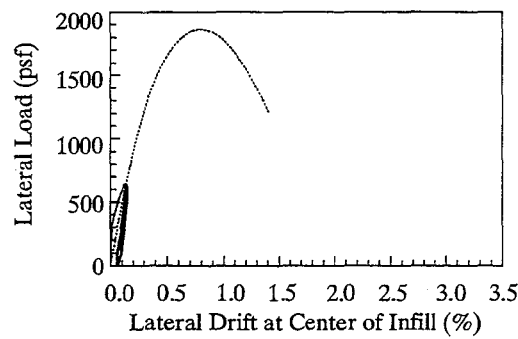
(a) – Specimen 4b



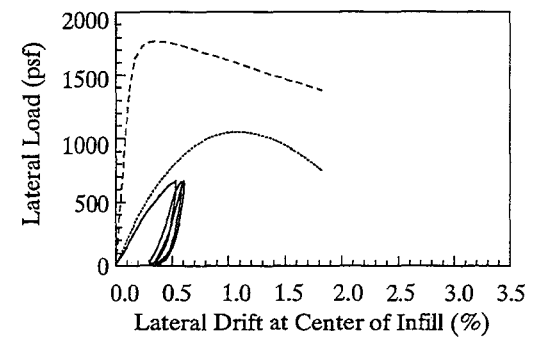
(b) – Specimen 5b



(c) – Specimen 6b



(d) – Specimen 6c



(e) – Specimen 8b

Fig. 52 Predicted Behavior

for Specimen 8b. This is attributed to a more severe amount of existing in-plane damage in the infill. For this panel, the analytical model produces an agreeable failure envelop.

6.7 Concluding Remarks

An analytical model based on arching action has been developed to evaluate the out-of-plane capacity of virgin, or previously damaged infill panels. Results obtained from the analytical model were correlated with experimental results.

Conclusions made based on the analytical model, and on the comparison between the experimental and analytical results are:

- Analytical results obtained from the model compared favorably to the experimental results.
- Analytical results obtained from the model represented well the deterioration in the out-of-plane strength caused by the existing in-plane damage.
- The analytical model accurately represented the initial stiffness of the panels.
- The analytical model accurately estimated the out-of-plane strength of the panels.
- The strain-stress curve correlated well with experimental results obtained from this and other projects.
- The out-of-plane strength and behavior of the panels greatly depend on the slenderness ratio of the panel, and on the compressive strength of the masonry.
- The out-of-plane strength and behavior was slightly dependent on the crushing strain of the masonry.
- The reduction in out-of-plane strength as a result of in-plane damage varied nonlinearly with the slenderness ratio of the panel.

CHAPTER 7

SUGGESTED EVALUATION PROCEDURE

Based on the analytical model presented in Chapter 6, an evaluation procedure is developed to estimate the out-of-plane strength of cracked or uncracked panels. The evaluation procedure approximates the out-of-plane strength by considering a unit strip of an infill that spans between two fully restrained supports. A series of parameters affecting the out-of-plane strength of the panels are studied including: (a) effects of masonry crushing strain, (b) effects of in-plane damage, (c) effects of the flexibility of the confining frame, and (d) effects of panel slenderness ratio.

7.1 Effects of Masonry Strain and Stress

The state of strain in the masonry is an important parameter to consider for the evaluation of out-of-plane strength. The strain in the masonry can be calculated from geometrical properties as presented in Section 6.1. A sensitivity analysis for masonry strain at peak load was done for a series of slenderness ratios.

The masonry strain when the out-of-plane strength is reached (ϵ_{max1}) varies with the slenderness ratio of the panel and crushing strain of the masonry. The change in masonry strain for a large range of slenderness ratios is presented in Fig. 53. The masonry strain (ϵ_{max1}) corresponding

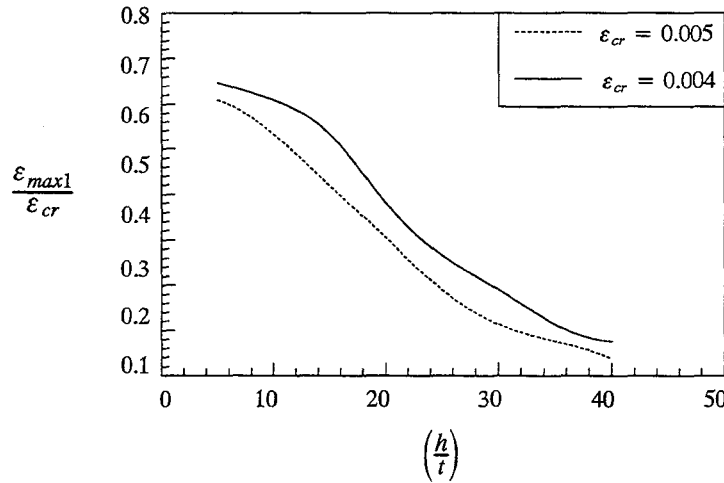


Fig. 53 Masonry Strain vs. Slenderness Ratio of the Panel

to the out-of-plane strength of the panel has been normalized in terms of the masonry crushing strain (ϵ_{cr}). The curves presented in Fig. 53 correspond to a nonlinear relationship between the two parameters represented at the axis. Nevertheless, a regression study of the data can be performed to estimate an equivalent linear relationship between $\frac{\epsilon_{max1}}{\epsilon_{cr}}$ and $\left(\frac{h}{t}\right)$ as illustrated by Fig. 54. The data used to plot the relationship was calculated based on an expression obtained from the regression

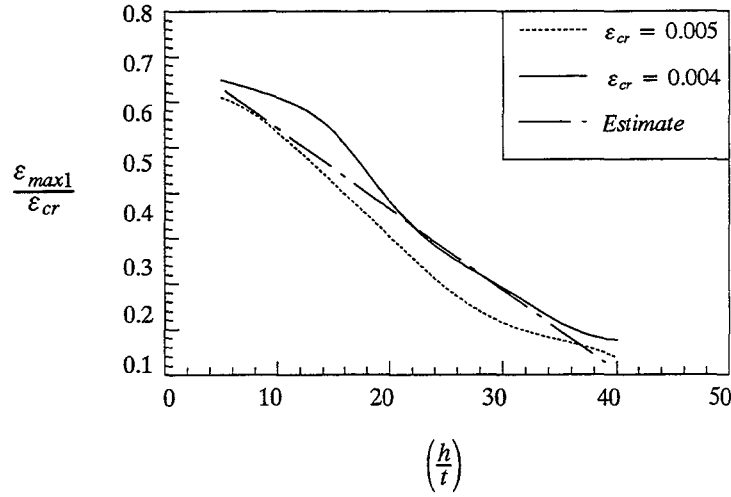


Fig. 54 Predicted Masonry Strain vs. Slenderness Ratio of the Panel

analysis (Eq. [54]). The obtained expression used to predict the relationship between $\frac{\varepsilon_{max1}}{\varepsilon_{cr}}$ and

$$\varepsilon_{max1} = \varepsilon_{cr} \left(0.73 - 0.016 \left(\frac{h}{t} \right) \right) \quad \text{Eq. [54]}$$

$\left(\frac{h}{t} \right)$ produces satisfactory results for the out-of-plane strength of the panel as explained in Sec.7.4.

The masonry strain related to the out-of-plane strength of the panels also affects the masonry stress. Based on the stress-strain relationship for masonry (Appendix H) Eq. [55] is obtained. This expression evaluates the stress developed in the panel, corresponding to the strain at which the out-of-plane strength is reached (ε_{max1}). This calculated stress is always smaller than the masonry compressive strength (f'_m).

$$f_b = \frac{27f'_m(250\varepsilon_{cr} - 1)}{4\varepsilon_{cr}^3} \varepsilon_{max1}^3 + \frac{27f'_m(1 - 333.3\varepsilon_{cr})}{4\varepsilon_{cr}^2} \varepsilon_{max1}^2 + 750f'_m \varepsilon_{max1} \quad \text{Eq. [55]}$$

7.2 Effects of In-Plane Damage

The out-of-plane strength decreases according to the magnitude of in-plane damage experienced by the panel. Experimental results proving this statement are presented in Chapter 5. The reduction observed in the panel strength, by varying the slenderness ratio of the panel and the maximum existing in-plane drift, is illustrated in Fig. 55. This curves were obtained from the analytical model modified to consider in-plane damage on the out-of-plane strength calculations as explained in Section 6.4. Δ represents the maximum lateral deflection that the panel has experienced, while Δ_{cr} is the lateral deflection required for cracking of the panel. As shown in Fig. 55, the out-of-plane strength is not linearly related to either the magnitude of the in-plane damage nor the slenderness ratio. The behavior observed in the panels was similar for both magnitudes of in-plane damage but at different scales (Fig. 55(a) and Fig. 55(b)). The deterioration in

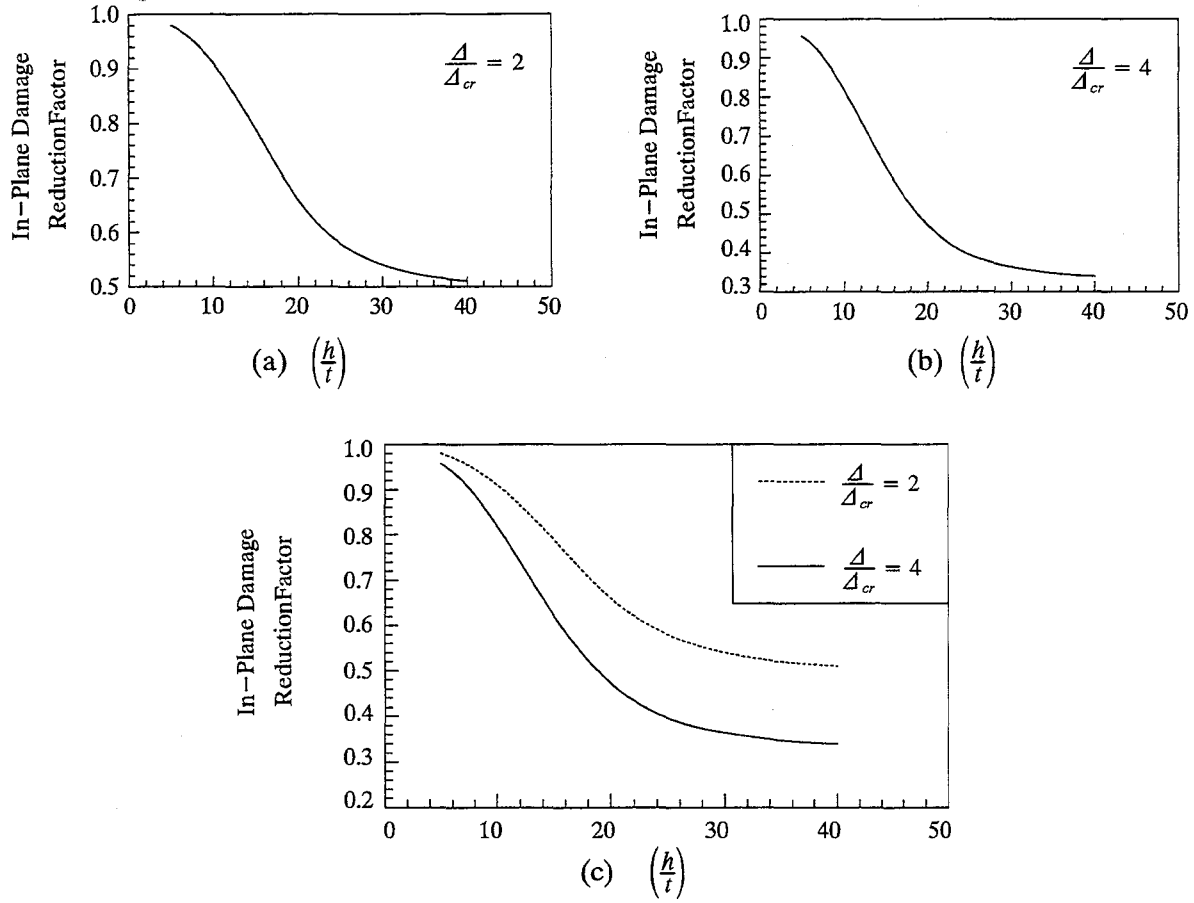


Fig. 55 In-Plane Damage Reduction Factor
vs. the Slenderness Ratio of the panel

out-of-plane strength associated with a maximum in-plane drift of twice the lateral drift at cracking was taken as the bases for determining a damage relation factor. The reduction resulting from a displacement equal to $2\Delta_{cr}$ was chosen because it could be checked against the obtained experimental results. Based on the type of behavior observed in Fig. 55(a), it was considered that a third degree polynomial with a total of four constants would be able to represent well this observed behavior. Based on the slope and reduction values for the strength of the panels at slenderness ratios of 5 and 40, Eq. [56] was developed. This expression has been evaluated for a series of slenderness ratios and

$$R = 1.08 + \left(\frac{h}{t}\right) \left(-0.015 + \left(\frac{h}{t}\right) \left(-0.00049 + 0.000013 \left(\frac{h}{t}\right) \right) \right) \quad \text{Eq. [56]}$$

results are presented in Fig. 56. Comparing Fig. 55(a) and Fig. 56 when $\frac{\Delta}{\Delta_{cr}} = 2$, shows very good correlation between the measured and the approximate reduction in the out-of-plane strength of the panels. For more severe in-plane damage, a general expression has been developed to evaluate

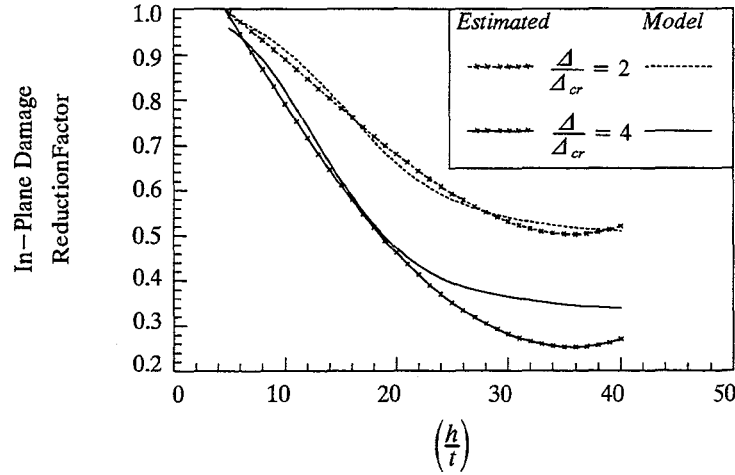


Fig. 56 Approximate In-Plane Damage Reduction Factor vs. the Slenderness Ratio of the panel

the corresponding out-of-plane strength reduction, as presented in Eq. [58]. The variation in

$$R_1 = 1 \text{ for } \frac{A}{2A_{cr}} < 0.5 \quad \text{Eq. [57]}$$

$$R_1 = \left[1.08 + \left(\frac{h}{t} \right) \left(-0.015 + \left(\frac{h}{t} \right) \left(-0.00049 + 0.000013 \left(\frac{h}{t} \right) \right) \right) \right]^{\frac{A}{2A_{cr}}} \text{ for } \frac{A}{2A_{cr}} \geq 0.5 \quad \text{Eq. [58]}$$

reduction factor has been considered by adding an exponential function in terms of both the maximum in-plane drift experienced by the infills and the in-plane drift related to the cracking of the panel. The curve obtained for $\frac{A}{A_{cr}} = 4$ is simply the square of the curve obtained for $\frac{A}{2A_{cr}}$. This value is obtained when the value for $\frac{A}{A_{cr}} = 4$ is substituted into the exponent of Eq. [58], $\frac{A}{2A_{cr}}$. The analytical model predictions and the approximate curves favorably compare.

7.3 Effects of Confining Frame Stiffness

The type of out-of-plane behavior predicted by the analytical model also depends on the stiffness of the confining frame. The analytical model is based on a fully restrained support. Panels located in the exterior bays, or the uppermost story, include one side of the confining frame that is not continuous. A reduction factor (R_2) has been included to account for the flexibility of the confining frame for panels at these edge locations. The reduction factor has been determined based on the flexibility of the frame for a number of different slenderness ratios. Based on a computer program developed by Dawe [22], a number of simulations of out-of-plane loadings on uncracked infill panels was carried out. The different panels in combination with a number of different frame properties produced a curve representing the influence of the confining frame on the out-of-plane strength of the panel. Based on the obtained curve, for simplification purposes, a simple double linear

relationship has been developed to account for the flexibility of the confining frame on the out-of-plane strength of the panels. The expressions assumed eccentric placement of the panel. Expressions for the reduction factor (R_2) are presented in Eq. [59], and Eq. [60] for two different ranges of frame stiffness. The flexural stiffness properties used in these equations should correspond

$$R_2 = 0.357 + 7.14 \times 10^{-8} EI \quad \text{for } 2.0E6 \text{ k-in} \leq EI \leq 9.0E6 \text{ k-in} \quad \text{Eq. [59]}$$

$$R_2 = 1 \quad \text{for } EI > 9.0E6 \text{ k-in} \quad \text{Eq. [60]}$$

to the smallest member of the confining frame at the panel edge with no continuity. These values were conservatively designed to account for the worst possible case scenario encountered.

7.4 Out-of-Plane Strength

The out-of-plane strength of a masonry panel can be evaluated with an analytical model based on arching action as presented in Chapter 6. A general expression was developed in Section 6.1 and is again presented in Eq. [61].

$$w = \frac{4 k_1 \left(\frac{b}{t}\right) f_b \frac{\cos \gamma}{\cos \theta} \sin \gamma}{\left(\frac{h}{t}\right)} \quad \text{Eq. [61]}$$

A number of simplifications have been done on the parameters influencing the strength of the panel (Eq. [61]) as illustrated in Eq. [62] through Eq. [70]. In addition, reduction factors to account for in-plane cracking (R_I Eq. [58]) and frame stiffness (R_2 Eq. [59]) are considered to produce a simpler expression (Eq. [71]).

$$\frac{\cos \gamma}{\cos \theta} \approx 1 \quad \text{Eq. [62]}$$

$$k_1 = 0.5, \quad k_2 = 0.33 \quad \text{Eq. [63]}$$

$$c_1 = \frac{1}{4} \varepsilon_{\max 1} = \frac{1}{4} \varepsilon_{cr} \left(0.73 - 0.016 \left(\frac{h}{t} \right) \right) \quad \text{Eq. [64]}$$

$$\frac{b}{t} \approx 0.25 \left[1 + \sqrt{1 - 2c_1 \left(\frac{h}{t} \right)^2} \right] \quad \text{Eq. [65]}$$

$$\tan \theta = \frac{c_1 \left(\frac{h}{t} \right)}{\left(\frac{b}{t} \right)} \quad \text{Eq. [66]}$$

$$\tan \beta = \frac{2 \left[1 - 2k_2 \left(\frac{b}{t} \right) \right]}{\left(\frac{h}{t} \right)} = \frac{2 - \frac{4}{3} \left(\frac{b}{t} \right)}{\left(\frac{h}{t} \right)} \quad \text{Eq. [67]}$$

$$\beta \approx \tan \beta, \quad \theta \approx \tan \theta \quad \text{Eq. [68]}$$

$$\sin \gamma = \sin(\beta - \theta) \quad \text{Eq. [69]}$$

$$\sin \gamma = \sin \left(\frac{2 - \frac{4}{3} \left(\frac{b}{t} \right) - c_1 \left(\frac{h}{t} \right)}{\left(\frac{h}{t} \right)} \right) \quad \text{Eq. [70]}$$

$$w = 2 f_b \left(\frac{b}{t} \right) R_1 R_2 \sin \gamma \quad \text{Eq. [71]}$$

7.5 Correlation With Experimental Results

Results obtained using Eq. [71] estimates out-of-plane strengths similar to the analytical model developed in Chapter 6. Comparison between out-of-plane strengths calculated by the analytical model and the expression for the evaluation method (Eq. [71]) are illustrated in Fig. 57(a) and Fig. 57(b). These results are also compared to the experimental results. Measured strengths have

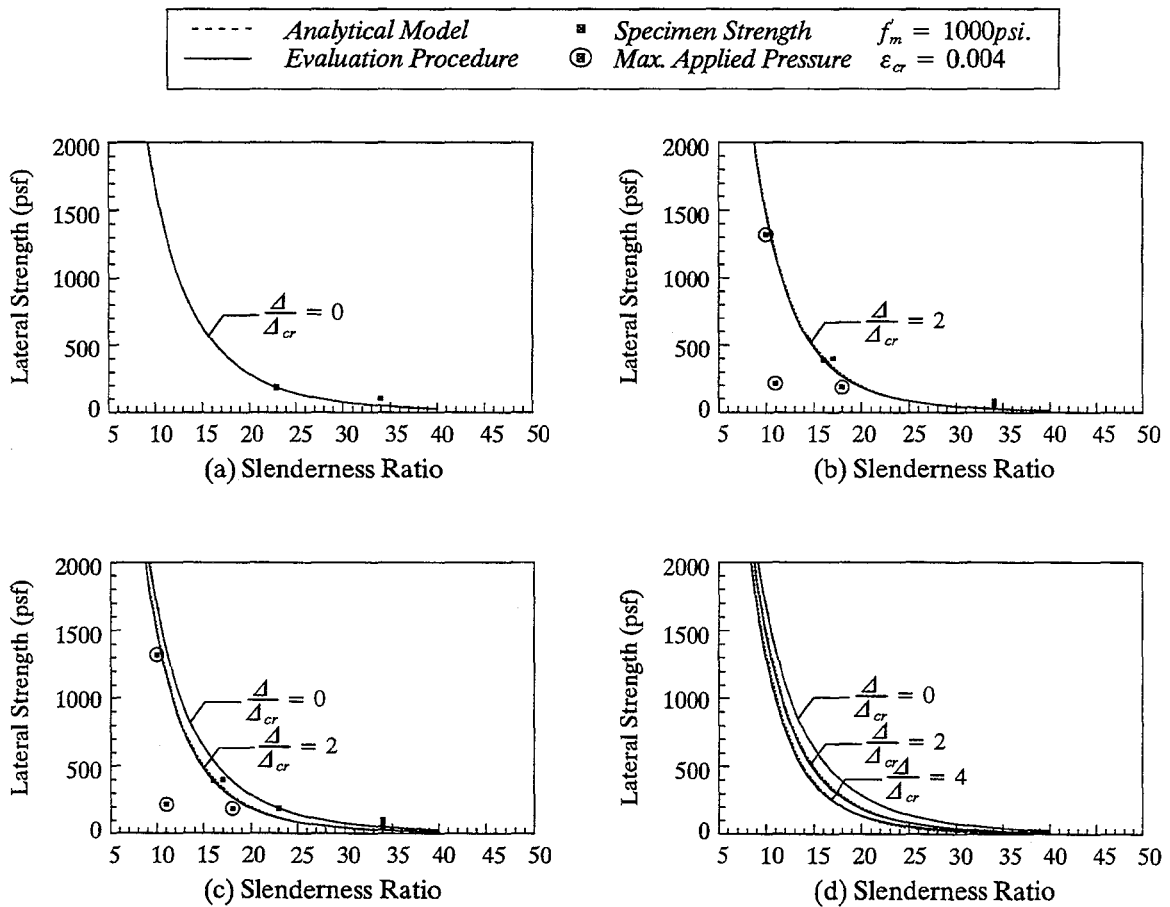


Fig. 57 Lateral Strength of Panels vs. Slenderness Ratio

been normalized to a compressive strength of 1000 psi for comparison with strength curves. Notice that some panels were not tested to failure since their strength exceeded the capacity of the loading rig. For these panels, the maximum applied pressure was recorded rather than their strength.

Predicted strengths for panels with no existing in-plane damage are illustrated in Fig. 57(a), while strengths for panels damaged in the in-plane direction corresponding to a maximum in-plane drift of twice the required for cracking of the panel are illustrated in Fig. 57(b). The out-of-plane strength reduction obtained from the applied in-plane damage along with all the experimental results are presented in Fig. 57(c). The pattern observed for the reduction of the out-of-plane strength of the panels for a series of different existing in-plane damage is illustrated in Fig. 57(d). As shown in Fig. 57(d), the strength of the panels varies with the slenderness ratio of the panel and with the magnitude of in-plane damage experienced by the panel.

7.6 Suggested Evaluation Procedure

7.6.1 Simplifications

Expression developed in section 7.4 for the out-of-plane strength of panels (Eq. [71]) are simplified by considering a constant masonry crushing strain. The crushing strain of the masonry was considered to be equal to 0.004. Parameters b/t , f_b , and $\sin(\gamma)$, depend on the crushing strain and on the slenderness ratio of the panel. These parameters are combined to obtain a dimensionless parameter λ (Eq. [72]). This dimensionless parameter was evaluated for a range of panel

$$\lambda = \left[\left(\frac{f_b}{f_m} \right) \left(\frac{b}{t} \right) \sin \gamma \right] \quad \text{Eq. [72]}$$

thicknesses, and results are presented in Table 12. Substituting λ into Eq. [71] produces expression Eq. [73].

$$w = \frac{2 f_m}{\left(\frac{h}{t} \right)} R_1 R_2 \lambda \quad \text{Eq. [73]}$$

According to the NEHRP Handbook for the Seismic Evaluation of Existing Buildings [56], a typical ten story building was analyzed under the worst possible conditions, and the maximum lateral

Table 12 Parameter Approximation

$\frac{h}{t}$	λ	R_1 for corresponding ratio of Δ/Δ_{cr}	
		1	2
5	0.129	0.997	0.994
10	0.060	0.946	0.894
15	0.034	0.888	0.789
20	0.021	0.829	0.688
25	0.013	0.776	0.602
30	0.008	0.735	0.540
35	0.005	0.716	0.512
40	0.003	0.727	0.528

acceleration that an infill panel would experience is approximately equal to 2.0 g's (Equivalent to a range of X to XII in the Modified Mercalli Intensity Scale). Based on the maximum expected acceleration, and considering the allowable masonry stresses and related factors of safety, panels with slenderness ratios smaller than 9 are considered safe (masonry compressive strength larger than 500 psi) and no further analysis is required.

7.6.2 The Evaluation Process

The evaluation process presented here follows, with a few exceptions, the same steps as procedures presented by the Federal Emergency Management Agency (FEMA)–178, National Earthquake Hazards Reduction Program (NEHRP) Handbook for the Seismic Evaluation of Existing Buildings [56].

This section presents a method for evaluation of the out-of-plane strength of an infill masonry panel that may be cracked or uncracked. The steps involved with a strength evaluation of a damaged URM infill should consist of the following steps:

1.) A visit to the site and data collection.

Field measurements should be made. Overall dimensions of the structure should be measured, and the structural damage should be assessed.

2.) Selection and review of evaluation statements.

Identify the exact problem to be evaluated.

3.) Tests of Materials.

Material mechanical properties of the element under evaluation should be obtained from compression tests in accordance to FEMA–178. The modulus of elasticity for the confining frame should be estimated based on the design compressive strength of the concrete or simply 30,000 ksi for steel. The quality of the mortar in all masonry infills should be determined by performing in-place shear tests in accordance with C.4.2.3. in FEMA–178. Masonry compressive strength and modulus of elasticity can be estimated from unit compressive strength and mortar type in accordance to UBC or ACI–530 codes. Masonry unit compressive strength tests should be performed in accordance to ASTM–C216. Masonry compressive strength may also be determined from tests done on samples in accordance with ASTM–E447. State of vertical stress of the infills may be (not necessary) evaluated using the flat-jack test as explained in Appendix C, or from a detailed estimate of the gravity loads that the infill carries. After completion of the field measurements and testing of the material properties, the parameters presented in Table 13 will be known.

4.) Analysis required for the evaluation of infill.

1.) In-plane damage assessment.

There are two methods for quantifying the magnitude of damage for cracked panels: 1) visual inspection, and 2) analysis of the maximum deflection experienced by the element in terms of the displacement observed at cracking of the infill panel.

Table 13 Frame—Infill Specimen Properties

Frame		Infill	
Physical Properties	Mechanical Properties	Physical Properties	Mechanical Properties
I_c (in ⁴)	E_c (ksi)	t (in)	f_m (psi)
I_b (in ⁴)		h (in)	E_m (ksi)
h' (in)		L (in)	f_a (psi)
L' (in)			f_v (psi)

Based on the visit to the site, and on assessments of building performance following past earthquakes, determine the state of maximum drift that the element has experienced (Δ) and the existing in-plane damage in the masonry infill panel. The maximum lateral displacement observed by the structure (Δ) may be obtained from different sources: 1) instrumentation in the building such as accelerographs or older seismographs, or 2) numerical analysis of the expected behavior of the building under the applied earthquake.

Determination of the lateral load required for cracking of the panel is based on results obtained from in-place shear tests. Results obtained from in-place shear tests are evaluated following the procedure presented in FEMA-178 C.4.2.3. Based on an estimated axial stress in the masonry and a coefficient of friction of unity, the mortar shear stress is calculated at a desired section using the following equations.

$$f_v = \frac{V_{test}}{A_{bed-joints}} - f_a \quad \text{Eq. [74]}$$

where:

f_v = masonry shear strength at in-place shear test location.
(20 percent of the calculated value)

A_b = mortar bed joint area resisting the pushing force.

f_a = measured or estimated compressive stress at location of in-place shear test.

$$f_{vm} = 0.56f_v + \frac{.75P_d}{A} \quad \text{Eq. [75]}$$

where:

f_{vm} = masonry shear strength at any desired location.

A = area of unreinforced masonry.

P_d = measured or estimated compressive stress at desired location.

Load required for cracking of the panel is calculated as:

$$P_{cr} = f_{vm} A = f_{vm} (Lt) \quad \text{Eq. [76]}$$

Determine the stiffness of the frame–infill element in question based on expression Eq. [77]. The expression estimates the stiffness of single frame–infill element. Determine the lateral displacement

$$K = \left[\frac{12E_c I_c}{h'^3 \left[1 + \frac{l_c}{l_b} \cot \theta \right]} + \frac{t f_m'}{6 \varepsilon_{cr}} \right] \quad \text{Eq. [77]}$$

corresponding to cracking of the panel (Eq. [78]).

$$\Delta_{cr} = \frac{P_{cr}}{K} \quad \text{Eq. [78]}$$

Based on the ratio $\Delta/2\Delta_{cr}$, a reduction factor for the out–of–plane strength of the panel is calculated based on the simplified linear expressions Eq. [79] and Eq. [80]. Expressions Eq. [79] and Eq. [80] have been obtained from simplifications of Eq. [57] and Eq. [58]. These simplifications have been developed for the engineer to use a linear function in terms of the slenderness ratio of the panel. The reduction factor is considered to account for the magnitude of existing in–plane damage in the panel being evaluated.

$$R_1 = 1 \text{ for } \frac{\Delta}{2\Delta_{cr}} < 0.5 \quad \text{Eq. [79]}$$

$$R_1 = \left[0.958 - 0.144 \left(\frac{h}{t} \right) \right]^{\frac{\Delta}{2\Delta_{cr}}} \text{ for } \frac{\Delta}{2\Delta_{cr}} \geq 0.5 \quad \text{Eq. [80]}$$

A simpler method used to evaluate the damage of a panel is visual inspection. Visual inspection of the panel can classify the magnitude of existing panel damage into three different categories as illustrated in Fig. 58. Reduction factors for a range of panel slenderness ratios have been

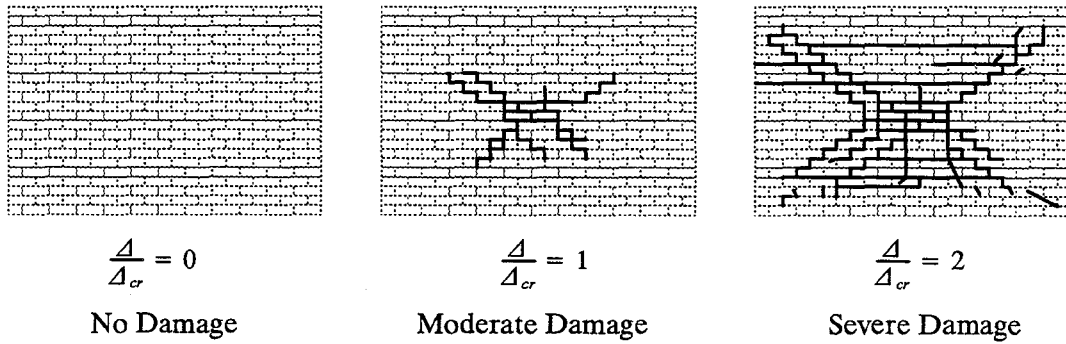


Fig. 58 Physical Infill Cracking Damage

tabulated (based on Eq. [57] and Eq. [58]) and results are presented in Table 12.

2.) Flexibility of confining frame.

Infill panels confined within frames with all sides continuous (neighboring panel in every direction) may assume to have fully restrained boundary conditions ($R_2 = 1$). For infill panels

confined within frames with at least one side not continuous (neighboring panel missing on any panel direction) a reduction factor for the out-of-plane strength is applied (R_2). Evaluation of the stiffness of the smallest frame member on the non-continuous panel side should be performed, and results are to be used in conjunction with Eq. [81] and Eq. [82].

$$R_2 = 0.357 + 7.14 \times 10^{-8} EI \quad \text{for } 2.0E6 \text{ k-in} \leq EI \leq 9.0E6 \text{ k-in} \quad \text{Eq. [81]}$$

$$R_2 = 1 \quad \text{for } EI > 9.0E6 \text{ k-in} \quad \text{Eq. [82]}$$

3.) Out-of-plane strength of the panel.

The out-of-plane strength of previously cracked, or uncracked infill panels within confining frames at any location of a structure may be evaluated by Eq. [83]. Allowable compressive stresses

$$w = \frac{2 \frac{1}{4} f_m}{\left(\frac{h}{t}\right)} R_1 R_2 \lambda \quad \text{Eq. [83]}$$

are limited to $1/4$ the compressive strength of the masonry (f_m). Values for λ for a range of slenderness ratio are given in Table 12.

4.) Retrofit or rehabilitation techniques.

Infill masonry panels may require rehabilitation due to lack of available out-of-plane strength. A rehabilitation technique to improve the out-of-plane strength of the panels is presented in Chapter 3, and is also discussed by Prawel [61] along with other useful rehabilitation techniques.

The repairing method recommended to increase the out-of-plane strength of the panel consists of parging a ferrocement coating to one or both faces of the infill panel. Application of the coating decreases the slenderness ratio of the panel, and also increases the compressive strength of the panel. The out-of-plane strength of the panel is then largely increased by the repair method since the strength depends: 1) linearly on the compressive strength of the material, and 2) on the square of the slenderness ratio of the panel.

The out-of-plane strength of repaired infill panels may be evaluated by Eq. [84] (R_1 is not considered because once the panel is repaired the existing in-plane damage does not affect the strength of the panel). The value for the slenderness ratio should consider the thickness of the panel

$$w = \frac{2 \frac{1}{4} f_{m-repaired}}{\left(\frac{h}{t}\right)} R_2 \lambda \quad \text{Eq. [84]}$$

once repairing has been completed. The compressive strength for the panel should be the lesser of the masonry or of the repair coating. Values for λ for a range of slenderness ratios are presented in Table 12.

7.7 Example

In this section an illustrative example is presented to show the sequence of calculations required for the use of the evaluation procedure.

A reinforced concrete building was subjected to lateral accelerations produced by a nearby earthquake, and damage to some of its elements occurred. A view of the building under observation is presented in Fig. 59. Although the lateral accelerations did not cause serious damage to the frame elements, they caused damage to a number of the masonry infills. Because of the in-plane damage to some of the infills, questions regarding the safety of the out-of-plane strength of the panels have been raised.

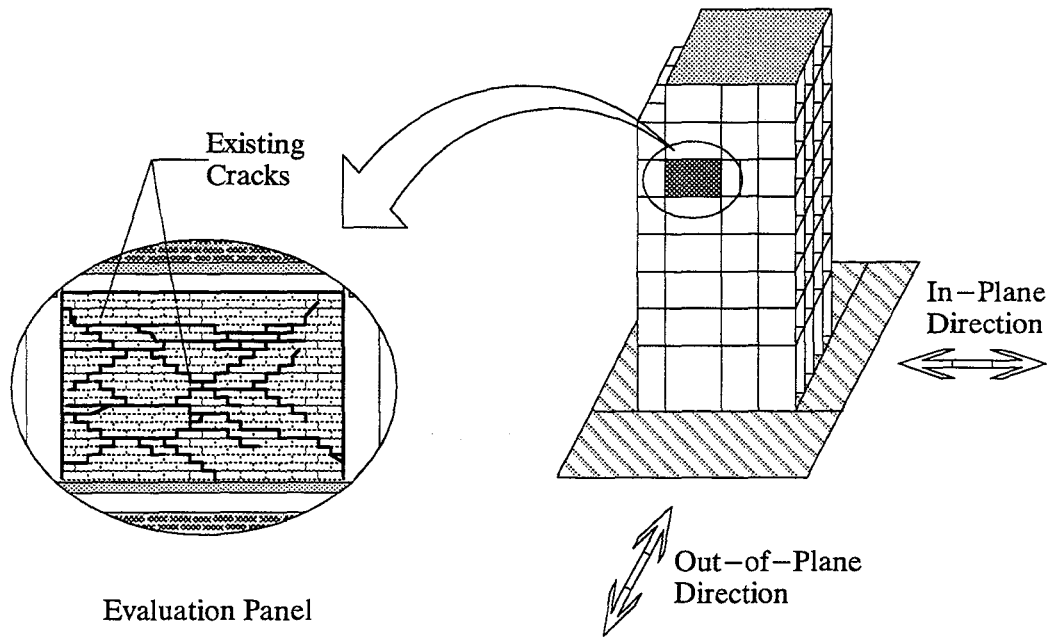


Fig. 59 Example Problem

The typical dimensions of the panels in the building were 12'x20'x7³/₈" (height, width, thickness). The panels consisted of older brick masonry built in double-wythe with a medium strength Type N mortar. In addition to the physical properties of the panels, evaluation of the corresponding mechanical properties are required. For this purpose, a series of masonry unit compression tests, and shove tests were carried out. The masonry unit compression tests provided that together with the mortar type produced the compressive strength of the masonry (f'_m), and the modulus of elasticity (E_m) in accordance to ACI-530 (masonry $\epsilon_{cr} = 0.004$). The shove tests provided values corresponding to the shear strength of the masonry (f_v). Results for these masonry properties are presented in Table 14.

The building had not been instrumented during the earthquake, therefore the damaged in the panels must be evaluated by visual inspection of the infill panels. Existing panel damage was considered to be severe as illustrated in Fig. 59. The building experienced a maximum lateral drift of approximately twice the required for cracking of the panel ($\frac{\Delta}{\Delta_{cr}} = 2$). This factor of two becomes

Table 14 Frame–Infill Properties

Frame		Infill	
Physical Properties	Mechanical Properties	Physical Properties	Mechanical Properties
$I_c = 13824 (in^4)$	$E_c = 3600 (ksi)$	$t = 7\frac{3}{8} in$	$f'_m = 1400 (psi)$
$I_b = 15625 (in^4)$		$h = 144 in$	$E_m = 750 (ksi)$
$h' = 269 (in)$		$L = 240 in$	$f_a = 40 (psi)$
$L' = 264 (in)$		$\left(\frac{h}{t}\right) = 20$	$f_v = 200 (psi)$

important for the estimation of the reduction in the out-of-plane strength of the panel caused by in-plane damage (R_I). Using Table 15 for a slenderness ratio of 20, R_I becomes 0.688.

The frame being evaluated is surrounded by continuous panels in all directions. This type of location provides full restraint for the panel; thus factor R_2 becomes 1.

The process used to evaluate the out-of-plane strength of a cracked or an uncracked panel is similar with the only difference being that the reduction factor for in-plane damage on the panel (R_I) becomes unity for uncracked panels. The procedure consists of substituting the required information that has been obtained for the panel into Eq. [85]. Given the physical and mechanical

$$w = \frac{2 \frac{1}{4} f_m}{\left(\frac{h}{t}\right)} R_1 R_2 \lambda \quad \text{Eq. [85]}$$

$$w = \frac{2 \frac{1}{4} f_m}{\left(\frac{h}{t}\right)} R_2 \lambda = \frac{2 \frac{1}{4} (1400 psi)}{(20)} (1) (0.021) = 105 psf \quad (\text{uncracked panel}) \text{Eq. [86]}$$

$$w = \frac{2 \frac{1}{4} f_m}{\left(\frac{h}{t}\right)} R_1 R_2 \lambda = \frac{2 \frac{1}{4} (1400 psi)}{(20)} (0.688)(1)(0.021) = 73 psf \quad (\text{cracked panel}) \text{Eq. [87]}$$

Table 15 Example–Parameter Approximation

$\frac{h}{t}$	λ	R_I for corresponding ratio of $\Delta/\Delta_{cr} = 2$
5	0.129	0.994
10	0.060	0.894
15	0.034	0.789
20	0.021	0.688
25	0.013	0.602
30	0.008	0.540
35	0.005	0.512
40	0.003	0.528

properties of the panel (Table 15), the expression has been evaluated and the results are presented. The estimated out-of-plane strength of 105 psf (1.37 g's) for an uncracked panel and 73 psf (0.94 g's) for the cracked panel show that the panels should be repaired to reach a higher strength (larger than 2.0 g's).

The panel rehabilitation technique to increase the out-of-plane strength consisted of a one-inch thick ferrocement coating parged to both faces of the infill panel. This operation was conducted after totally cleaning the wall obtaining a smooth surface. A single sheet wire mesh was placed on each face. The new thickness of the panel became approximately 9³/₈" (slenderness ratio equal to 15). Plaster compressive strength obtained from cylinder testing reached 2800 psi. Thus for the strength evaluation of the panel, the lesser compressive strength of the material was used (1400 psi for existing masonry). Strength of the repaired panel was estimated to be 228 psf (2.34 g's) as given in Eq. [88]. The lateral strength of the repaired infill was satisfactory exceeding the lower limit of 2.0

$$w = \frac{2 \frac{1}{4} f_m}{\left(\frac{h}{t}\right)} R_2 \lambda = \frac{2 \frac{1}{4} (1400 \text{ psi})}{(15)} (1)(0.034) = 228 \text{ psf (repaired panel)} \quad \text{Eq. [88]}$$

g's, and the evaluation of the panels was successfully completed.

7.8 Summary and Conclusions

An evaluation procedure based on the analytical model presented in Chapter 6 to estimate the out-of-plane strength of masonry infills was developed. Comparisons were made between experimental results and results calculated using the evaluation procedure and the analytical model. A linear regression curve to account for the strain in the masonry at which the strength of the panel is reached was described. Expressions were also developed to account for reduction in the out-of-plane strength of the panel caused by the existing in-plane damage, and the flexibility of the confining frame. These parameters are plotted against the slenderness ratio to illustrate their relationship.

Conclusions made based on the analytical model, and on comparison between the evaluation procedure, the analytical model and the experimental results are:

- Out-of-plane strength estimates based on the evaluation procedure as well as on the analytical model compared well with the experimental results.
- The reduction observed in out-of-plane strength resulting from different magnitudes of in-plane damage varied for the same slenderness ratio.
- The reduction observed in out-of-plane strength resulting from in-plane damage varied with the slenderness ratio.

CHAPTER 8

SUMMARY AND CONCLUSIONS

This chapter summarizes the content of the report and presents the most important conclusions observed on the behavior and strength of masonry infills. A brief description of the experimental part of the project is presented including the panel repairing technique and the use of non-destructive evaluation methods. In-plane and out-of-plane test results are presented in addition to the major conclusions observed in their behavior as observed from the experimental results. Finally an analytical model and a suggested evaluation procedure for the prediction of the behavior and the strength of masonry infill panels are presented.

8.1 Experimental Program Overview

A series of eight unreinforced masonry infill panels confined within a reinforced concrete frame were constructed and tested to failure in the Newmark Civil Engineering Laboratory. The uniqueness of this study lies in the evaluation of the panel out-of-plane strength reduction due to a constant existing lateral in-plane damage. The masonry infill panels were tested by subjecting them to a monotonically increasing out-of-plane pressure using an air bag. Prior to the out-of-plane testing, all but one of the specimens were subjected to a series of static reversed in-plane shear forces that followed a predetermined displacement sequence. The same sequence was applied to the specimens with a maximum range equal to twice the lateral displacement required to crack a panel.

The infill specimens were confined by a reinforced concrete frame. Masonry units consisted of reclaimed clay brick or concrete block. The reclaimed brick was obtained from a demolished building, and the concrete masonry block was obtained from a local supplier. The type of mortars varied between a Type N mortar, and a lime type mortar.

The masonry infill panels were confined within the same reinforced concrete frame to obtain the same type of confinement for all the specimens. The slenderness ratio of the panels was a parameter that was considered important to evaluate. The slenderness ratios corresponding to the tested panels ranged from 9 to 34 for clay brick infills, and from 11 to 18 for concrete masonry infills.

For panels where the out-of-plane strength was low, a repairing method was used. The repairing method consisted of parging a ferrocement coating to one or both sides of the masonry panel. The same method may be utilized for rehabilitation of structures that have not been previously damaged.

Finally, two non-destructive testing techniques were used to obtain information required for the evaluation of specimen strength. The flat-jack test and the in-place shear test (shove test) were used. The flat-jack test evaluated the vertical stress acting on the panel, while the in-place shear test evaluated the shear strength of the masonry. These techniques provided unique insight on the type of behavior expected for the specimens.

8.2 In-Plane Tests

Results from the in-plane tests are presented in Appendix E. A discussion of the measurements is presented in Chapter 4. A series of topics affecting the in-plane behavior of the frame/infill specimens were addressed. Comparisons between the tests results, and results obtained from existing analytical models and different types of nondestructive tests, were done.

The most important conclusions made regarding in-plane behavior of masonry infill panels were:

- The lateral stiffness greatly decreased once the cracking of the infill occurred.
- Masonry shear strength was affected by the type of mortar type used.
- The lateral stiffness was directly proportional to the masonry compressive strength.
- The lateral stiffness was well predicted up to cracking of the masonry based on equivalent strut theories.
- The shove test estimated a lower conservative bound for the actual lateral strength of the specimens.

8.3 Out-of-Plane Tests

A series of experiments focusing on the out-of-plane strength and behavior of unreinforced masonry panels were performed. The masonry infill panels varied from uncracked specimens, cracked specimens and repaired specimens, to specimens tested with loads applied in both the in-plane and the out-of-plane directions. Finally, static test results were compared to dynamic results obtained from similar but half-scale models, and to results from tests carried out in masonry panels located in an existing building scheduled for demolition.

Conclusions regarding out-of-plane behavior of masonry infill panels were:

- Out-of-plane strength greatly depends on the slenderness ratio.
- Out-of-plane strength depends on compressive strength of the masonry and not on the tensile strength.
- Repetitive loadings within the elastic region did not affect the stiffness of the specimen.
- In-plane shear stress and panel gravity loads slightly increased the initial out-of-plane stiffness, but the out-of-plane strength of the panel was not affected.
- In-plane cracking reduced the out-of-plane strength of the slender panels by a factor as high as two.

- Repairing technique increased the out-of-plane strength of damaged infills by a factor as high as five, with no concern for the magnitude of existing panel damage.
- Out-of-plane strength and stiffness of the cracked test panels are overestimated by existing analytical models.

8.4 Development of a New Analytical Model and a Suggested Evaluation Procedure

An analytical model based on arching action was developed to evaluate the out-of-plane capacity of virgin, or previously damaged infill panels. The model was based on the prediction of a unit wide strip of the panel that spans between two fully restrained supports. The model was used to evaluate the behavior and strength of the test panels. Results from the analytical model were compared with experimental results. Parameters studied with the analytical model included the type of failure mode, the slenderness ratio of the panel, and the reduction of the out-of-plane strength of the panel due to existing in-plane damage.

Conclusions made based on the correlation of experimental and analytical results were:

- The analytical model estimated accurately the measured out-of-plane strength of the panels.
- The reduction in out-of-plane strength resulting from in-plane damage varied non-linearly with the slenderness ratio of the panel.

Based on the analytical model and on observations from experimental results, an evaluation procedure was developed to predict the out-of-plane strength of masonry infills. The procedure considered the effects of existing in-plane damage and frame flexibility on the out-of-plane strength evaluation of panels.

8.5 Further Studies

General directions for further study are recommended based on the experiments, and on the analysis. Additional experimental results would be helpful as supporting data for the analytical model. Out-of-plane tests of specimens previously loaded in the in-plane direction to different damage levels would support the empirical results obtained from the developed analytical model and also the suggested evaluation procedure.

Experiments using different structural configurations would provide further insight into the behavior of masonry panels. Configuration variables may include the number of stories, the number of bays, the type of confining frame, the flexibility of the frame, the type of boundary conditions between the frame and the infill panel, the type of masonry unit used for construction of the infill, the number and size of openings in the infill, and the magnitude of existing in-plane damage in the infill.

Finally, research on development of different repairing and rehabilitation techniques for panels that obtained a lower than desirable out-of-plane strength should be done. These repairing

techniques would be useful in the mitigation of earthquake hazards on prone zones for these types of structures.

8.6 Summary

An analytical model based on arching action was developed to predict the out-of-plane strength and behavior of masonry infill panels. Experimental testing of a series of specimens was done to verify predictions by the analytical model. Based on the analytical model and on the supporting experimental results, this research resulted in the development of a seismic evaluation and rehabilitation procedure for unreinforced masonry infill panels loaded normal to their plane. The procedure outlines the steps to follow during an evaluation, and an example is presented.

APPENDIX A

DESCRIPTION OF TESTING EQUIPMENT

A.1 Loading Apparatus

This appendix describes the testing equipment, and the test setup that was used for the in-plane and out-of-plane tests. In addition, a description of the instrumentation used is presented in the latter part of this appendix.

A.1.1 In-Plane Test Set-Up

The specimens were loaded in-plane by a pair of servo-hydraulic actuators. The load applied by the actuators was resisted by a prestressed concrete masonry reaction wall built specifically for testing this type of specimens. The overall testing setup for during the in-plane testing of the frame-infill specimens is illustrated in Fig. 60. A detailed description of the design, properties and behavior of the reaction frame used for the in-plane tests is presented by Shah and Abrams [68]. The hydraulic actuators were directly connected to the specimen at a connection stub built at the mid-span of the top beam. This connection stub was especially designed for the set of available actuators to prevent them from sliding during the test. The lateral load was applied to the top beam along its center of gravity to prevent creation of unnecessary moments on the frame. The lateral load

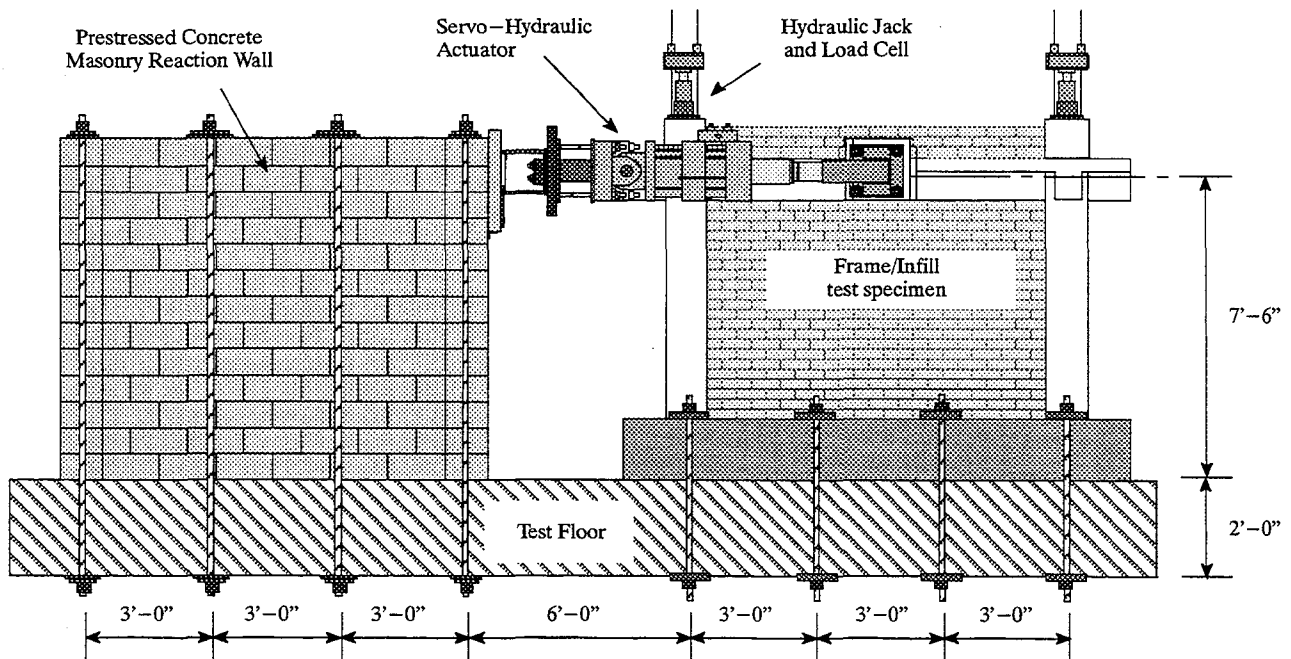


Fig. 60 Elevation of Overall In-Plane Test Setup

was applied at the mid-span of the top beam to obtain symmetrical behavior of the specimen under the predefined cyclic histogram as illustrated in Fig. 18.

A.1.2 Out-of-Plane Test Set-Up

A uniform load applied throughout the surface area of the infill was used to test the infills in the out-of-plane direction. A commercial GoodYear rubber pneumatic airbag, with a deflated surface area approximately equal to that of the infill was used. The relative location and size of the air bag with respect to the infill is illustrated in Fig. 61. The air bag was confined in place by the air

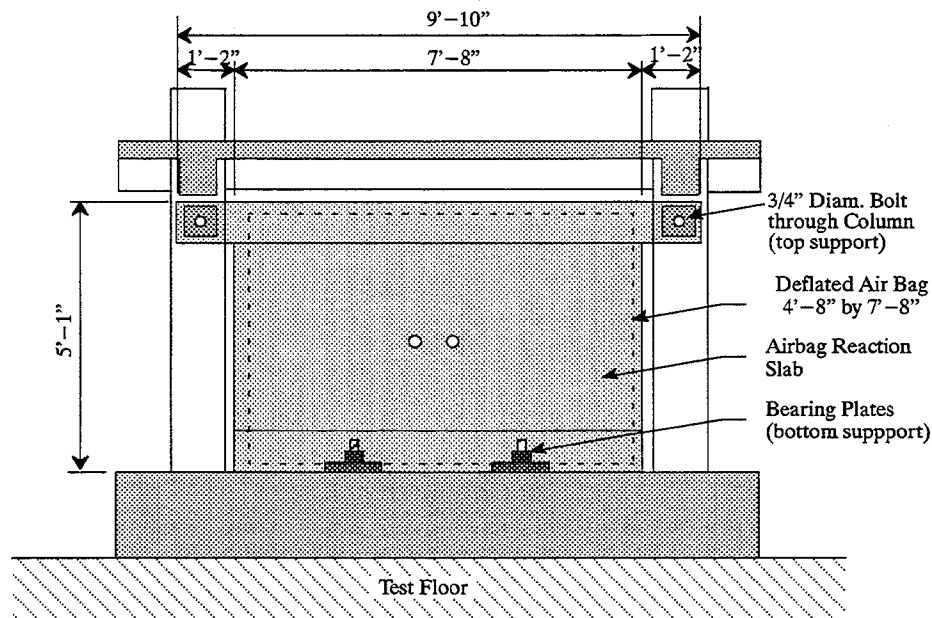


Fig. 61 Air Bag Location

bag reaction slab which was supported at four points on the reinforced concrete frame. The air bag reaction slab was designed as a one way slab spanning between two beams under the influence of a uniform load. A detailed description of the air bag reaction slab design is presented in Fig. 62. The top beam was designed to resist the applied pressures as a simply supported beam spanning 9 feet between supports. The applied loads consisted of the maximum expected pressure applied by the air bag, times its tributary area. The bottom beam was designed in the same fashion with a different span length and tributary area. Cross-sections for both top and bottom beams are also presented in Fig. 62. An elevation view of the out-of-plane testing set-up is presented in Fig. 63. A layer of half inch thick foam rubber covering the entire infill surface area was placed against the infill to generate a smooth bearing surface for the air bag and protect the air bag from surface roughness. Also, a thin layer of greased plastic was placed on both sides of the air bag to prevent any type of movement restriction on the air bag during inflation. The air bag reaction slab was supported at four points: two on the base beam and two on the columns. A detailed illustration of the connection is presented in

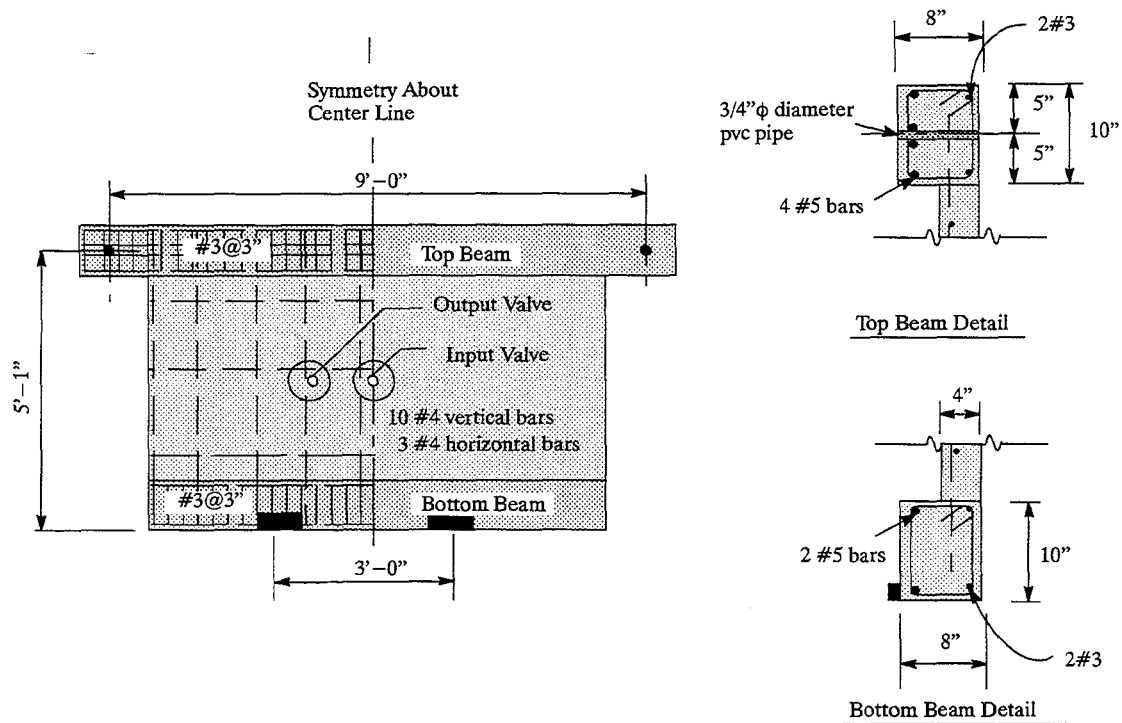


Fig. 62 Airbag Reaction Wall

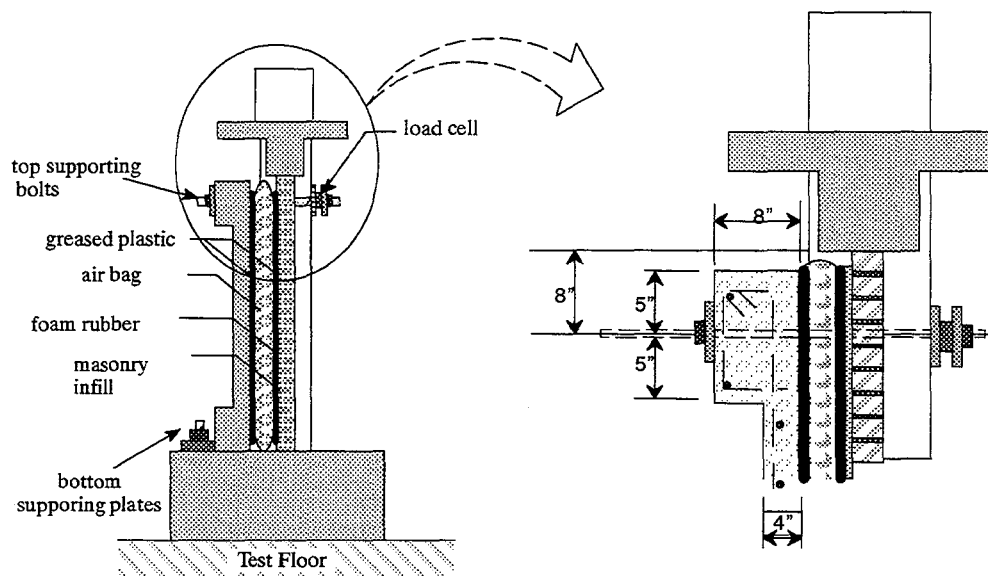


Fig. 63 Air Bag Reaction System

Fig. 63. The supports on the base beam transferred the horizontal load through bearing of the air bag reaction slab against the supporting plates as illustrated. The top supports were directly connected to the columns by a pair of bolts. The input pressure in the airbag was controlled by a hand operated air pressure regulator that increased the pressure at a uniform rate. For small pressures, the air bag

pressure was also monitored with a water manometer as a check for the readings recorded by the pressure transducer. The airbag reaction frame was designed for a maximum pressure capacity of 720 psf applied over the entire surface area of the infill.

A.1.3 Gravity Loading

The simulation of gravity loads is important for the representation of real structures. Typical values of compressive stress on the concrete columns were estimated and corresponding vertical loads calculated. The vertical loads applied to obtain the desired column stresses were 50 kips per column. These loads were chosen to simulate typical gravity loads transferred from upper levels to the bottom story. The vertical load was applied by tensioning a pair of 0.5" diameter strands at the top of the column with hydraulic jacks. The top and bottom connections used during the tests for the application of the vertical load to the columns is presented in Fig. 64 and Fig. 65 respectively. Two 270 ksi

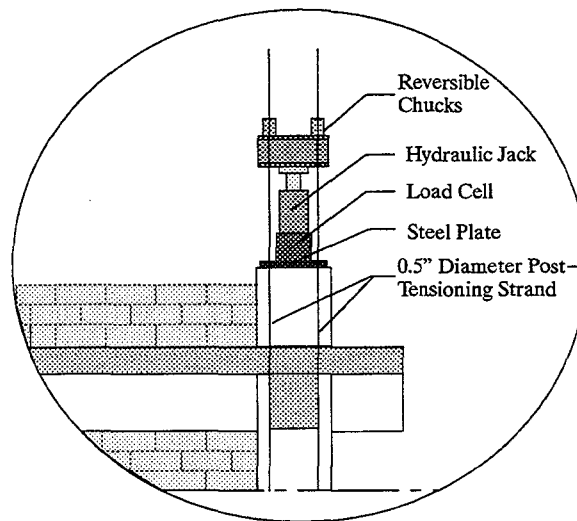


Fig. 64 Elevation of Vertical Loading System (Top-Beam Column Joint)

stress-relieve strands were placed concentrically in the column. The strands were isolated from the concrete by encasing them in 1 inch diameter plastic conduit fully greased to minimize friction. The bottom connection for the strands consisted of a steel plate designed to distribute uniformly the applied loads to the concrete, and a pair of 0.5 inch re-useable high-strength chucks that restrain the strand to generate the desired loads. The connection was attached to the base-beam steel cage to prevent any movement during the casting operation. Intensive vibration around the bottom connection was executed during casting of the base beam to prevent honeycomb pocket development. The top gravity loading connection was placed once the concrete frame had been completed. The top connection entails a more complex arrangement. A steel plate was mounted on top of the column after spreading a layer of hydrocal to assure a smooth bearing area. This was done to insure a uniform stress distribution. A 60-kips capacity load cell connected directly to the computer was placed on top of the

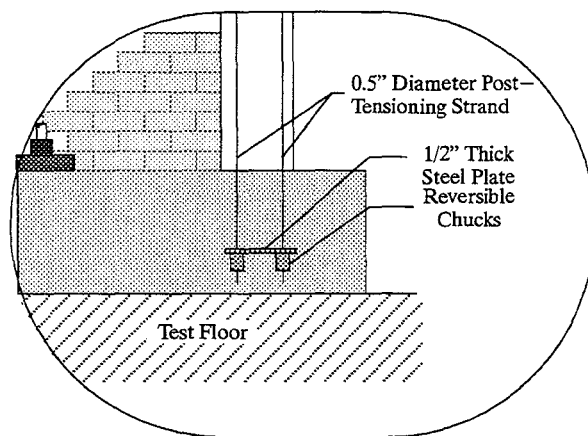


Fig. 65 Elevation of Vertical Loading System
(Column-Base Beam Joint)

steel plate to monitor the vertical load applied to the column during the course of the tests. A set of hydraulic jacks were located on top of the load cell as illustrated in Fig. 64. The jacks were pressurized up to a predefined pressure by using a hand controlled electric power hydraulic pump. The pressure in the jacks was held constant throughout the tests. A pair of adjustable reusable chucks were placed above a small beam that distributed the load applied by the jacks to the two strands inserted in the concrete. The chucks used on the upper strand connection were adjustable to assure an equal load distribution between both strands.

A.1.4 Base-Beam

A detailed design for the base-beam is presented in Fig. 66. The large and massive base beam design simulates a rigid foundation. Heavily reinforced steel cages were assembled to resist the large compression forces obtained from post-tensioning of the anchoring bolts. After securing the base beam cage in place, both column cages were dropped in their corresponding locations and tightened to restrain them from movement. The base-beam was then cast in-place with a concrete mix ordered from a local supplier. Once the base beam had cured and the frame was completed, eight Dywidag $1\frac{3}{8}$ " ϕ bars, with a force of 160 kips each, were used to post-tension the base-beam to the laboratory testing floor to prevent any sliding or slippage of the frame.

A.2 Instrumentation and Data Acquisition

A combination of instrumentation was used to monitor the behavior of the frame and the infill during the in-plane and the out-of-plane tests. The electronic data acquisition equipment consisted of an IBM PC-AT based 32 channel acquisition system capable of individually programmed sampling. The IBM personal computer was equipped with two 16-channel analog-to-digital conversion boards that were controlled by a program written in Quick-Basic for this purpose. The Quick-Basic program used board-specific subroutines provided by the manufacturing company (Metrabyte DASH16 analog-to-digital board). The instrumentation consisted of LVDT's (linear variable displacement transducers), conventional strain gages and different types of load cells.

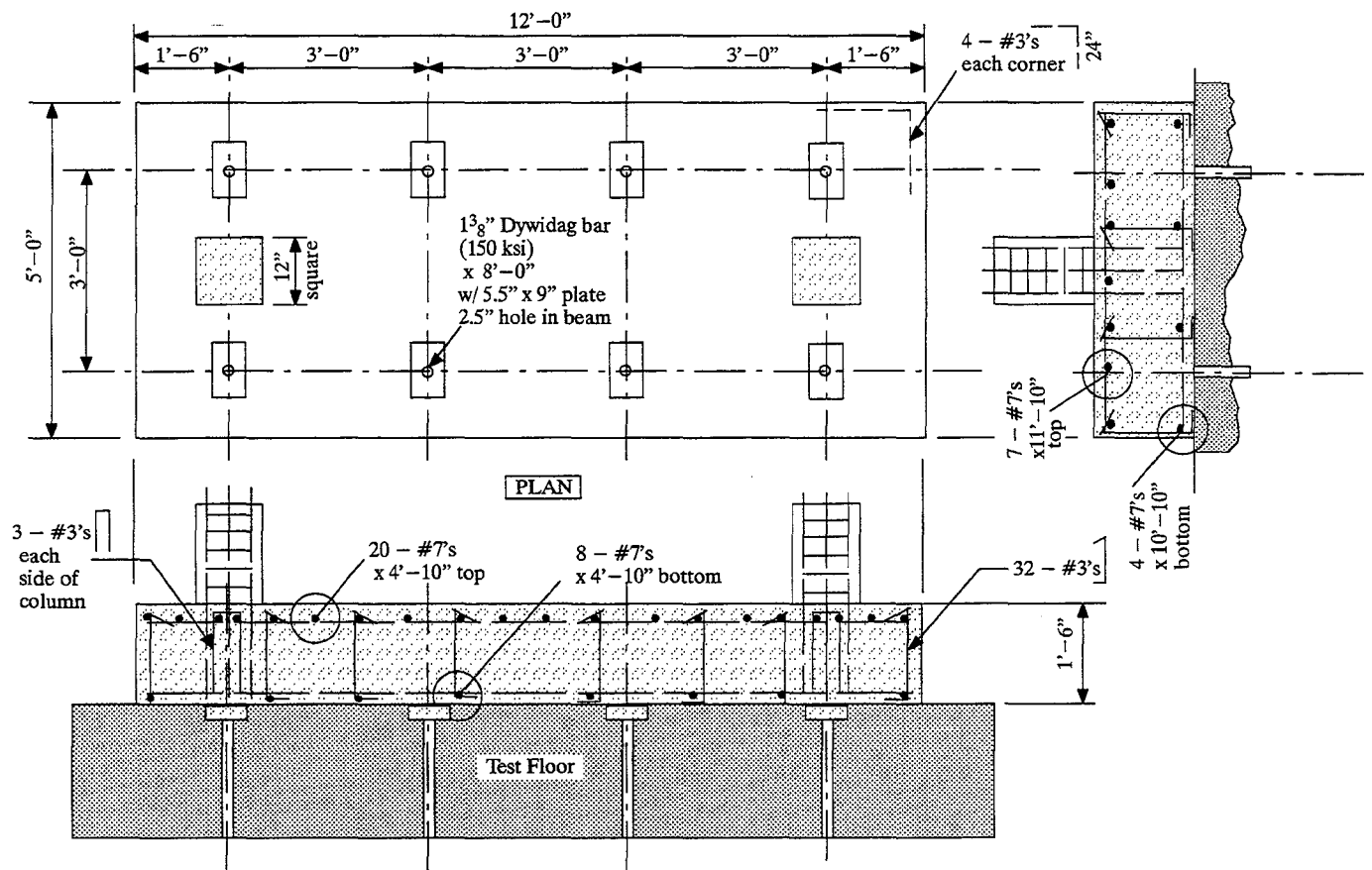


Fig. 66 Detail For Base Beam

A.2.1 In-Plane Test

A total of thirty two channels were read by the data acquisition computer system for the in-plane tests. The information obtained during the tests by the computer was viewed directly on the screen and then saved on magnetic media for further processing. Two different monitoring windows were established on the computer screen. One of the windows plotted the relative rotation of both of the columns at the base. The second window plotted the total lateral force applied to the frame vs. the average deflection of the frame measured from the center of the top beam to a stationary station. The second window with the force vs. deflection plot was used as the controlling device for the displacement controlled in-plane tests.

The instrumentation consisted of a total of sixteen strain gages, twelve displacement transducers and four load cells. Location of all instrumentation used during the in-plane tests is presented in Fig. 67 and Fig. 68. The sixteen strain gages monitored directly the behavior of the reinforcement steel during the tests. These strain gages were placed on the center steel bars of the members at their critical sections as illustrated. A total of eight strain gages were placed at the bottom

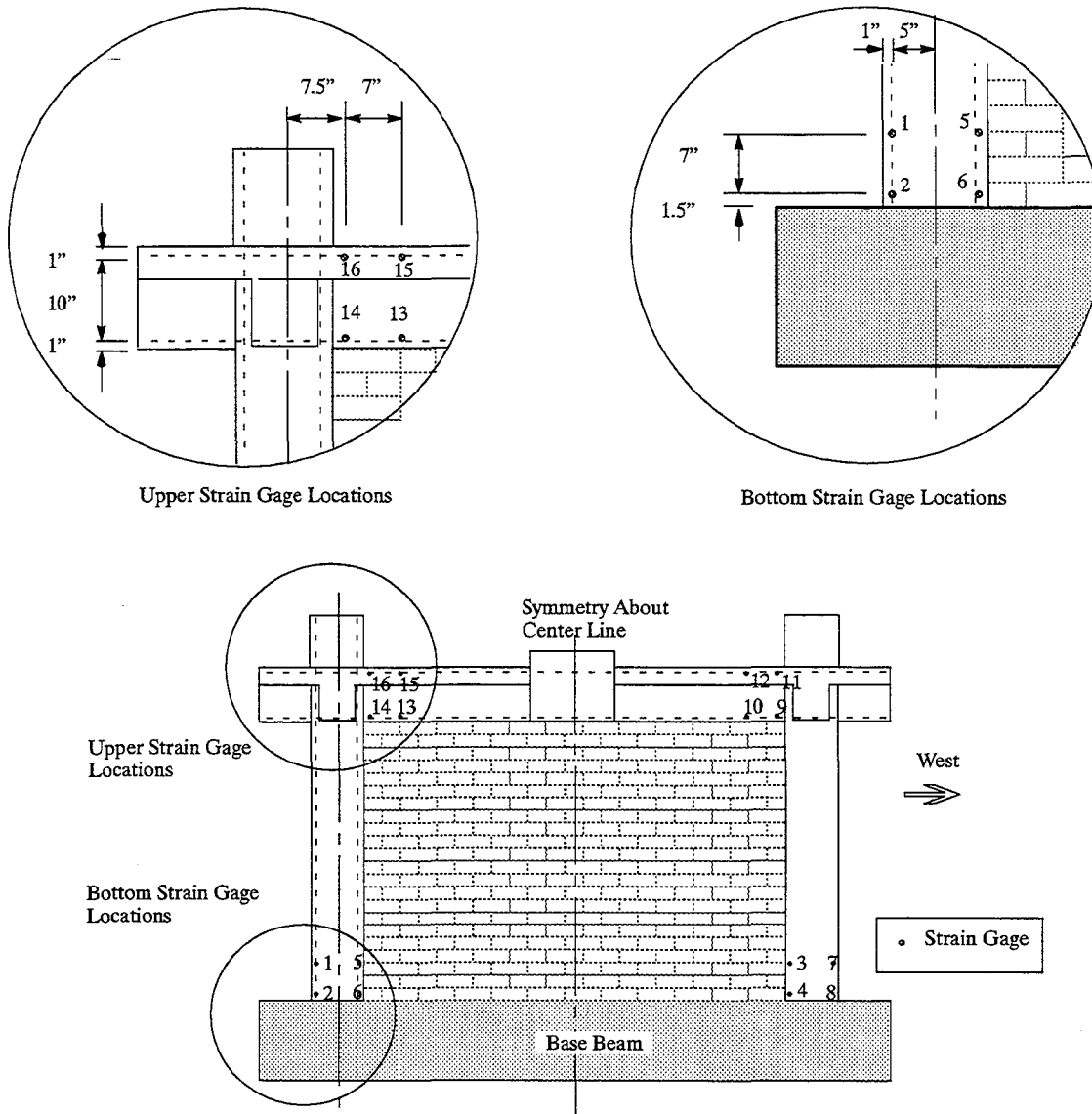


Fig. 67 Reinforcing Strain Gage Locations For Concrete Frame

of the critical sections in the column/base beam connection. For the concrete frame, the weakest member in the column/top beam connection was the beam, and therefore, the eight remaining strain gages were placed in the critical sections of the beam as illustrated in Fig. 67.

The remaining number of channels open for instrumentation equipment were distributed among twelve LVDT's (Linear Voltage Displacement Transducer), and four load cells as illustrated in Fig. 68. Eight LVDT's were placed at the critical sections of the frame to estimate the relative rotation of the members. In addition, two LVDT's were placed in a X-shape pattern on the infill. The purpose of these LVDT's was to measure the global shear strain that developed on the infill during

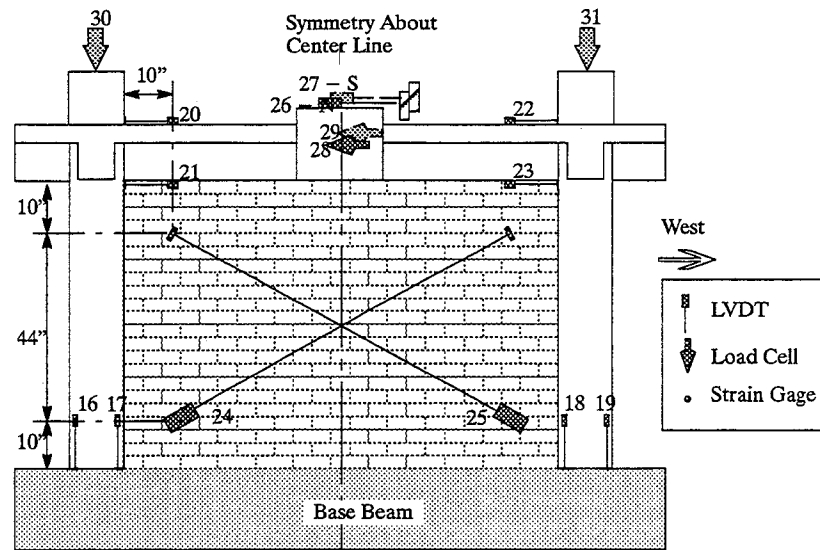


Fig. 68 Location for LVDT's and Load Cells

loading. The last two LVDT's measured the lateral drift of the frame. This lateral drift was measured as the lateral displacement of the center stub of the top beam. The final four available channels were used to record two different sets of load cells. A set of load cells was placed on top of the columns to record the axial load resisted by the columns during the testing of the specimen. Finally, and most importantly, a set of internal load cells controlling the system mechanisms of the hydraulic actuators were recorded.

A.2.2 Out-of-Plane Test

A total of ten channels were recorded by the computer during the out-of-plane tests. There were a total of seven displacement transducers placed at various locations across the infill as illustrated in Fig. 69; these displacement transducers monitored the overall deflection shape of the infill under the applied uniform load. In addition, there were two load cells placed at the top connections of the airbag reaction frame and the columns of the concrete frame. The purpose for these load cells was to verify the contact area of the airbag on the infill. Determination of an equivalent pressure acting on the entire infill surface area is possible from these load cells. The procedure used for the determination of the equivalent pressure is as follows: the air-bag pressure measured by the pressure transducer is converted to an equivalent uniform pressure by equating the external work done by the air-bag across the known contact area to that of the work done by equivalent pressures applied uniformly across the entire surface of the infill panel. Finally, the last recorded channel was used to monitor the pressure transducer for the air-bag.

The monotonic test was run in pressure control up to a maximum allowable capacity in the system of 720 psf. Test specimens with capacities larger than the capacity of the loading rig were tested

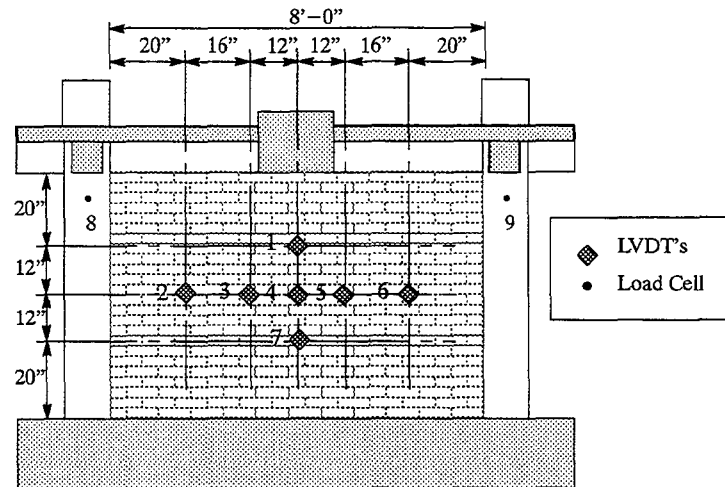


Fig. 69 Out-of-Plane LVDT'S Location

cyclically several times (by alternatively deflating and inflating the bag) to observe the elastic behavior of the frame/infill system even after out-of-plane cracking in the infill had occurred.

The type of instrumentation used during the in-plane and the out-of-plane tests is summarized in Table 16 and Table 17.

Table 16 In-Plane Test Instrumentation

Instrument type	Model	Range	Location
Strain Gages	Measurements Group, INC. EA-06-250BG-120	0.001"	Reinforcement Steel
LVDT	TRANS-TEK 0350-000	0.050"	Base Beam-Column Connections, Column-Top Beam Connections
LVDT	TRANS-TEK 0243-000	0.500"	Center part of Infill, Relative Max. Frame Displacements
Load-Cells	MTS 661.22 serie No. 516	110 kips	Inserted in the actuators
Load-Cells	Home Made	60 kips	Top of Columns

A.2.3 Masonry Strain Distribution

Gravity loads in frame-infill structures often apply a compressive stress to the masonry infill. The vertical stress distribution across the infill varies with the geometrical and mechanical properties of both the frame and the infill in the specimen. A number of displacement transducers (range of 0.050" LVDT) and displacement gages (0.010" gage) were placed across the frame-infill specimen to monitor the strain distribution as the vertical forces were applied to the columns. The monitoring instrumentation was placed on the specimen as shown in Fig. 70. This strain monitoring sequence was

Table 17 Out-of-Plane Test Instrumentation

Instrument type	Model	Range	Location
LVDT	TRANS-TEK 0244-000	1.000"	Center Part of Infill
Load-Cells	Home Made	8 kips	Reinforced Frame—Air Bag Reaction Frame Connections
Pressure Transd.	ASHCROFT M1	5 psi	Air Bag

performed solely for Specimen 2a. Based on the strain distribution experienced by the infill panel, and multiplied by the corresponding elastic modulus, the vertical compressive stress distribution was determined. Results from readings observed using this approach estimated a vertical stress in the panel similar to values from the flat jack test for Specimen 2a (40 psi). The forces applied to the columns were mostly carried by the columns with a minimal portion distributed to the infill. The vertical stress distribution was triangularly-shaped with largest values at the base of the specimen.

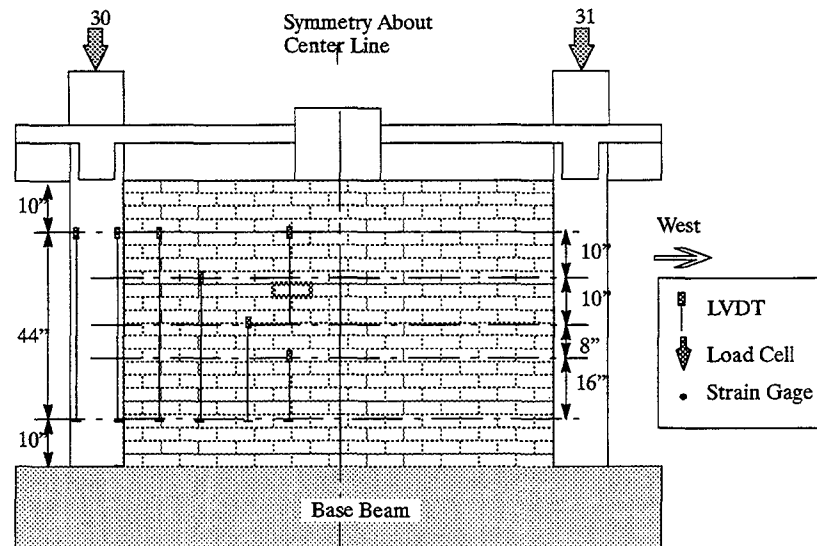


Fig. 70 Masonry Strain Monitoring Setup

APPENDIX B

CONSTRUCTION MATERIALS

This section summarizes the properties of the construction materials used to build the frame as well as properties of the various clay brick and concrete block masonry infills. Materials tested included masonry units, masonry prisms, mortar samples, concrete cylinders and beams, and steel bars. All of these test samples were built or cast during the construction of the specimen. All test samples were tested at the same time as the frame/infill specimen.

B.1 Frame Properties

Mechanical properties for the frame were chosen to properly model current design practices. A brief description of the materials used for construction of the reinforced concrete frame is presented in this section.

B.1.1 Base Beam

The base – beam for the frame was designed to represent a rigid support. The beam was strong and heavily reinforced as shown in Fig. 66. The behavioral aspects of this beam was not of primary concern. The concrete mixed used for the base beam was a common concrete mix ordered from the local supplier to meet a compressive strength of 4000 psi.

B.1.2 Concrete

The concrete was mixed using in – house mixing equipment. The equipment is a state of the art automatic concrete mixer. The desired mix was inputted into the mixer, and the exact amounts of materials were automatically mixed. This method of mixing was preferred when a high quality control material mix was required.

Two mechanical properties were obtained from standard testing methods for the concrete used in the frame: the compressive strength (ASTM C–39), and the modulus of rupture (ASTM C–78). Concrete samples for these tests are shown in Fig. 71 and Fig. 72 respectively.

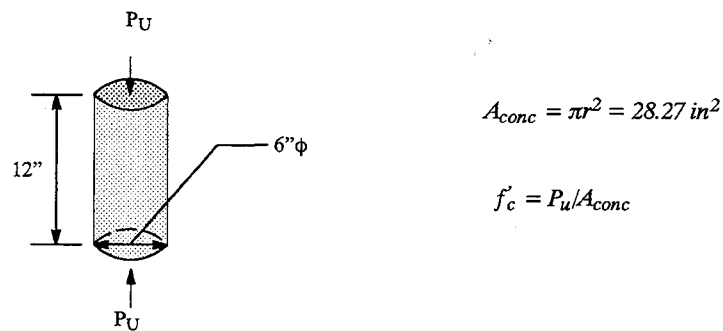
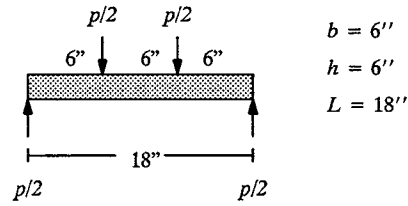


Fig. 71 Cylinder Test (ASTM C–39)

The concrete mix used for the frame was mixed in – house with a recipe obtained from the PCI handbook [57]. The concrete mix is presented in Table 18. Results for the compressive strength, and

Four point load



$$S_g = \frac{b d^2}{6} = \frac{6 * (6)^2}{6} = 36 \text{ in.}^3$$

$$M = \frac{P L}{6} = \frac{P * 18}{6} = 3 * P \text{ lbs} - \text{in}$$

$$M = f_r S_g \rightarrow f_r = \frac{M}{S_g} = \frac{3 * P}{36} = \frac{P}{12}$$

Fig. 72 Beam Test (ASTM C-78)

the modulus of rupture are presented at the end of this appendix in Table 19. The average concrete compressive strength of the frame was 8000psi with a coefficient of variation of 3.5%. These values were obtained from 15 cylinder tests carried out at the same time as the specimen testing. The average modulus of rupture for the frame was 700 psi with 9% coefficient of variation.

B.1.3 Steel

The yield stress and the tensile strength of the reinforcing steel bars used in the frame are summarized at the end of this section in Table 20. The type of steel used in the specimens had a yield stress of 60 ksi and complied with ASTM Standard A615–Grade 60. The tests were carried out in accordance with the ASTM Standard. The tensile force in the bar was measured by a load cell in the testing machine; and the steel deformations were measured by a four–inch extensometer. From the extensometer measurements, the strain in the bars was calculated. From the load cells, the stress was calculated. Based on the measured stress–strain curve for the steel the values for the modulus of elasticity was estimated, and it compared well with the generally used value of 29,000 ksi.

B.2 Masonry Unit

The two masonry unit types used in this research were clay brick and concrete block. Rationale for the selection of these specific units are discussed in the following section, and a summary of their material properties is provided at this end of the appendix.

B.2.1 Brick Type (ASTM C-62, ASTM C-67)

Representation of existing construction was of prime interest. Accomplishment of this task was done by obtaining reclaimed brick and using them in conjunction with a specific mortar type to obtain the desired strength. The mortar types are discussed in the following section.

Reclaimed bricks were the main masonry unit used as a typical unit for existing construction. The purchasing of 8000 bricks was completed with the cooperation of a distributor of reclaimed bricks located in Chicago. Various ASTM standard tests were used to evaluate basic mechanical properties of the bricks including the initial rate of absorption, the modulus of rupture and the flat–wise compressive strength (ASTM C67). The average compressive strength of the bricks was 3480 psi with a coefficient of variation of 6%.

B.2.2 Block Type (ASTM C-90)

Concrete masonry consists of units molded in different sizes that contain a mix of cement and aggregate. The concrete masonry units were obtained from a local material supplier. Common 4" and 6" wide blocks were chosen to represent the required h/t slenderness ratio. The ASTM C90 designation for the units is hollow load-bearing concrete masonry unit Grade N, Type 1. Grade N specifies that the unit may be used in walls above and below grade which may or may not be exposed to moisture or weather. Type 1 specifies that the unit meets the requirement to be considered as a moisture-controlled unit. Several ASTM standard tests were used to evaluate basic mechanical properties of these concrete units including the initial rate of absorption, and the flat-wise compressive strength over the gross area.

B.3 Mortar (ASTM C-109)

Two mortar types were chosen to represent older and recent construction. Representing older construction was lime type mortar. Lime mortar contained proportions 1:3 (lime:sand). This mixture yielded poor mechanical properties. The mortar type chosen to represent recent construction was Type N mortar. This mortar type contained a mixture in the ratio 1:1:6 (cement:lime:sand). Type N mortar yielded a higher compressive strength as well as better overall mechanical properties. Type S mortar was used for the first specimen. Type S mortar, with a mixture ratio 1:1/2:4 1/2 (cement:lime:sand), observed similar mechanical properties as Type N mortar. Several two-inch cubes were made during different stages of construction of the infills. These cubes were then tested to failure in uniaxial compression following ASTM C109 in an universal MTS compression machine. An average compressive strength of 900 psi for lime mortar and 1200 psi for Type N mortar were obtained from tests in accordance to the ASTM standard.

B.4 Prism Test (ASTM E447-84)

An average of four prisms were built during the construction of every infill in accordance to ASTM E447-84. The prisms were tested at the same time as the frame/infill specimen for consistency. The tests were carried out in a MTS universal 50-kip capacity machine. The rate of loading was controlled according to ASTM test standards. Fig. 73 shows the prism test setup used for the compression tests. Prism compressive strengths were based on the maximum required applied load divided by the measured cross-sectional area of the prism. The modulus of elasticity was estimated from load-deflection plots recorded during the prism tests. The load was recorded directly by the computer from the internal load-cell in the MTS machine. The displacements were measured by two LVDT's attached directly to the masonry for accurate results. An LVDT was placed on each face of the prism to estimate the average deformation through the center of the prism. Results from prism tests are presented in Table 21 at the end of this appendix.

B.5 Diagonal Tension Test (ASTM E519-81)

The diagonal tension test determines the shear strength of the masonry. The tests were performed by loading in compression, at a 45 degree angle, a single wythe 4'x4' masonry panel. These

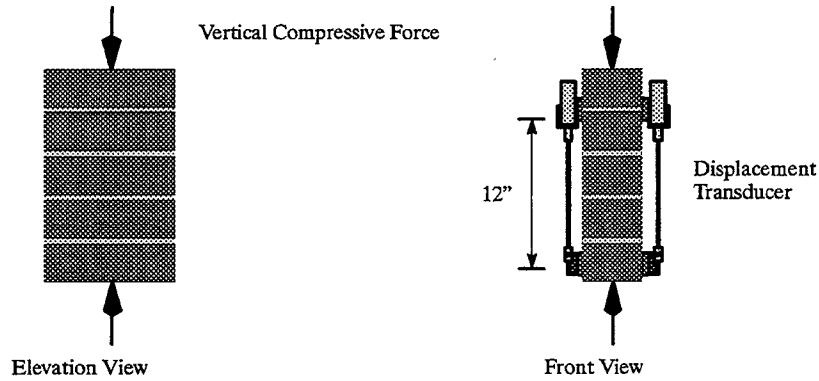


Fig. 73 Prism Compression Test

panels were loaded to the failure load of the specimen as described in the ASTM E519 standard. In addition to estimating the shear capacity of the infill, the test also permits the evaluation of the shear modulus of the masonry. The shear modulus was calculated from readings recorded by displacement transducers during the testing of the specimens. The placement of the displacement transducers as well as the overall test setup utilized is illustrated in Fig. 74. Three 4'x4' panels were built by the

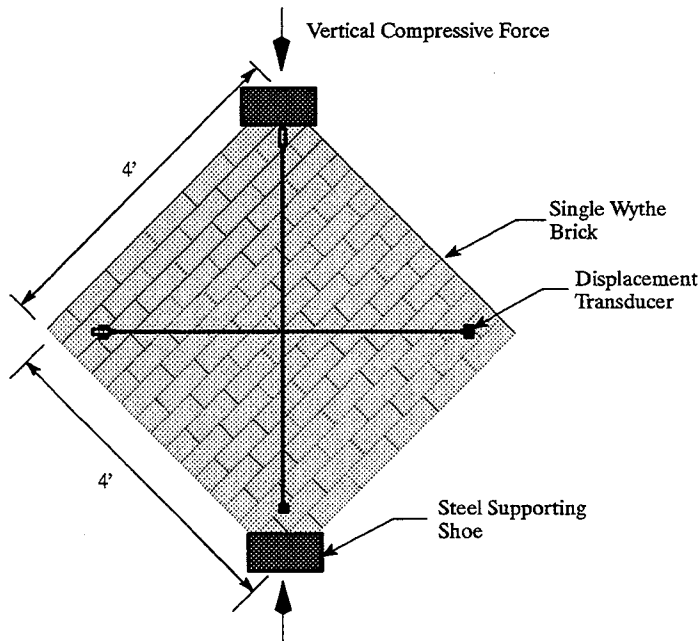


Fig. 74 Diagonal Compression Test

masons at the same time as the specimen was constructed. These tests were performed prior to testing of the specimen to better predict the strength for that specific frame/infill specimen. Measurements and calculations were done in accordance to ASTM E519-81 standards. Complications during the tests prevented the testing of two of the specimens. The specimens failed prematurely due to lack of a strong masonry bond strength. The tested specimen yielded a strength of 60 psi at cracking. The

common failure mode observed for these tests consisted of a vertical crack pattern extending from support to support. The cracks occurred mostly through the mortar joints with a couple of split bricks at the center of the specimen.

B.6 Quadlet Test

The quadlet test estimates the shear strength in the masonry. As shown in Fig. 75, a simple arrangement of four bricks was built. Quadlet samples were cured for the same period of time and under the same atmospheric conditions as the actual infill specimen. The testing of these quadlets was done at the same time as the testing of the infill/frame specimen. A typical quadlet and the overall testing setup used is shown in Fig. 75. Lime mortar type specimens did not perform as desired, and

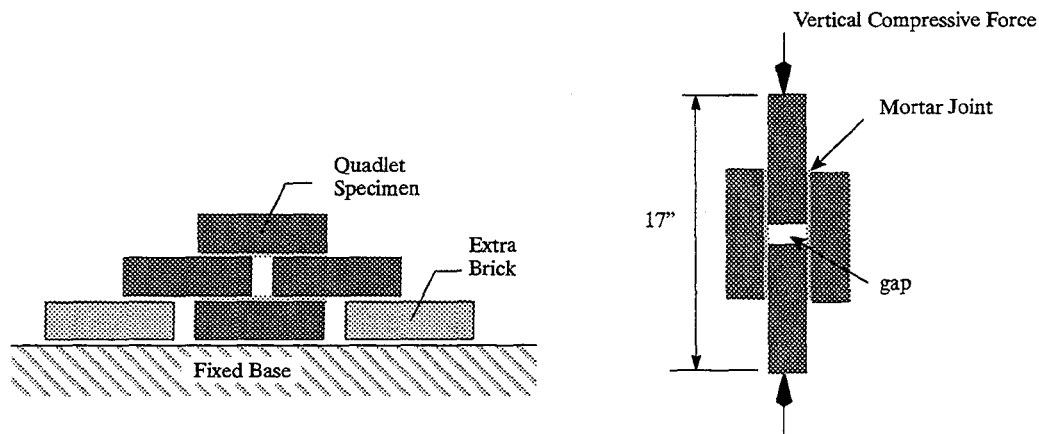


Fig. 75 Quadlet Test Specimen

broke prematurely due to lack of tensile strength. Type N mortar, was used in the remainder of the tests. The average shear strength for these specimens was found to be 56 psi with a coefficient of variation of 49%. The data scatter was too large for meaningful interpretation of results.

B.7 Test for Flexural Tensile Strength

The flexural tensile strength of the masonry is important when evaluating masonry construction for cracking strength. The flexural tensile strength of the masonry depends on factors such as the direction of the bed mortar joint with respect to the direction of the applied load, the type of mortar, and the bond strength. Evaluation of these properties is outlined in this section.

B.7.1 Perpendicular to bed joint (ASTM E518–80)

Flexural tensile strength perpendicular to the bed joint is an important mechanical property of the masonry. Evaluation of this property was performed according to ASTM E518–80. A typical specimen used in this testing procedure consists of a total of 10 bricks laid on top of each other in a stack bond pattern. The overall testing setup used to determine the flexural tensile strength perpendicular to the bed joint is illustrated in Fig. 76. The specimen was tested by applying two point loads placed at equidistant locations. The load was applied by a hydraulic jack controlled by a manual

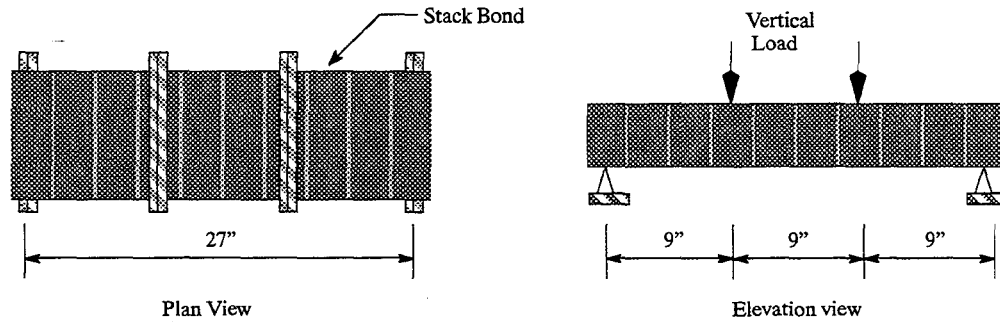


Fig. 76 Flexural Bond Strength of Masonry Perpendicular to Bed Joints

hand pump. This load was recorded by a load-cell that kept track of the highest load applied. The flexural tensile strength was then calculated as the moment applied by the two point loads divided by the section modulus at the failure section. The average value of 32 psi (c.o.v. of 32%) was obtained from testing of specimens built with Type N mortar.

B.7.2 Parallel to bed joint

The flexural tensile strength parallel to the bed joints for masonry is also an important parameter. This type of testing was executed in accordance to ASTM E518-80. The construction of the test specimen is not standard. The chosen configuration consisting of ten bricks long by 4 courses high was decided to be the most representative sample of actual construction. The placement of the loads, and the equipment utilized to acquire the data were similar to the ones used for the evaluation of the tensile strength of the masonry perpendicular to the bed joint. The testing setup for this test is presented schematically in Fig. 77. The calculated flexural tensile strength was based on the moment

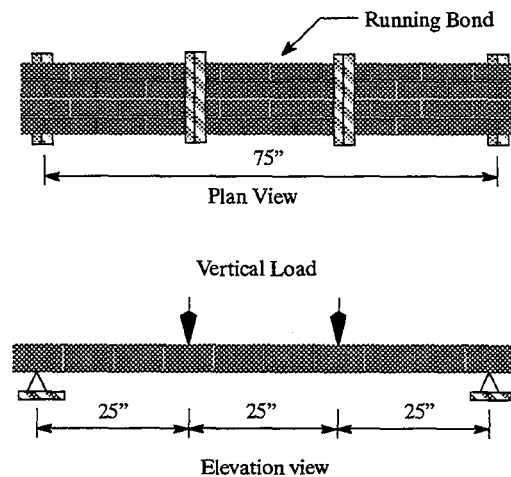


Fig. 77 Flexural Bond Strength of Masonry Parallel to Bed Joints

applied divided by the section modulus at the failure section. The average value of over 220 psi (c.o.v.

of 28%) was obtained from these tests for specimens build with type N mortar, and reclaimed clay masonry units.

Table 18 Concrete Mix for Concrete Frame

Material	Weight	Ratio of Content	Standard Units
Cement (type I)	331 lbs	0.215	3.52 bags
Water	173 lbs		20.8 gallons
Fine Aggregate (coarse sand)	693 lbs	0.450	5.8 ft ³
Coarse Aggregate (pea gravel)	518 lbs	0.340	4.3 ft ³

Typical Batch size = 0.45 cy = 1640 lbs. Slump (average of 3) = 4"
Water/Cement Ratio = 0.52

Table 19 Concrete Properties for Frame*

Batch #	P _{u(rupture)} (kips)	f _r (ksi)	P _{u(comp.)} (kips)	f _c (ksi)
1	7.825	0.652	228.8	8.09
2	7.577	0.632	218.5	7.73
3	8.630	0.719	235.4	8.32
4	9.512	0.792	226.3	8.00
Average Values =		0.699		8.04

* Each entry represents the average of three tests

Table 20 Steel Properties for Frame*

Bar #	P _y (kips)	F _y (ksi)	P _u (kips)	F _u (ksi)
3	7.22	65.6	11.7	106.1
4	13.33	66.3	19.3	96.7
5	21.97	70.9	34.2	110.3
7	39.20	66.4	59.9	101.6

* Each entry represents the average of three tests

Table 21 Results for Prism Tests in Concrete Frame*

Infill #	f_m (psi)	E_m (ksi)
1	1670	1138
2	1575	1167
3	1470	756
4	3321	1804
5	3113	1686
6	665	310
7	1596	424
8	507	342

* Each entry represents the average of four tests

APPENDIX C

NDE TESTING

Non-destructive tests were done prior to testing to determine mechanical properties. The flat-jack test and the in-place shear (shove) test were done. A detailed description of the non-destructive evaluation techniques used in this report are presented by Epperson and Abrams [26].

C.1 Effect of Column Axial Compression and Infill Compression Stress

Compressive forces were applied to the columns simulating the state of stress of actual structures. The vertical force transfers partly through the infill and mostly directly to the columns. The state of stress is of interest for the evaluation of the panel; for that purpose, the flat jack test is used. The corresponding testing procedure is described in this section.

The flat-jack test determines the vertical compressive stresses present in masonry walls. A cut is made in the mortar bed joint. The locations for performing the flat jack test are presented in Fig. 78. A diagram of the hydraulic jack is shown in Fig. 79. The hydraulic flat jack utilized in this project was designed to be used for infills with thicknesses as small as 2 inches. When placing the flat jack, the void in the masonry joint was filled with a wet hydrocal mix used to obtain a continuous bearing surface between the surface of the flat jack and the surface of the exposed masonry.

The distance between two fixed points on adjacent sides of the cut bed joint was measured before and after cutting the mortar joint. The setup used for this procedure is presented in Fig. 80. The state of stress in the infill before and after cutting is illustrated in Fig. 80. The masonry initially had a relative distance between the two selected fixed points that reduced when the removal of the joint occurred. Once the flat jack was placed within the removed joint and the hydrocal mix had cured, the jack was pressurized. Then, the pressure in the jack was increased with the use of a manual hydraulic pump at a constant rate until the displacement of the undisturbed masonry (D_f) was

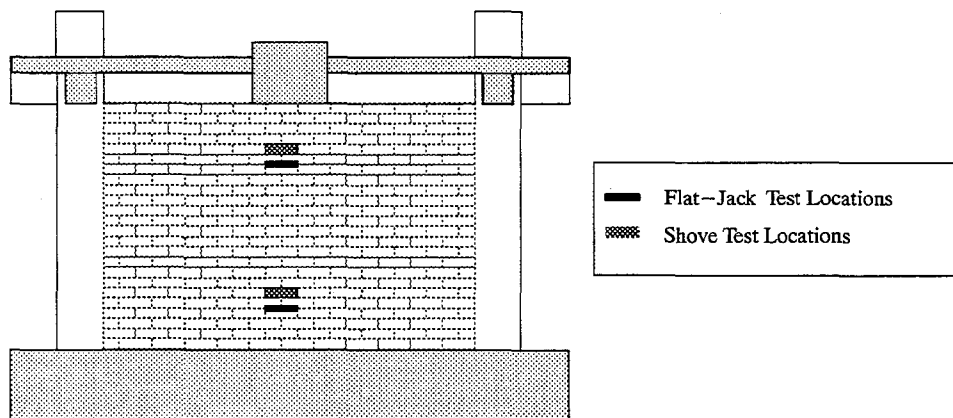


Fig. 78 Locations for Flat-Jack tests, and Shove Tests

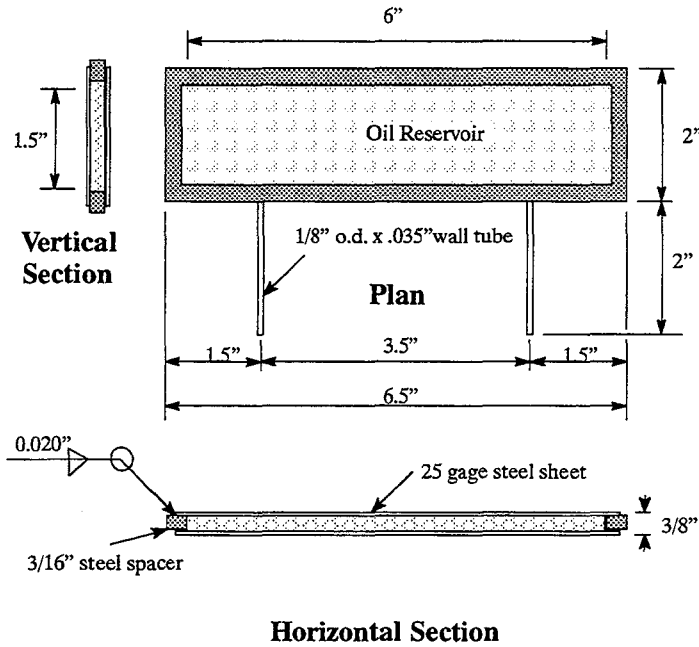


Fig. 79 Flat Jack

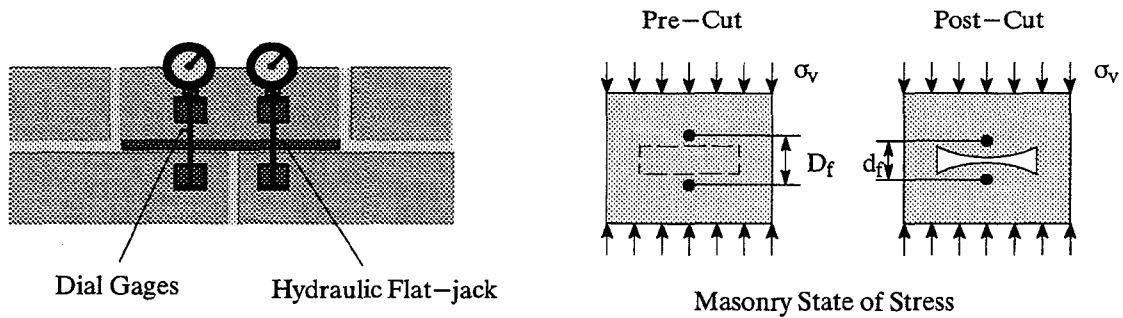


Fig. 80 Flat-Jack Test Setup

reached. The pressure in the hydraulic jack and the relative distance between the fixed points were recorded.

The flat jack applied stress on the masonry was computed as:

$$\sigma_f = K_j K_a P_f$$

where :

σ_f = applied stress by flat jack on masonry

K_j = jack constant

K_a = area constant

P_f = hydraulic pressure in flat jack

Due to a small amount of pressure required to initially deform the flat jack, the hydraulic pressure

within the jack is higher than the stress applied to the masonry by the jack. The factor K_j is the jack stiffness constant and was determined by pressurizing the flat jack against the platens of an uniaxial testing machine. A factor of 0.96 was determined for K_j .

The surface area on which the flat jack acted was not of the same magnitude as the surface area of the removed mortar joint. A correction factor that considered the effective area on which the flat-jack bears against the masonry was then applied to the recorded flat jack pressures. K_a is the factor that considers the flat-jack bearing area on the masonry and is defined as the ratio of the flat jack area to the area of the removed mortar bed joint. The area of the flat-jack was smaller than the area of the cut joint, and an average value of 0.76 was determined for K_a .

Once the flat-jack test was completed, repair of the masonry was done by injection of mortar into the open joints, until the gap was totally full. The mortar was the same kind as previously used. It was left to cure until its strength was comparable to the rest of the masonry.

The vertical stress distribution was monitored using several dial gages located throughout the infill and the frame as illustrated in Fig. 70. Relative strains recorded from the dial gages were then multiplied by the corresponding masonry modulus of elasticity. The modulus of elasticity used for this purpose were obtained from previously tested masonry prisms. The vertical stress distribution measured using the dial gages was triangularly shaped. Monitoring of stress distribution in the infill by dial gages was done only for Specimen 2a.

Results from the flat jack test and the reading obtained from the dial gages placed throughout the infill agreed with the presence and magnitude of the vertical stress for Specimen 2a. Flat jack test results are presented in Table 9. The vertical stress corresponded to a typical vertical load of 50k on each column of the frame. From flat jack test results it was concluded that the infill carried approximately 7% of the vertical forces applied to the columns.

C.2 Masonry Shear Strength

The shear strength is one of the most important properties of masonry. A shear strength estimate is vital for evaluation of the lateral load capacity of existing masonry structures. Shear strength of existing masonry depends on the types of materials used and on the quality of the workmanship during construction. In situ tests can therefore provide unique information about the strength of existing construction. Although this type of testing has been used for various types of masonry members, its use for masonry infills is scant.

The shove test measures the shear strength along the brick/mortar interface of a single brick in a masonry panel. A brick is removed to allow placement of a small hydraulic jack and a low range load cell. The mortar head joint on the opposite end of the single brick to be tested is also removed to allow movement of the brick and to better estimate the effective mortar area resisting the applied force. The overall test setup is illustrated in Fig. 81. The relative movement was monitored at all times by a displacement transducer. The general load-deflection behavior of the brick was monitored

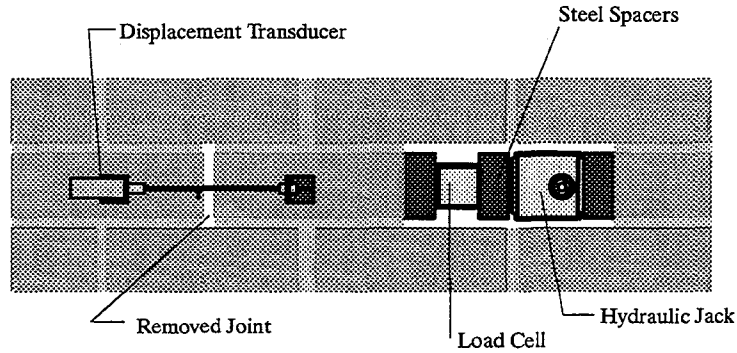


Fig. 81 Shove Test Setup

during testing. The shear strength of the masonry was estimated as the maximum pushing force read by the load cell divided by the effective area of the mortar joints resisting this force. Typical locations for performing the shove test are illustrated in Fig. 78. Results for the shove-tests are presented in Table 22. By measuring the shear strengths under a range of different vertical stresses, an expression for the shear strength based on the amount of vertical stress was developed. The expression is in the same format as presented in FEMA-178:

$$v_m = 0.56v_t + \frac{0.75P_D}{A} \quad \text{Eq. [89]}$$

where:

v_m = masonry shear strength

P_D = superimposed dead load at the top of the pier
under consideration

A = area of unreinforced masonry

v_t = 20% of v_{to} , and

$$v_{to} = \frac{V_{\text{shove-test}}}{A_b} - p_{D+L} \quad \text{Eq. [90]}$$

where:

$V_{\text{shove-test}}$ = shove test results

$p_{(D+L)}$ = stress resulting from actual dead load plus live load
in place at the time of testing (psi)

A_b = total area of bed joints above and below the
test specimen for each in-place shear test.

Results obtained for the shear strength using the expression from FEMA-178 are presented in Table 22 for comparison with the shove test results.

The hydraulic jack used in this study was an Enerpac Model RSM-200, with a capacity of 50,000 pounds. A load cell model Sensotek 53 with a range of operation of 0-50,000 pounds was used to record the applied load. Movement of the test brick was monitored by a Trans-Tek Series 351

displacement transducer (working range of plus or minus 0.100 inches). The load and displacement channels were recorded with an IBM-AT computer with a MetraByte DASH-16F high speed A/D board, and with modified software from utility subroutines supplied with the A/D board.

Table 22 Shear Test Results*

Infill #	Load (lbs)	Area (in ²)	Shear Strength (psi)	
			Shove Test	FEMA-178
2	3200	25.6	125	40
3	2225	25.6	87	32
6	1975	57.6	35	16
7	3933	56.0	70	26
8	1675	55.3	30	12

* Each entry represents the average of two tests

APPENDIX D

CRACK PATTERNS

Cracking patterns, recorded following each in-plane and out-of-plane test, are presented in this appendix.

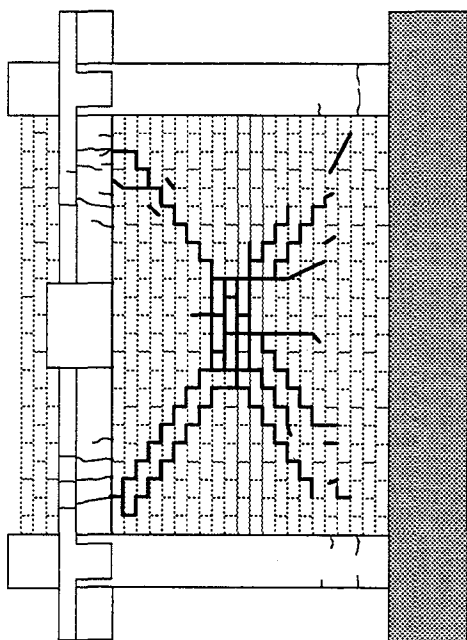


Fig. 82 Specimen 1 Brick Infill $h/t = 34$ Type S Mortar

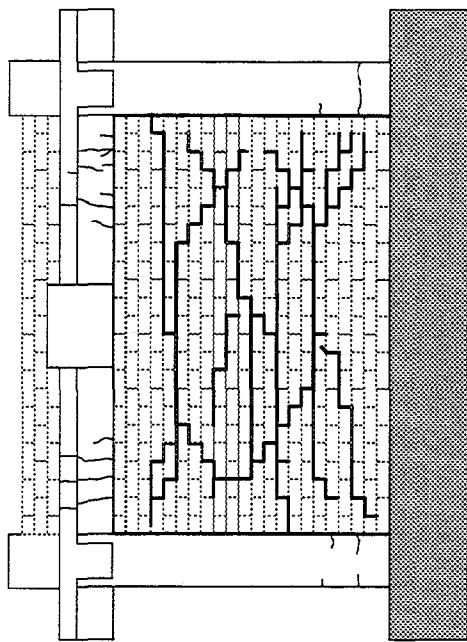


Fig. 83 Specimen 2a Brick Infill $h/t = 34$ Type N Mortar

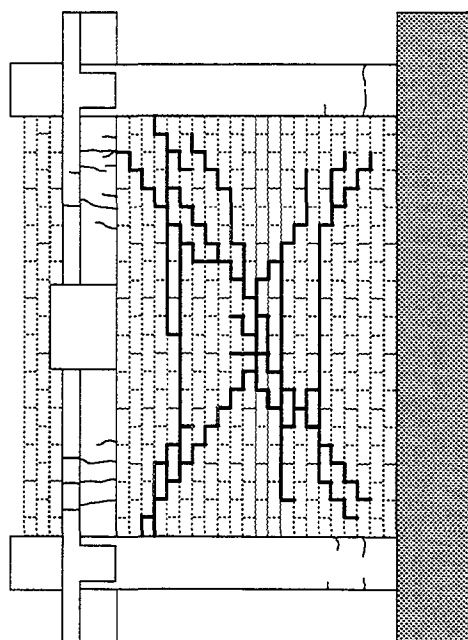


Fig. 84 Specimen 2b Brick Infill $h/t = 34$ Type N Mortar

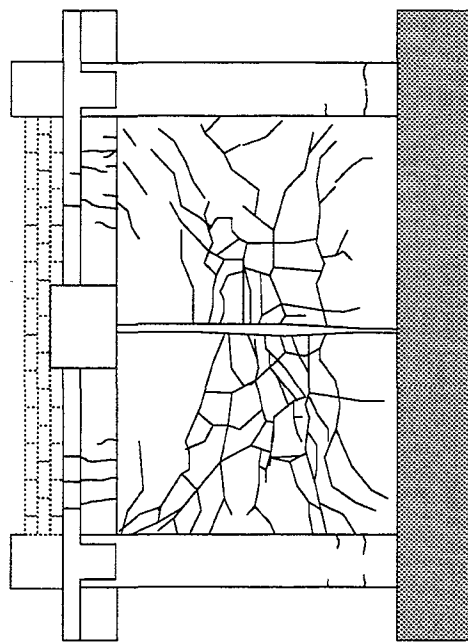


Fig. 85 Specimen 2c Repaired Brick Infill $h/t = 21$

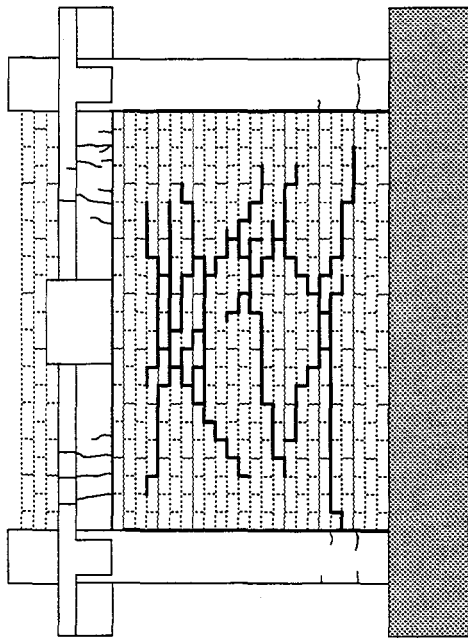


Fig. 86 Specimen 3a Brick Infill $h/t = 34$ Lime Mortar

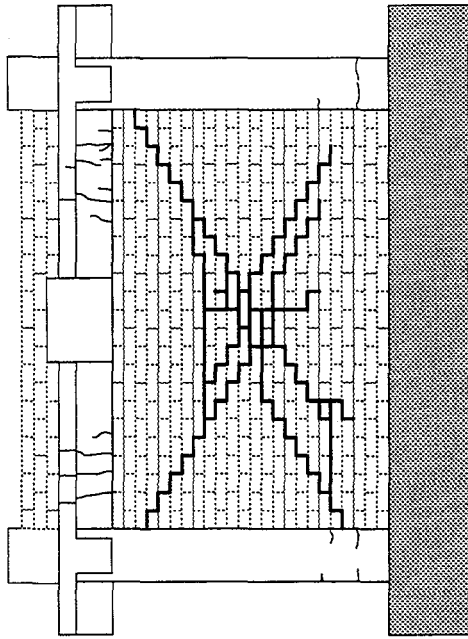


Fig. 87 Specimen 3b Brick Infill $h/t = 34$ Lime Mortar

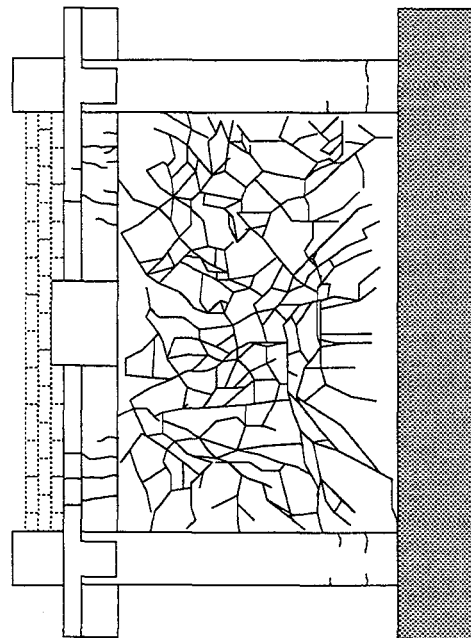


Fig. 88 Specimen 3c Repaired Brick Infill $h/t = 21$

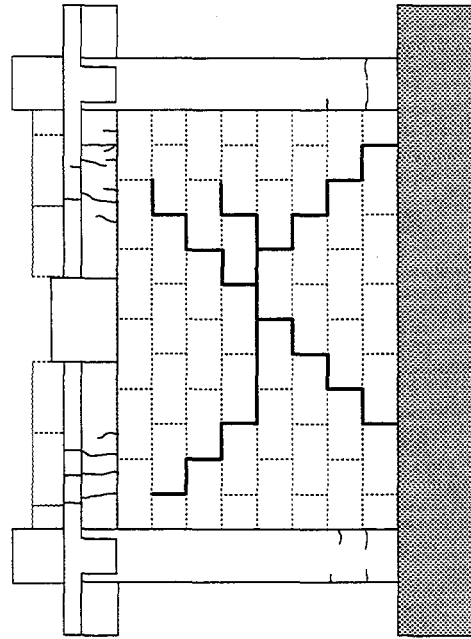


Fig. 89 Specimen 4a Block Infill $h/t = 18$ Type N Mortar

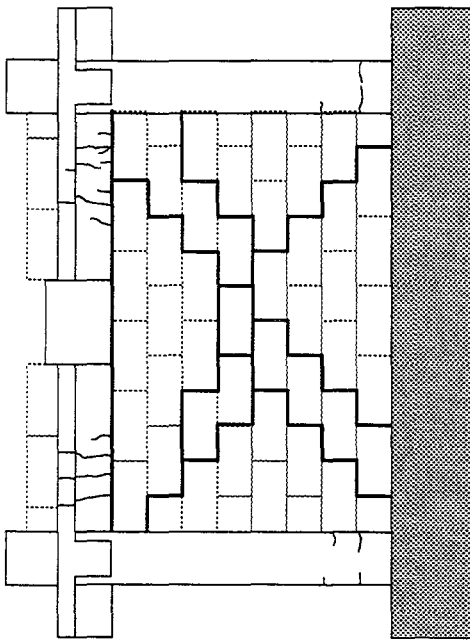


Fig. 90 Specimen 4b Block Infill $h/t = 18$ Type N Mortar

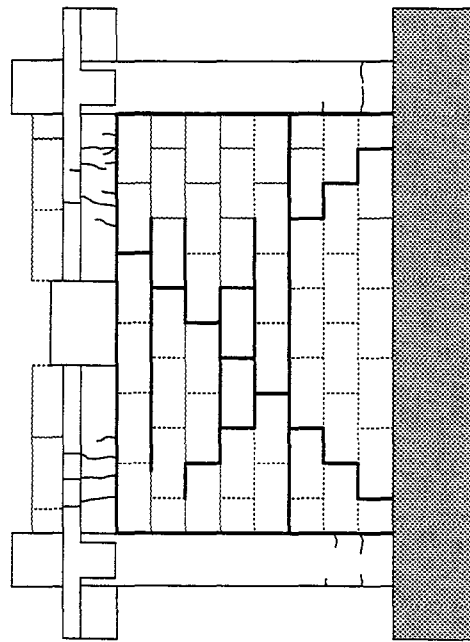


Fig. 92 Specimen 5b Block Infill $h/t = 11$ Type N Mortar

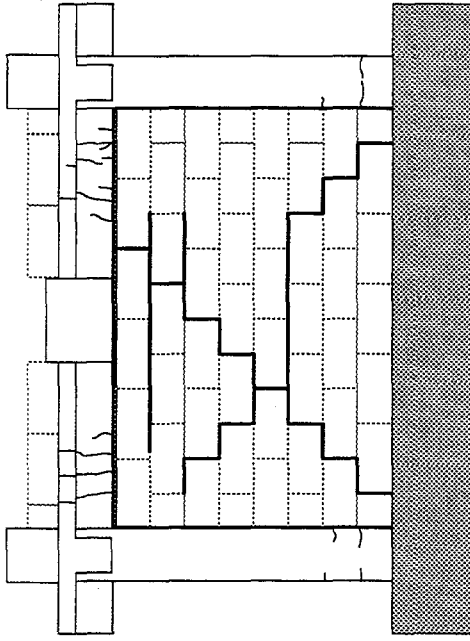


Fig. 91 Specimen 5a Block Infill $h/t = 11$ Type N Mortar

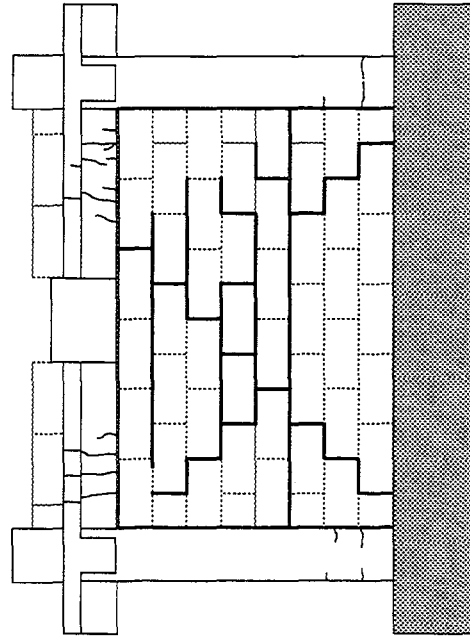


Fig. 93 Specimen 5d Block Infill $h/t = 11$ Type N Mortar

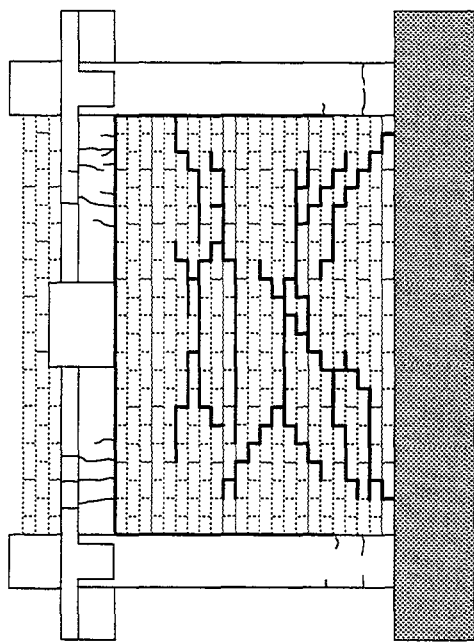


Fig. 94 Specimen 6a Brick Infill $h/t = 18$ Lime Mortar

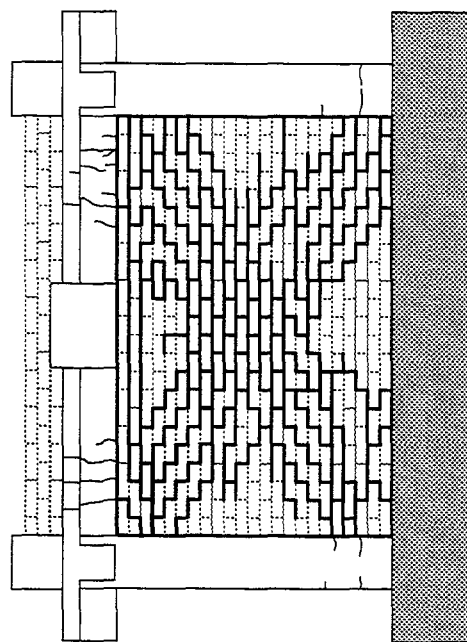


Fig. 96 Specimen 6b2 Brick Infill $h/t = 18$ Lime Mortar

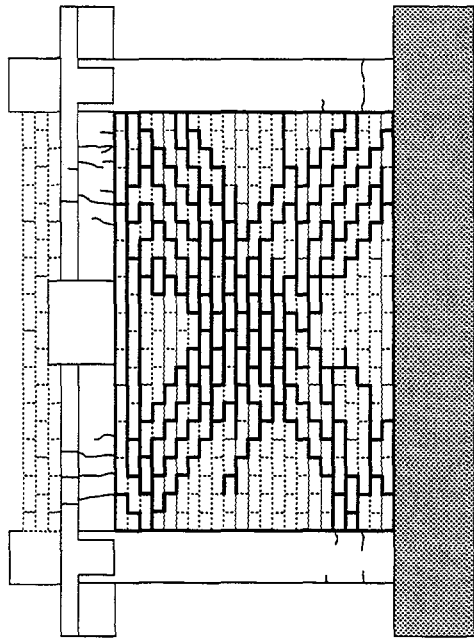


Fig. 95 Specimen 6b Brick Infill $h/t = 18$ Lime Mortar

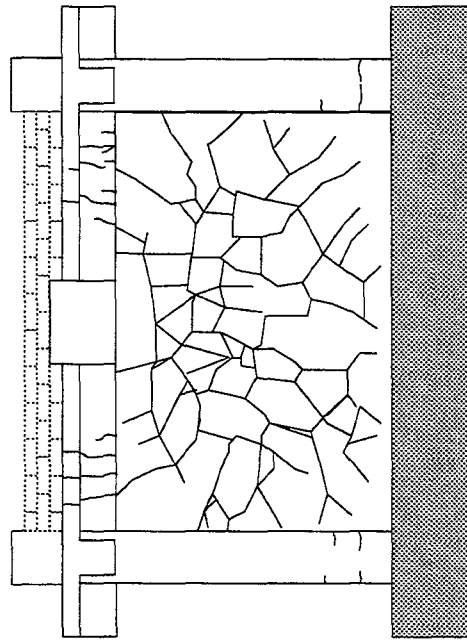


Fig. 97 Specimen 6c Brick Infill $h/t = 18$ Lime Mortar

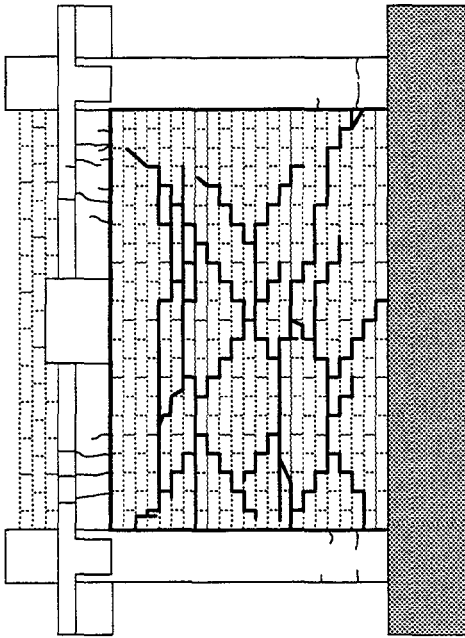


Fig. 98 Specimen 7a Brick Infill $h/t = 18$ Type N Mortar

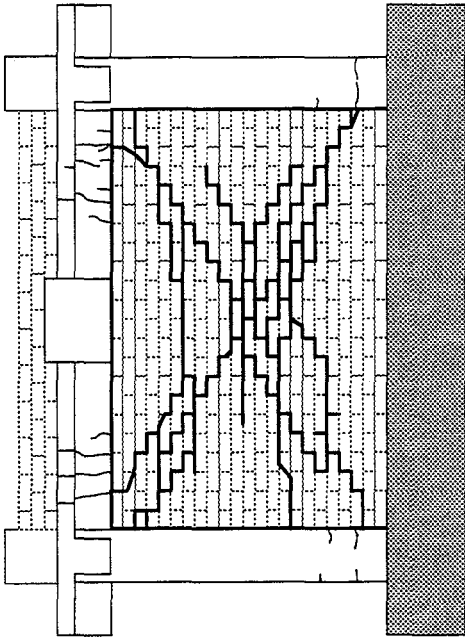


Fig. 99 Specimen 7b Brick Infill $h/t = 18$ Type N Mortar

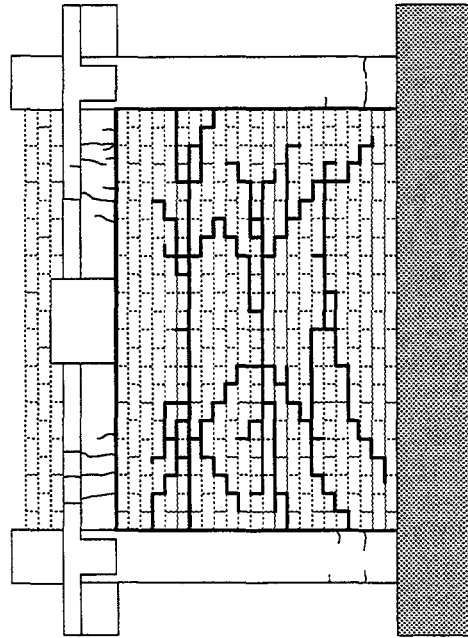


Fig. 100 Specimen 8a Brick Infill $h/t = 8$ Lime Mortar

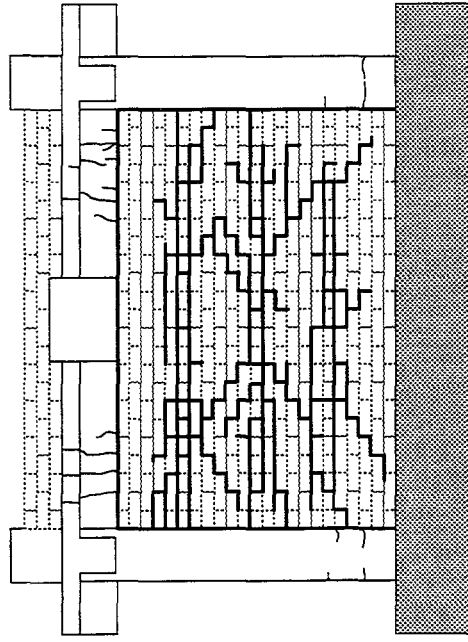


Fig. 101 Specimen 8b Brick Infill $h/t = 8$ Lime Mortar

APPENDIX E

IN-PLANE TEST RESULTS

A list of all plots obtained for the in-plane tests is presented in Table 23. These plots include plots for measured data and plots of calculated quantities for infill and frame as derived from the measured data.

Table 23 Summary of In-Plane Data

Figure Description
Lateral Load vs. Lateral Deflection
Lateral Load vs. Lateral Drift
Lateral Load vs. Shear Strain
Shear Stress vs. Shear Strain
Lateral Load vs. East Column Rotation
Lateral Load vs. West Column Rotation
Lateral Load vs. Rotation at East Side of Beam
Lateral Load vs. Rotation at West Side of Beam
LVDT vs. Strain Gage at East Column East Face
LVDT vs. Strain Gage at East Column West Face
LVDT vs. Strain Gage at West Column East Face
LVDT vs. Strain Gage at West Column West Face
LVDT vs. Strain Gage at East of Beam on Bottom
LVDT vs. Strain Gage at East of Beam on Top
LVDT vs. Strain Gage at West of Beam on Bottom
LVDT vs. Strain Gage at West of Beam on Top
Lateral Load vs. Thrust Developed on East Column
Lateral Load vs. Moment Developed on East Column
Lateral Load vs. Thrust Developed on West Column
Lateral Load vs. Moment Developed on West Column

E.1 Lateral Force vs. Shear Strain Relations

Lateral force vs. shear strain and shear stress vs. shear strain plots were developed based on acquired data from the test specimens. Equipment used to calculate the required data is presented in Fig. 102. Procedures for calculating the corresponding shear stresses and shears strains is illustrated and explained in Chapter 4.

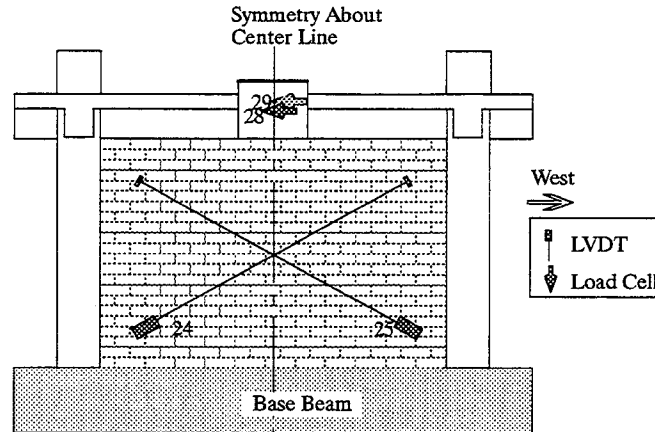
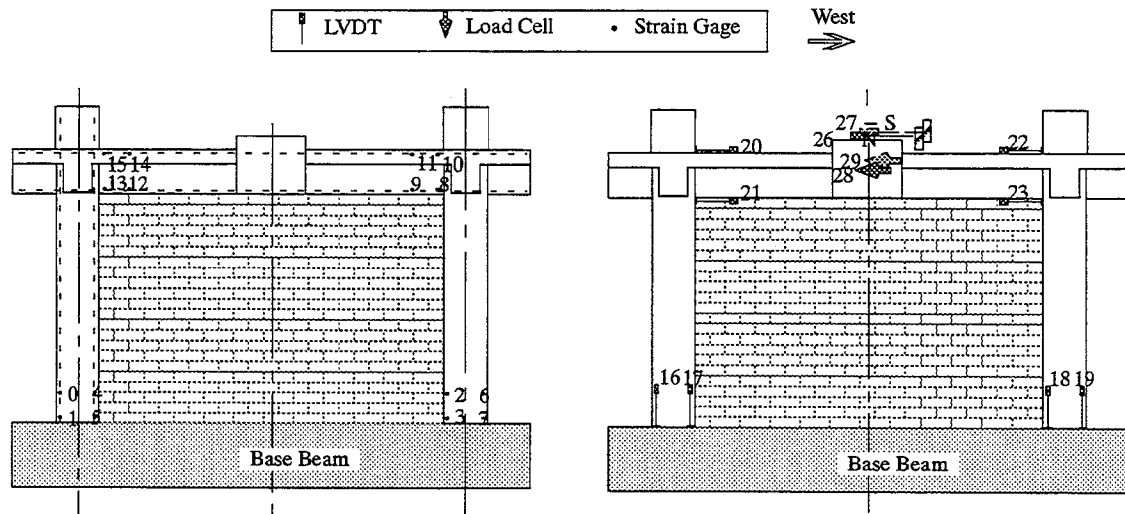


Fig. 102 Location for LVDT's Placed on the Infill and Load Cells in the Hydraulic Actuators

E.2 Frame Monitoring Instrumentation

Reinforced concrete frame behavior was monitored at its critical sections by strain gages placed directly on reinforcing bars, and by displacement transducers placed on the surface of the frame members. The instrumentation used to monitor the behavior of the frame is illustrated in Fig. 103. Relative hinge rotation at the ends of the beams and the columns were calculated as illustrated by Fig. 104. Applied lateral force vs. the calculated rotations were plotted and are presented at the end of this appendix.

E.3 Derivation of Frame Axial Loads and Resisting Moments



$$\theta = \frac{\delta_1 + \delta_2}{d}$$

$d = 9''$ for columns

$d = 14''$ for beam

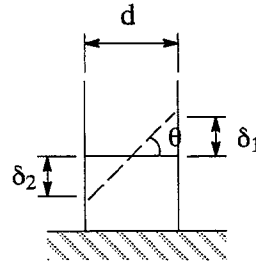


Fig. 104 Determination of θ

Lateral forces applied to the specimens during the in-plane tests created moments resisted by the specimen. Based on the recorded behavioral response of the frame during the tests, and by using several expressions developed in the next section, the applied moments and axial forces were evaluated.

Based on strain gage readings and on geometry, several expressions were developed for evaluation of axial forces resisted by the reinforcement and by the concrete in the columns. Axial forces in the reinforcement were simply evaluated as the strain recorded (always smaller than yielding strain) multiplied by the modulus of elasticity and by the corresponding layer steel area. Forces acting on the concrete were more complicated. Two different cases were considered depending on the location of the neutral axis based on the strain distribution in the column. The neutral axis laid within

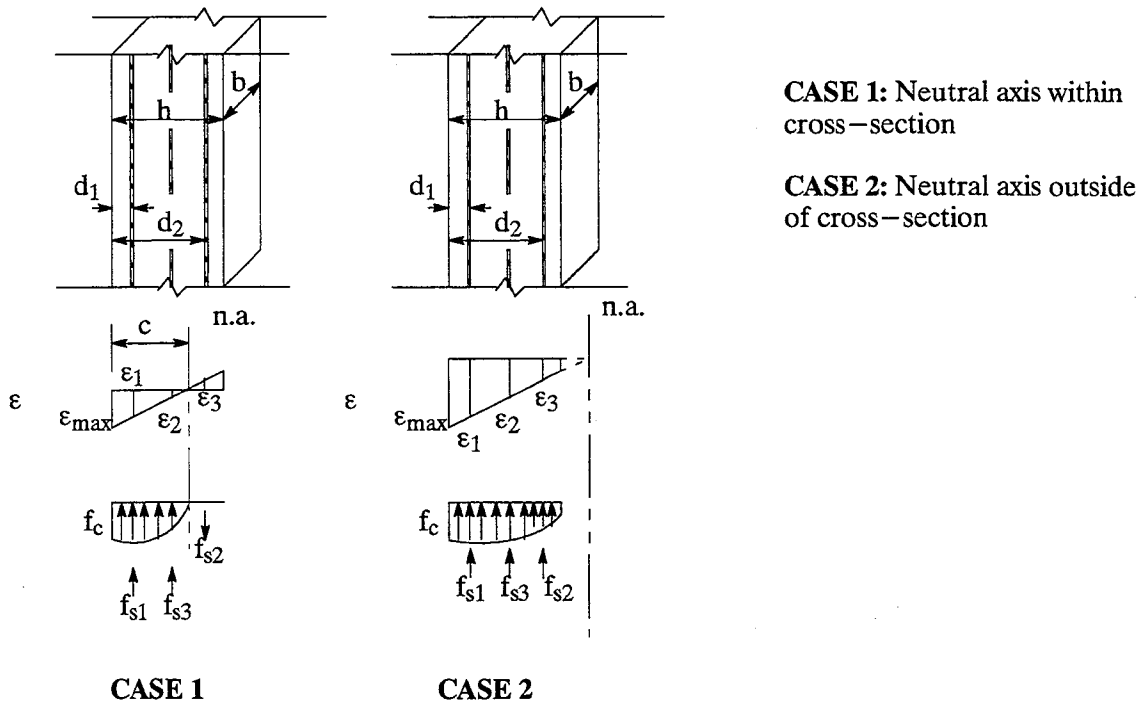
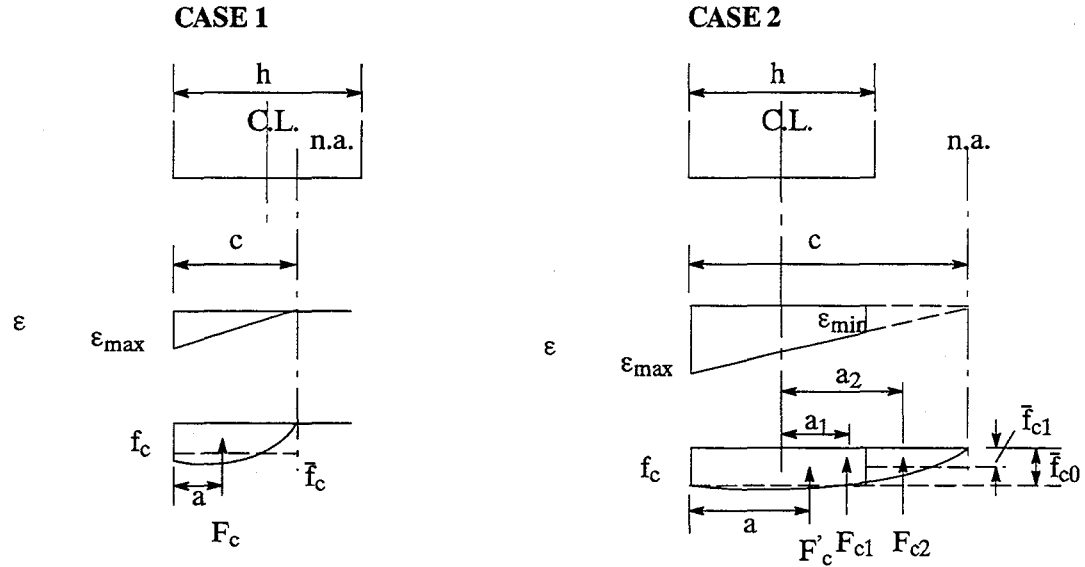


Fig. 105 Stress-Strain Distributions

the column or outside the column as illustrated in Fig. 105. Based on the maximum compressive strain in the columns and on the stress-strain distribution for concrete in compression, several equations were developed to evaluate the axial force in the columns as illustrated in Fig. 106. In the case where the neutral axis laid outside the column, superposition was used to subtract the force acting on the area outside the column.



Assume stress-strain distribution for concrete in compression is best represented by Todeschini continuous curve (MacGergor PP. 56-60)

$$\begin{aligned} \bar{f}_c &= \beta_1 f'_c & \bar{f}_{c0} &= \beta_{21} f'_c & \beta_{21} &= \frac{\ln(1 + x_1^2)}{x_1} & x_1 &= \frac{\epsilon_{\max}}{\epsilon_0} \\ \beta_1 &= \frac{\ln(1 + x_1^2)}{x_1} & x_1 &= \frac{\epsilon_{\max}}{\epsilon_0} & \bar{f}_{c1} &= \beta_{22} f'_c & \beta_{22} &= \frac{\ln(1 + x_2^2)}{x_2} & x_2 &= \frac{\epsilon_{\min}}{\epsilon_0} \\ F_{c1} &= \bar{f}_c c b & F_{c1} &= \bar{f}_{c0} c b & F_{c2} &= \bar{f}_{c1} (c - h) b \\ a &= \left[1 - \frac{2(x_1 - \tan^{-1} x_1)}{x_1^2 \beta_1} \right] c & F'_c &= F_{c1} - F_{c2} \\ a_{c.l.} &= a - \frac{h}{2} & & & & & & & & \end{aligned}$$

Distances from concentrated force to centerline of the columns is found in the same way as in case 1

Fig. 106 Development of Concrete Forces

Once axial forces were evaluated, the moment was determined by summing the calculated forces times their corresponding eccentricities with respect to the center line of the column. Eccentricities for the steel layers were constant and they were considered to be the distance from the center line of the column to the center line of the steel layer. The center steel layer did not contribute

to the moment resisting mechanism of the column. Expressions for the eccentricities of the developed concrete compressive axial forces are presented in Fig. 106. The values for these eccentricities depended on the geometry of the column and on the strain distribution as illustrated. Superposition of concrete and steel forces and moments was used in the evaluation of the total axial forces and moments. These evaluated axial forces and moments are plotted against the applied lateral force and results are presented at the end of this appendix for the test specimens.

E.4 Test Results

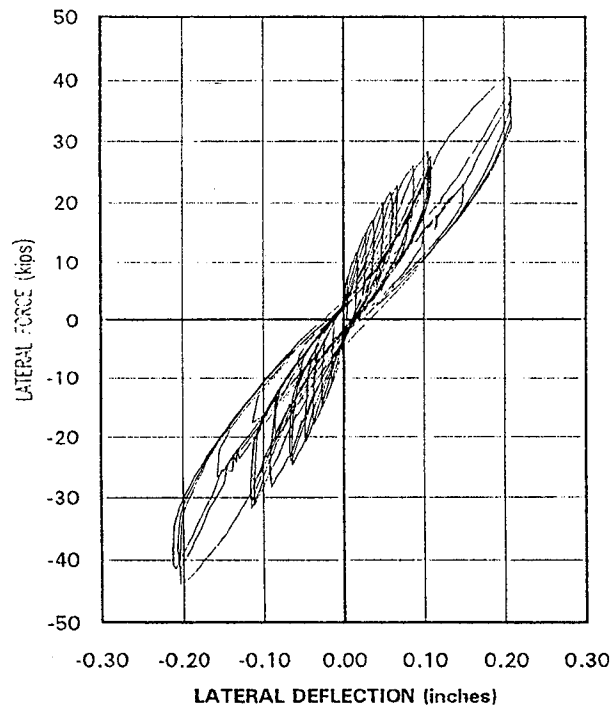
Test results are presented in ascending specimen number. A total of 5 sheets per test are presented and corresponding order is presented in Table 24.

Table 24 Summary of In-Plane Data

Figure Description	Spec. #	2a	3a	4a	5a	6a	7a	8a
Lateral Load vs. Lateral Deflection		○	○	○	○	○	○	○
Lateral Load vs. Lateral Drift		○	○	○	○	○	○	○
Lateral Load vs. Shear Strain		○	○	○	○	○	○	○
Shear Stress vs. Shear Strain		○	○	○	○	○	○	○
Lateral Load vs. East Column Rotation		○	○	○	○	○	○	○
Lateral Load vs. West Column Rotation		○	○	○	○	○	○	○
Lateral Load vs. Rotation at East Side of Beam		○	○	○	■	○	○	○
Lateral Load vs. Rotation at West Side of Beam		○	○	○	○	○	○	○
LVDT vs. Strain Gage at East Column East Face		○	○	○	○	○	○	○
LVDT vs. Strain Gage at East Column West Face		○	○	○	○	○	○	○
LVDT vs. Strain Gage at West Column East Face		○	○	○	○	○	○	■
LVDT vs. Strain Gage at West Column West Face		○	○	○	○	○	○	○
LVDT vs. Strain Gage at East of Beam on Bottom		○	○	○	■	○	○	○
LVDT vs. Strain Gage at East of Beam on Top		○	■	■	■	○	○	○
LVDT vs. Strain Gage at West of Beam on Bottom		○	○	○	○	○	○	○
LVDT vs. Strain Gage at West of Beam on Top		○	○	○	○	○	○	○
Lateral Load vs. Thrust Developed on East Column		○	○	○	○	○	○	○
Lateral Load vs. Moment Developed on East Column		○	○	○	○	○	○	○
Lateral Load vs. Thrust Developed on West Column		○	○	○	○	○	○	○
Lateral Load vs. Moment Developed on West Column		○	○	○	○	○	○	○

○ Good

■ Not Plotted



**Fig. 107 Test 2A—
Lateral Force vs. Deflection**

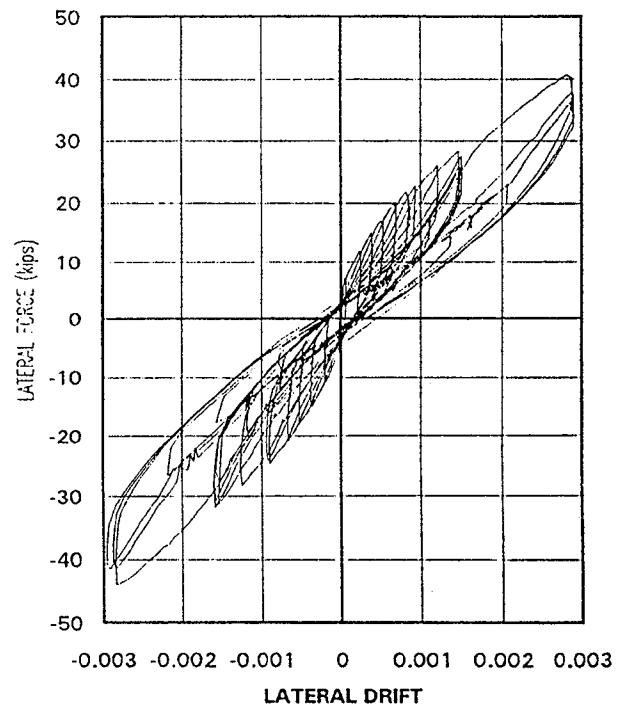


**Fig. 108 Test 2A—
Lateral Force vs. Drift**

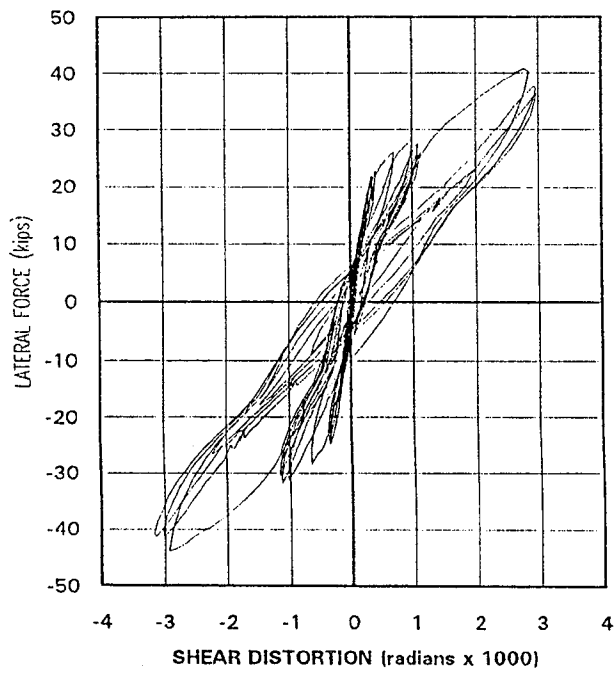


**Fig. 109 Test 2A—
Lateral Force vs. Shear Distortion**

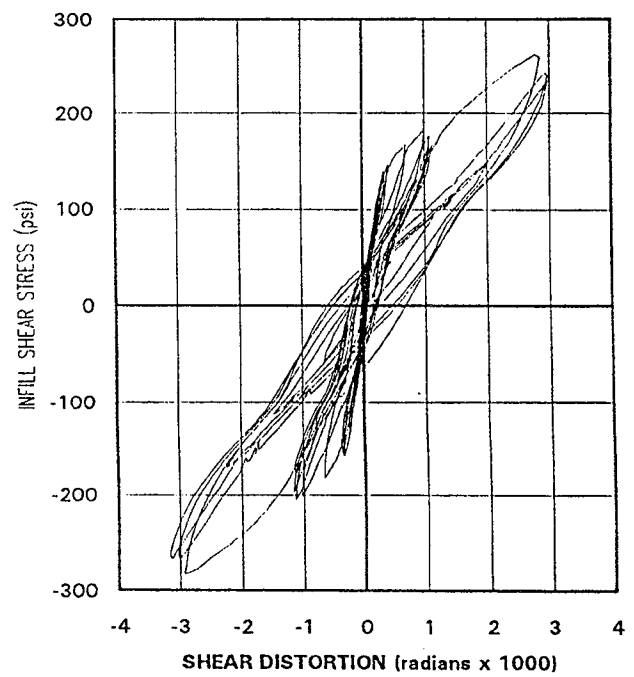


**Fig. 110 Test 2A—
Infill Shear Stress vs. Shear Distortion**

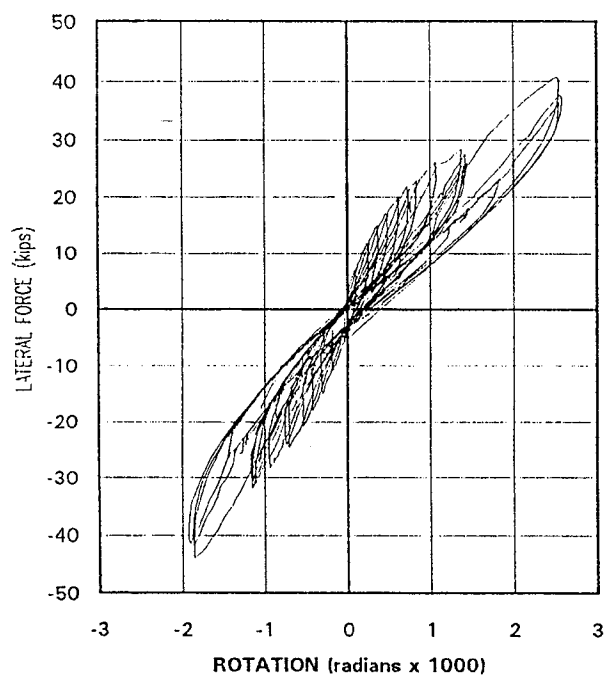


**Fig. 111 Test 2A—
Lateral Force vs. East Column Base Rotation**

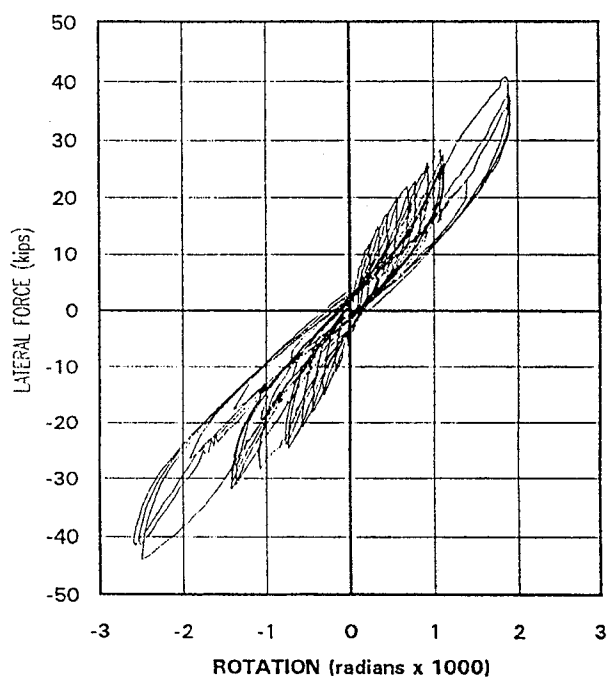


**Fig. 112 Test 2A—
Lateral Force vs. West Column Base Rotation**

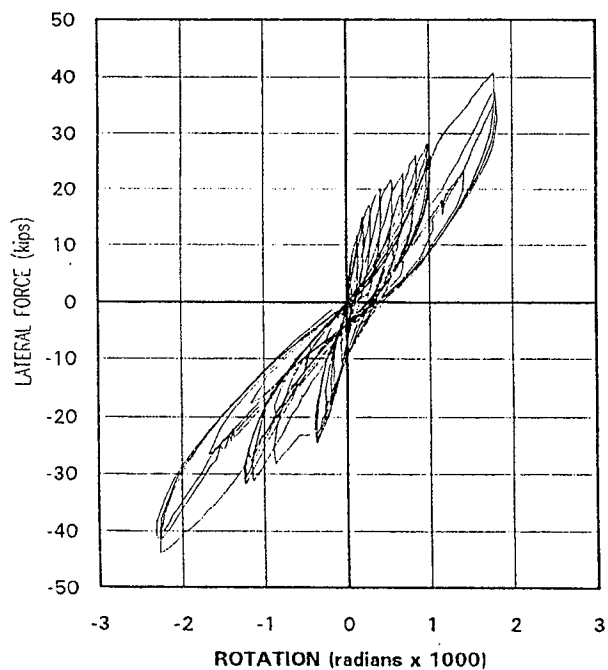


**Fig. 113 Test 2A—
Lateral Force vs. Beam East End Rotation**

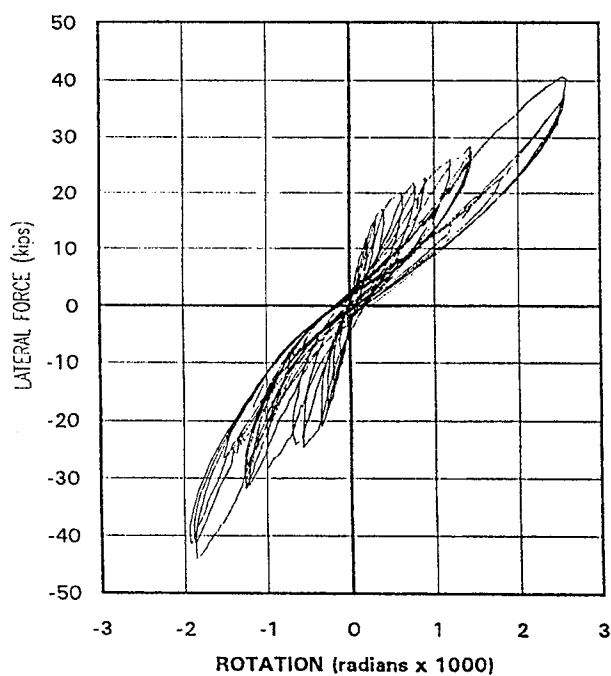


**Fig. 114 Test 2A—
Lateral Force vs. Beam West End Rotation**

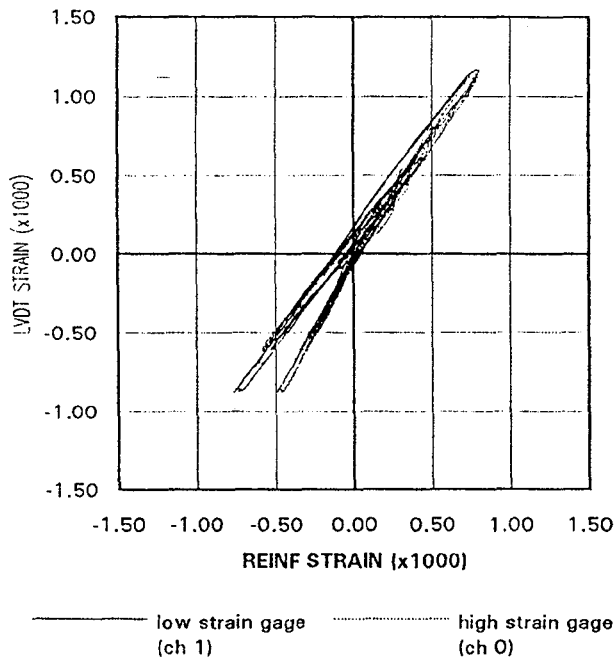


**Fig. 115 Test 2A— East Column East
Base LVDT Strain vs. Reinf Strain**

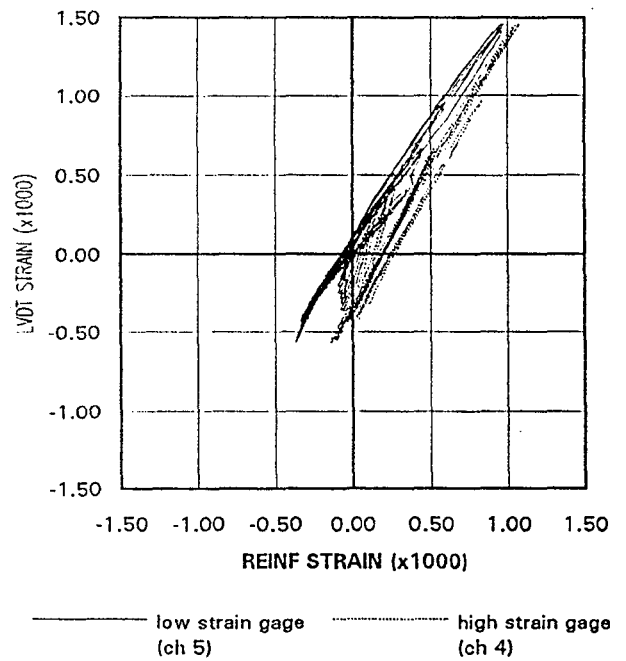


**Fig. 116 Test 2A— East Column West
Base LVDT Strain vs. Reinf Strain**

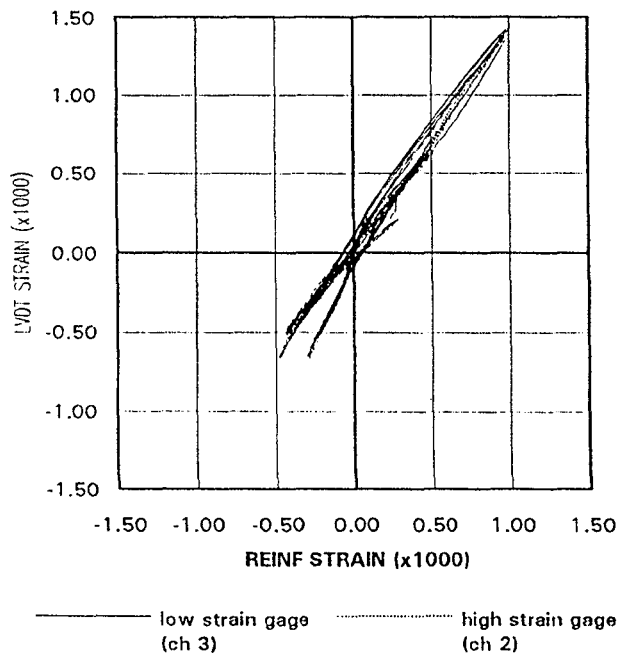


**Fig. 117 Test 2A— West Column East
Base LVDT Strain vs. Reinf Strain**

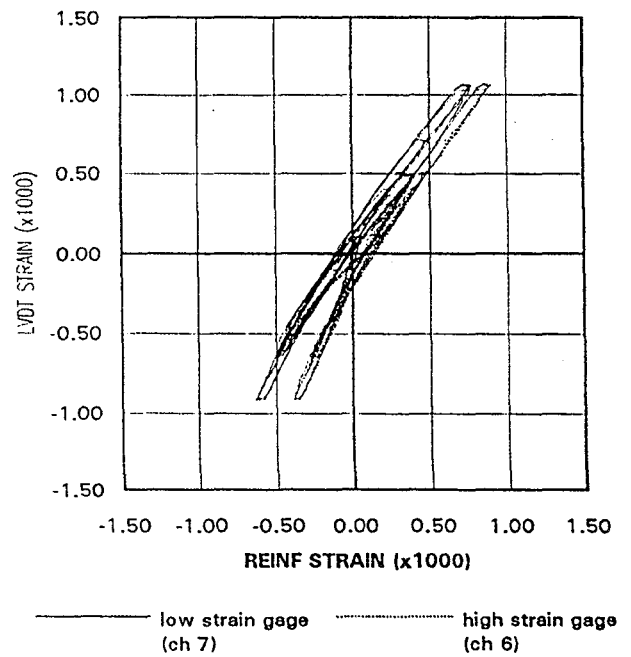


**Fig. 118 Test 2A— West Column West
Base LVDT Strain vs. Reinf Strain**

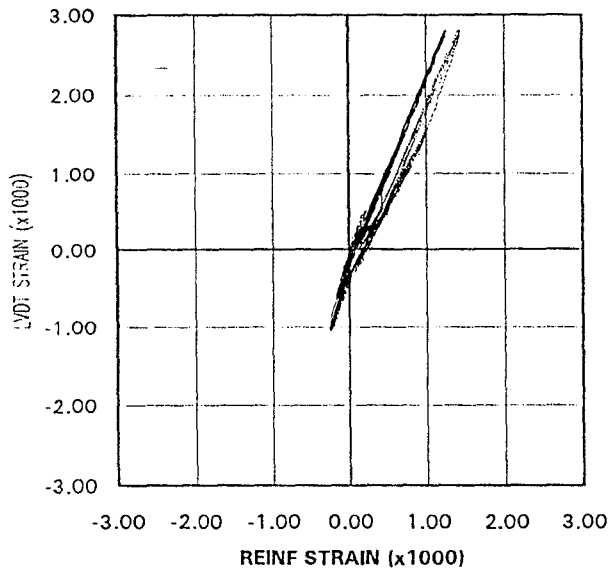


**Fig. 119 Test 2A— East End Beam
Bottom LVDT Strain vs. Reinf Strain**

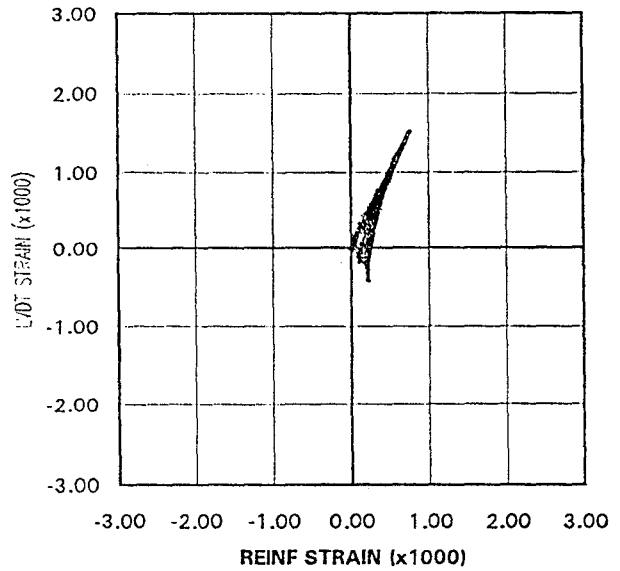


**Fig. 120 Test 2A— East End Beam
Top LVDT Strain vs. Reinf Strain**

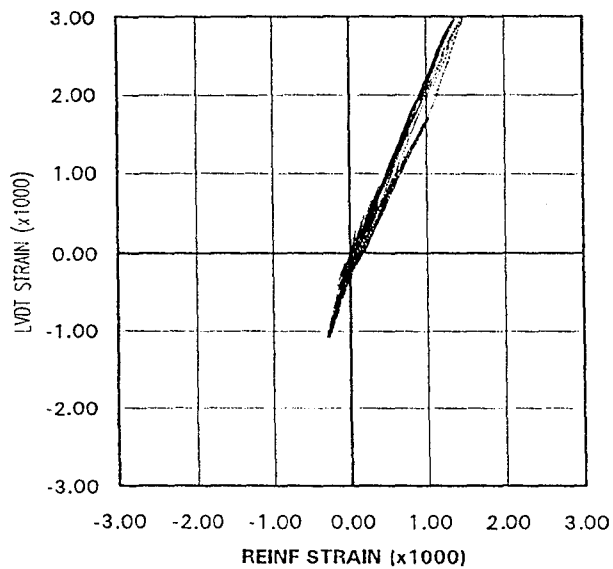


**Fig. 121 Test 2A— West End Beam
Bottom LVDT Strain vs. Reinf Strain**

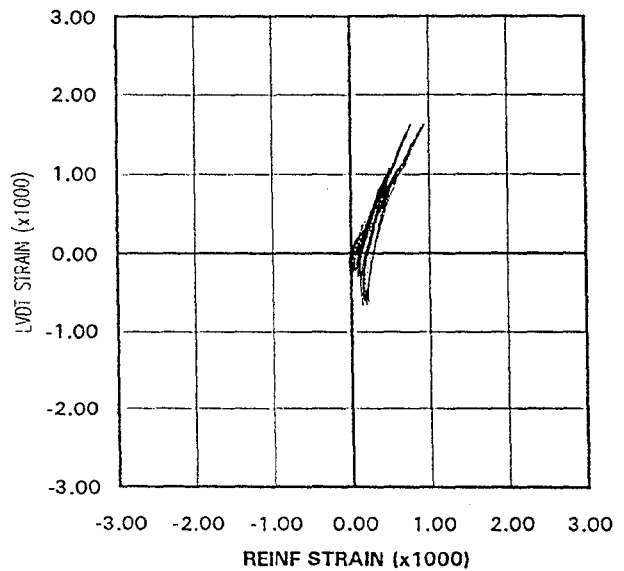


**Fig. 122 Test 2A— West End
Top LVDT Strain vs. Reinf Strain**

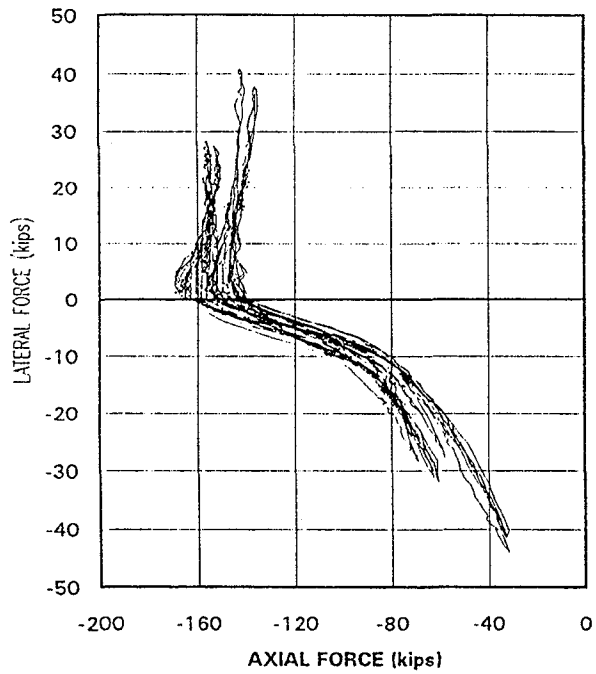


**Fig. 123 Test 2A—
Lateral Force vs. East Column Axial Force**

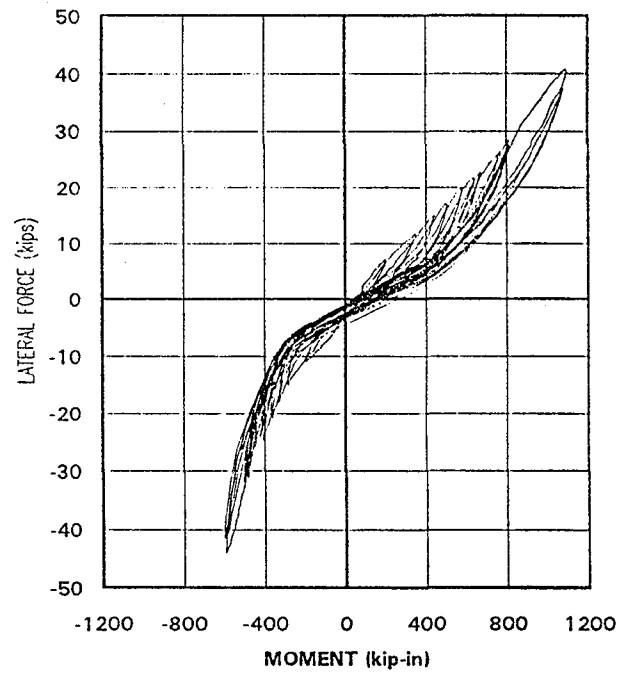


**Fig. 124 Test 2A—
Lateral Force vs. East Column Moment**

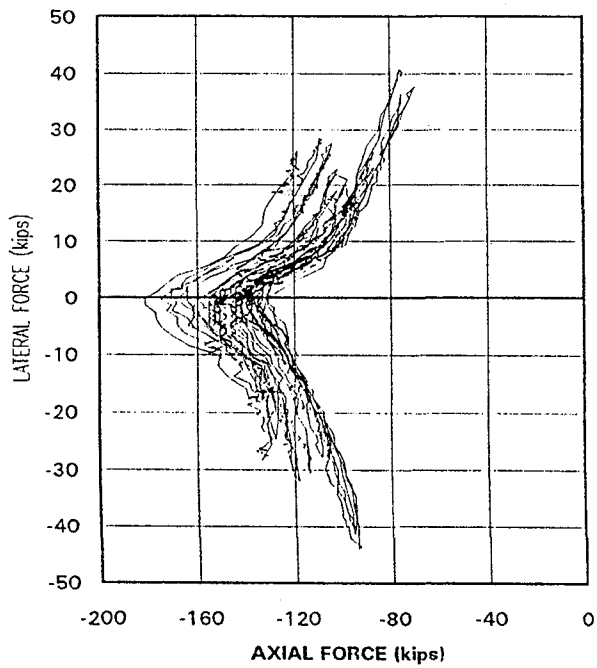


**Fig. 125 Test 2A—
Lateral Force vs. West Column Axial Force**

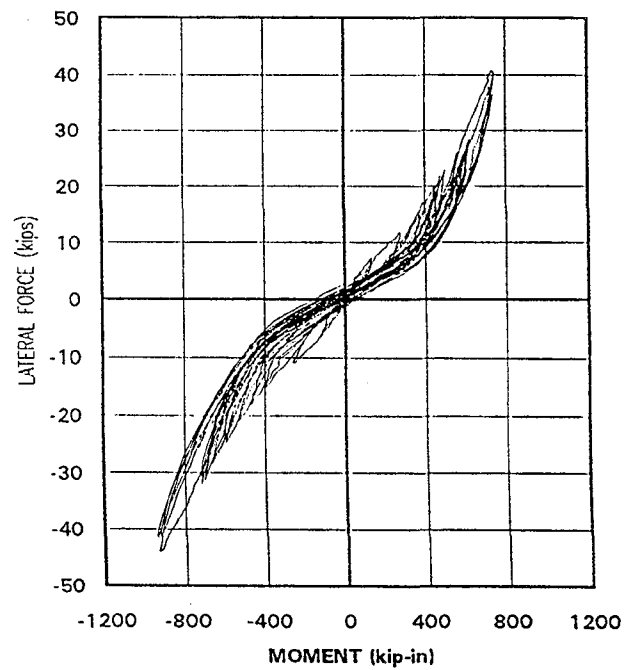


**Fig. 126 Test 2A—
Lateral Force vs. West Column Moment**

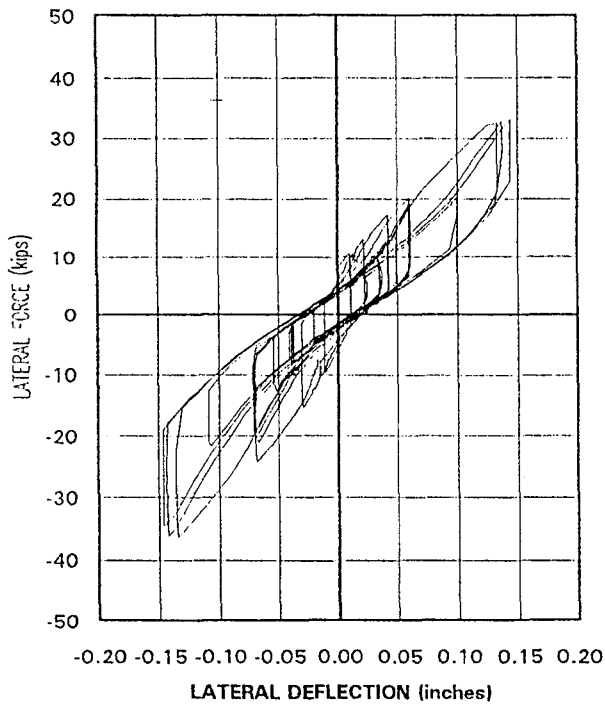


**Fig. 127 Test 3A—
Lateral Force vs. Deflection**

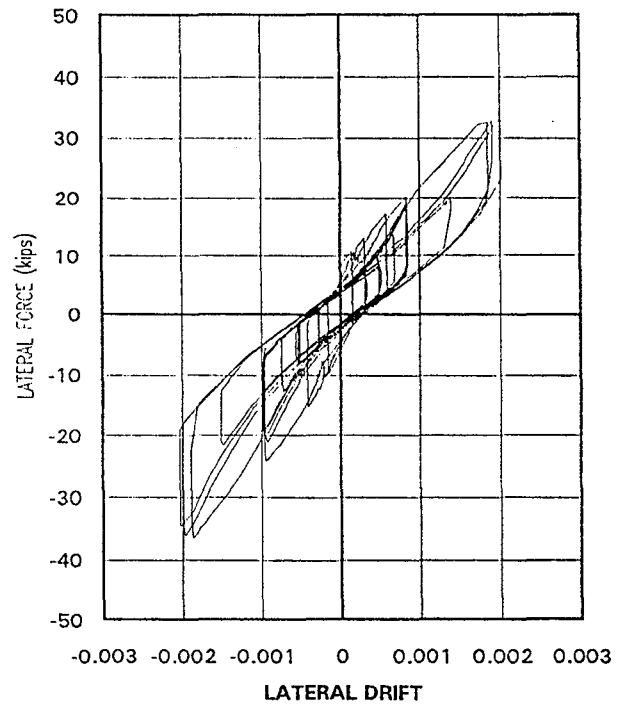


**Fig. 128 Test 3A—
Lateral Force vs. Drift**

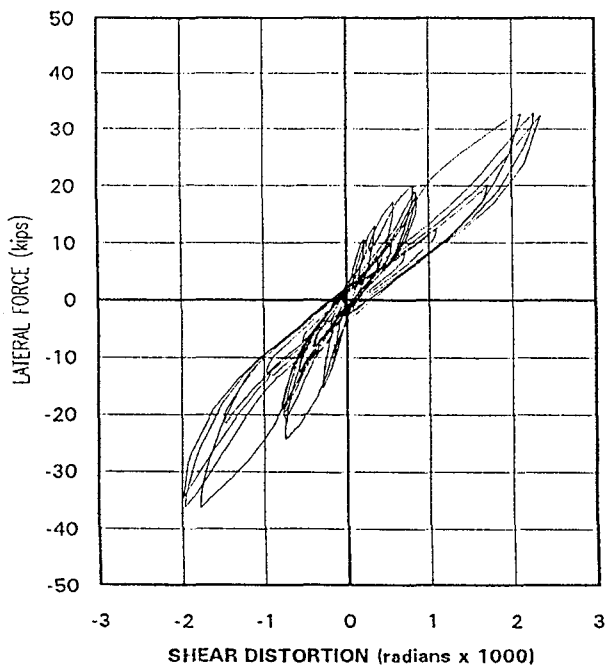


**Fig. 129 Test 3A—
Lateral Force vs. Shear Distortion**

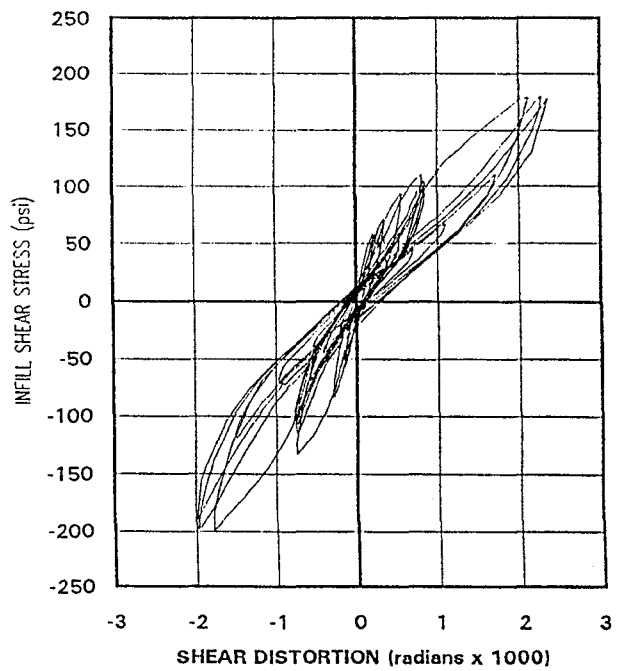


**Fig. 130 Test 3A—
Infill Shear Stress vs. Shear Distortion**

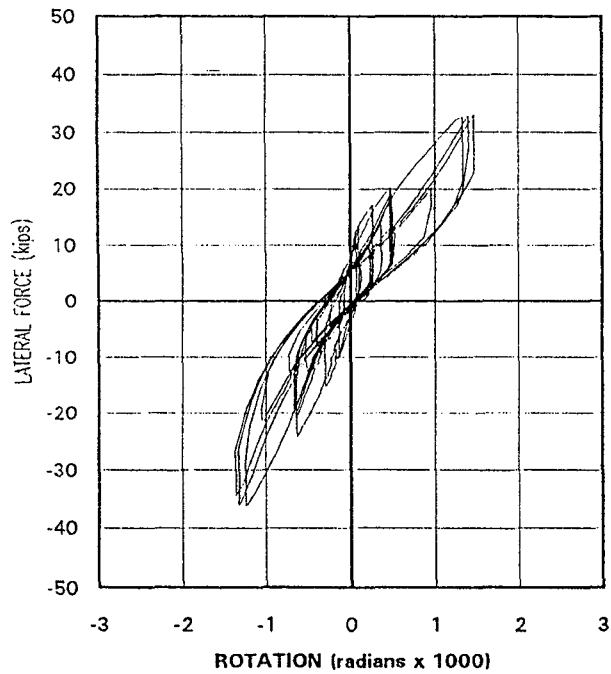


**Fig. 131 Test 3A—
Lateral Force vs. East Column Base Rotation**

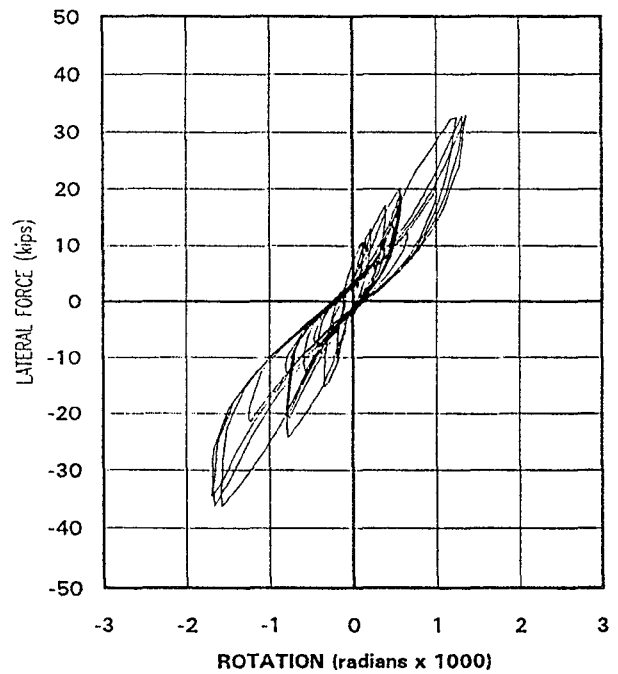


**Fig. 132 Test 3A—
Lateral Force vs. West Column Base Rotation**

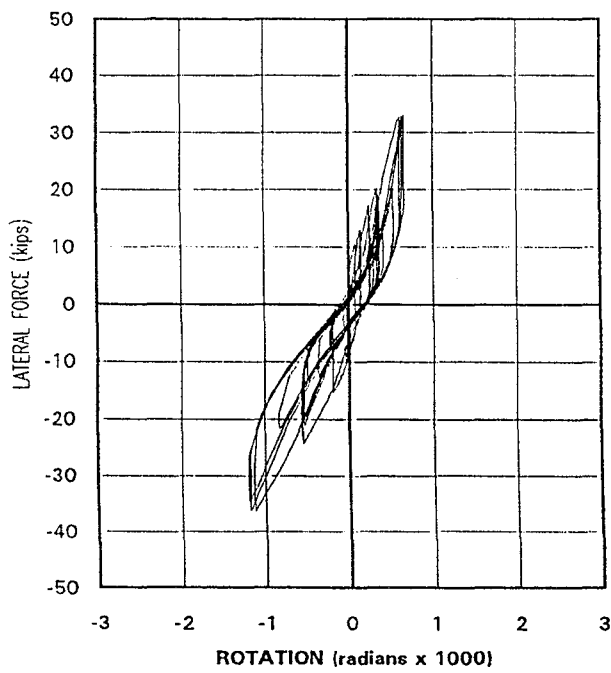


**Fig. 133 Test 3A—
Lateral Force vs. Beam East End Rotation**

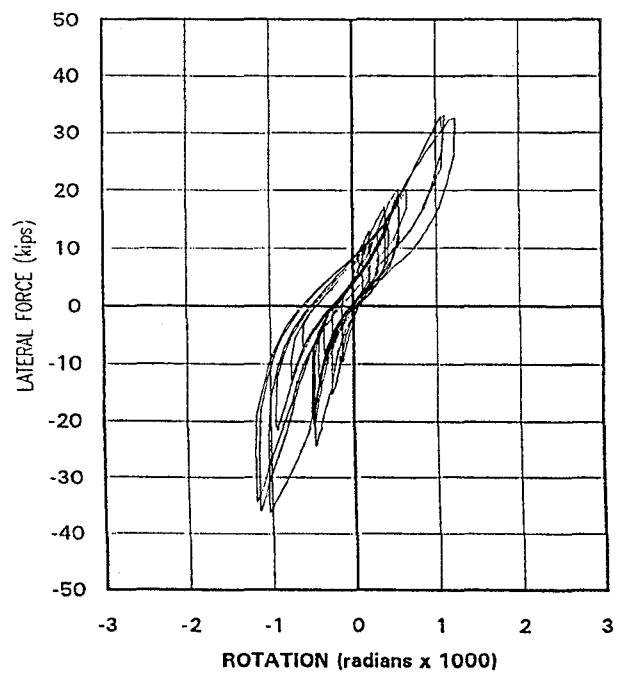


**Fig. 134 Test 3A—
Lateral Force vs. Beam West End Rotation**

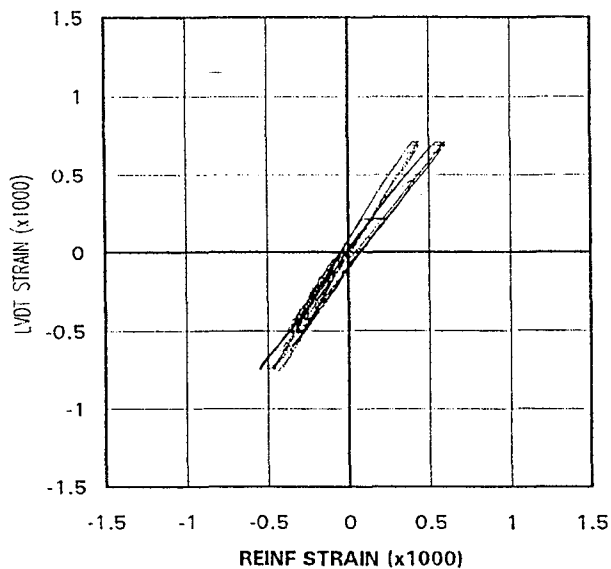


**Fig. 135 Test 3A— East Column East
Base LVDT Strain vs. Reinf Strain**

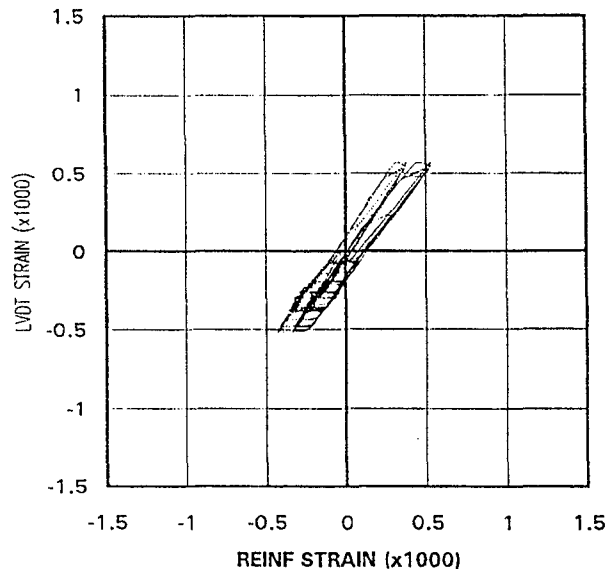


**Fig. 136 Test 3A— East Column West
Base LVDT Strain vs. Reinf Strain**

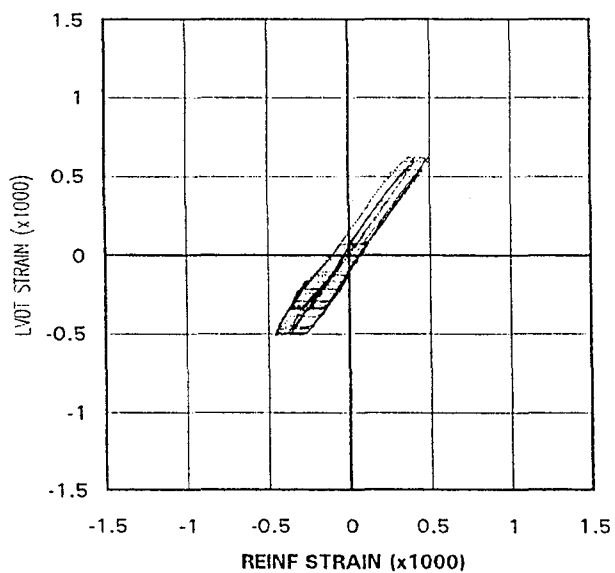


**Fig. 137 Test 3A— West Column East
Base LVDT Strain vs. Reinf Strain**

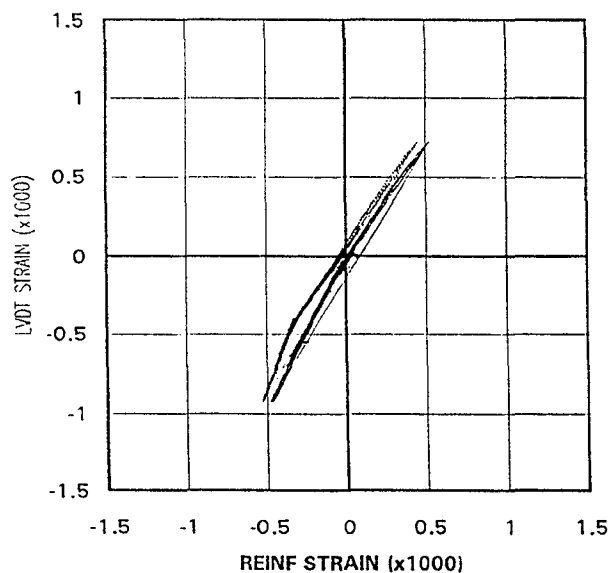


**Fig. 138 Test 3A— West Column West
Base LVDT Strain vs. Reinf Strain**

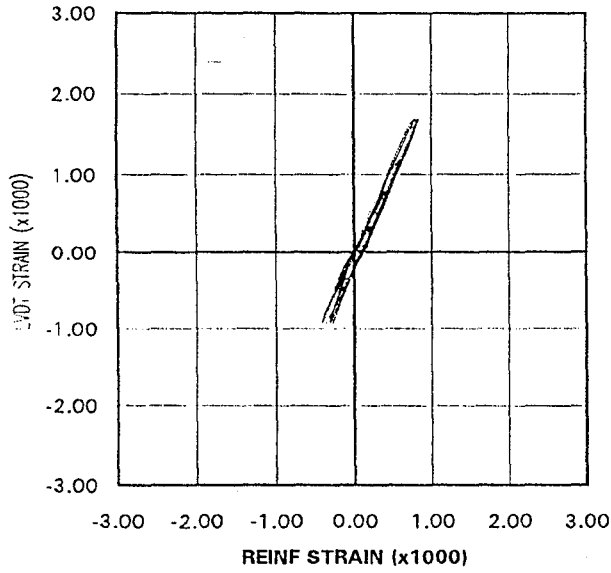


**Fig. 139 Test 3A— East End Beam
Bottom LVDT Strain vs. Reinf Strain**

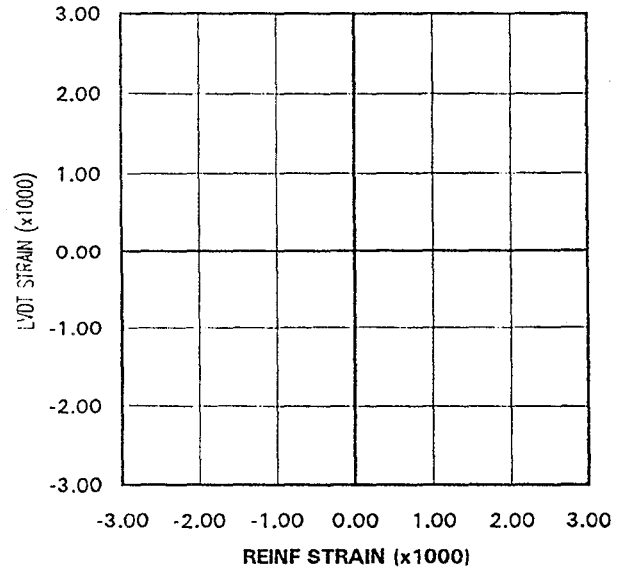


**Fig. 140 Test 3A— East End Beam
Top LVDT Strain vs. Reinf Strain**

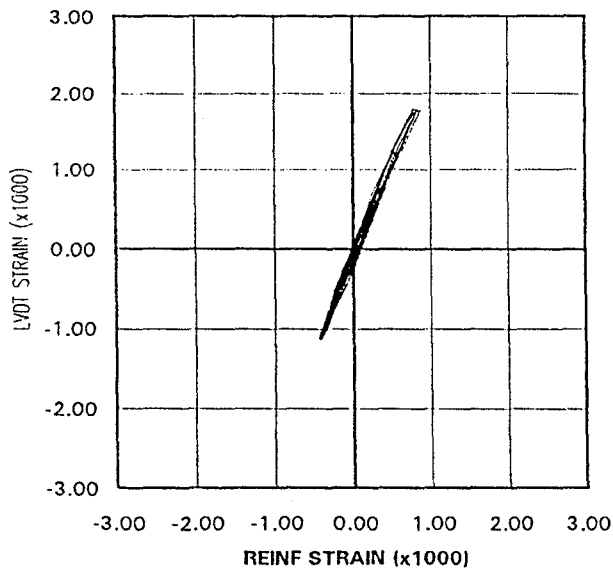


**Fig. 141 Test 3A— West End Beam
Bottom LVDT Strain vs. Reinf Strain**

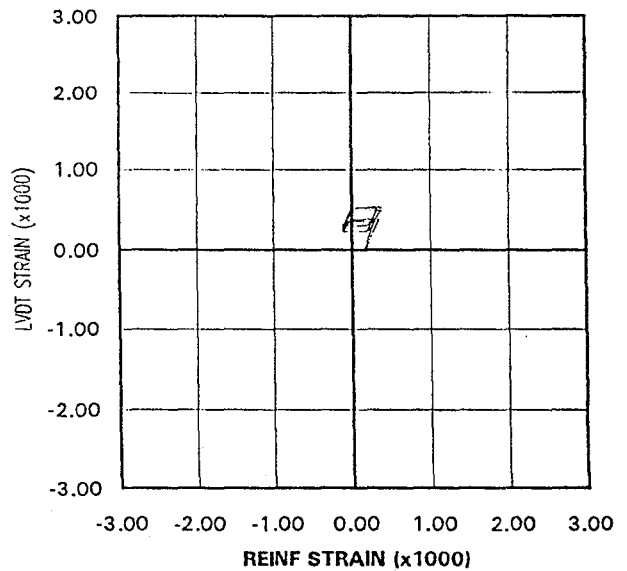


**Fig. 142 Test 3A— West End
Top LVDT Strain vs. Reinf Strain**

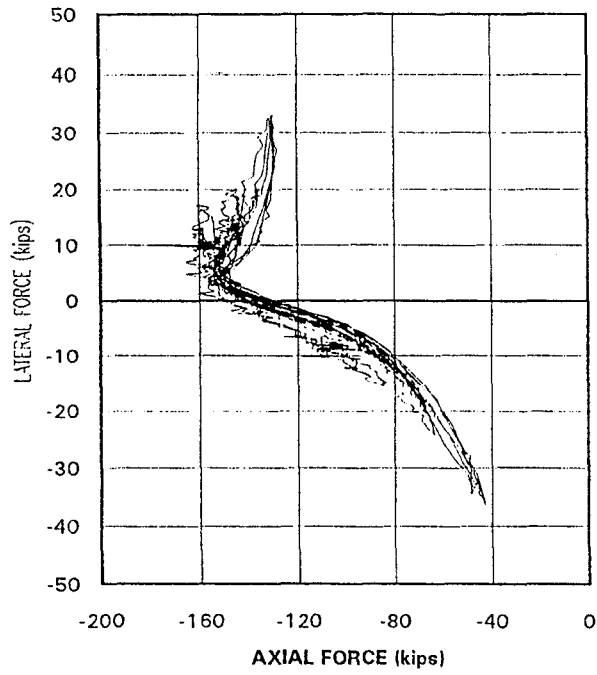


**Fig. 143 Test 3A—
Lateral Force vs. East Column Axial Force**

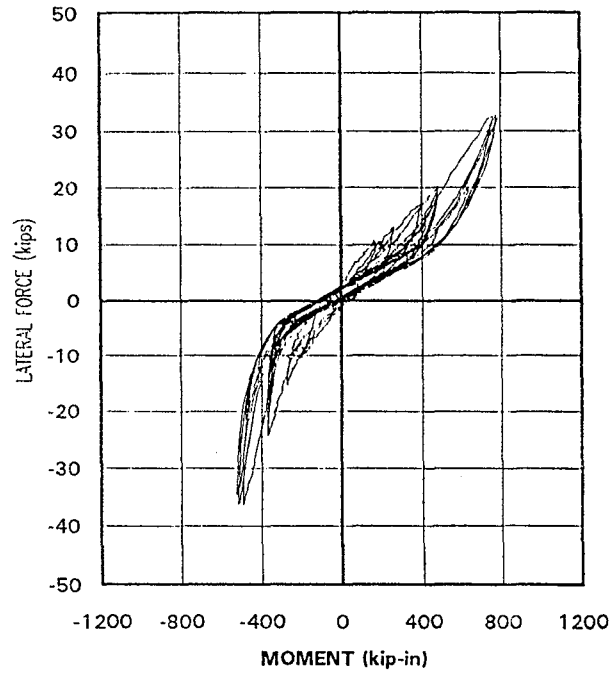


**Fig. 144 Test 3A—
Lateral Force vs. East Column Moment**

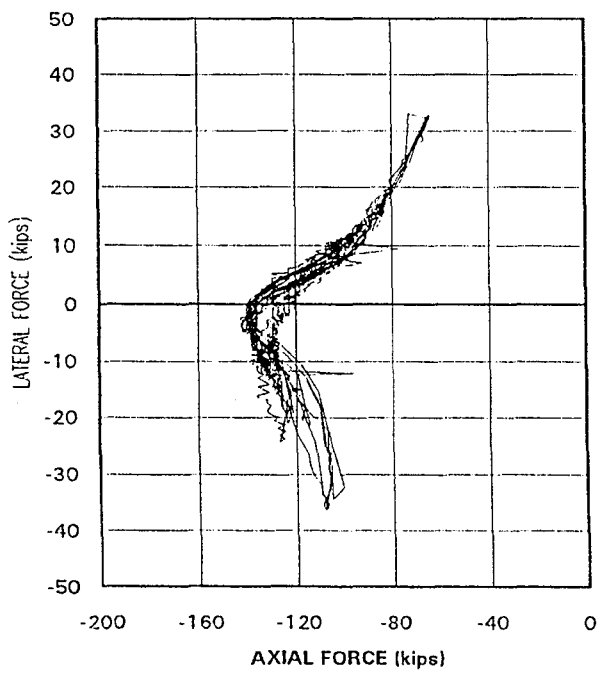


**Fig. 145 Test 3A—
Lateral Force vs. West Column Axial Force**

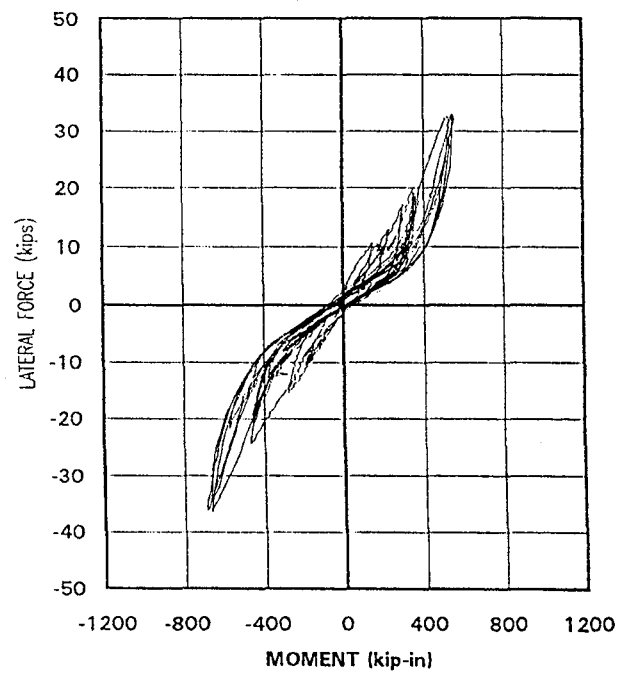


**Fig. 146 Test 3A—
Lateral Force vs. West Column Moment**

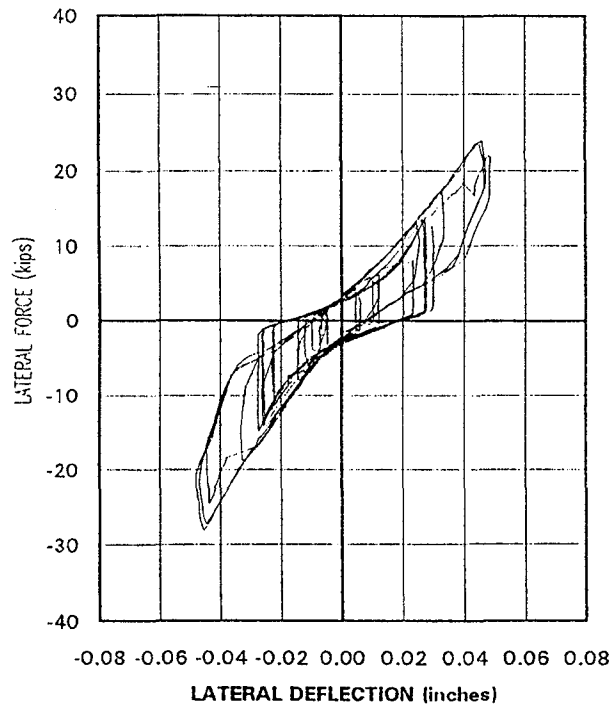


**Fig. 147 Test 4A—
Lateral Force vs. Deflection**

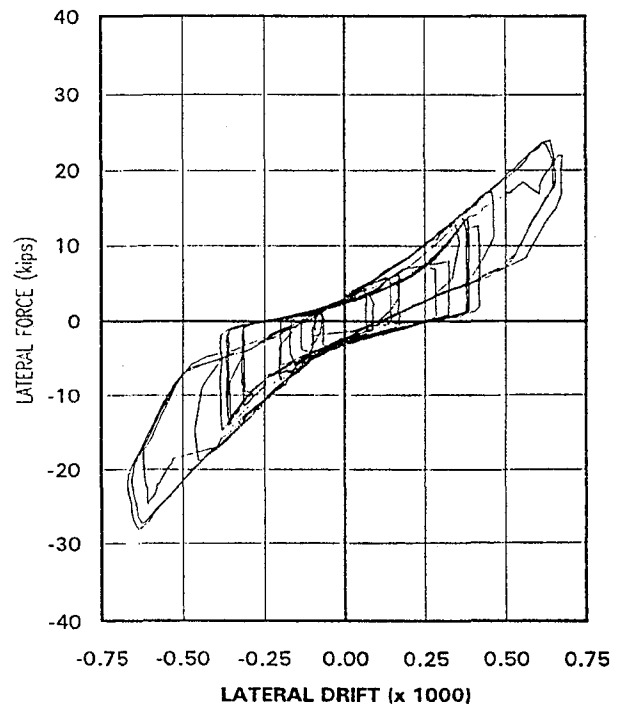


**Fig. 148 Test 4A—
Lateral Force vs. Drift**

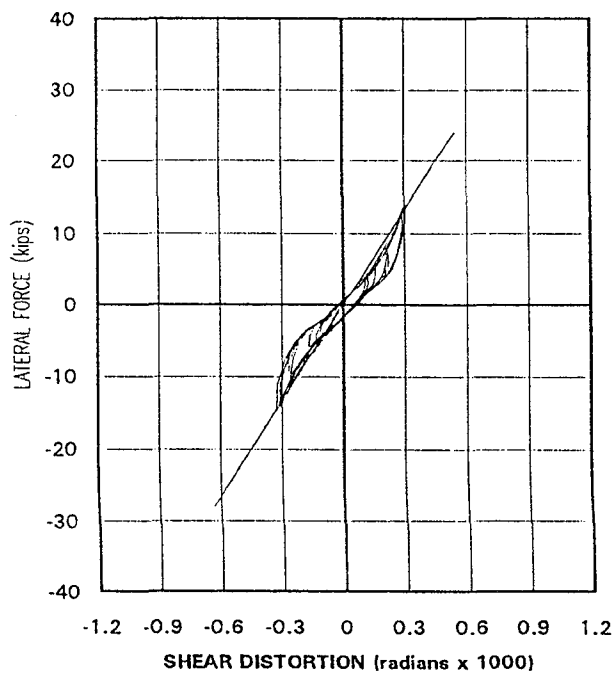


**Fig. 149 Test 4A—
Lateral Force vs. Shear Distortion**

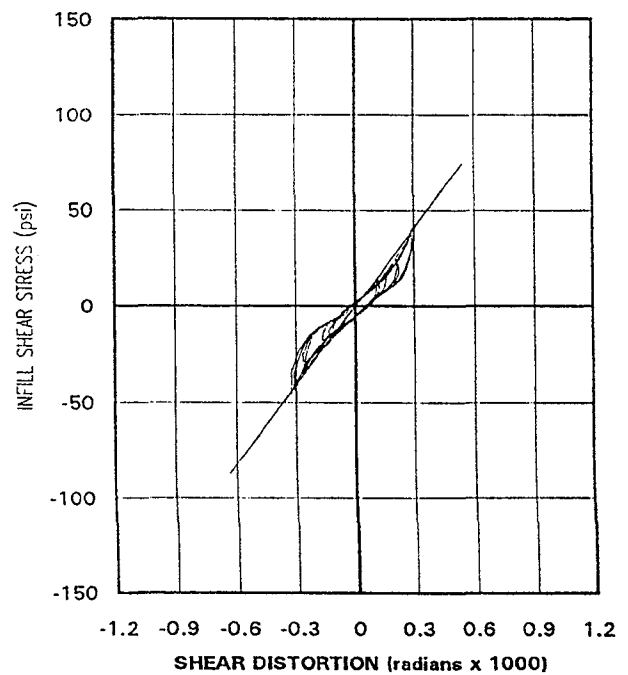


**Fig. 150 Test 4A—
Infill Shear Stress vs. Shear Distortion**

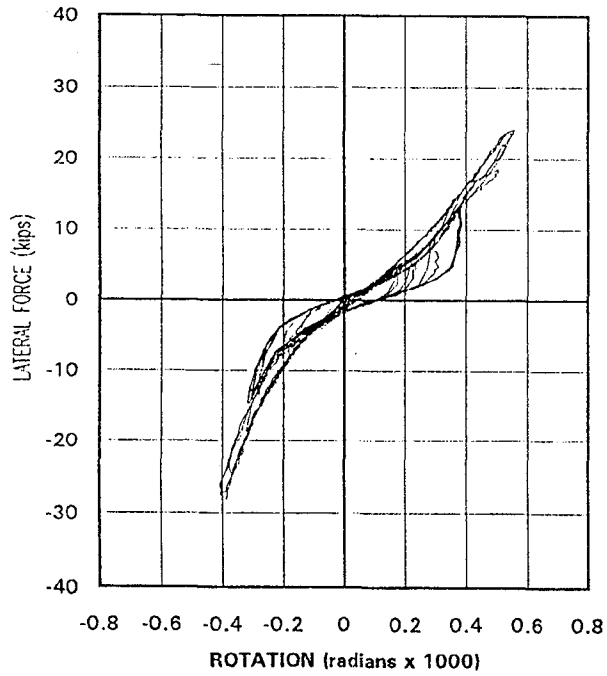


**Fig. 151 Test 4A—
Lateral Force vs. East Column Base Rotation**

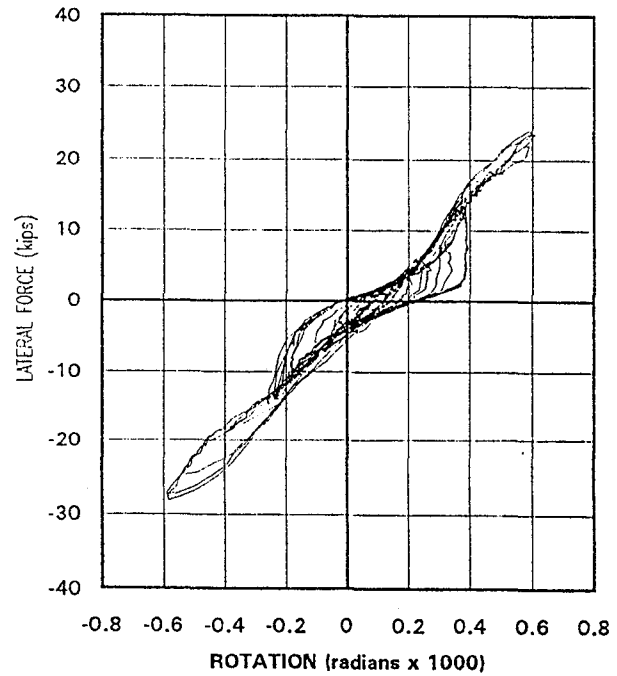


**Fig. 152 Test 4A—
Lateral Force vs. West Column Base Rotation**

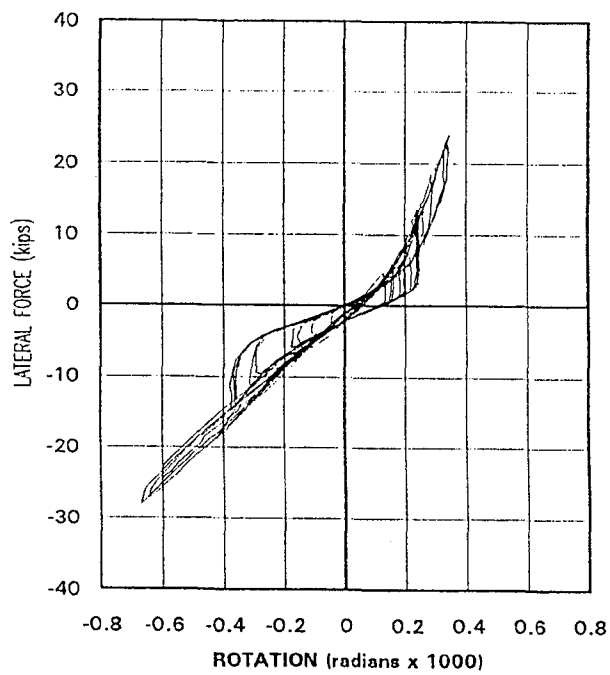


**Fig. 153 Test 4A—
Lateral Force vs. Beam East End Rotation**

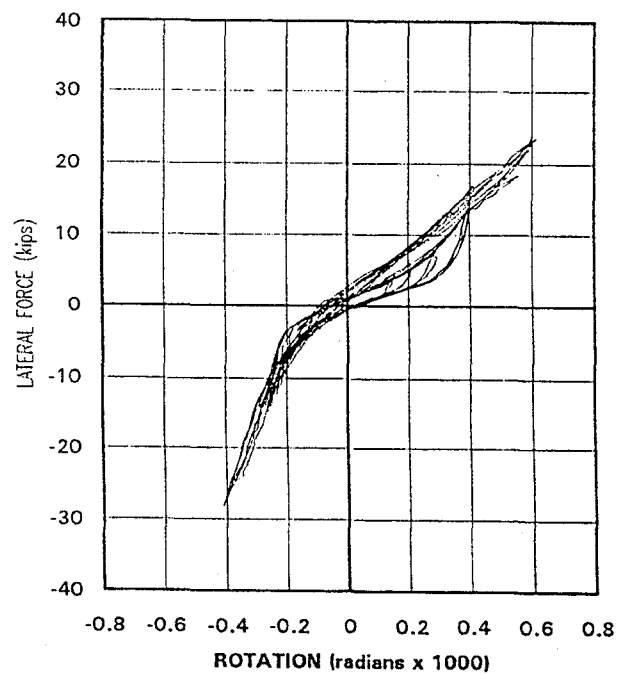


**Fig. 154 Test 4A—
Lateral Force vs. Beam West End Rotation**

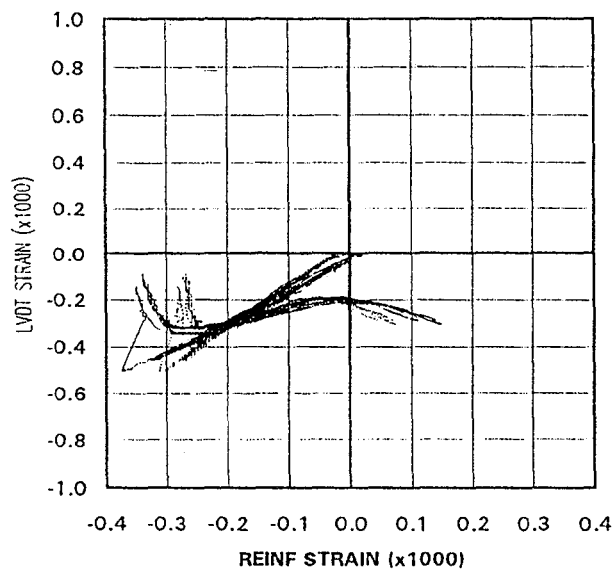


**Fig. 155 Test 4A— East Column East
Base LVDT Strain vs. Reinf Strain**

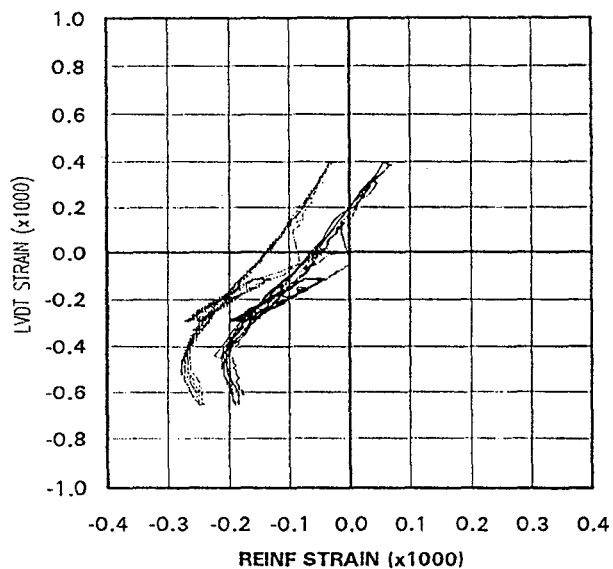


**Fig. 156 Test 4A— East Column West
Base LVDT Strain vs. Reinf Strain**

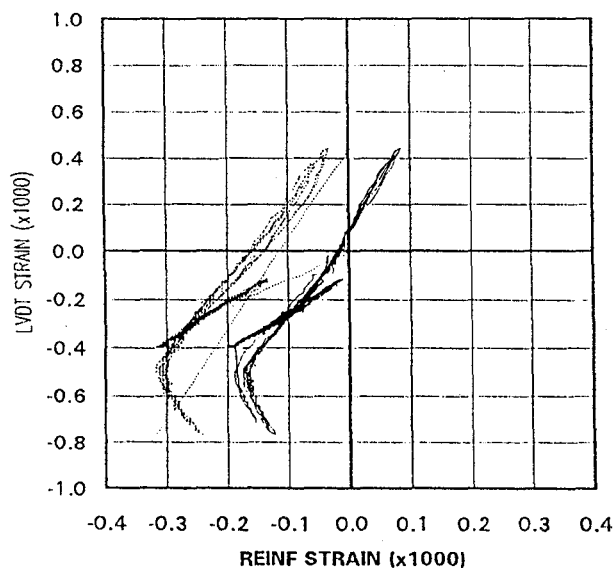


**Fig. 157 Test 4A— West Column East
Base LVDT Strain vs. Reinf Strain**

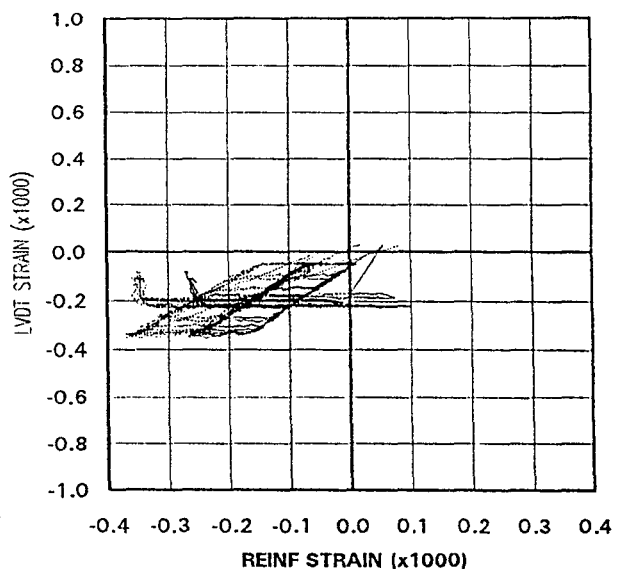


**Fig. 158 Test 4A— West Column West
Base LVDT Strain vs. Reinf Strain**

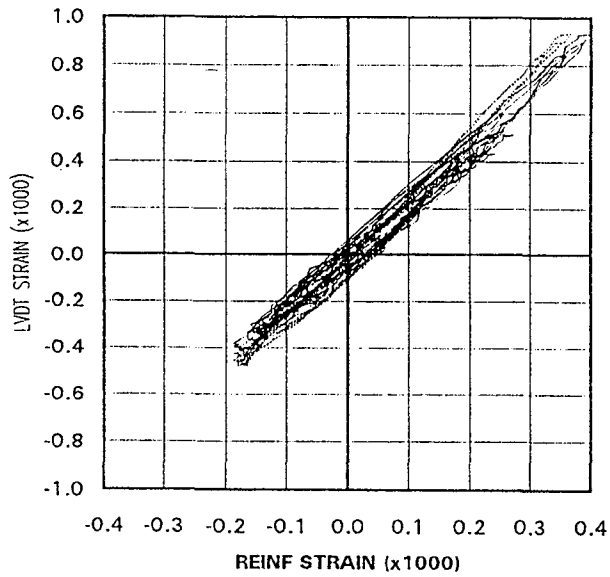


**Fig. 159 Test 4A– East End Beam
Bottom LVDT Strain vs. Reinf Strain**

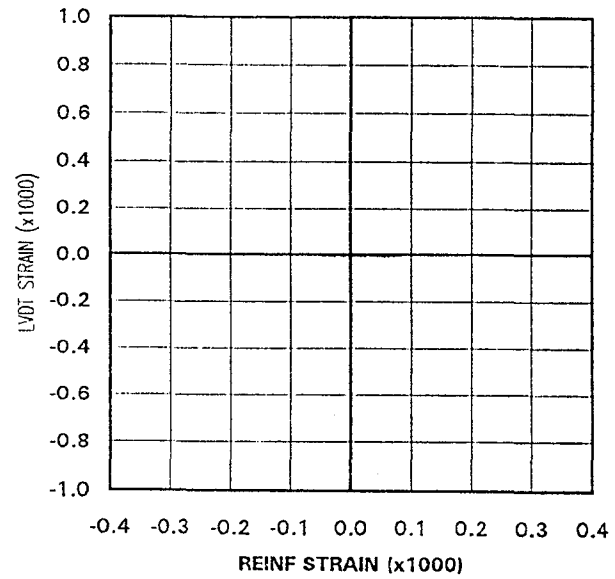


**Fig. 160 Test 4A– East End Beam
Top LVDT Strain vs. Reinf Strain**

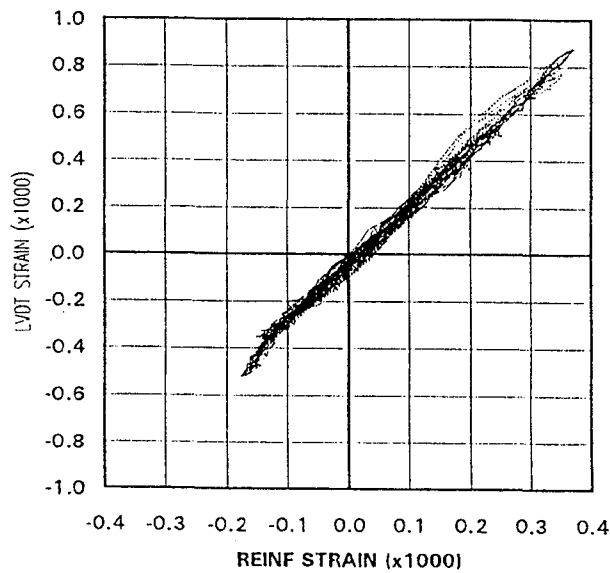


**Fig. 161 Test 4A– West End Beam
Bottom LVDT Strain vs. Reinf Strain**

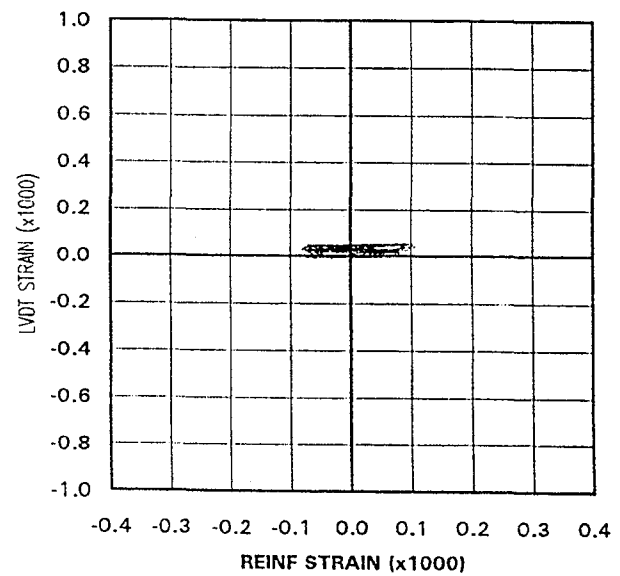


**Fig. 162 Test 4A– West End
Top LVDT Strain vs. Reinf Strain**

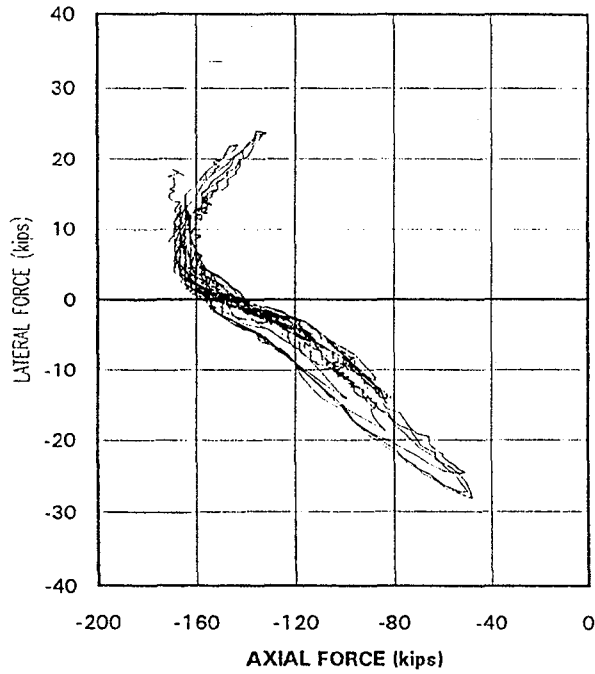


**Fig. 163 Test 4A—
Lateral Force vs. East Column Axial Force**

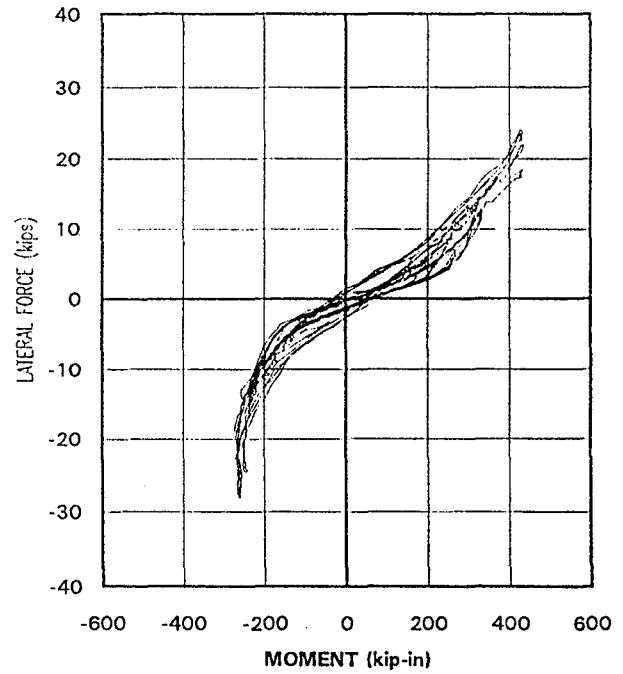


**Fig. 164 Test 4A—
Lateral Force vs. East Column Moment**

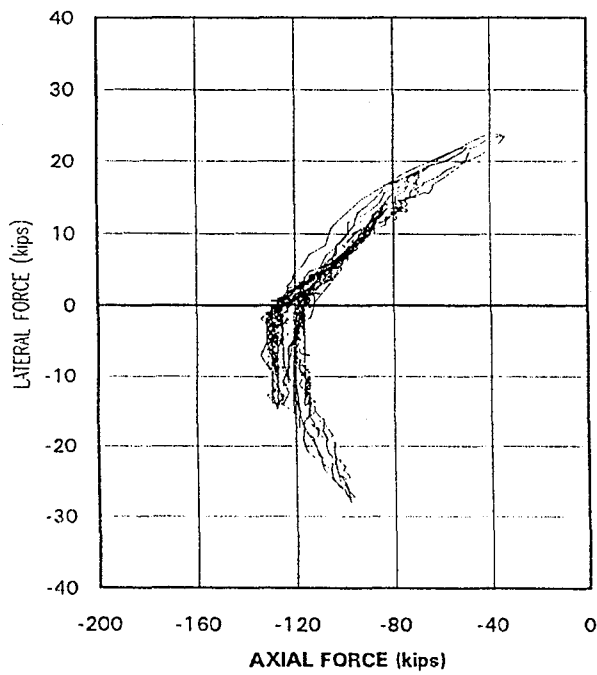


**Fig. 165 Test 4A—
Lateral Force vs. West Column Axial Force**

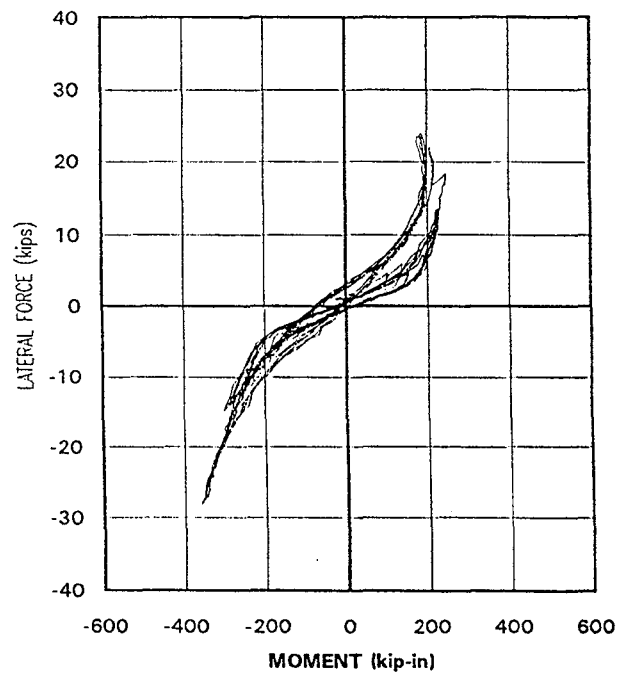


**Fig. 166 Test 4A—
Lateral Force vs. West Column Moment**

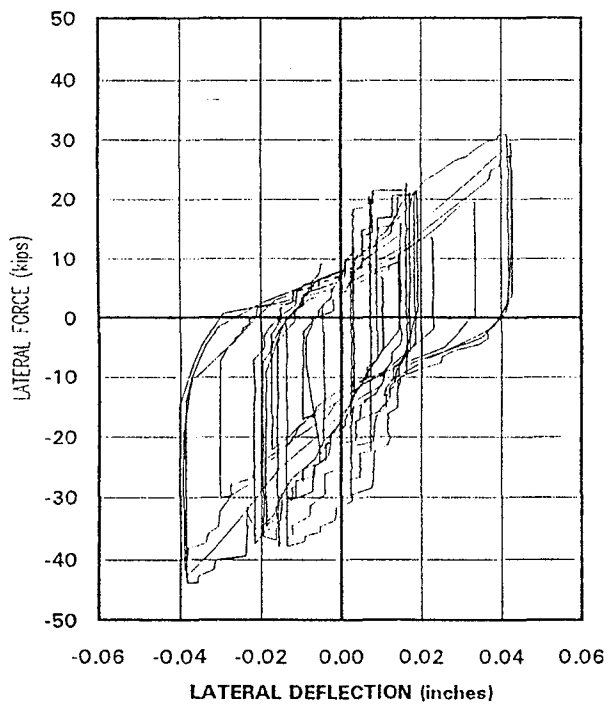


**Fig. 167 Test 5A—
Lateral Force vs. Deflection**

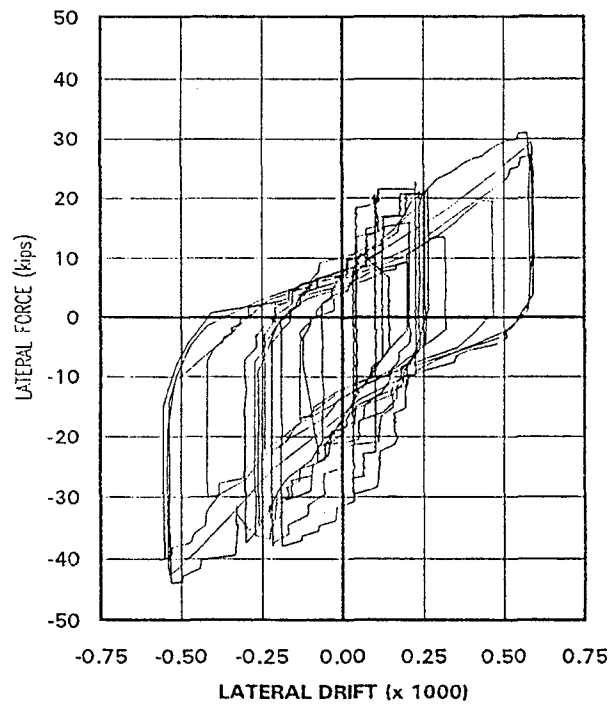


**Fig. 168 Test 5A—
Lateral Force vs. Drift**

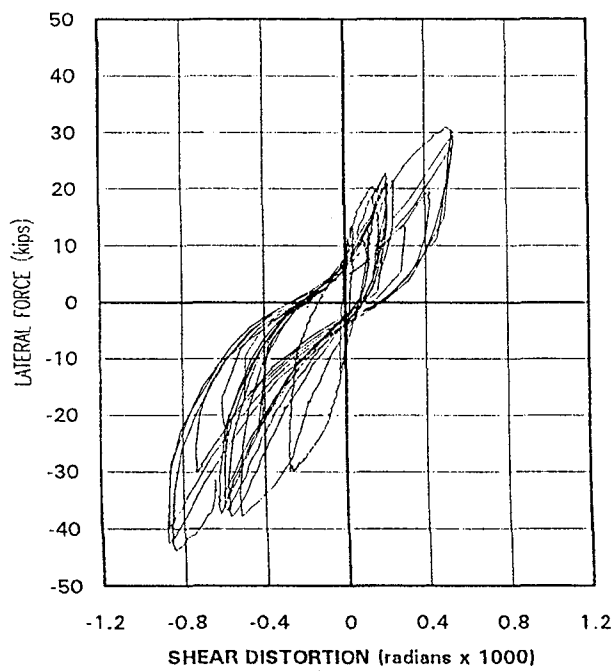


**Fig. 169 Test 5A—
Lateral Force vs. Shear Distortion**

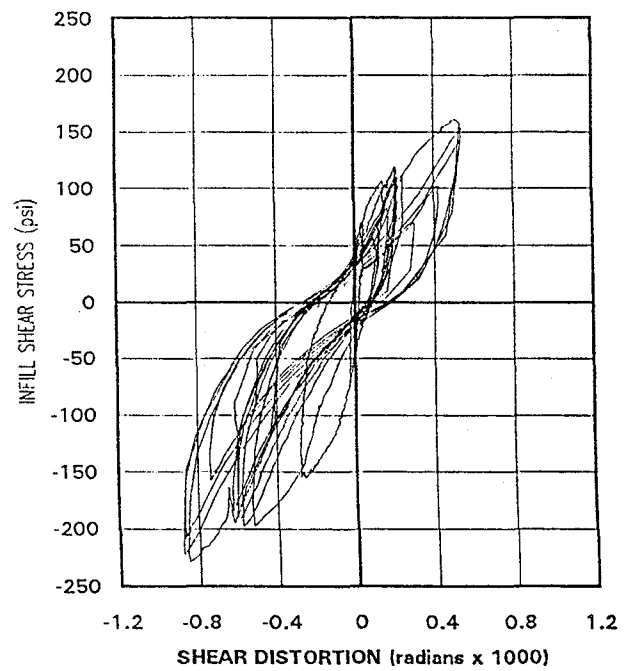


**Fig. 170 Test 5A—
Infill Shear Stress vs. Shear Distortion**

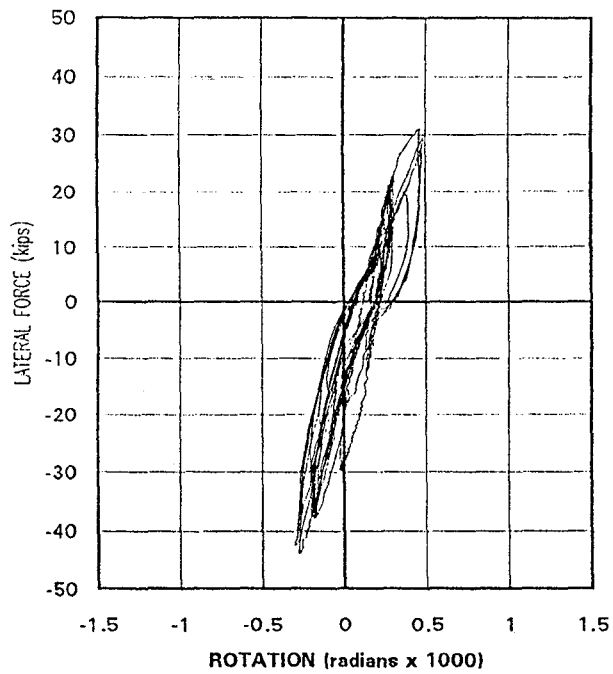


**Fig. 171 Test 5A—
Lateral Force vs. East Column Base Rotation**

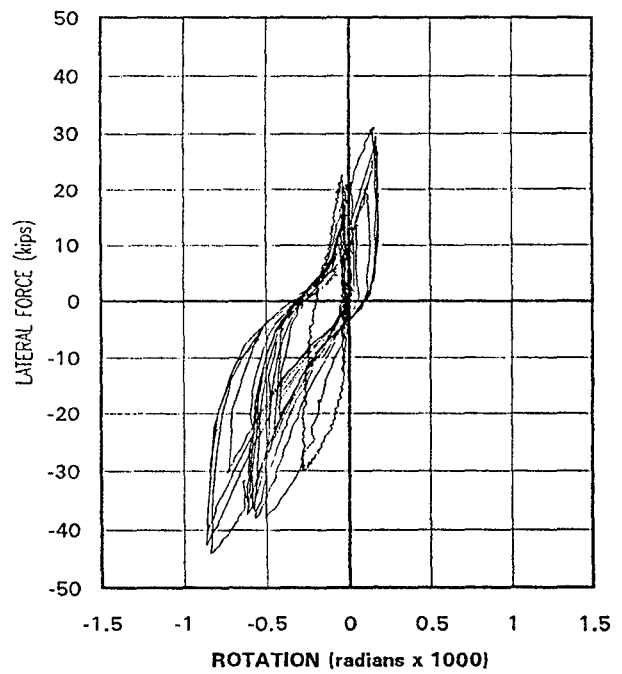


**Fig. 172 Test 5A—
Lateral Force vs. West Column Base Rotation**

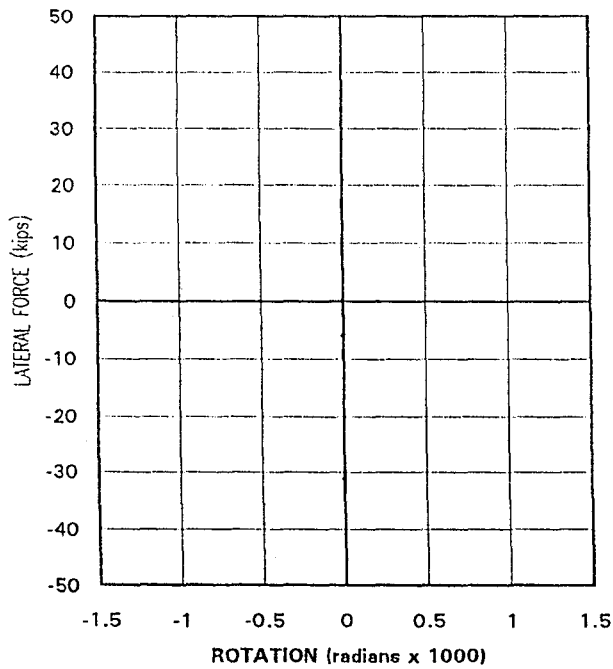


**Fig. 173 Test 5A—
Lateral Force vs. Beam East End Rotation**

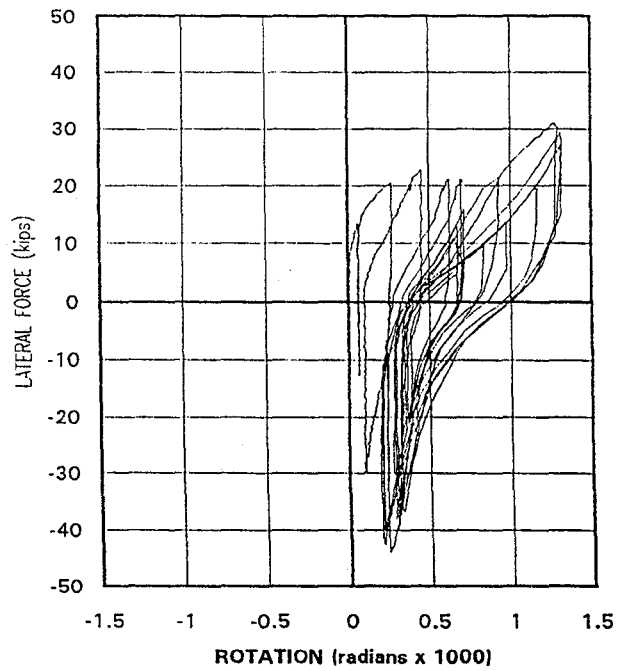


**Fig. 174 Test 5A—
Lateral Force vs. Beam West End Rotation**

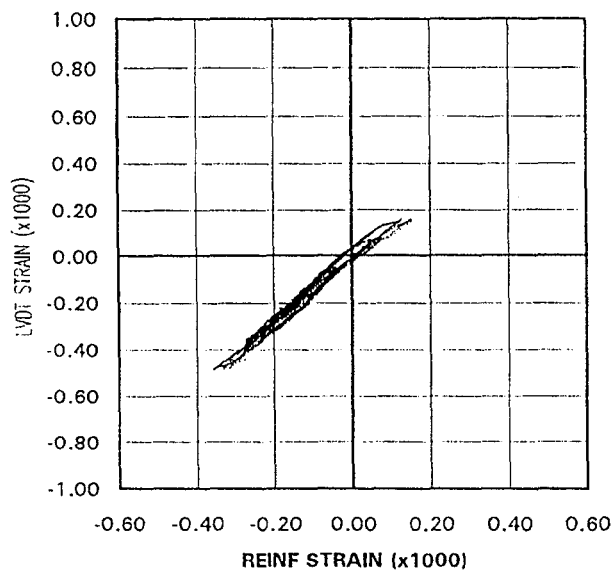


**Fig. 175 Test 5A— East Column East
Base LVDT Strain vs. Reinf Strain**

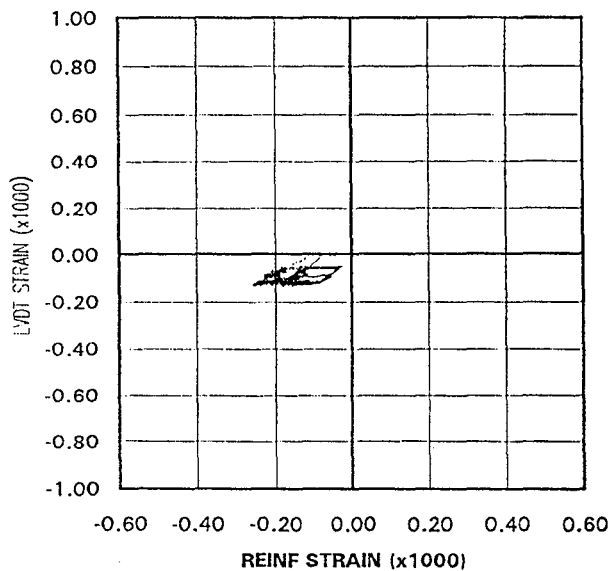


**Fig. 176 Test 5A— East Column West
Base LVDT Strain vs. Reinf Strain**

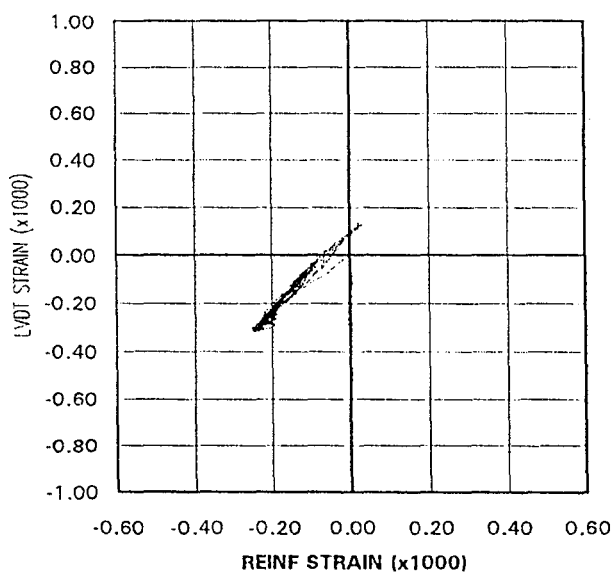


**Fig. 177 Test 5A— West Column East
Base LVDT Strain vs. Reinf Strain**

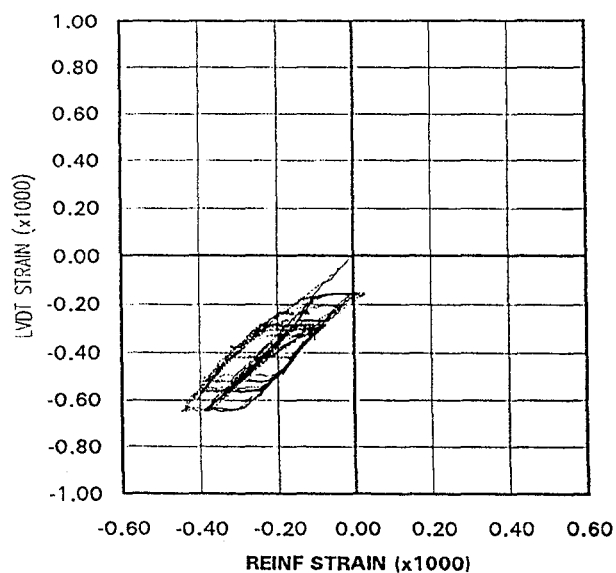


**Fig. 178 Test 5A— West Column West
Base LVDT Strain vs. Reinf Strain**

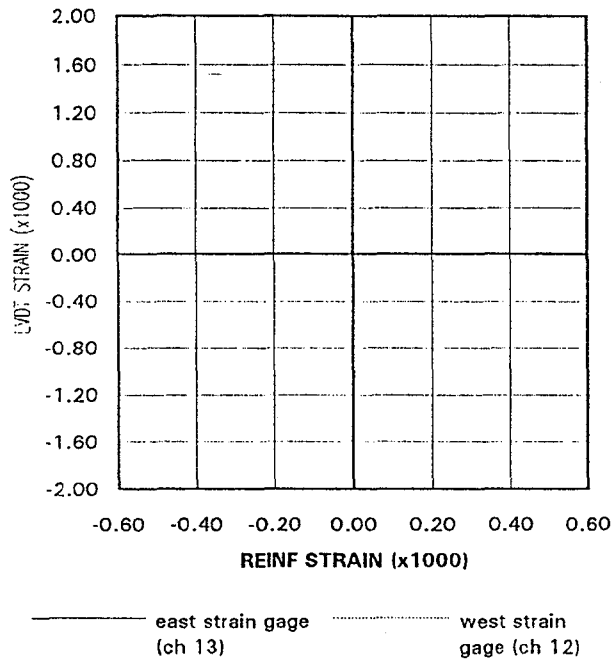


**Fig. 179 Test 5A – East End Beam
Bottom LVDT Strain vs. Reinf Strain**

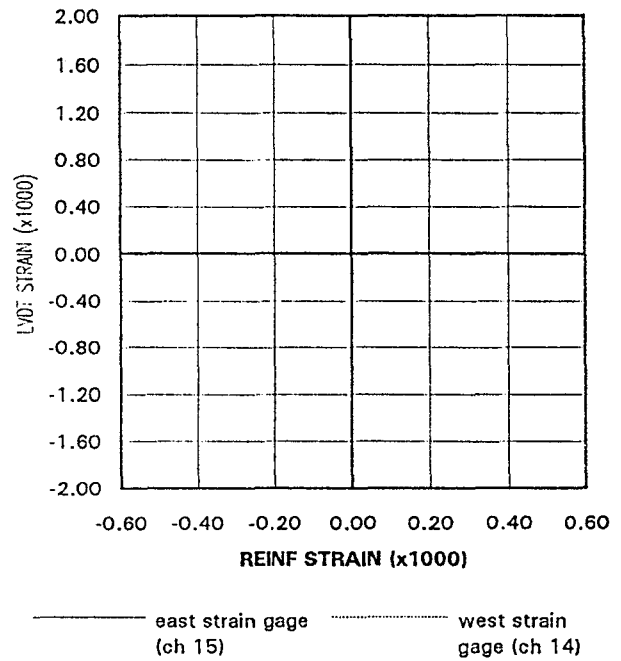


**Fig. 180 Test 5A – East End Beam
Top LVDT Strain vs. Reinf Strain**

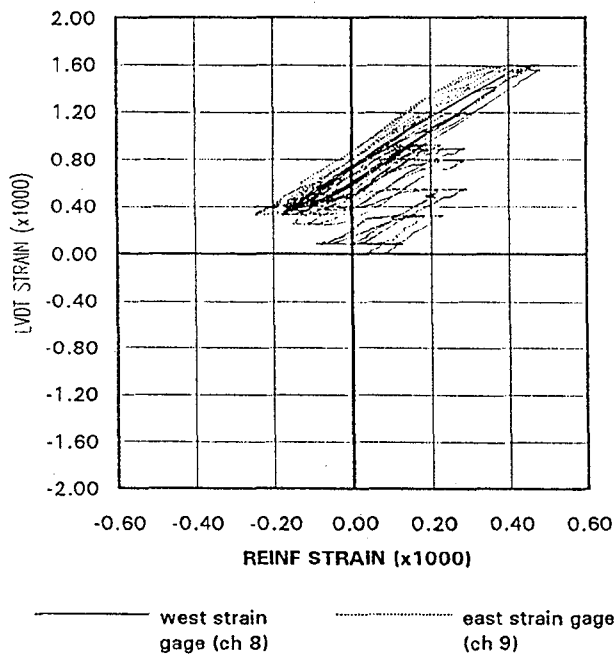


**Fig. 181 Test 5A – West End Beam
Bottom LVDT Strain vs. Reinf Strain**

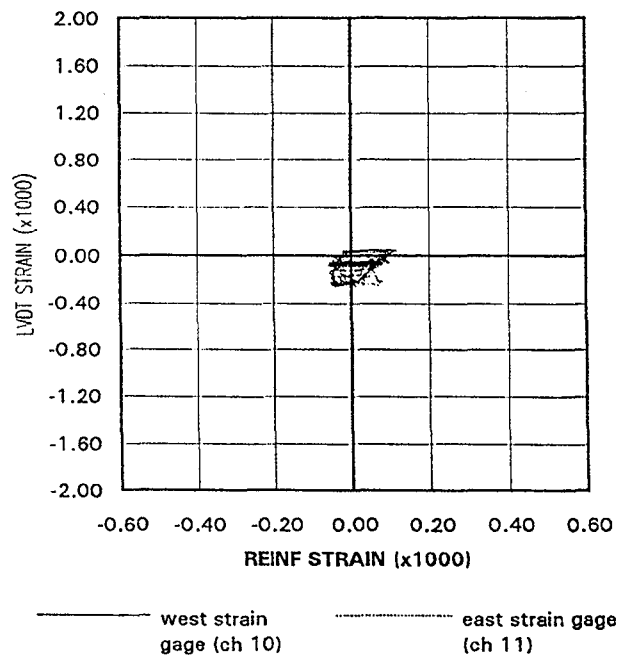


**Fig. 182 Test 5A – West End Beam
Top LVDT Strain vs. Reinf Strain**

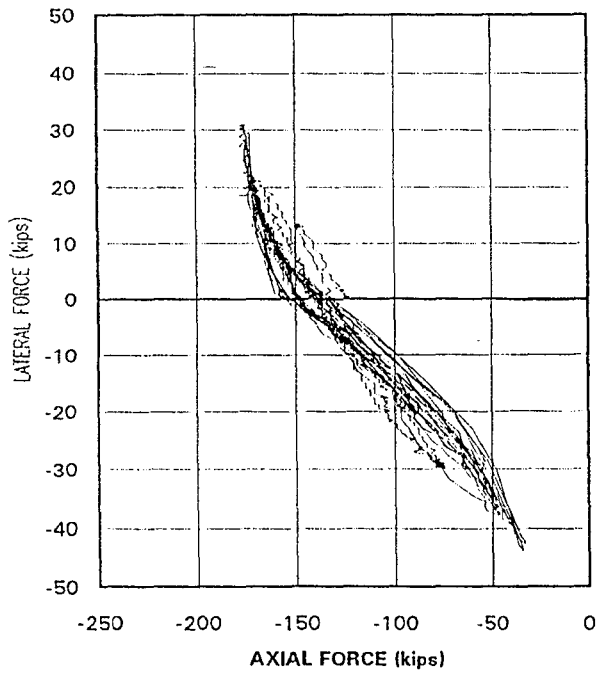


**Fig. 183 Test 5A—
Lateral Force vs. East Column Axial Force**

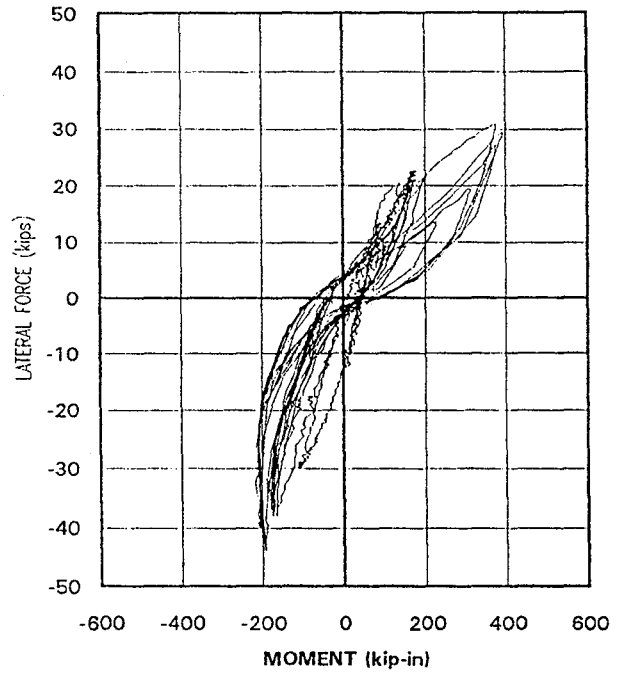


**Fig. 184 Test 5A—
Lateral Force vs. East Column Moment**

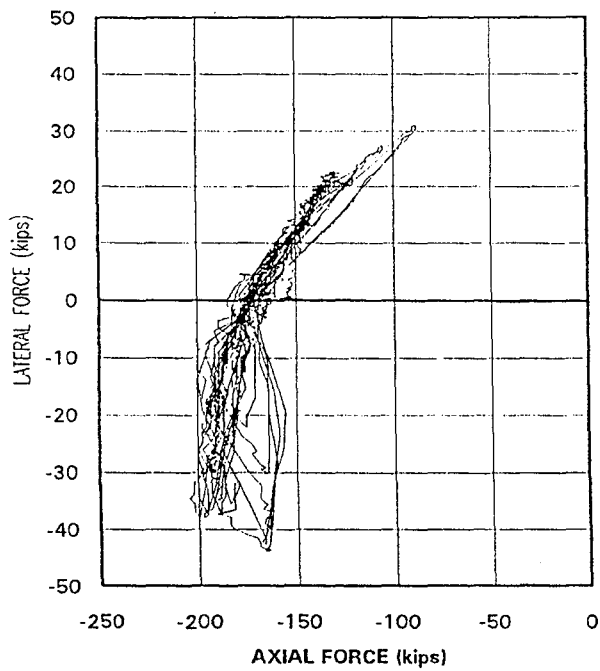


**Fig. 185 Test 5A—
Lateral Force vs. West Column Axial Force**

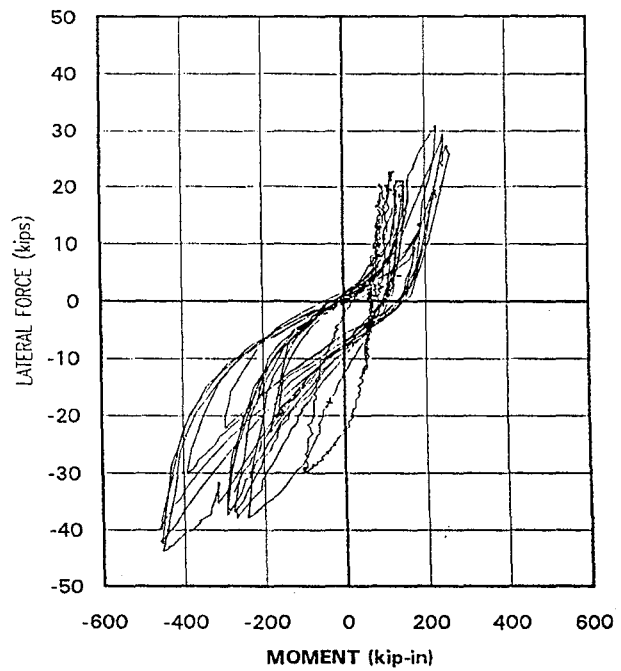


**Fig. 186 Test 5A—
Lateral Force vs. West Column Moment**

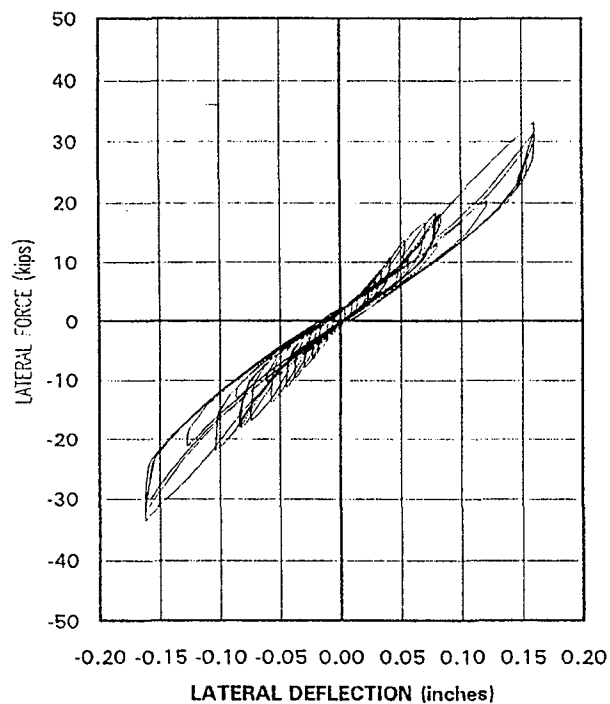


**Fig. 187 Test 6A—
Lateral Force vs. Deflection**

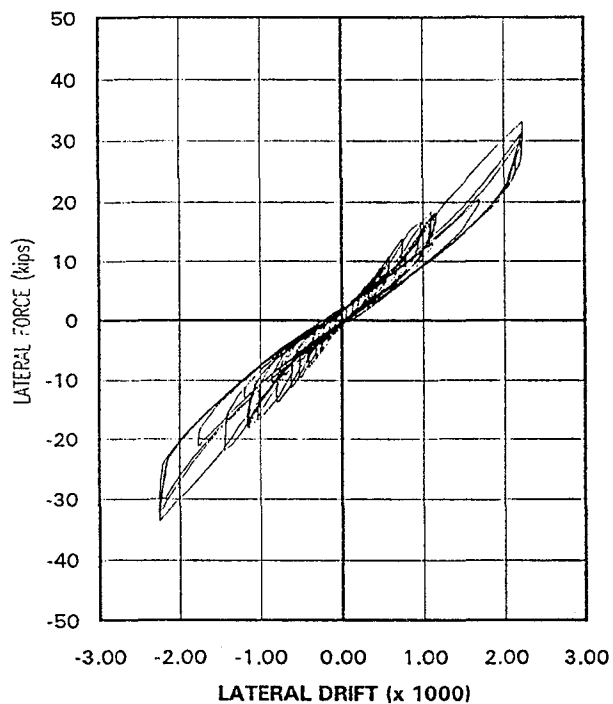


**Fig. 188 Test 6A—
Lateral Force vs. Drift**

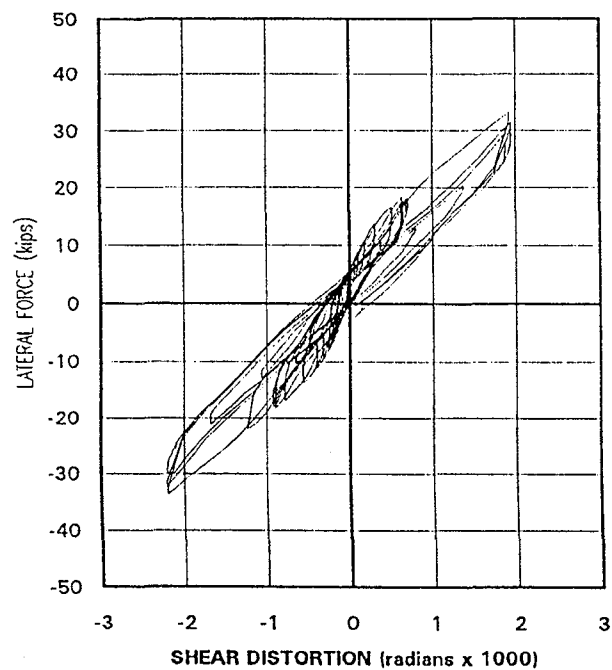


**Fig. 189 Test 6A—
Lateral Force vs. Shear Distortion**

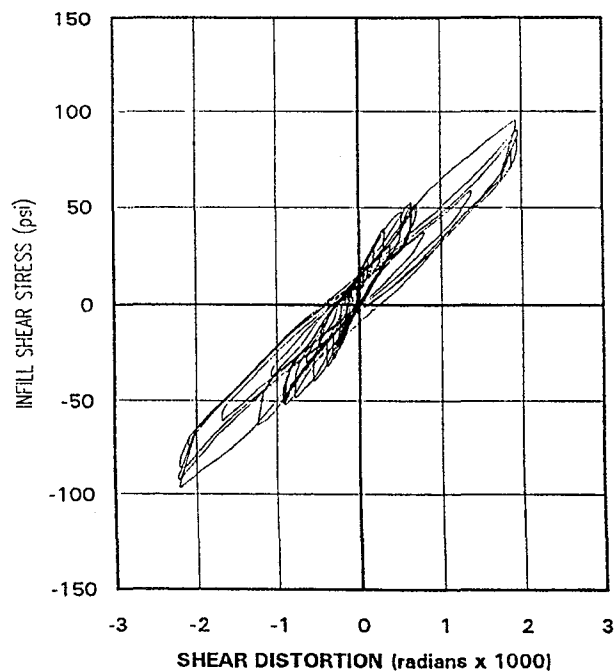


**Fig. 190 Test 6A—
Infill Shear Stress vs. Shear Distortion**

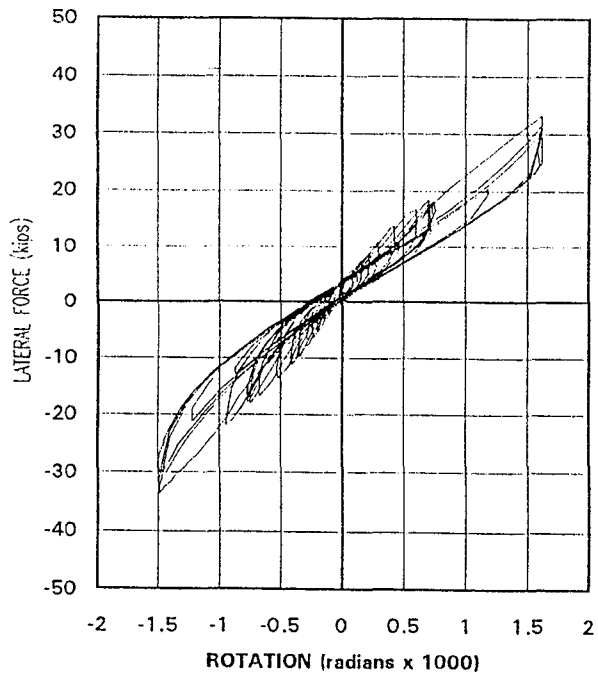


**Fig. 191 Test 6A—
Lateral Force vs. East Column Base Rotation**

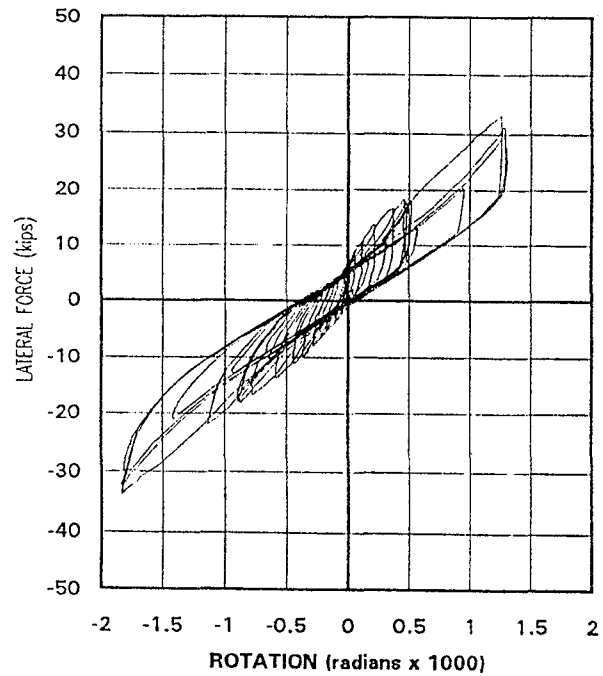


**Fig. 192 Test 6A—
Lateral Force vs. West Column Base Rotation**

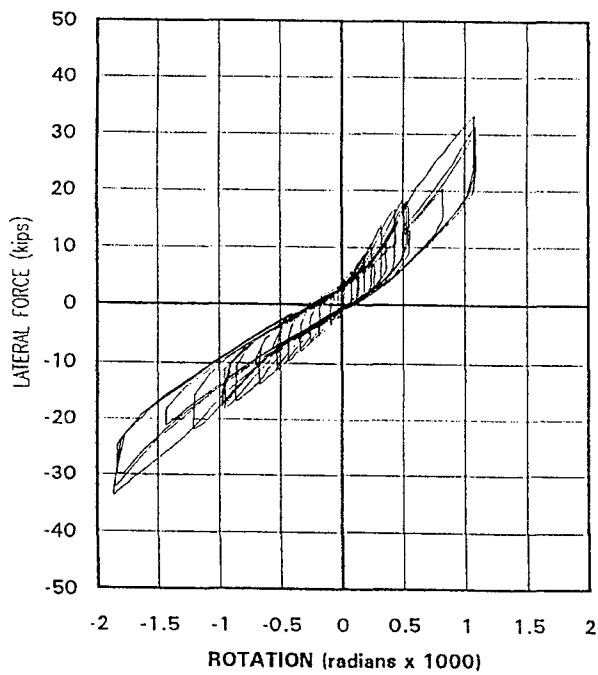


**Fig. 193 Test 6A—
Lateral Force vs. Beam East End Rotation**

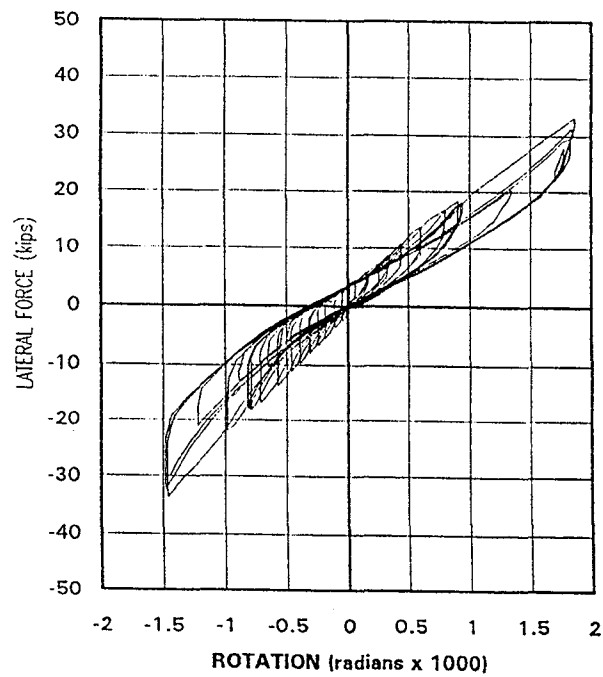


**Fig. 194 Test 6A—
Lateral Force vs. Beam West End Rotation**

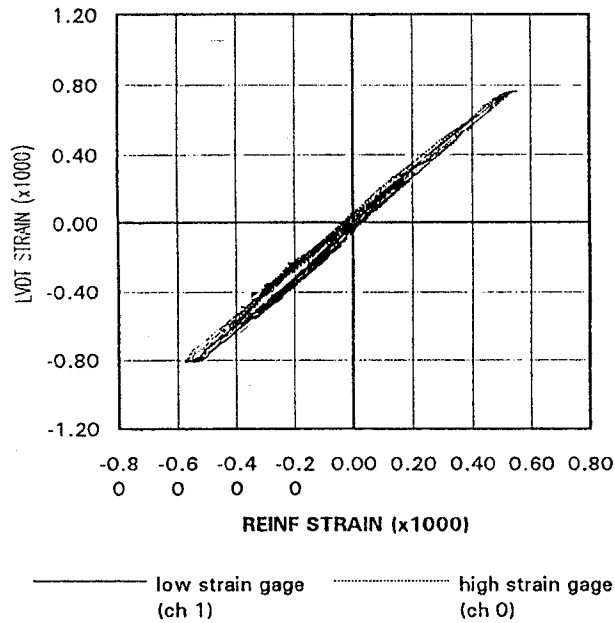


**Fig. 195 Test 6A— East Column East
Base LVDT Strain vs. Reinf Strain**

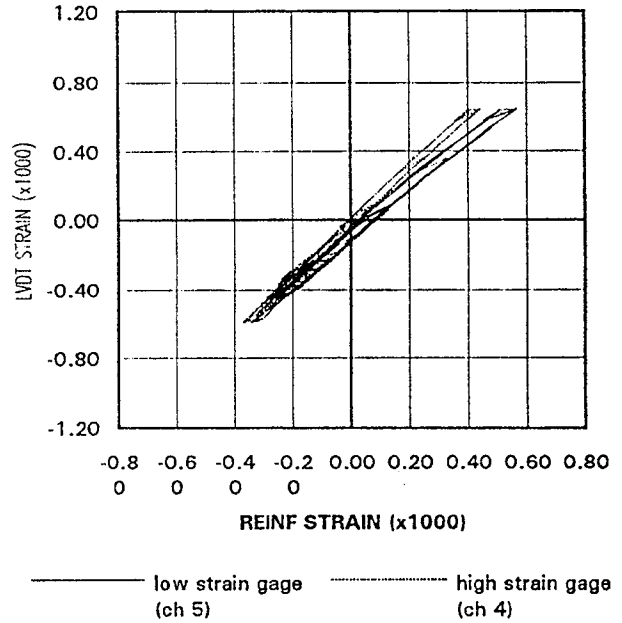


**Fig. 196 Test 6A— East Column West
Base LVDT Strain vs. Reinf Strain**

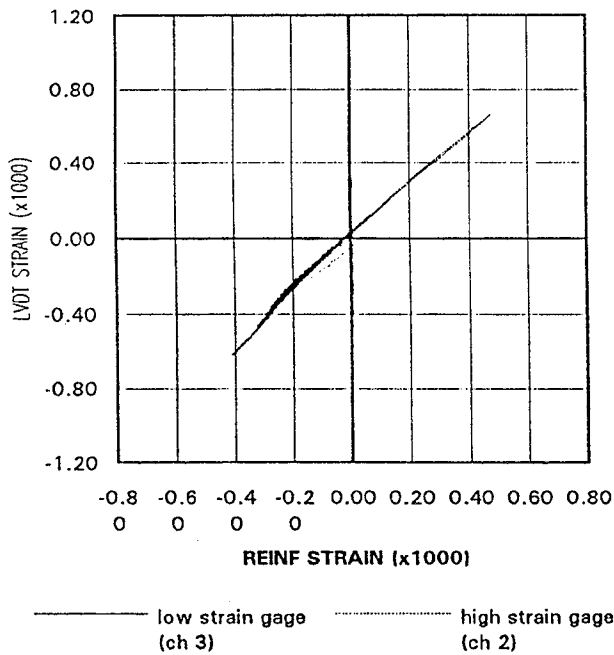


**Fig. 197 Test 6A— West Column East
Base LVDT Strain vs. Reinf Strain**

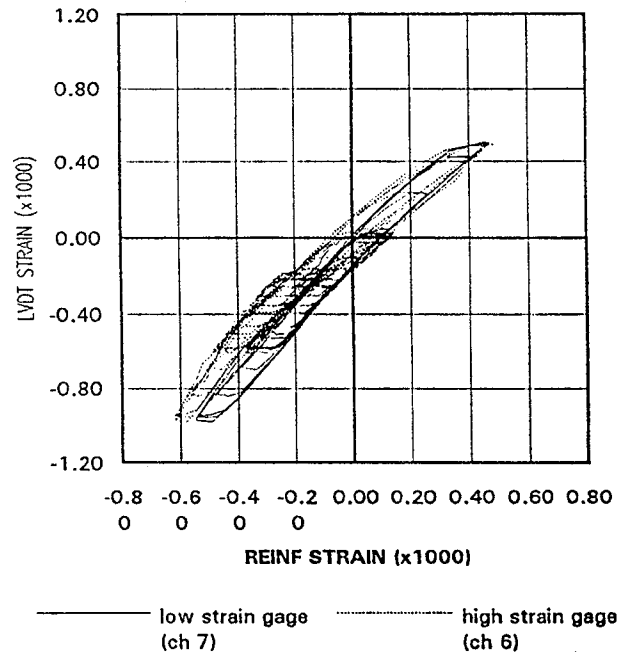


**Fig. 198 Test 6A— West Column West
Base LVDT Strain vs. Reinf Strain**

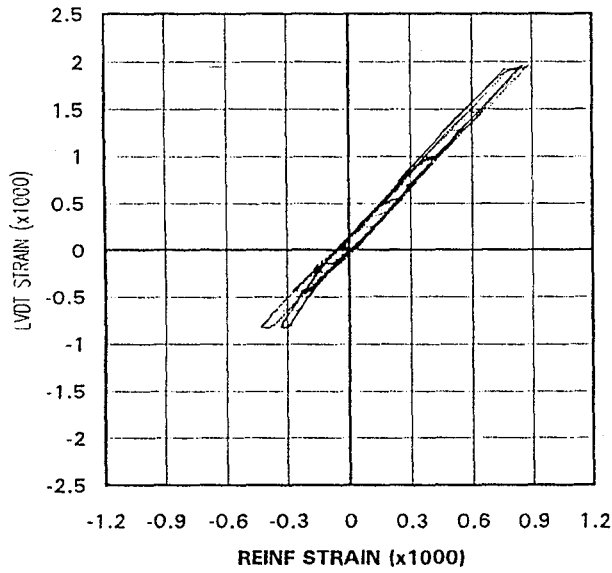


**Fig. 199 Test 6A— East End Beam
Bottom LVDT Strain vs. Reinf Strain**

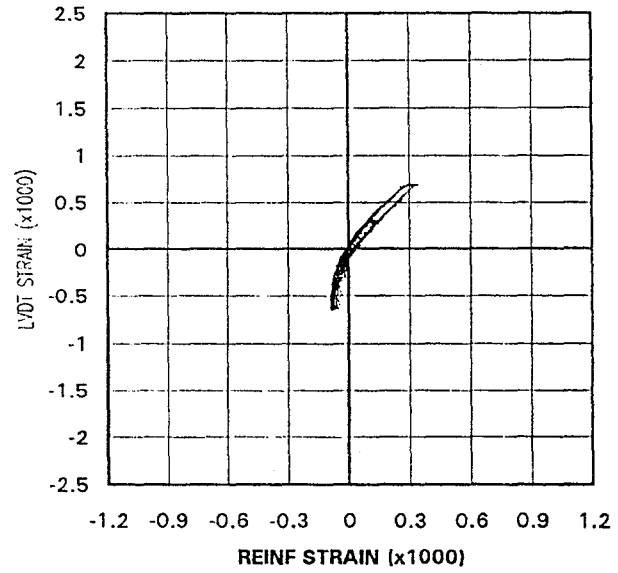


**Fig. 200 Test 6A— East End Beam
Top LVDT Strain vs. Reinf Strain**

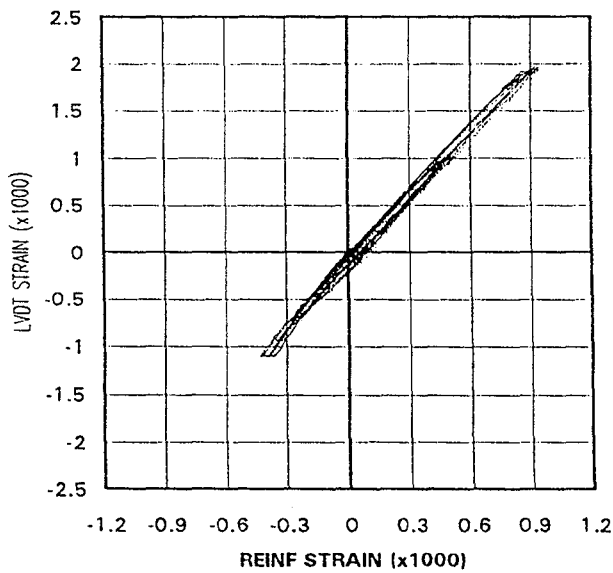


**Fig. 201 Test 6A— West End Beam
Bottom LVDT Strain vs. Reinf Strain**

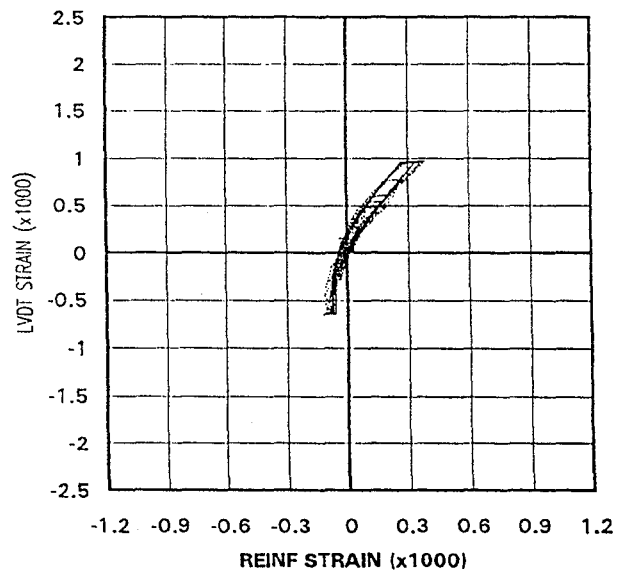


**Fig. 202 Test 6A— West End
Top LVDT Strain vs. Reinf Strain**

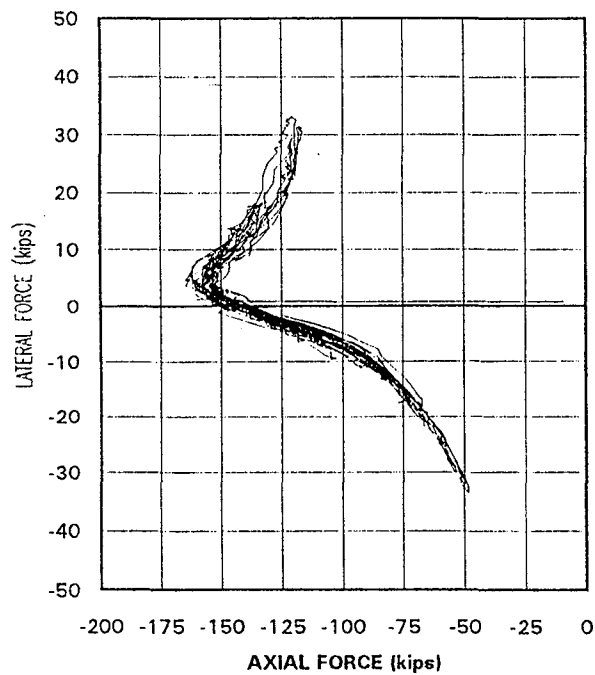


**Fig. 203 Test 6A—
Lateral Force vs. East Column Axial Force**

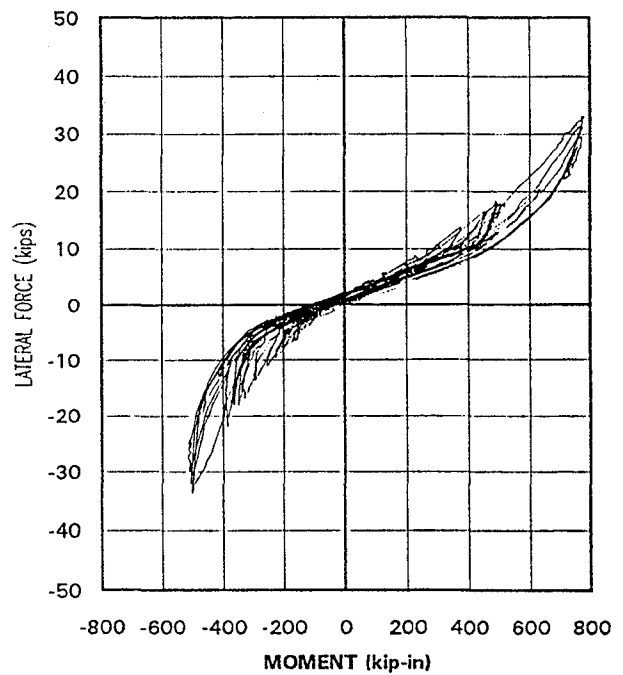


**Fig. 204 Test 6A—
Lateral Force vs. East Column Moment**

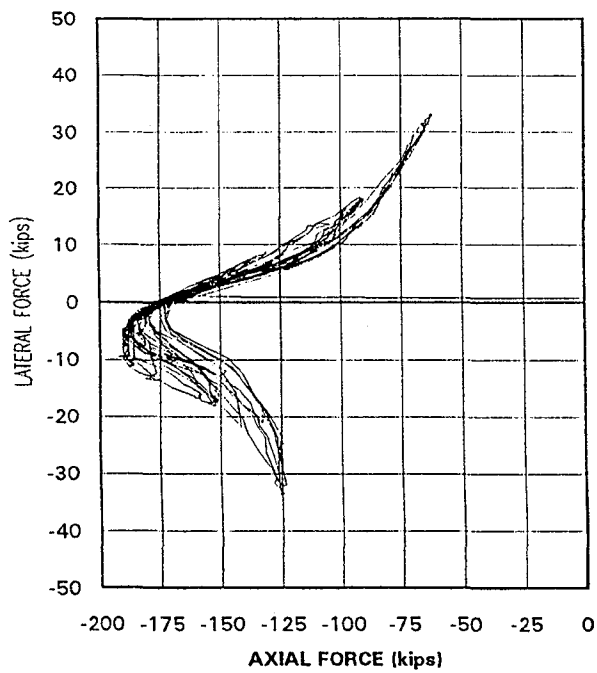


**Fig. 205 Test 6A—
Lateral Force vs. West Column Axial Force**

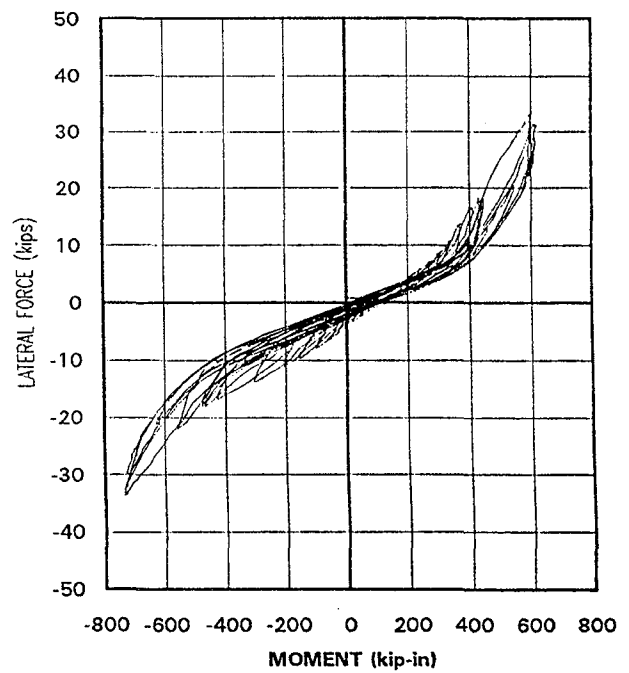


**Fig. 206 Test 6A—
Lateral Force vs. West Column Moment**

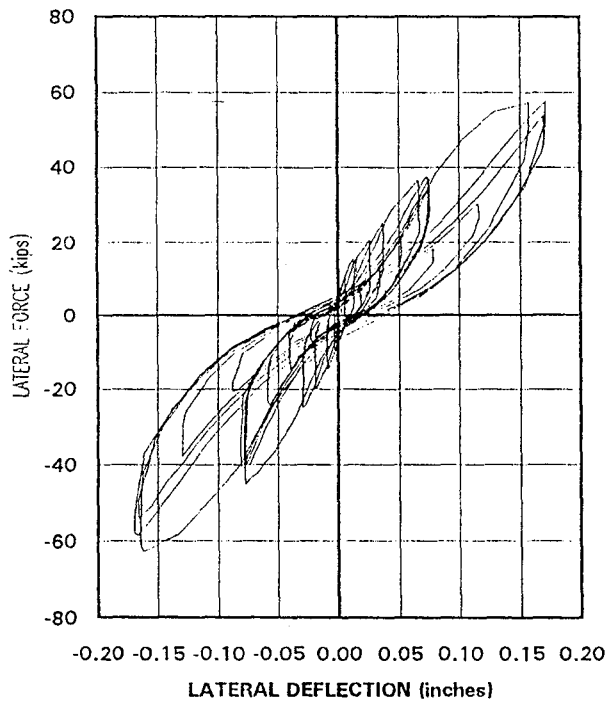


**Fig. 207 Test 7A—
Lateral Force vs. Deflection**

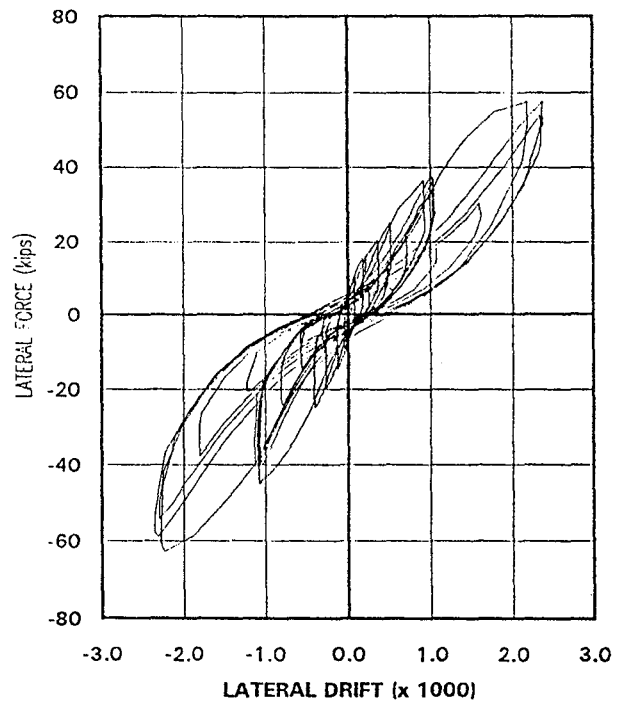


**Fig. 208 Test 7A—
Lateral Force vs. Drift**

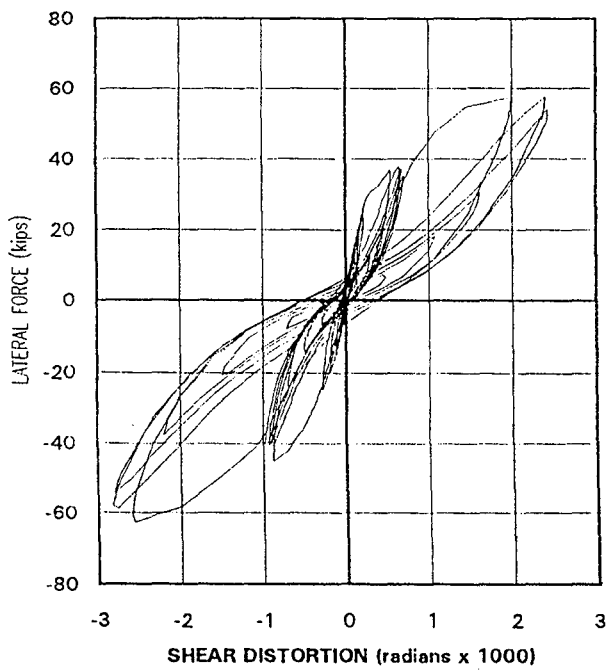


**Fig. 209 Test 7A—
Lateral Force vs. Shear Distortion**

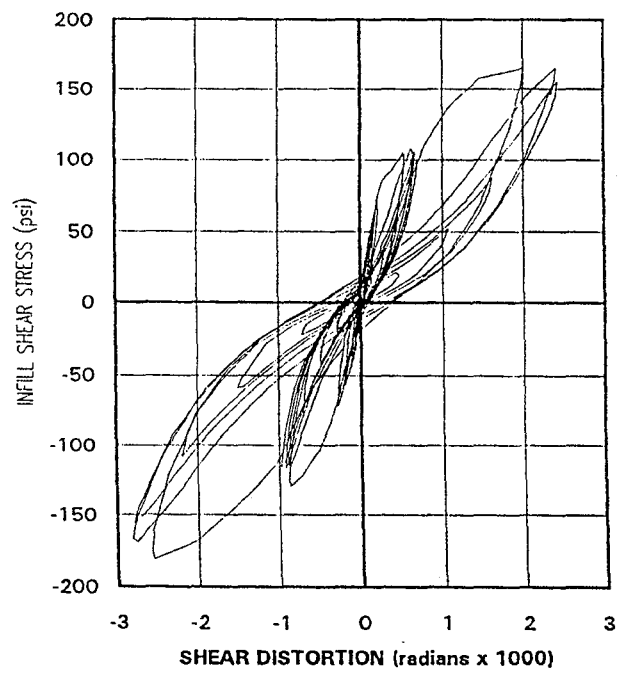


**Fig. 210 Test 7A—
Infill Shear Stress vs. Shear Distortion**

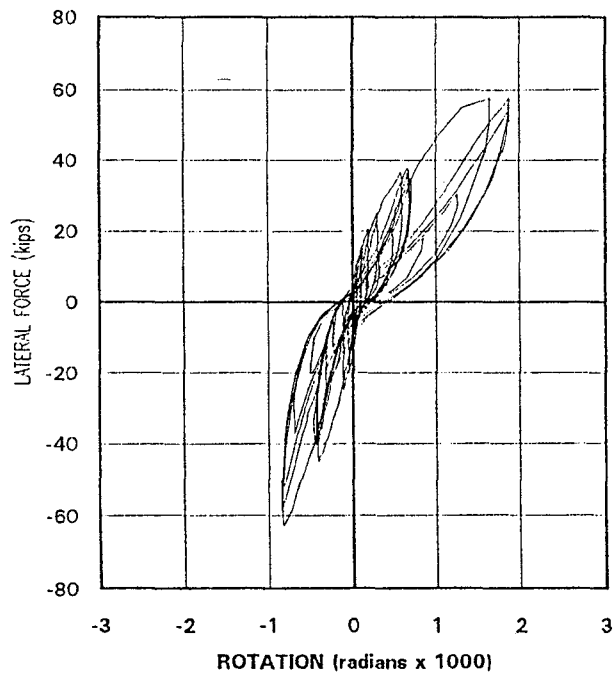


**Fig. 211 Test 7A—
Lateral Force vs. East Column Base Rotation**

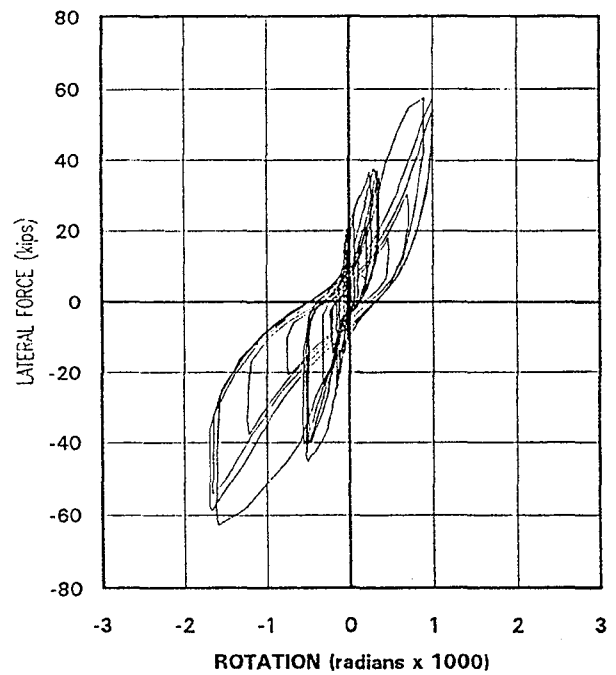


**Fig. 212 Test 7A—
Lateral Force vs. West Column Base Rotation**

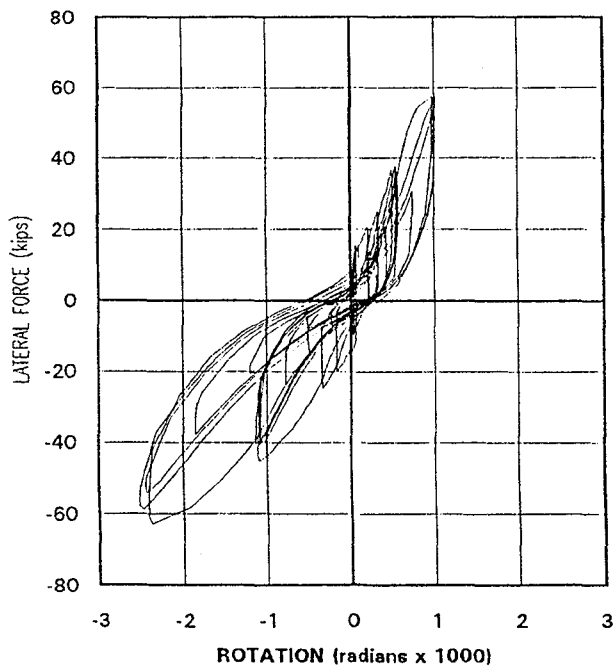


**Fig. 213 Test 7A—
Lateral Force vs. Beam East End Rotation**

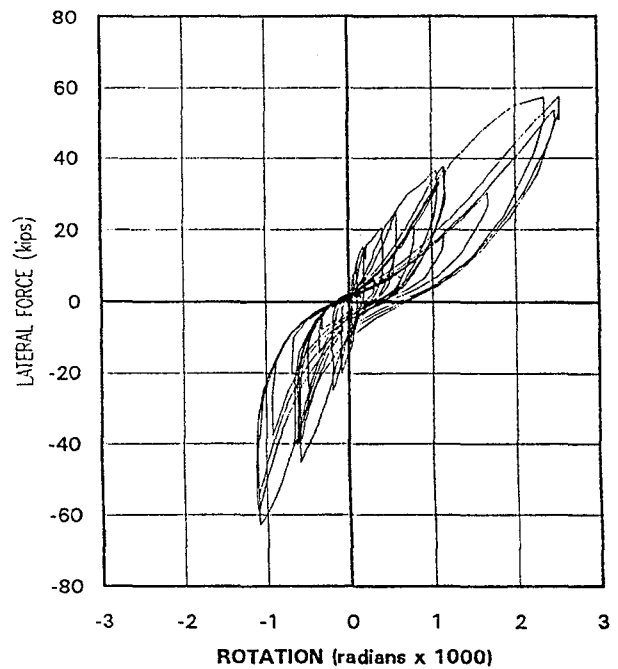


**Fig. 214 Test 7A—
Lateral Force vs. Beam West End Rotation**

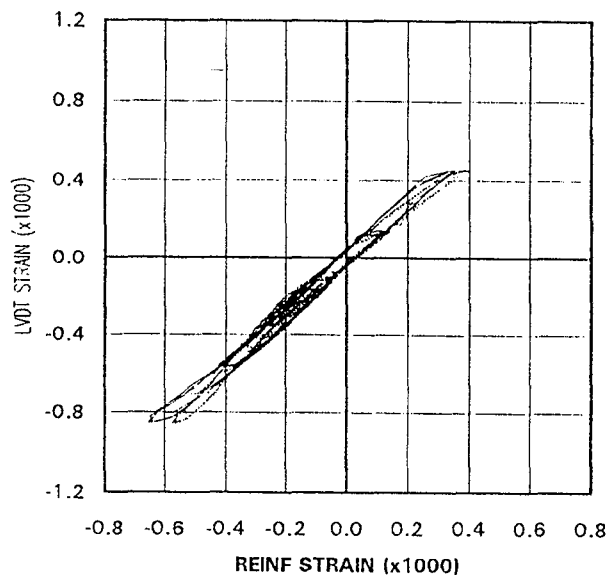


**Fig. 215 Test 7A— East Column East
Base LVDT Strain vs. Reinf Strain**

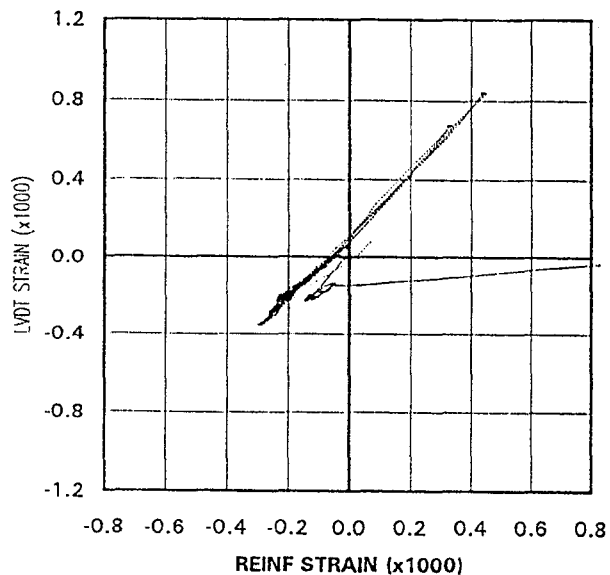


**Fig. 216 Test 7A— East Column West
Base LVDT Strain vs. Reinf Strain**

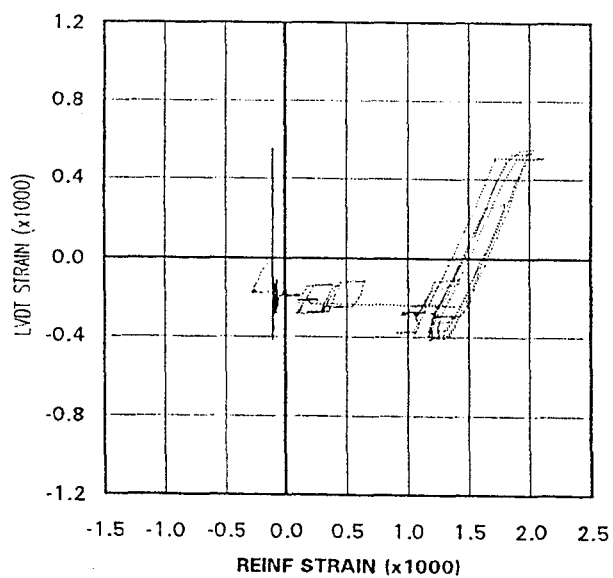


**Fig. 217 Test 7A— West Column East
Base LVDT Strain vs. Reinf Strain**

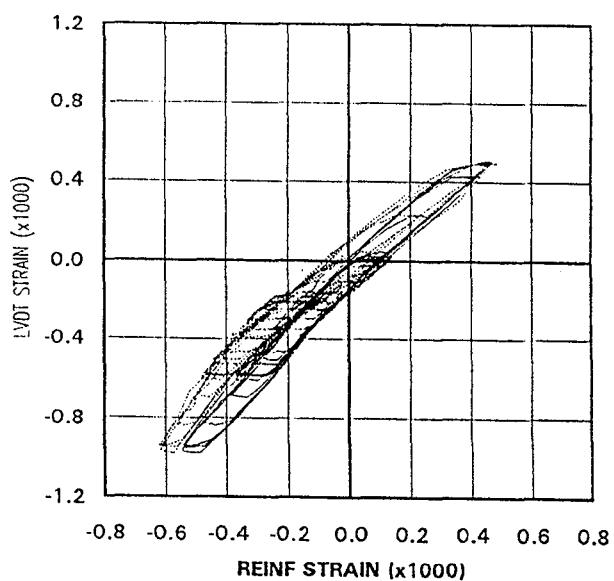


**Fig. 218 Test 7A— West Column West
Base LVDT Strain vs. Reinf Strain**

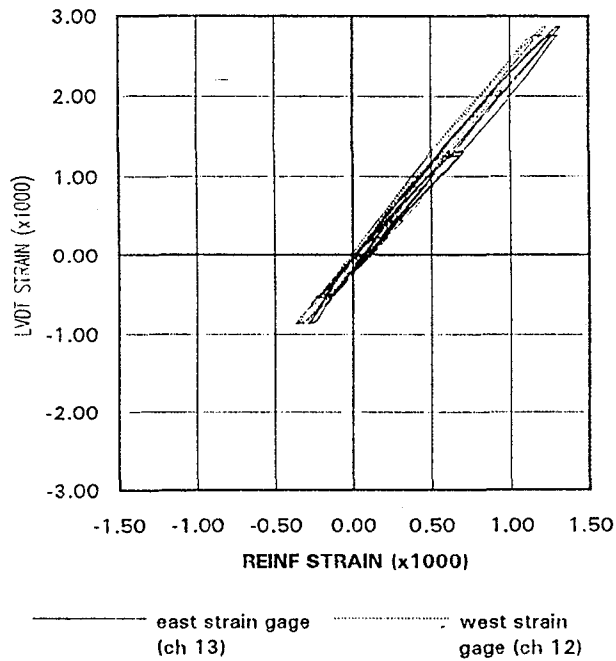


**Fig. 219 Test 7A– East End Beam
Bottom LVDT Strain vs. Reinf Strain**

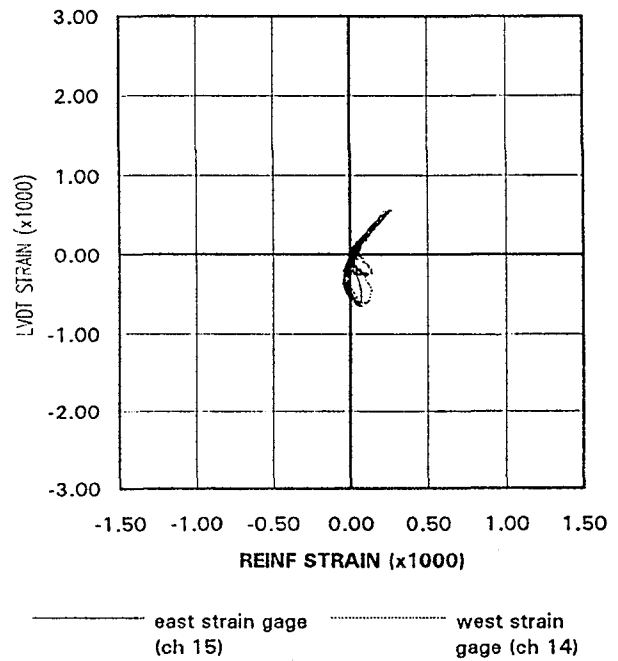


**Fig. 220 Test 7A– East End Beam
Top LVDT Strain vs. Reinf Strain**

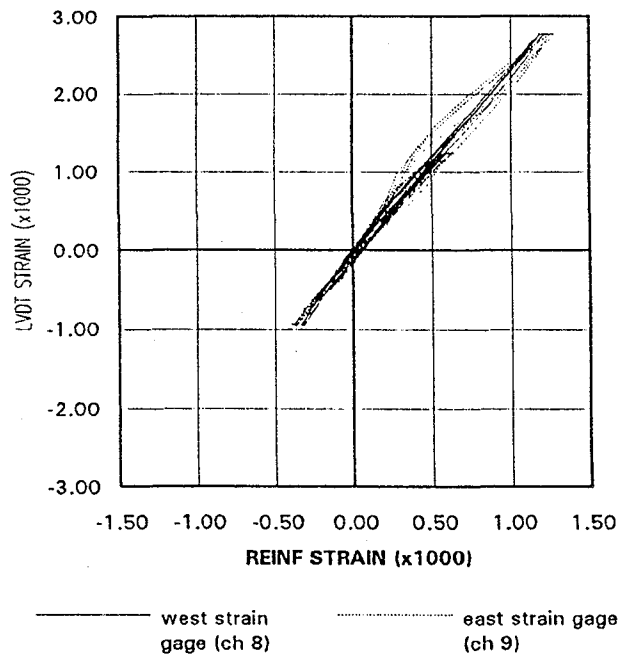


**Fig. 221 Test 7A– West End Beam
Bottom LVDT Strain vs. Reinf Strain**

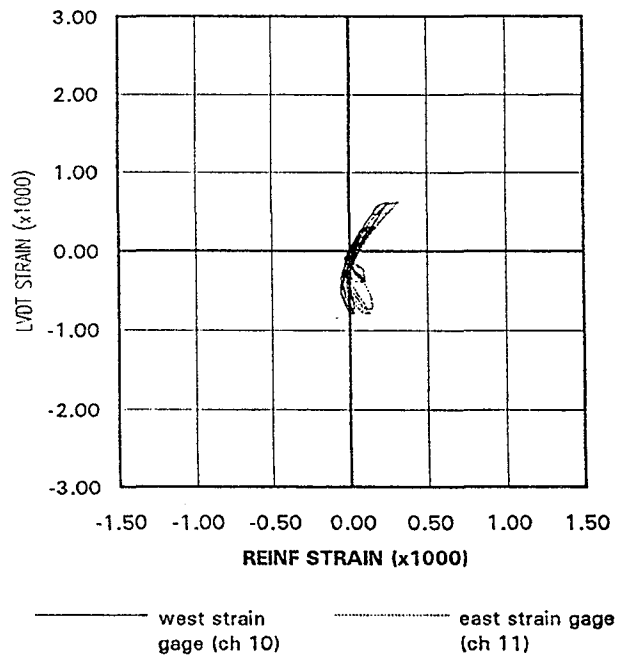


**Fig. 222 Test 7A– West End
Top LVDT Strain vs. Reinf Strain**

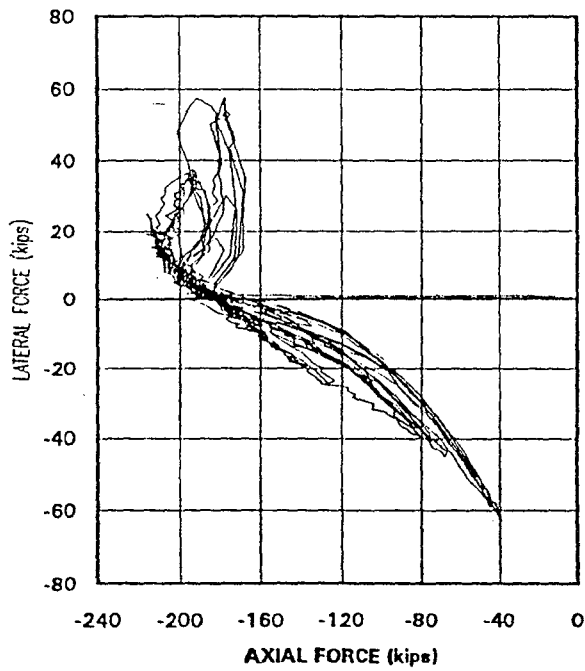


Fig. 223 Test 7A—
Lateral Force vs. East Column Axial Force

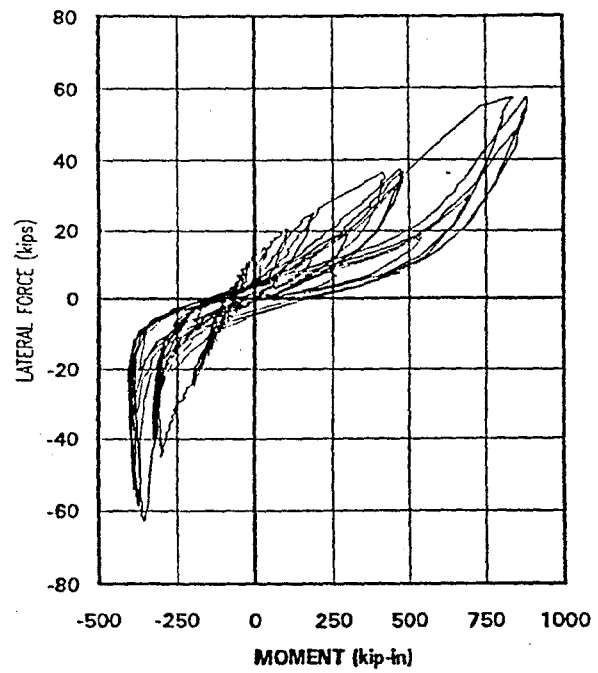


Fig. 224 Test 7A—
Lateral Force vs. East Column Moment

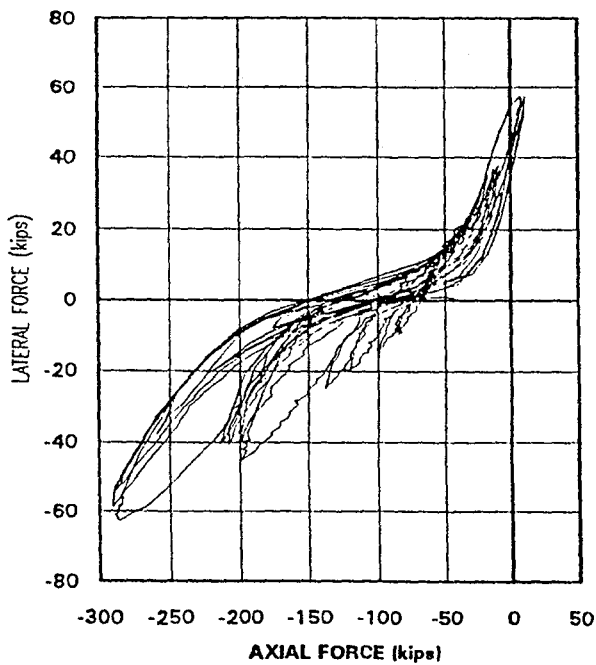


Fig. 225 Test 7A—
Lateral Force vs. West Column Axial Force

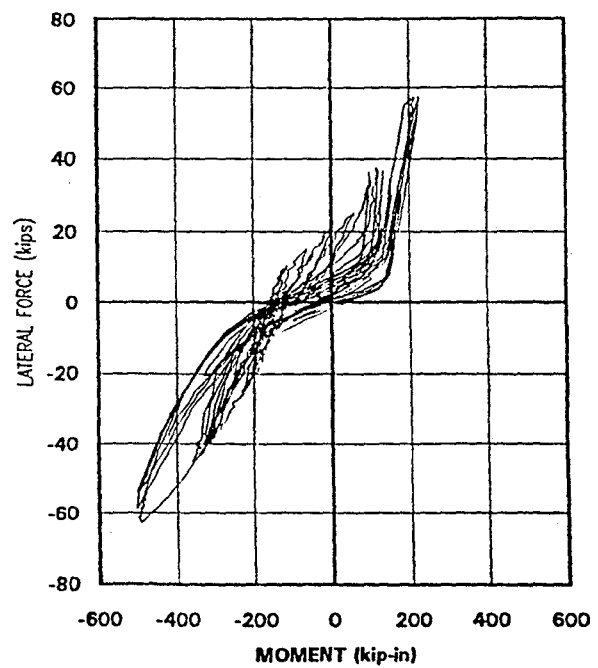
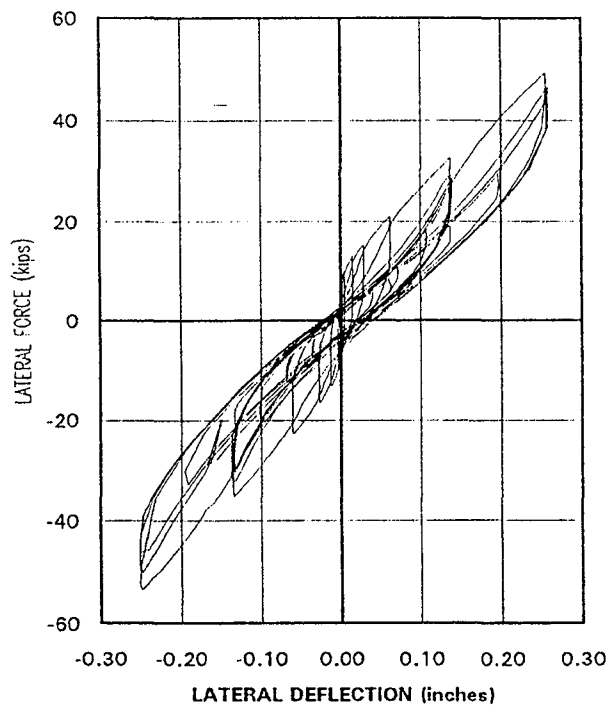
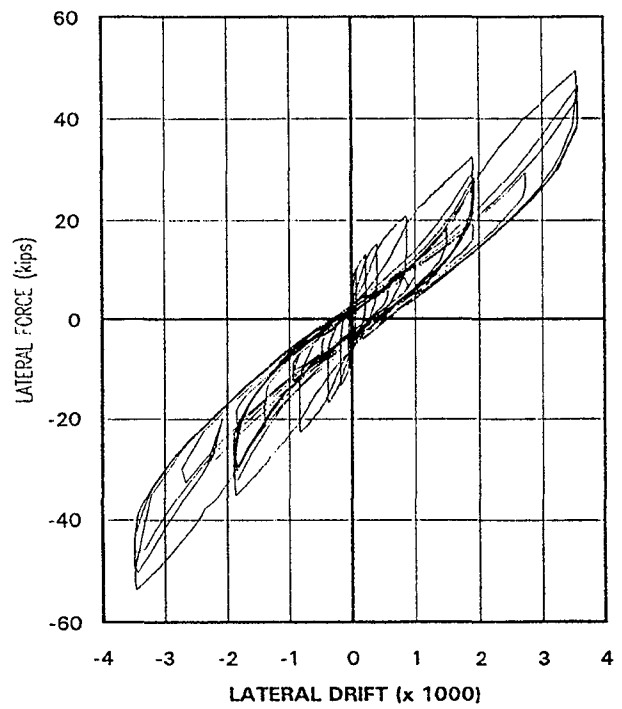


Fig. 226 Test 7A—
Lateral Force vs. West Column Moment



**Fig. 227 Test 8A—
Lateral Force vs. Deflection**



**Fig. 228 Test 8A—
Lateral Force vs. Drift**

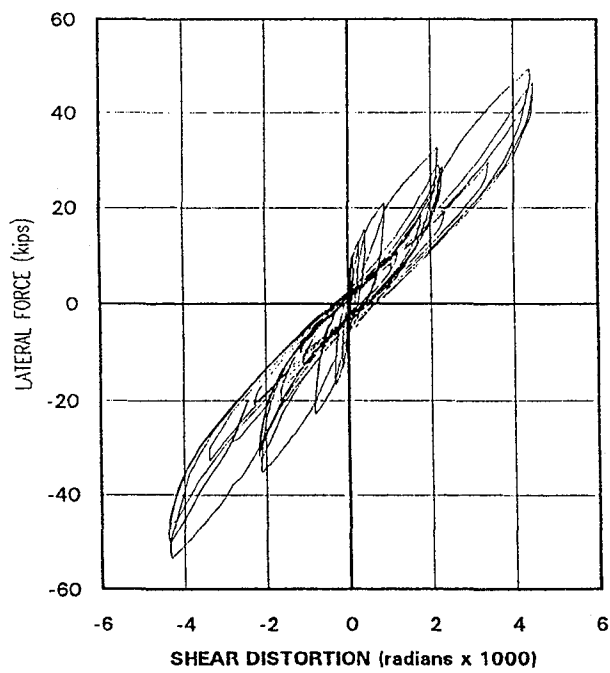


**Fig. 229 Test 8A—
Lateral Force vs. Shear Distortion**

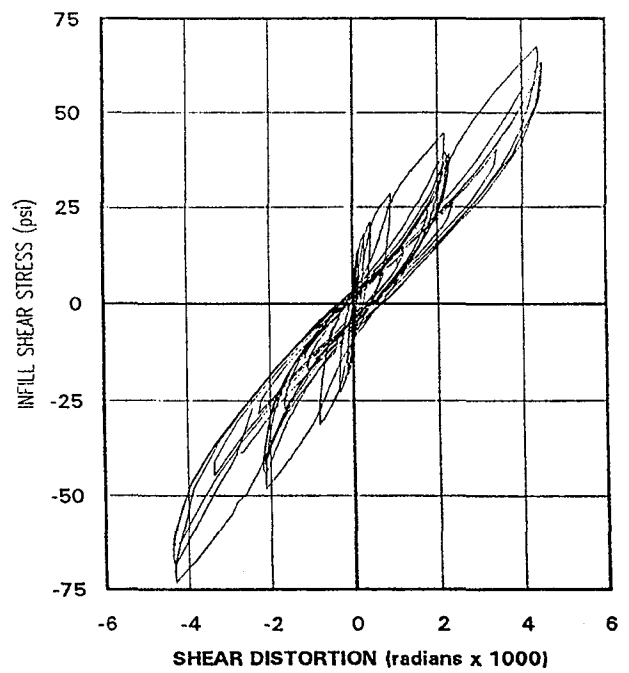


**Fig. 230 Test 8A—
Infill Shear Stress vs. Shear Distortion**

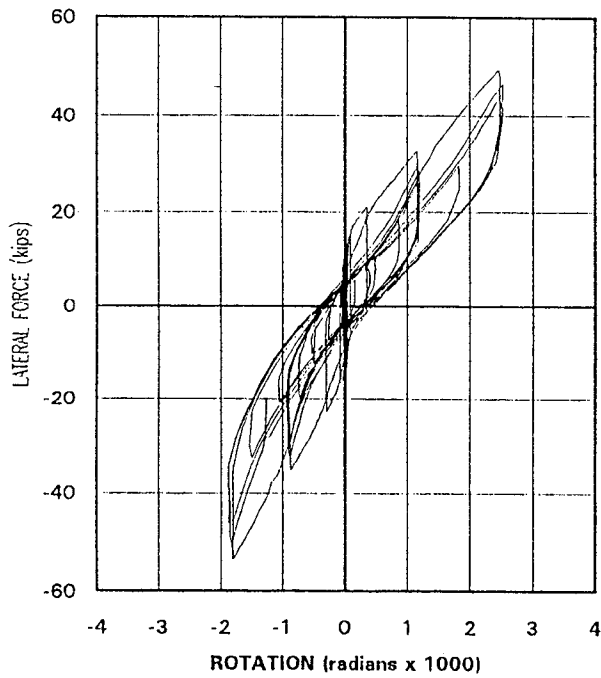


**Fig. 231 Test 8A—
Lateral Force vs. East Column Base Rotation**

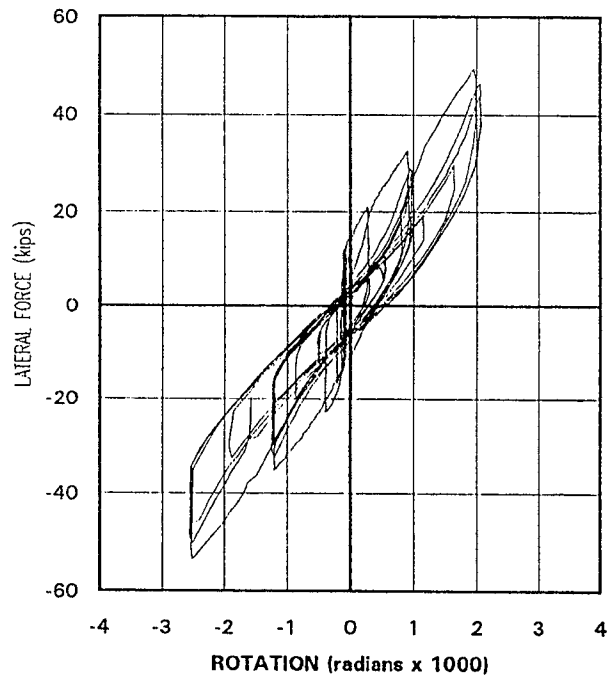


**Fig. 232 Test 8A—
Lateral Force vs. West Column Base Rotation**

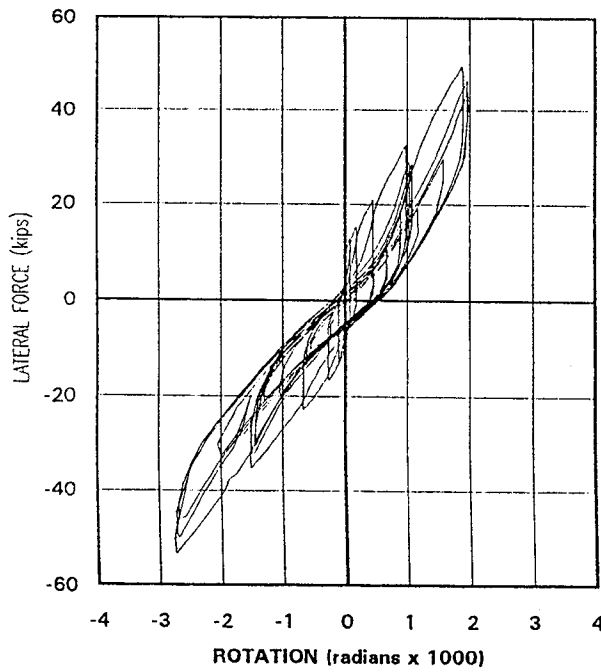


**Fig. 233 Test 8A—
Lateral Force vs. Beam East End Rotation**

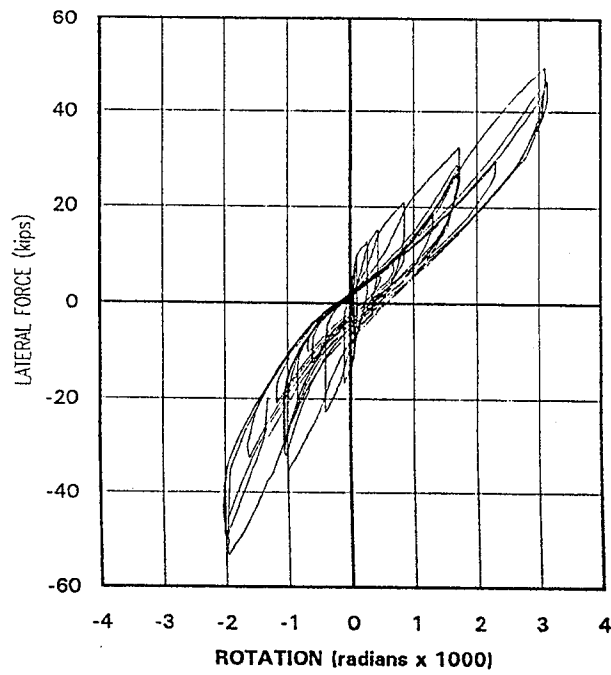


**Fig. 234 Test 8A—
Lateral Force vs. Beam West End Rotation**

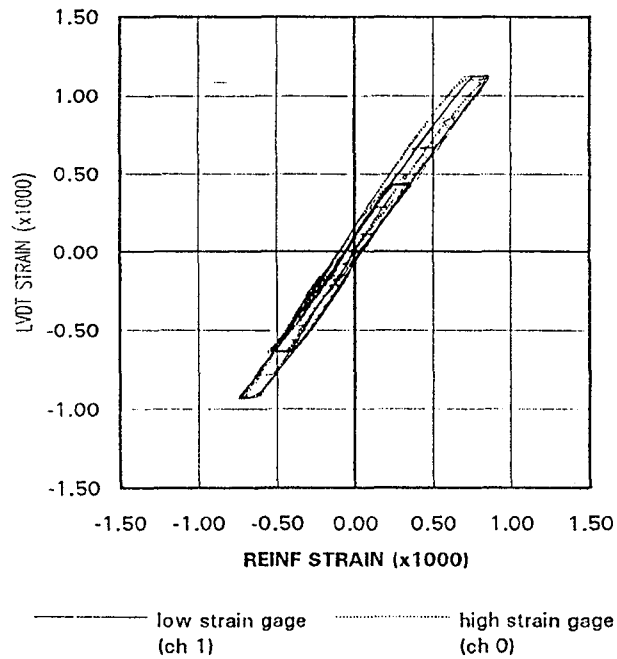


Fig. 235 Test 8A— East Column East Base LVDT Strain vs. Reinf Strain

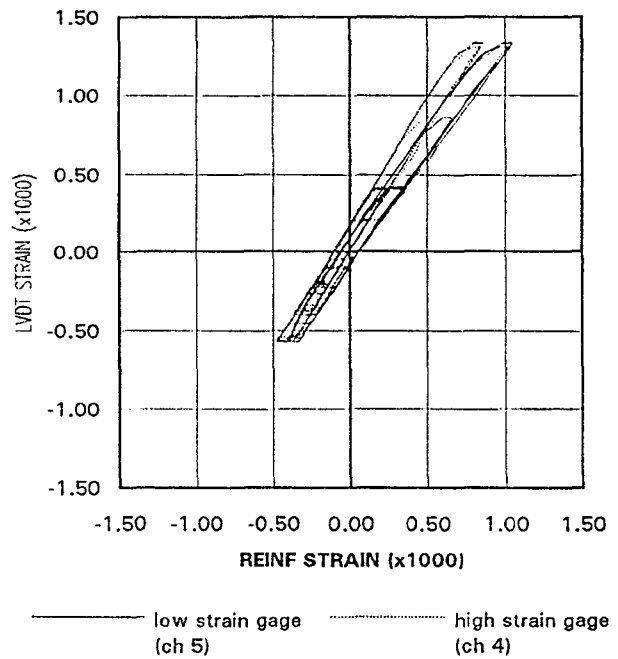


Fig. 236 Test 8A— East Column West Base LVDT Strain vs. Reinf Strain

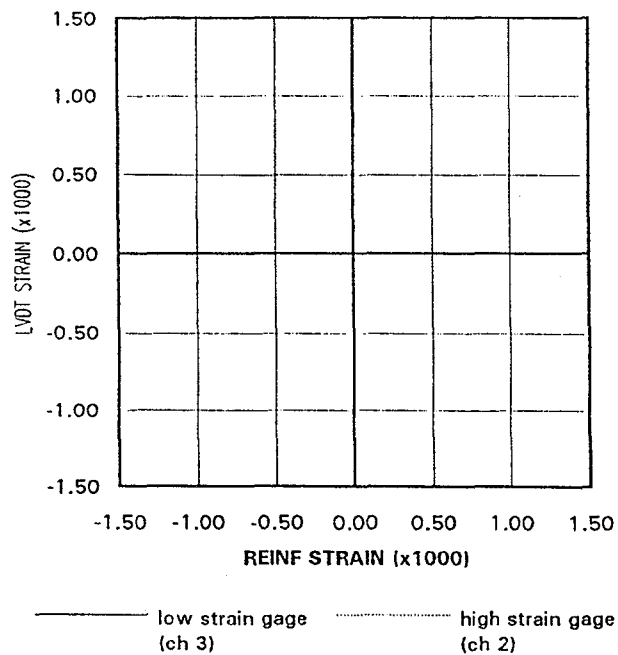


Fig. 237 Test 8A— West Column East Base LVDT Strain vs. Reinf Strain

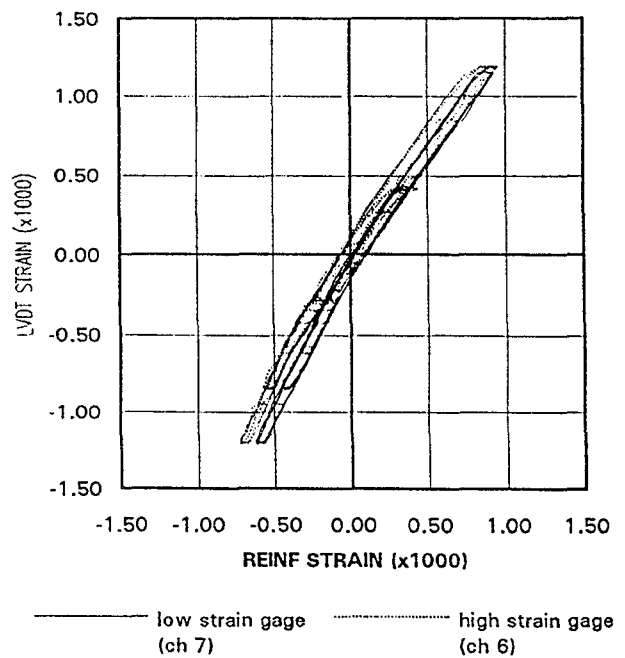
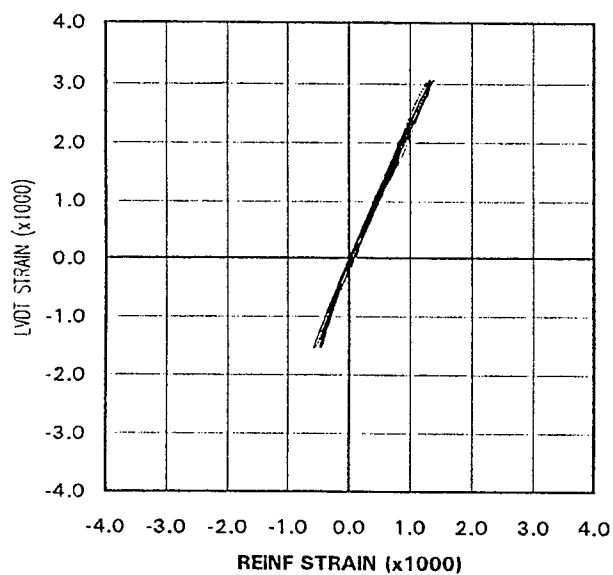
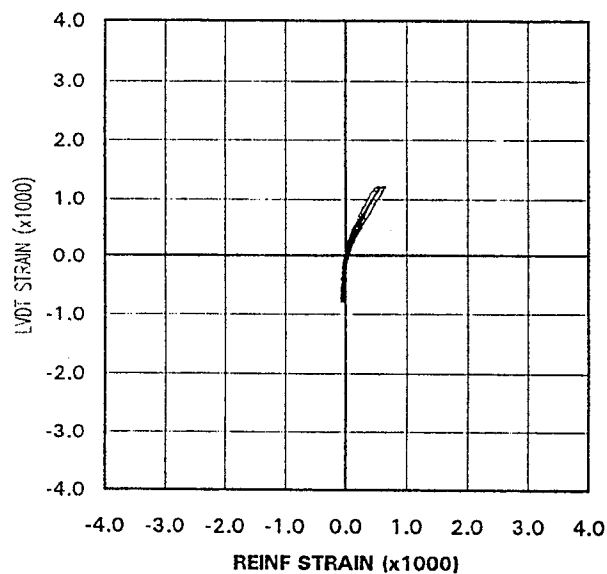


Fig. 238 Test 8A— West Column West Base LVDT Strain vs. Reinf Strain



**Fig. 239 Test 8A— East End Beam
Bottom LVDT Strain vs. Reinf Strain**



**Fig. 240 Test 8A— East End Beam
Top LVDT Strain vs. Reinf Strain**

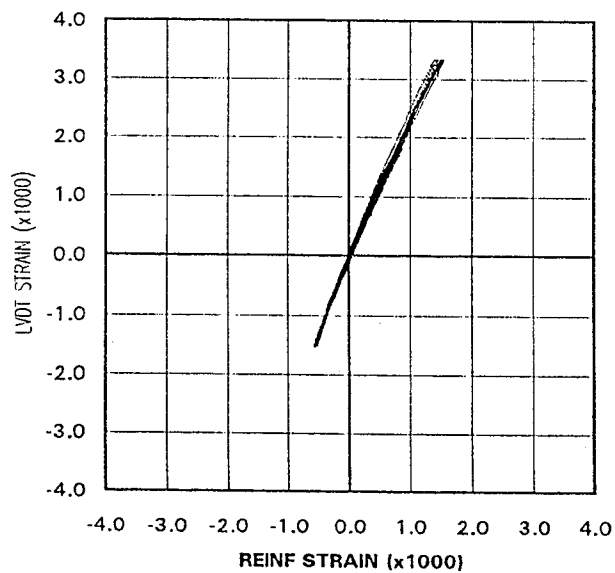


**Fig. 241 Test 8A— West End Beam
Bottom LVDT Strain vs. Reinf Strain**

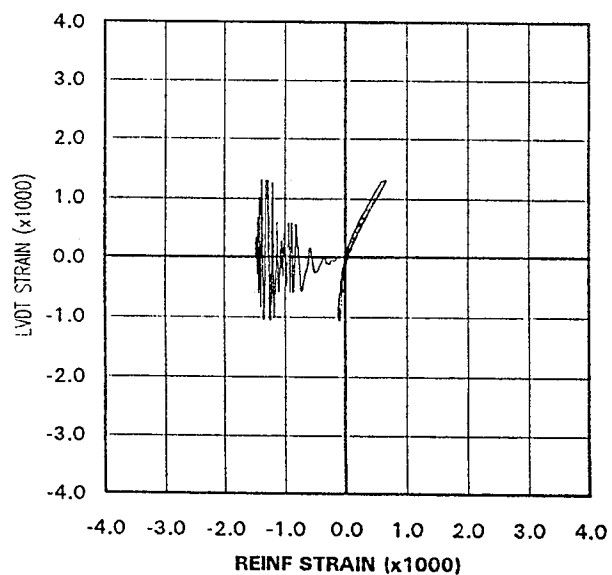


**Fig. 242 Test 8A— West End
Top LVDT Strain vs. Reinf Strain**

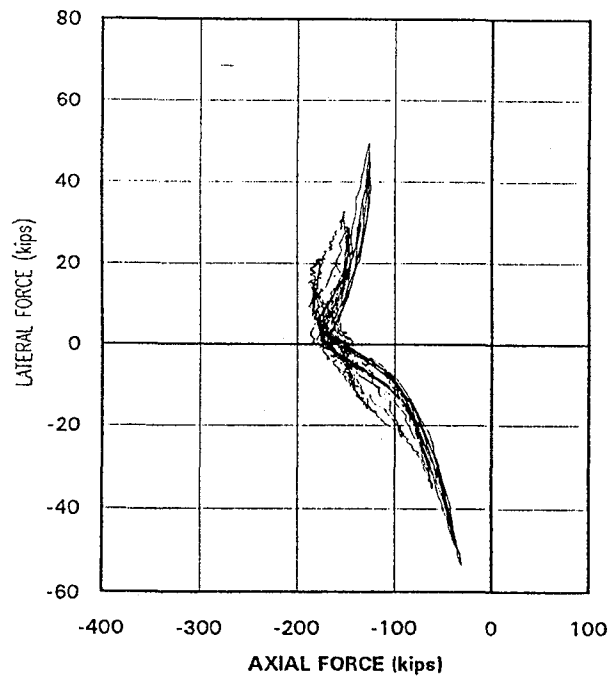


**Fig. 243 Test 8A—
Lateral Force vs. East Column Axial Force**

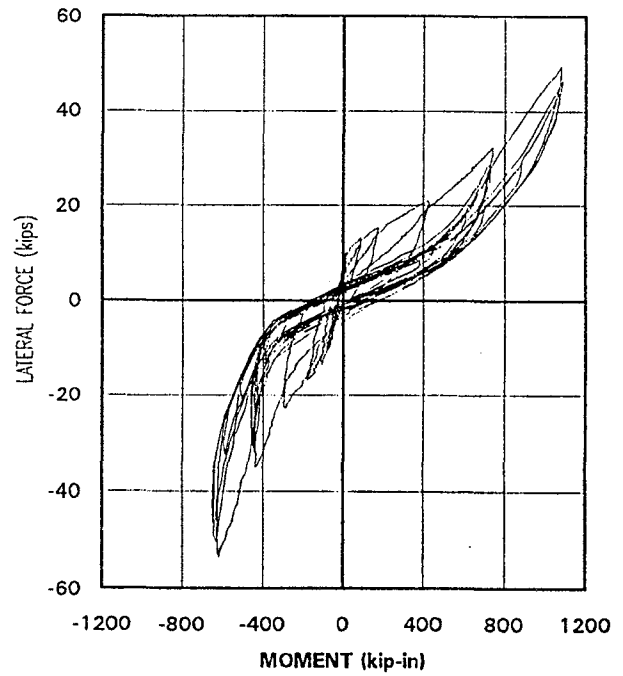


**Fig. 244 Test 8A—
Lateral Force vs. East Column Moment**

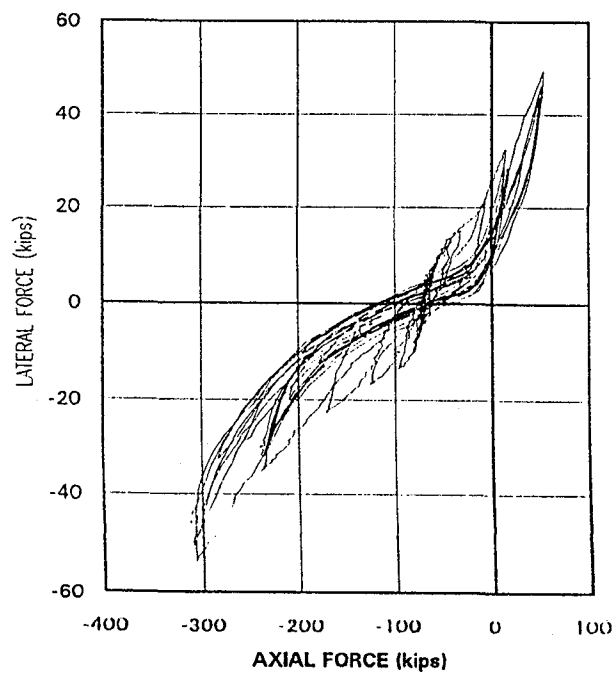


**Fig. 245 Test 8A—
Lateral Force vs. West Column Axial Force**

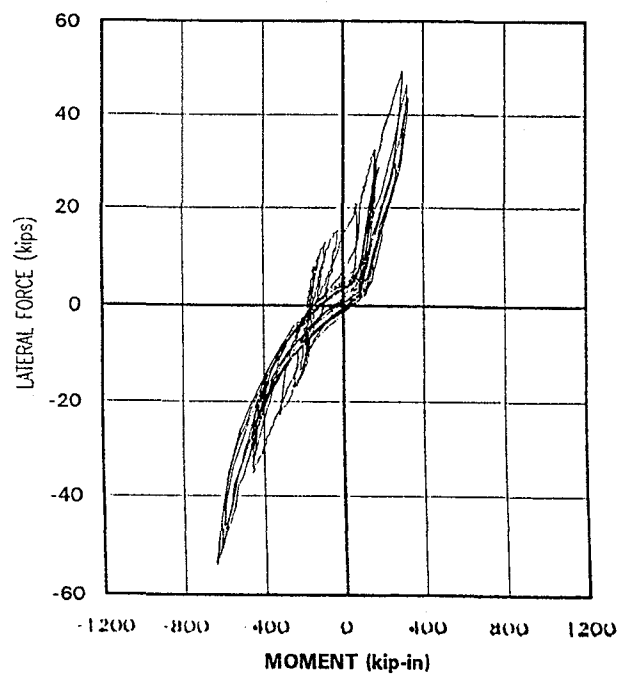


**Fig. 246 Test 8A—
Lateral Force vs. West Column Moment**

APPENDIX F

OUT-OF-PLANE TEST RESULTS

Out-of-plane test results for the test specimens are presented in this appendix. Discussion and analysis of the results are presented in Chapter 5. Detail description of the specimens and important chronological data is presented in Table 25.

Table 25 Specimen Chronological Information

Specimen#	# of Courses	Mortar	Date Built	Date Tested
1	22	Type S	7/16/91	10/31/92
2a	22	Type N	11/15/91	4/2/92
2b	22	Type N	11/15/91	4/10/92
2c	22	Repaired	4/30/92	5/8/92
3a	24	Lime Mortar	5/14/92	6/3/92
3b	24	Lime Mortar	5/14/92	6/4/92
3c	24	Repaired	6/12/92	6/18/92
4a	8	Type N	6/24/92	7/10/92
4b	8	Type N	6/24/92	7/14/92
5a	8	Type N	7/21/92	7/28/92
5b	8	Type N	7/21/92	7/29/92
5d	8	Type N	7/21/92	7/30/92
6a	23	Lime Mortar	8/6/92	8/31/92
6b	23	Lime Mortar	8/6/92	9/1/92
6b2	23	Lime Mortar	8/6/92	9/3/92
6c	23	Repaired	9/10/92	9/24/92
7a	23	Type N	10/2/92	12/7/92
7b	23	Type N	10/2/92	12/17/92
8a	23	Lime Mortar	1/11/93	2/3/93
8b	23	Lime Mortar	1/11/93	2/5/93

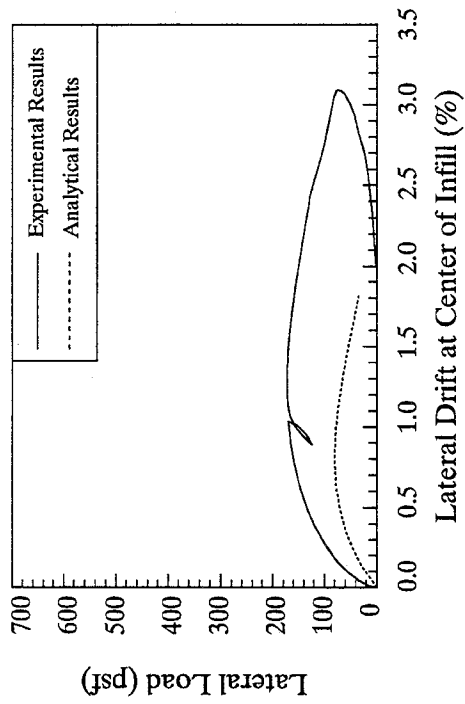


Fig. 247 Results for Test #1

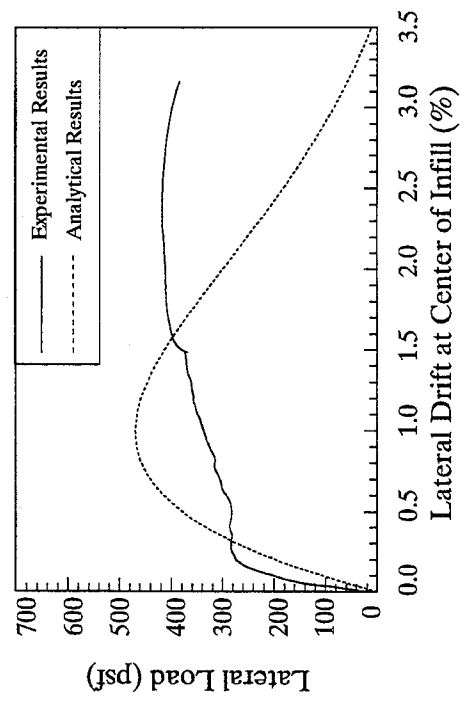


Fig. 249 Results for Test #2c

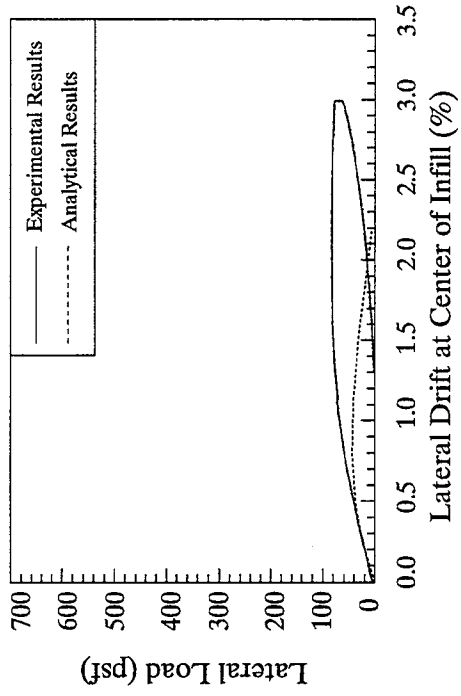


Fig. 248 Results for Test #2b

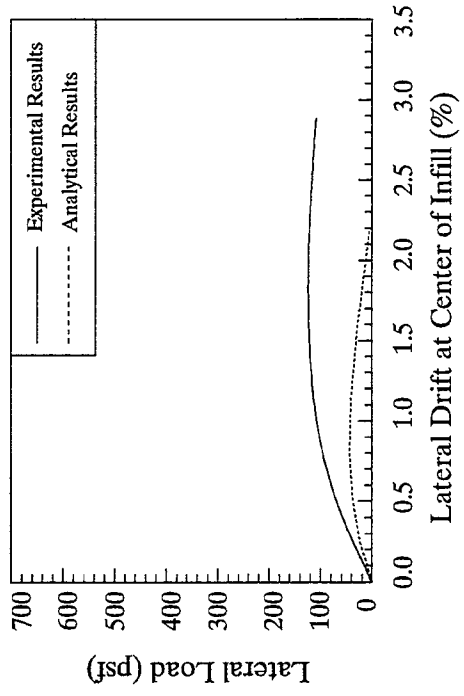


Fig. 250 Results for Test #3b

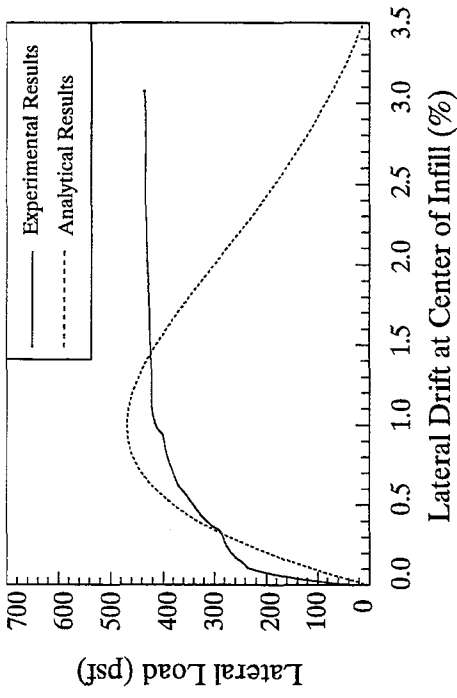


Fig. 251 Results for Test #3c

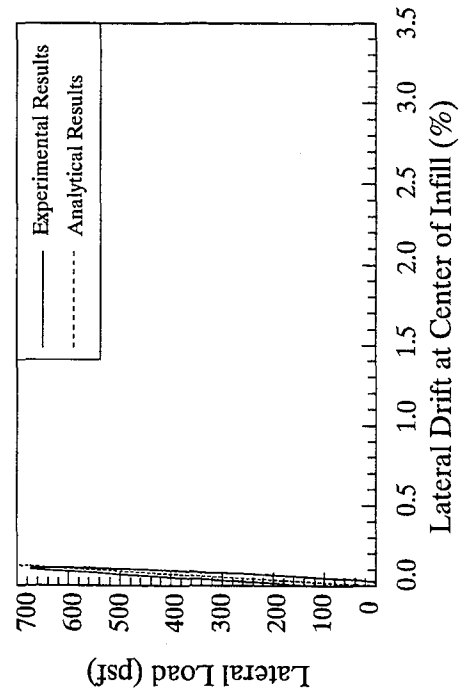


Fig. 253 Results for Test #5b

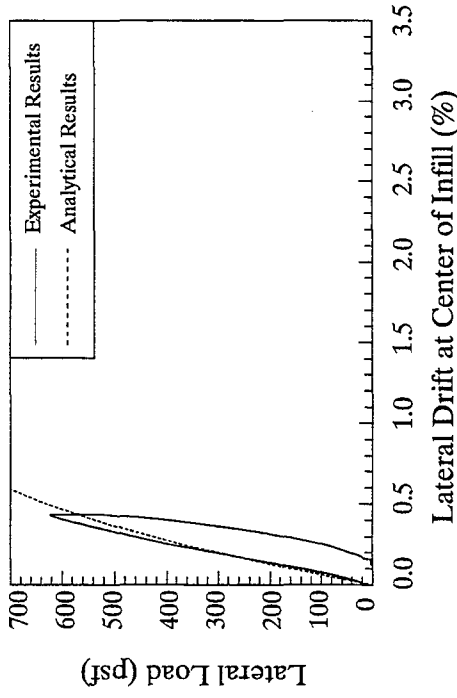


Fig. 252 Results for Test #4b

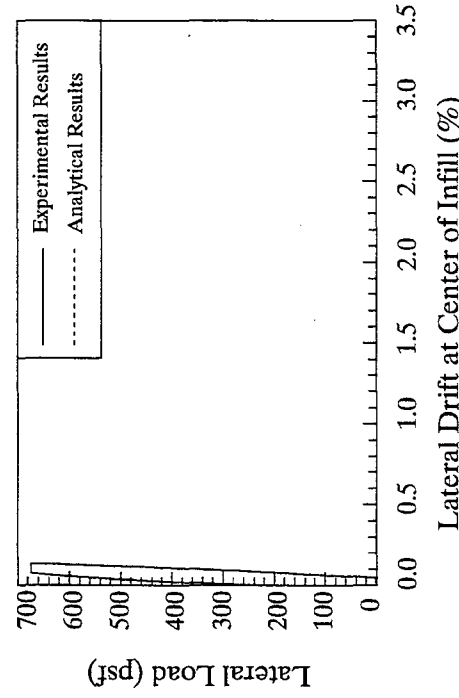


Fig. 254 Results for Test #5d

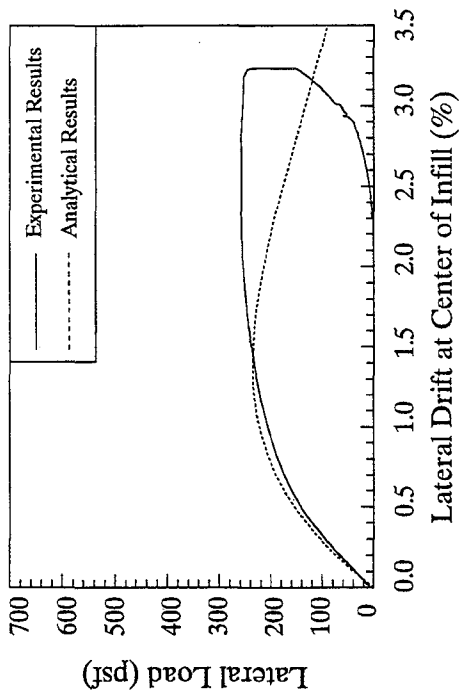


Fig. 255 Results for Test #6b

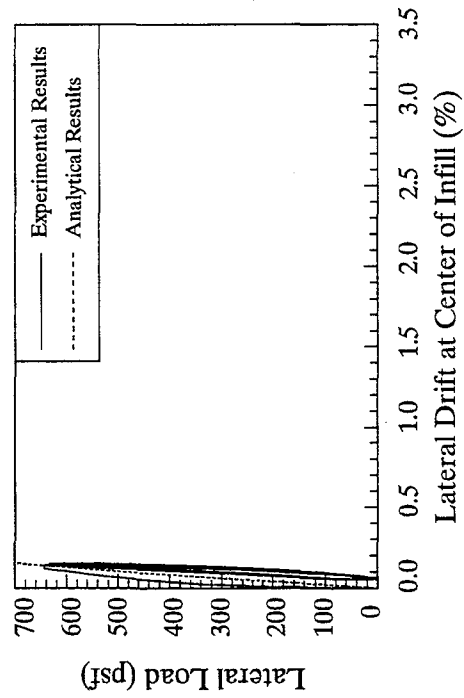


Fig. 257 Results for Test #6c

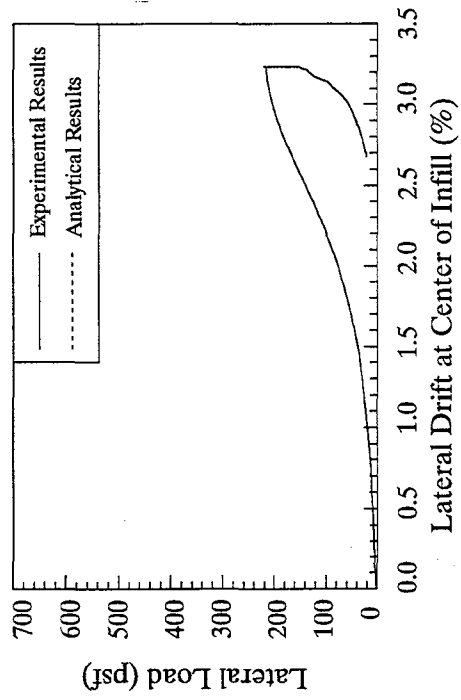


Fig. 256 Results for Test #6b2

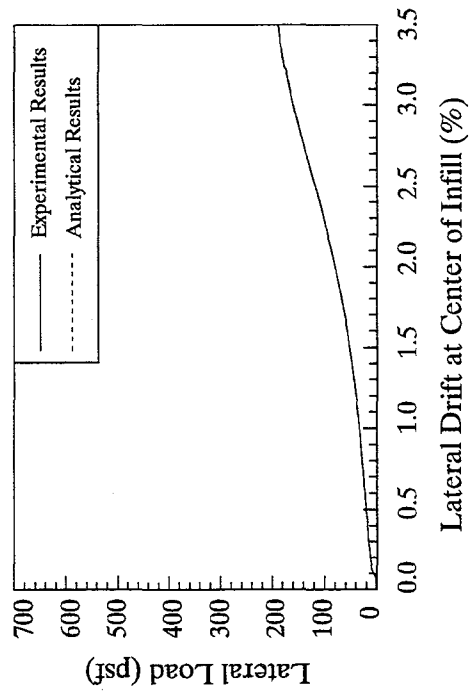


Fig. 258 Results for Test #6d

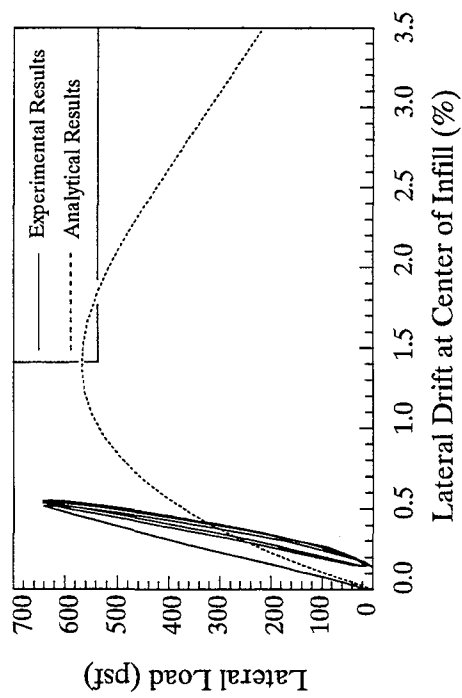


Fig. 259 Results for Test #7b

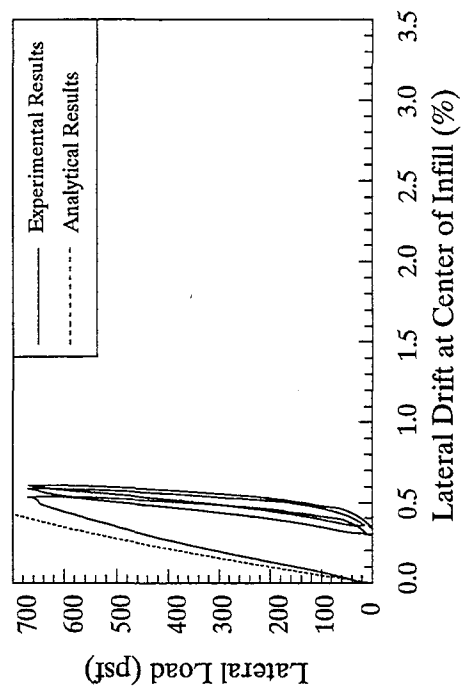


Fig. 260 Results for Test #8b

crushing strain (ϵ_{cr}) of 0.003 the values for k_1 and k_2 are 0.62 and 0.36, while for a crushing strain (ϵ_{cr}) of 0.004 the values for k_1 and k_2 are 0.67 and 0.37 respectively.

The influence of k_1 and k_2 on the out-of-plane strength of the panel are discussed separately. For a range of values for k_1 it was found that the out-of-plane strength of the panel increases with k_1 . The strength of a panel for a range of k_1 values are presented in Fig. 262. Panel strength has been

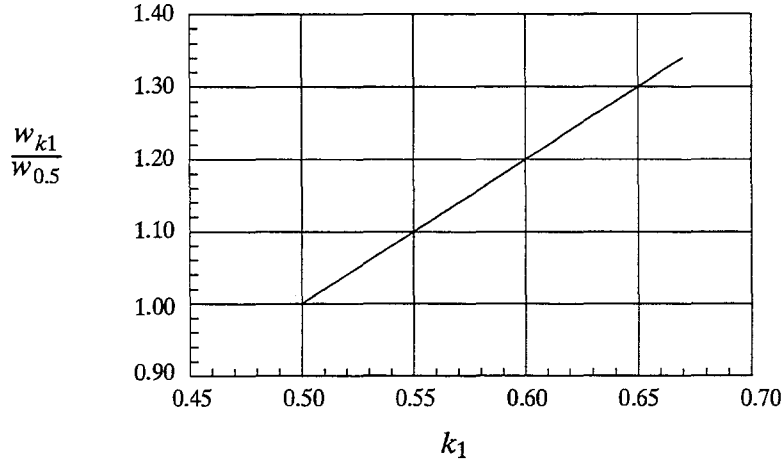


Fig. 262 Panel Strength Reduction vs. k_1

normalized with respect to the panel strength corresponding to a k_1 value of 0.5. The value of $w_{0.5}$ corresponds to the out-of-plane strength of the panel for the case where k_1 is the lowest value of 0.5. The value of w_{k1} corresponds to the out-of-plane strength of the panel where k_1 ranges from 0.5 to 0.7. Based on Fig. 262 and assuming in the calculations that k_1 equals to 0.5, the strength estimated for the panel based on Eq. [24] may be underestimated by up to 26%. The calculated estimate is on the conservative side. A series of increasing values for k_2 decreases linearly the out-of-plane strength of the panel. The panel strength for a range of values corresponding to k_2 are normalized to the strength of the panel corresponding to k_2 equal to 0.33 and results are presented in Fig. 263. Based on Fig. 263 and assuming in the calculations that k_2 equals to 0.33, the strength estimated for the panel based on Eq. [24] may be overestimated by up to 12%. The calculated estimate is on the unconservative side.

Analysis of the effects of k_1 and k_2 on the out-of-plane strength of the panels were observed to cause opposite reactions; that is, while for increasing values for k_1 the strength of the panel increased, for increasing values of k_2 the strength of the panel decreased. The effects on panel strength caused by the change in k_1 and k_2 depend on the type of stress-strain distribution assumed for the masonry. Therefore, the values of k_1 and k_2 are related and must be selected in pairs. The probable combinations for a number of different masonry stress-strain distributions are $k_1=0.50$, $k_2=0.33$; $k_1=0.63$, $k_2=0.40$; $k_1=0.63$, $k_2=0.43$ and $k_1=0.68$, $k_2=0.43$. The obtained out-of-plane strengths of the panels with any k_1 and k_2 combinations are computed based on results presented in Fig. 262 and

APPENDIX G

SENSITIVITY ANALYSIS FOR K_1 AND K_2

In this appendix a sensitivity analysis for the effect of k_1 and k_2 on the out-of-plane strength of the panel is presented. The values of k_1 and k_2 are compared to a series of values corresponding to different stress-strain distributions and a relative accuracy range is presented.

Out-of-plane strength of masonry panels can be evaluated by using the analytical model developed in Chapter 7. An expression to evaluate the out-of-plane strength of the panels in terms of all the influencing parameters is presented in Eq. [24]. This expression contains two parameters that have been considered constant. These are k_1 , and k_2 which are concealed in γ (Eq. [38]). k_1 is defined as the ratio of the average stress on the bearing area in compression to the maximum compressive stress at the support. k_2 is defined as the ratio of the distance from the extreme compressive fiber to the resultant compressive force to the bearing width.

A stress-strain relationship for the masonry has been developed as explained in Appendix H, and an illustration of this relationship is presented in Fig. 261.

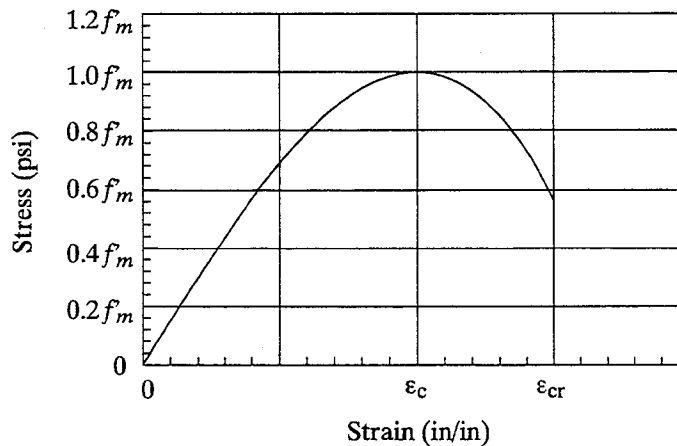


Fig. 261 Idealized Stress-Strain Relation in Compression

During the out-of-plane testing of the panels, the strain in the extreme fiber of the panels increases and the lateral displacement of the panel increases. Thus, during the course of the test, the strain in the extreme fiber of the panel varies up to its corresponding crushing limit. The corresponding stress distribution in the masonry varies between an almost triangular shape for low strain values, to a parabolic shape for strain values reaching the crushing limit. The value that the two parameters in question take varies according to the stress-strain distribution as follows: for a triangular distribution, $k_1 = 0.5$, $k_2 = 0.33$; for a parabolic distribution diagram $k_1 = 0.67$, $k_2 = 0.40$ and for a curve with partial descending branch, k_1 ranges between 0.63 and 0.68, while k_2 is equal to 0.43. For the stress-strain curves the k_1 and k_2 change according to the crushing strain of the masonry. For a

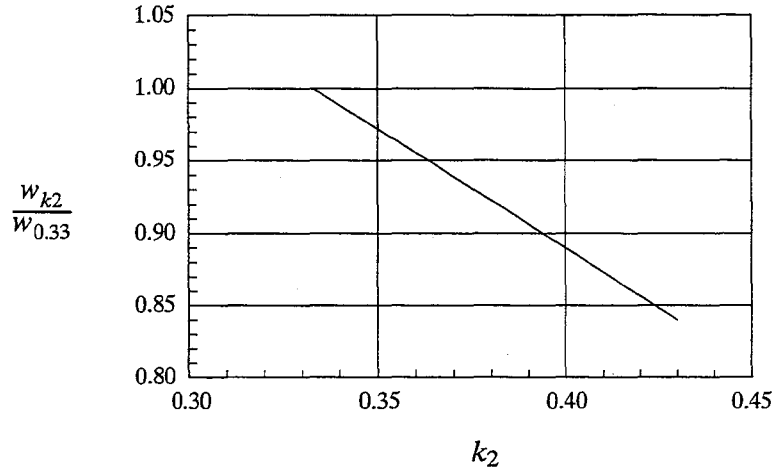


Fig. 263 Panel Strength Reduction vs. k_2

Fig. 263 and are normalized to the strength of the panel calculated for the case when k_1 and k_2 are 0.5 and 0.33 respectively. The obtained ratios for $\left(\frac{w_{k_1, k_2}}{w_{0.50, 0.33}}\right)$ versus k_2 are shown in Fig. 264.

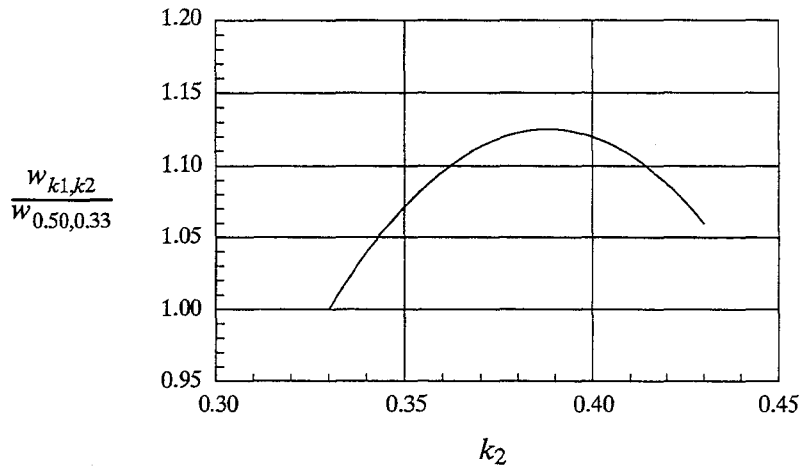


Fig. 264 Panel Strength Reduction vs. k_2

For assumed values of $k_1 = 0.50$ and $k_2 = 0.33$, Eq. [24] produces a maximum underestimation value for the out-of-plane lateral strength of 14%. This 14% strength underestimation is the upper limit on the conservative side. Thus, the values of $k_1 = 0.50$ and $k_2 = 0.33$ are suggested to be adopted in Eq. [24]. This assumption is simple, conservative, and the error is acceptable.

APPENDIX H

THE MAXIMUM COMPRESSIVE STRESS f_b AT THE SUPPORT

The stress–strain relation for both concrete block and clay brick masonry units is of interest for the determination of its corresponding behavior when subjected to axial or bending stresses. A number of proposed curves describing this behavior are available, but no standard model has been adopted for general use.

Stress–strain relationships including those presented by G. C. Hart et. al. [38] and by Priestley and Elder [62] were studied and compared to different experimental results obtained for both clay brick and concrete block masonry. Experimental stress–strain results were obtained from a number of reports presented as part of a U.S.–Japan Coordinated Program For Masonry Building Research [14, 20, 35]. A curve for the stress–strain behavior of the masonry was developed, based on experimental results obtained from the U.S.–Japan Coordinated Program. The shape of the stress–strain relationship is presented in Fig. 265. This proposed curve was developed to represent

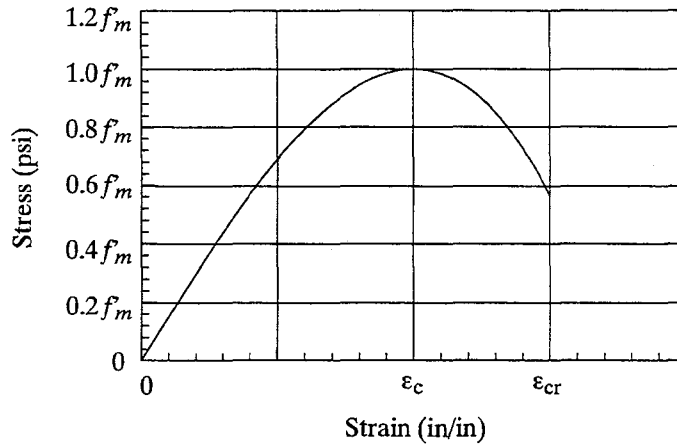


Fig. 265 Idealized Stress–Strain Relation in Compression
Zone for Flexural Compressive Masonry Member

the behavior observed for both concrete block and clay brick masonry during the bending of the masonry.

The equation for the stress–strain relationship (Fig. 265) was designed to meet a number of four different available parameters in the masonry. The four parameters included the location of the origin of the curve with both coordinates at zero. A second parameter defined the compressive strain (ϵ_c) in the masonry at which the strength of the masonry (f_m) was achieved in terms of the crushing strain of the masonry (ϵ_{cr}). The last two parameters consisted of the initial slope of the curve to equal the corresponding modulus of elasticity of the masonry ($750f_m$), and the slope observed at ϵ_c to equal zero. The four parameters are illustrated in Fig. 266. Based on these four parameters, it is observed that the developed equation must contain four different constants; therefore, this relation must follow a third degree polynomial distribution as shown in Eq. [91]. Evaluating the equation (Eq. [91]) with

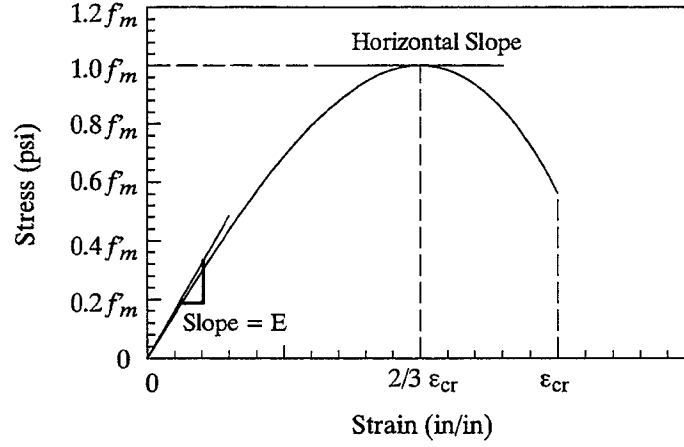


Fig. 266 Parameters for The Idealized Stress–Strain Relation

$$f_b = a\varepsilon^3 + b\varepsilon^2 + c\varepsilon + d \quad \text{Eq. [91]}$$

the four different parameters allow the constants in the equation to be solved. Corresponding constant values are given in Eq. [92] through Eq. [95].

$$a = \frac{750f_m \frac{2}{3}\varepsilon_{cr} - 2f_m}{\left(\frac{2}{3}\varepsilon_{cr}\right)^3} = \frac{27f_m(250\varepsilon_{cr} - 1)}{4\varepsilon_{cr}^3} \quad \text{Eq. [92]}$$

$$b = \frac{-2 * 750f_m \frac{2}{3}\varepsilon_{cr} + 3f_m}{\left(\frac{2}{3}\varepsilon_{cr}\right)^2} = \frac{27f_m(1 - 333.3\varepsilon_{cr})}{4\varepsilon_{cr}^2} \quad \text{Eq. [93]}$$

$$c = E = 750f'_m \quad \text{Eq. [94]}$$

$$d = 0 \quad \text{Eq. [95]}$$

After solving for the four equation constants, and substituting the corresponding values, Eq. [91] produces the final expression for the masonry stress–strain relationship (Eq. [96]).

$$f_b = \frac{27f_m(250\varepsilon_{cr} - 1)}{4\varepsilon_{cr}^3}\varepsilon^3 + \frac{27f_m(1 - 333.3\varepsilon_{cr})}{4\varepsilon_{cr}^2}\varepsilon^2 + E\varepsilon \quad \text{Eq. [96]}$$

APPENDIX I

NOTATION

This appendix concentrates in the definition of nomenclature used during the entire course of the project. They are organized in alphabetical order.

- a distance from the center line to the point no longer in contact with the support
- A_s steel cross sectional area in the concrete members
- A_g gross concrete cross sectional area
- A_v is the shear area of the wall
- b bearing width of the panel on the confining frame
- $\left(\frac{b}{t}\right)_{min1}$ ratio of masonry bearing width to thickness of the panel corresponding to $\left(\frac{h}{t}\right)_{max1}$
- $\left(\frac{b}{t}\right)_{min2}$ ratio of masonry bearing width to thickness of the panel corresponding to $\left(\frac{h}{t}\right)_{max2}$
- c factor equal to $\frac{d}{h}$ or $\frac{1}{4}\varepsilon_{max}$
- d deflection at mid span of panels
- E_c modulus of elasticity of concrete frame
- E_m modulus of elasticity of masonry
- f_a axial compressive stress in the masonry
- f_b compressive stress of the masonry corresponding to the compressive strain observed by the panels at their extreme fiber
- f'_c specified compressive strength of concrete
- f_{kx} flexural tensile strength of the masonry in the direction perpendicular to the bed joint
- f_{ky} flexural tensile strength of the masonry in the direction parallel to the bed joint
- f'_m specified compressive strength of masonry
- f_{v1} masonry shear stress at cracking of the panel
- f_{v2} masonry shear stress at twice the lateral displacement required for cracking of the panel
- G_m masonry shear modulus = $0.4 E_m$
- h height of the masonry infill panels

h'	height of the confining frame
h/t	slenderness ratio of the panel
$\left(\frac{h}{t}\right)_{max1}$	critical slenderness ratio (for the case when $\left(\frac{b}{t}\right)$ does not have a real number solution)
$\left(\frac{h}{t}\right)_{max2}$	critical slenderness ratio (for the case of arching action vanishing, i. e. $\gamma = 0$)
I_b	gross moment of inertia of the beams
I_c	gross moment of inertia of the columns
I_g	gross moment of inertia of the panel
k_1	ratio of the average stress on the bearing area in compression to the maximum compressive stress at the support
k_2	ratio of the distance from the extreme compressive fiber to the resultant compressive force to the bearing width
K	in-plane stiffness of the specimen
L	infill length
L'	frame width
M_u	ultimate moment capacity of the reinforced concrete frame (k-in)
P	applied horizontal force
q_a	allowable out-of-plane lateral pressure resisted by the panel
q_u	ultimate out-of-plane lateral pressure resisted by the panel
R_1	out-of-plane strength reduction factor to account for existing in-plane damage
R_2	out-of-plane strength reduction factor to account for confining frame flexibility
t	masonry infill panel thickness
T	developed thrust forces in the panels due to arching action
V_u	ultimate shear capacity of the reinforced concrete frame (k)
w	uniform lateral load
$w_{0.5}$	lateral strength of the panels corresponding to $k_1 = 0.5$
w_{k1}	lateral strength of panels corresponding to a certain k_1 value
$w_{0.33}$	lateral strength of panels corresponding to $k_1 = 0.33$

w_{k2}	lateral strength of panels corresponding to a certain k_2 value
$w_{0.50,0.33}$	lateral strength of panels corresponding to $k_1 = 0.50$ and $k_2 = 0.33$
$w_{k1,k2}$	lateral strength of panels corresponding to certain k_1 and k_2 values
β	angle between the longitudinal fiber of panels and the thrust force of arches
δ	displacement of the center line of the panel
Δ	maximum in-plane lateral displacement observed by the specimen
Δ_1	axial shortening of extreme fiber
Δ_{cr}	in-plane lateral displacement of the specimen required for the infill panel to crack
ϵ_m	masonry compressive strain
ϵ_{max}	strain of extreme fiber
ϵ_{max1}	strain of extreme fiber corresponding to the out-of-plane strength of the panel
ϵ_{cr}	ultimate crushing strain of masonry
ϵ_c	strain corresponding to f_m'
λ	parameter used to combine several terms in the out-of-plane strength expression
γ	angle between the thrust force and the vertical line
ρ	beam steel ratio (%)
ρ_g	columns steel ratio (%)
θ	rotation of the half panel

REFERENCES

- [1] "Bases Regionales para Elaborar Codigos de Vivienda Sismoresistente de Bajo Costo," *Centro de Investigacion de la Facultad de Ingenieria*, Universidad de Los Andes, Bogota Colombia, Noviembre de 1990.
- [2] "Dynamic Behavior of Brick Structural Elements Infilled to Strengthen R.C. Structures," *Proceedings of the Fifth International Brick Masonry Conference*, Washington, D.C., U.S.A., October 5–10, 1979, pp. 294–301.
- [3] "Methodology for Mitigation of Seismic Hazards in Existing Unreinforced Masonry Buildings: Wall Testing, Out-of-plane," *ABK Topical Report 04*, El Segundo, CA, December 1981.
- [4] Abrams, D.P. and R. Angel, "Lateral Strength of Cracked URM Infills," *Proceedings of Unreinforced Hollow-Clay Tile Workshop*, San Francisco, September 21–22, 1992.
- [5] Abrams, D.P., "Diagnosing Lateral Strength of Existing Concrete or Masonry Buildings," Structural Engineering in Natural Hazards Mitigation, *Proceeding of the Structures Congress 1993*.
- [6] Abrams, D.P., and R. Angel, "Strength, Behavior and Repair of Masonry Infills," Structural Engineering in Natural Hazards Mitigation, pp. 1439–1444, *Proceeding of the Structures Congress 1993*.
- [7] Abrams, D.P., R. Angel, and J. Uzarski, "Transverse Strength of Damaged URM Infills," *Proceedings of Sixth North American Masonry Conference*, Drexel University, Philadelphia, June June 6–9, 1993.
- [8] Abrams, D.P., R. Angel, and J. Uzarski, "Transverse Strength of Damaged URM Infills," *The Masonry Society Journal*, Volume 12, Number 1, pp. 45–52, August 1993.
- [9] Adam, S.A., "Out-of-Plane Response of Masonry Walls," *Proceedings of the Third North American Masonry Conference*, June, 1985.
- [10] Al-chaar, Ghassan, R. Angel, and Abrams, D.P., "Dynamic Testing of Unreinforced Brick Masonry Infills," *To be published in the proceedings of the Symposium on Advances in Engineering for Concrete and Masonry Structures*, April 24–28, 1994.
- [11] Anderson, C., "Lateral Loading Tests on Concrete Block Walls," *The Structural Engineer*, Pt. 2, Vol. 54, No 7, July 1976, pp 239–246.
- [12] Anderson, C., "Arching Action in Transverse Laterally Loaded Masonry Wall Panels," *The Structural Engineer*, Vol. 62B, No. 1, 1984, pp. 12–23.
- [13] Anderson, C., "Tests on Walls Subjected to Uniform Lateral Loading and Edge Loading," *Proceedings of the Seventh International Brick Masonry Conference*, Melbourne, Australia, February 1985, pp. 889–899.

- [14] Assis, G.F., Hamid, A.A., and Harris, H.G., "Material Properties for Grouted Block Masonry," *Report No. 1.2(a)-2, U.S.-Japan Coordinated Program for Masonry Building Research*, Department of Civil and Architectural Engineering, Drexel University, Philadelphia, PA, August 1989.
- [15] Axley, J.W. and V.V. Bertero, "Infilled Panels: Their Influence on the Seismic Response of Buildings," *Earthquake Engineering Research Center Report EERC 79-28*, University of California, Berkeley, September 1979.
- [16] Benjamin, J.R., and H.A. Williams, "The Behavior of One-Story Brick Shear Walls," *Journal of the Structural Division*, ASCE, Vol. 84 ST4, July 1958.
- [17] Bostjancic, Joze, "Use of a Modelling Approach in The Analysis of The Effects of Repairs to Earthquake-Damaged Stone-Masonry Buildings," *Dimiceva 12*, Ljubljana, Yugoslavia (Slovenia).
- [18] "Building Code Requirements for Reinforced Concrete," ACI 318-56.
- [19] "Building Code Requirements and Commentary for Reinforced Concrete," ACI 318-89.
- [20] Brown, R.H., and Young, J.M., "Compressive Stress Distribution of Grouted Hollow Clay Masonry Under Strain Gradient," *Report No. 1.2(b)-1, U.S.-Japan Coordinated Program for Masonry Building Research*, Department of Civil Engineering, Clemson University, Clemson, OH, May 1988.
- [21] Cohen, E., and Laing, E., "Discussion of Arching Action Theory of Masonry Walls," *Journal of the Structural Division*, ASCE, Volume 82 No. ST5, September 1956.
- [22] Dawe, J.L., and C.K. Seah, "Out-of-Plane Resistance of Concrete Masonry Infilled Panels," *Journal of the Canadian Society of Civil Engineering*, January 1990, pp. 854-864.
- [23] De Veckey, R.C. and West, H.W.H. "The Flexure Strength of Concrete Blockwork," *Magazine of Concrete Research*, Vol. 32, No. 113, Dec. 1980, pp 206-218.
- [24] Drysdale, R.G., and A.S. Essawy, "Out-of-Plane Bending of Concrete Block Walls," *Journal of the Structural Division*, American Society of Civil Engineers, Vol. 114, No. ST1, 1988, pp. 121-133.
- [25] El-Attar, Adel G., White, Richard N., "Shake Table Test of a one-eighth scale three-story reinforced concrete frame building designed primarily for gravity loads," *6th Canadian Conf. Earthquake Engineering*, 1991.
- [26] Epperson, G.S., and D.P. Abrams, "Nondestructive Evaluation of Masonry Buildings," *Report No. 89-26-03, Advanced Construction Technology Center*, University of Illinois at Urbana-Champaign, October 1989.

- [27] Epperson, G.S., and D.P. Abrams, "Evaluation of Lateral Strength of Existing Unreinforced Brick Masonry Piers in the Laboratory," *Proceeding of Fifth North American Masonry Conference*, pp. 735–746, University of Illinois at Urbana–Champaign, June 1990.
- [28] Essawy, A., and R.G. Drysdale, "Capacity of Block Masonry under Uniformly Distributed Loading Normal to the Surface of the Wall," *Proceedings of the Third Canadian Masonry Symposium*, Edmonton, Canada, June 1983, pp. 39–1 to 39–16.
- [29] Essawy, A. and Drysdale, R.G., "Evaluation of Available Design Methods for Masonry Walls Subject to Out-of-Plane Loading," *Proceedings, Fourth North American Conference*, August, 1987, paper 32.
- [30] Fedorkiw, J.P., and M.A. Sozen, "A Lump Parameter Model to Simulate Response of Reinforced Concrete Frames with Masonry Filler Walls," *Civil Engineering Studies, Structural Research Series No. 338*, University of Illinois, Urbana, 1968.
- [31] Fiorato, A.E., M.A. Sozen, and W.L. Gamble, "An Investigation of Reinforced Concrete Frames with Masonry Filler Walls," *Civil engineering Studies, Structural Research Report No. 370*, University of Illinois, Urbana, November 1970.
- [32] Franklin, H.A., "Nonlinear Analysis of Reinforced Concrete Frame and Panels," *Structures and Materials Research Report SESM 70–5*, Department of Civil Engineering, University of California, Berkeley, March 1970.
- [33] Gabrielsen, B.L., and K. Kaplan, "Arching in Masonry Walls Subjected to Out-of-Plane Forces," *Proceedings of National Workshop on Earthquake Resistant Masonry Construction*, National Bureau of Standards, NBS Science Series No. 106, September 1977.
- [34] Guh, T.J., "Seismic Retrofit of Building Structures With Unreinforced Masonry Infill Walls," *Structural Engineering in Natural Hazards Mitigation, Proceeding of the Structures Congress 1993*.
- [35] Hamid, A.A., Assis, G.F., and Harris, H.G., "Material Properties for Grouted Block Masonry," *Report No. 1.2(a)–1, U.S.–Japan Coordinated Program for Masonry Building Research*, Department of Civil and Architectural Engineering, Drexel University, Philadelphia, PA, August 1988.
- [36] Haseltine, B.A., "Design of Laterally Loaded Wall Panels," *Proceedings of the British Ceramic Society, Loadbearing Brickwork*, Vol. 5, No. 24, Stoke-on-Trent, U.K., pp. 115–126.
- [37] Haseltine, B.A., West, H.W.H., and Tutt, J.N., "Design of Walls to Resist Lateral Loads," *The Structural Engineers, Pt 2*, Vol. 55, No. 10, Oct. 1977, pp 422–430.
- [38] Hart, G.C., Sajjad, N.A., Kingsley, F.R., and Noland, J. L., "Analytical Models for the Stress–Strain Behavior of Confined and Unconfined Concrete Masonry," *Proceedings Fifth Canadian Masonry Symposium*, Vancouver, B.C., June 1989.

- [39] Henderson, R.C., W.D. Jones, and M.L. Porter, "Out-of-Plane and In-Plane Testing of URM Infills," *Structural Engineering in Natural Hazards Mitigation, Proceeding of the Structures Congress 1993*.
- [40] Hendry, A.W. "The Lateral Strength of Unreinforced Brickwork," *The Structural Engineers*, Vol. 51, No. 2, Feb. 1973, pp 43–50.
- [41] Hendry, A.W. , and A.M.A. Kheir, "The Lateral Strength of Certain Brickwork Panels," *Proceedings of the Fourth International Brick Masonry Conference*, Brugge, Belgium, pp. 4.a.3.1–4.a.3.4, 1976.
- [42] Hill, J.A., "Full-Scale Testing of Unreinforced Masonry Infill Frame Panels," *Structural Engineering in Natural Hazards Mitigation, Proceeding of the Structures Congress 1993*.
- [43] Hodgkinson, A.W., West, H.W.H., and Haseltine, B.A., "Preliminary Tests on the Effect of Arching in Laterally Loaded Walls," *Proceedings of the Fourth International Brick Masonry Conference*, 1976.
- [44] Holmes, M., "Steel Frames with Brickwork and Concrete Infilling," *Proceedings of the Institution of Civil Engineers*, Vol. 19, No. 6501, Aug. 1961, pp. 473–475.
- [45] Holmes, M., "Combined Loading on Infilled Frames," *Proceedings of the Institution of Civil Engineers*, Vol. 25, May 1963, pp. 31–38.
- [46] Jara, Manvel, "Typical Cases of Repair and Strengthening of Concrete Buildings," *Earthquake Spectra: The Professional Journal of the Earthquake Engineering Research Institute*, Vol. 5, Feb. 1989, pp. 175–93.
- [47] Jirsa, James, "Repairing and Strengthening Damage Reinforced Concrete Buildings," *Proceedings of the third U.S.–Mexico Workshop on 1985 Mexico Earthquake Research*, The University of Texas at Austin, Austin 1989.
- [48] Klingner, R., and V.V. Bertero, "Infilled Frames in Aseismic Construction," *Earthquake Engineering Research Center Report EERC 76–32*, University of California, Berkeley, December 1976.
- [49] Lefter, J., and J. Colville, "Reinforcing Existing Buildings to Resist Earthquake Forces," *Proceedings of CENTO Symposium on Earthquake Engineering and Engineering Seismology*, Middle East Technical University, Ankara, Turkey, November 1974.
- [50] McDowell, E.L., K.E. McKee and E. Sevin, "Arching Action Theory of Masonry Walls", *Proceedings of the American Society of Civil Engineers, Journal of the Structural Division*, Vol. 82, No. ST2, March 1956, pp. 915–1 to 915–18.
- [51] McDowell, E.L., K.E. McKee and E. Sevin, "Discussion of Arching Action Theory of Masonry Walls", *Proceedings of the American Society of Civil Engineers, Journal of the Structural Division*, September 1956, pp. 1067–27 to 1067–40.

- [52] McKee, K.E., and E. Sevin, "Design of Masonry Walls for Blast Loading," *ASCE Transactions, Paper No. 1512*, Vol. 124, 1958.
- [53] Maio, N.A., "Dynamic Behavior of Brick Structural Elements Infilled to Strengthen R.C. Structures," *Proceedings of Vth International Brick Masonry Conference*.
- [54] Mehrabi, A.B. and P.B. Shing, "Performance of Masonry–Infilled R/C Frames under In–Plane Lateral Loads: Analytical Modeling," *Proceedings of NCEER Workshop on: Seismic Response of Masonry Infills*, San Francisco, CA., February 4 and 5, 1994.
- [55] Monk, C.B., "Resistance of Structural Clay Masonry to Dynamic Forces," *Research Report No. 7*, Structural Clay Products Research Foundation, Geneva, Illinois, November 1958.
- [56] "NEHRP Handbook for the Seismic Evaluation of Existing Buildings," *Federal Emergency Management Agency FEMA–178*, Earthquake Hazards Reduction Series 47, June 1992.
- [57] "PCI Design Handbook, Precast and prestressed Concrete," Third Edition, Prestressed Concrete Institute, Chicago, Illinois 1985.
- [58] Page, A.W., "Finite Element Model for Masonry," *Journal of the Structural Division*, ASCE, Vol. 104, ST8, August 1978.
- [59] Paulson, T.J., and D.P. Abrams, "Correlation between Static and Dynamic Response of Model Masonry Structures," *Earthquake Spectral*, Vol.6, Number 4, 1990, Earthquake Engineering Research Institute.
- [60] Plummer, Harry C. and Blume, John A., "Reinforced Brick Masonry and Lateral Force Design," *Structural Clay Products Institute*, 1953.
- [61] Prawel, S.P., "Summary of Research Tasks and Methods to be Used: Renovation/Retrofit/Repair of Brick Masonry," *Project No. 891004*, University at Buffalo, April 1990.
- [62] Priestley M.J.N., and Elder, D.M., "Stress–Strain Curves for Unconfined and Confined Concrete Masonry," *Journal of the American Concrete Institute*, May/June 1983/ No. 3 Proceedings V.80.
- [63] Remic, D., Zarnic, R., Cerne, G., and Kos, J., "Repair and Strengthening of a 19th Century School Building – A Case Study," *Seminar Rii*, Skopje 1988.
- [64] Rivero, C.E., and W.H. Walker, "An Analytical Study of the Interaction of Frames and Infill Masonry Walls," *Civil Engineering Studies, Structural Research Series No. 502*, University of Illinois, Urbana, September 1982.
- [65] Sachanski, S., "Analysis of the Earthquake Resistance of Frame Buildings Taking into Consideration the Carrying Capacity of the Filling Masonry," *Proceedings of the Second World Conference on Earthquake Engineering*, Vol. 3, p.2127–2141, Tokyo, 1960.
- [66] Seah, Chin Kong, "Out–of–Plane Behavior of Concrete Masonry Infilled Panels," *M.S. Thesis, the University of New Brunswick*, Canada, April 1988.

- [67] Seubkem F., A.G. Kurkchubasche, and G.R. Kingsley, "Three-Dimensional Analysis Model for Complete Masonry Buildings," *Structural Engineering in Natural Hazards Mitigation, Proceeding of the Structures Congress 1993*.
- [68] Shah, N. and D.P. Abrams, "Design, Construction and Utilization of a Post Tensioned Masonry Laboratory Reaction Structure," *Proceedings of Sixth Canadian Masonry Symposium*, University of Saskatchewan, June, 1992.
- [69] Sheppard, Peter F., "Dynamic Characteristics of Tall, Pre-1965 Masonry Buildings, as a basis for their Seismic Analysis and Strengthening," *Institute for Testing and Research in Materials and Structures*, Dimiceva, Ljubljana, Yugoslavia.
- [70] Shing, P.B., "Joint U.S.-Italy-Yugoslavia Research on Evaluation and Retrofit of Masonry-Infilled Reinforced Concrete Frames," Boulder, Colorado.
- [71] Shing, P.B., Noland, James L., "Response of Single-Story Reinforced Masonry Shear Wall to In-Plane Lateral Loads," *Report No. 3.1(a)-2*, Advanced Construction Technology Center, University of Colorado at Boulder, Boulder, January 1991.
- [72] Sinha, B.P., "A Simplified Ultimate Load Analysis of Laterally Loaded Model Orthotropic Brickwork Panels of Low Tensile Strength," *The Structural Engineer*, Vol. 56B, No. 4, December 1978, pp. 81-84.
- [73] Sinha, B.P., Loftus, M.D., and Temple, R., "Lateral Strength of Brickwork Panels," *Proc. Int. Civ. Engrs., Pt 2*, Vol. 67, March 1979, pp 191-197.
- [74] Smith, S., "Lateral Stiffness of Infilled Frames," *Journal of the Structural Division*, ASCE, Vol. 88, No. 3355, December 1962, pp. 183-199.
- [75] Smith, S., "Behavior of Square Infilled Frames," *Journal of the Structural Division*, ASCE, Vol. 92, No. ST1, February 1966, pp. 381-403.
- [76] Storm, J.H., "A Finite Element Model to Simulate the Nonlinear Response of Reinforced Concrete Frames with Masonry Filler Walls," *Ph.D. Thesis*, University of Illinois, Urbana, 1973.
- [77] Tassios, T.P., "Masonry, Infill and R.C. Walls under Cyclic Actions. An Invited State-of-the-Art Report," *CIB Symposium: Wall Structures*, Warsaw, 1984.
- [78] Thomas, F.G., "The Strength of Brickwork," *The Structural Engineer*, Part 2, Vol. 31, 1953, pp. 35-41.
- [79] Timoshenko, S., and S. Woinowsky-Krieger, "Theory of Plates and Shells," McGraw-Hill, 1959.
- [80] Trigo, D.A., "Estructuras de Paineis sob a accao de Solicitacoes Horinzotais," *Laboratorio National de Engenharia Civil*, Lisbon, 1968.
- [81] *Uniform Code for Building Conservation*, 1991 Edition, International Conference of Building Officials, Whittier, California.

- [82] West, H.W.H., H.R. Hodgkinson, and W.F. Web, "Lateral Load Test on Walls with Different Boundary Conditions," *Proceedings of Third International Brick Masonry Conference*, Essen, Germany, 1973, pp. 180–186.
- [83] West, H.W.H., Hodgkinson, H.R., and Haseltine, B.A., "The Resistance of Brickwork to Lateral Loading," *The Structural Engineers, Pt 2*, Vol. 55, No. 10, Oct. 1977, pp 441–421.
- [84] Whitney, C.S., Anderson, B.G., and Cohen E., "Design of Blast Resistant Construction for Atomic Explosions," *Journal of the American Concrete Institute*, Vol. 5, 1955.
- [85] Wilton, C., and B. Gabrielsen, "Shock Tunnel Tests of Preloaded and Arched Wall Panels," *URS Report 7030–10*, URS Research Co., San Mateo, California, June 1973.
- [86] Yong, P.M.F. "Cyclic Testing of a Strengthened In–Plane Brick Masonry Panel," Ministry of Works and Development, *Central Laboratories, Report No. 5–81/7*, Gracefield, New Zealand, August 1981.
- [87] Yorulmaz, M., and M.A. Sozen, "Behavior of Single–Story Reinforced Concrete Frames with Filler Walls," *Technical report to Department of Defense, Contract OCD–PS–64–201*, University of Illinois, Urbana, 1967.
- [88] Zarnic, R., and D.P. Abrams, "Considerations for Reinforced Concrete Frames filled with Masonry," *Structures Journal of American Concrete Institute*, May 1990.
- [89] Zarnic, R., M. Tomazevic, and T. Velechovsky, "Experimental Study of Methods for Repair and Strengthening of Masonry Infilled Reinforced Concrete Frames," *Proceedings of the Eighth European Conference on Earthquake Engineering*, Lisbon, September 1986, Vol. 5, pp.11.1/41–11.1/48.
- [90] Zarnic, R., and M. Tomazevic, "An Experimentally Obtained Method for Evaluation of the Behavior of Masonry Infilled R.C. Frames," *Proceedings of Ninth World Conference of Earthquake Engineering*, Tokyo–Kyoto, August 1988.
- [91] Zarnic, R., "Strengthening of Masonry Vaults By Foam Concrete Application," *Seminar RII*, Skopje 1988.

